ELECTROCHEMICAL ADVANCED OXIDATION OF SELECTED PHARMACEUTICALS AND DISINFECTION BY-PRODUCTS IN WATER SAMPLES

BY

HAKIMU NSUBUGA

A Dissertation Presented to the

DEANSHIP OF GRADUATE STUDIES

KING FAHD UNIVERSITY OF PETROLEUM & MINERALS

DHAHRAN, SAUDI ARABIA

In Partial Fulfillment of the
Requirements for the Degree of

DOCTOR OF PHILOSOPHY

In

CHEMISTRY

MARCH, 2019

KING FAHD UNIVERSITY OF PETROLEUM & MINERALS
DHAHRAN- 31261, SAUDI ARABIA

DEANSHIP OF GRADUATE STUDIES

This thesis, written by **HAKIMU NSUBUGA** under the direction of his thesis advisor and approved by his thesis committee, has been presented and accepted by the Dean of Graduate Studies, in partial fulfillment of the requirements for the degree of **DOCTOR OF PHILOSOPHY IN CHEMISTRY.**

Dr. Chanbasha Basheer
(Advisor)

Dr. Khalid R. Alhooshani
Department Chairman

Dr. Muhammad B. Haider
(Co-Advisor)

Dr. Salam A. Zummo
Dean of Graduate Studies

Dr. Abdel-Nasser Kawde
(Member)

28/3/19
Date

Dr. Hasan A.S.Al-muallem
(Member)

Dr. Abdulrahman A. Al-Arfaj
(Member)

DEDICATED

TO

My loving parents, wife and children for their continued prayers & Support

ACKNOWLEDGMENTS

All praise and thanks be to the Almighty Allah, The Most Gracious, The Most Merciful, for all the favors bestowed on me. Without His infinite mercy, this thesis work would never come to fruition.

I am eternally thankful to King Fahd University of Petroleum and Minerals (KFUPM) for granting me a scholarship opportunity to pursue my doctoral studies. The chemistry department under the wise leadership of the current chairman Dr. Khalid Alhooshani and the previous chairman Dr. Abdulaziz Al-saadi, together with their quality teams of staff and faculties are highly appreciated for their immense support and mentorship.

I am extremely indebted to my advisors Dr. Basheer Chanbasha and Dr. Muhammad B. Haider for their invaluable encouragement, support and advise. Their commitment and wisdom greatly shaped my thesis. Through them, I have learnt that one has to remain happy and optimistic despite the research challenges met.

I am profoundly grateful to my thesis committee members for their immensurable guidance during my thesis preparation.

My sincere gratitude goes to the administrators and staff of both graduate studies and research centers for their invaluable support. I am also thankful to Islamic University in Uganda (IUIU) for enlivening my passion for knowledge advancement.

I am also grateful to the deanship of scientific research at King Fahd University of Petroleum and Minerals (KFUPM) through a project grant No.151024 for the financial support.

I will always be thankful and grateful to my loving parents, wife and children for their prayers, endurances and sacrifices during my absence. Much as you were miles away from me, I was always with you in my heart! May Allah continue to bless you with happiness, long and good lives.

Lastly, I would like thank all my colleagues in the chemistry department and housing for their invaluable heartwarming moments especially off the busy working schedules.

TABLE OF CONTENTS

LIST OF TABLES

LIST OF FIGURES

LIST OF ABBREVIATIONS

ECs	**:**	Emerging Contaminants
AOPs	**:**	Advanced Oxidation Processes
EAOPs	**:**	Electrochemical Advanced Oxidation Processes
AO	**:**	Anodic Oxidation
LOQ	**:**	Limit of Quantitation
LOD	**:**	Limit of Detection
RSD	**:**	Relative Standard Deviation
LDR	**:**	Dynamic Linear Range
SAED	**:**	Selected Area Electron Diffraction
TEM	**:**	Transmission Electron Microscopy
XRD	**:**	X-ray powder diffraction
AO-H_2O_2	**:**	Anodic oxidation with electrogenerated H_2O_2
EF	**:**	Electro-Fenton
hEF	**:**	Heterogeneous Electro-Fenton
PIN	**:**	Pindolol
ACE	**:**	Acebutolol

ATE	**:**	Atenolol
PROP	**:**	Propranolol
ALP	**:**	Alprenolol
ß-blockers	**:**	Beta blockers
LC-MS/MS	**:**	Liquid chromatography–tandem mass spectrometry
DFEF	**:**	Droplet-flow assisted electro-Fenton reactor
RSM	**:**	Response Surface Methodology
CCD	**:**	Central Composite Design
ANOVA	**:**	Analysis Of Variance
pH	**:**	Hydrogen potential
UV	**:**	Ultraviolet
A_0	**:**	Coefficient constant
A_{ii}	**:**	Coefficient of the quadratic term
A_{ij}	**:**	Interaction coefficient
Df	**:**	Degree of freedom
F	**:**	Fisher-Snedecor value
R^2	**:**	Determination coefficient (correlation coefficient)

R^2 adj	**:**	Adjusted coefficients of determination
HWW	**:**	Hospital wastewater
NDPA	**:**	N-nitrosodibutylamine
NDBA	**:**	N-nitrosodipropylamine
GC-MS	**:**	Gas chromatography–mass spectrometry
DFEF	**:**	Droplet flow assisted electro-Fenton
PEF	**:**	Photoelectro-Fenton
DF-PEF	**:**	Droplet flow assisted photoelectro-Fenton
DF-PEF/RHS/TiO_2	**:**	Droplet flow assisted photoelectro-Fenton-photocatalyst
BDD	**:**	Boron doped diamond
GFE	**:**	Graphite felt electrode
ORR	**:**	Oxygen reduction reaction

ABSTRACT (ENGLISH)

Full Name : [HAKIMU NSUBUGA]

Thesis Title : [ELECTROCHEMICAL ADVANCED OXIDATION OF SELECTED PHARMACEUTICALS AND DISINFECTION BY-PRODUCTS IN WATER SAMPLES]

Major Field : [CHEMISTRY]

Date of Degree : [DECEMBER 2018]

This study focusses on the electrochemical advanced oxidation methods (EAOPs) for effective degradation and monitoring of selected emerging contaminants (ECs) in complex aquatic environments. The beauty of these methods lies in their strong abilities to continuously electrogenerate reactive oxygen species (ROS) (hydrogen peroxide, H_2O_2 and hydroxyl radical (•OH)) in-situ. The high removal efficiencies exhibited by these methods are due to several mechanisms such as direct, indirect oxidation and adsorption/electro-sorption. As such, the efficiency and selectivity of EAOPs for enhanced and sustainable in-situ electrogeneration of ROS mainly depend on reactor design, nature, and type of the electrode surfaces. Because of ROS strong oxidizing abilities, they unselectively react with organic pollutants till complete degradation. The first part of this thesis work was aimed at assessing the potential formation of trace level β-blockers in hospital wastewater (HWW) using an ecofriendly micro-solid phase extraction (μ-SPE) method based on rice husk silica sorbent and Liquid chromatography–tandem mass spectrometry (LC-

MS/MS) analysis. After multivariate chemometric optimization, the method was found suitable for determining trace level β-blockers in complex aquatic environments.

We then developed and fabricated a novel droplet-flow assisted electro-Fenton (DFEF) system for effective degradation of beta-blockers in HWW using sol-gel synthesized biogenic iron–carbon nanocomposites as heterogeneous Fenton catalysts. We demonstrated for the first time how natural air could be used as a nebulizing agent for fast, simultaneous, continuous catholyte air saturation, pollutant and Fenton catalyst transfer to the cathode electrode during DFEF operations. Under neutral pH conditions, a degradation efficiency of ß-blockers was up to 99.9%. In another study, treated graphite electrodes were functionalized by copper-boron-ferrite (Cu-B-Fe) composites via rice husk silica-based sol-gel approach. The integrated electrodes were then investigated as efficient electrodes for fast in-situ electro-generation of ROS via a continuous DFEF system. Using this proposed method and at optimized conditions, higher and faster degradation efficiencies of up to 100% for both propranolol and atenolol in HWW were demonstrated in less than 10 minutes. The fabricated cathode electrodes showed stable catalytic activities even after 20 experimental replicates. Lastly, a droplet flow-assisted photoelectron-Fenton system in combination with heterogeneous photocatalysis were investigated for effective degradation of N-nitrosamines (N-nitrosodibutylamine and N-nitrosodipropylamine). This work involved graphite electrode functionalization and microwave-assisted synthesis and immobilization of titanium oxide on rice husk nanosilica spheres via hydrolytic sol-gel routes. The immobilized catalyst and functionalized cathode were evaluated for effective and fast degradation of N-nitrosamines in swimming pool water. The influence of key operational parameters was investigated using central composite design. Under optimum conditions, the degradation efficiency of N-nitrosamines in swimming pool water was up to 100%.

ملخص الرسالة

الاسم الكامل: حكيمو نسوبوقا

عنوان الرسالة :الأكسدة الإلكتروكيميائية المتقدمة لمركبات صيدلانية مختارة وتعقيم عينات المياه من النواتج الجانبية لهذه المركبات.

التخصص: كيمياء.

تاريخ الدرجة العلمية :ديسمبر2018

هذه الدراسة تركز علي طرق الاكسدة الكهروكيميائية المتقدمة للتكسير الفعال والمتحكم للملوثات الناشئة المختارة في البيئات المائية المعقدة .تكمن هذه الطرق في قدرتها القوية علي استمرارية التوليد الكهربي لجسيمات الاكسجين النشطة والهيدروجين بيروكسيد وكذلك جسيم الهيدوكسيل النشط.بسبب قدرات المؤكسد القوي التي تتفاعل مع الملوثات العضوية حتي يكتمل التكسير. الجزء الاول من عمل هذه الرسالة يهدف الي تقييم التكون الجهدي للمستويات الضئيلة لبيتا الحاصرات في مياه الصرف الصحي للمستشفيات بإستخدام طريقة الاستخلاص الطور المصغر الصلبة الصديقة للبيئة التي تعتمد علي ماصة السليكا لقشر الارز و سائل التحليل الكروماتوجرافي – تحليل مطياف الكتلة . MS/MS) - (LC

بعد متعدد المتغيرات الكيميائية المثالي ، تم العثور على طريقة مناسبة لتحديد المستويات الضئيلة لحاصرات بيتا في البيئات المائية المعقدة. ثم قمنا بتطوير وتصنيع مفاعل كهربائي فينتون بمساعدة تدفق القطيرات (DFEF) نظام للتكسير الفعال للحاصرات بيتا في HWW باستخدام تقنية الصل -جل لتوليف بيولوجي المنشأ مركبات الكربون النانوية كعوامل حفازة غير متجانسة فينتونية. لقد أظهرنا لأول مرة كيف يمكن استخدام الهواء الطبيعي كعامل للإرهاق من أجل تشبع هواء كاثودي سريع ومتزامن ومستمر ،نقل محفز الملوثات والفنتون إلى القطب الكهربائي خلال عمليات DFEF. تحت درجة الحموضة متعادلة الظروف ، كانت كفاءة تدهور حاصرات ß تصل إلى 99.9 ٪. في دراسة أخرى ، الجرافيت المعالجة تم عمل الأقطاب الكهربائية بواسطة مركبات نحاس والبورون والحديد (Cu-B-Fe) عن طريق السيليكا الموجودة في قشر الأرز لفكرة الصل -جل. ثم تم تقييم الأقطاب

الكهربائية المتكاملة كأقطاب فعالة لسرعة التوليد الكهربائي لأنواع الأكسجين التفاعلية (H2O2 و • OH) عن طريق نظام مفاعل DFEF المستمر.

باستخدام هذه الطريقة المقترحة وفي الظروف المثالية ، كفاءة أعلى وأسرع تكسير يصل إلى 100 ٪ لكلا البروبرانولول والأتينولول في HWW ظهر في أقل من 10 دقائق. الأظهر القطب الكاثود ملفقة الأنشطة الحفزية مستقرة حتى بعد 20 مكررات التجريبية. أخيرا تدفق قطرة بمساعدة نظام الضوئية-فنتون في تركيبة مع التحفيز الضوئي غير المتجانسة تم التحقيق في التدهور الفعال لاثنين من نيتروزامين N (نيتروسوديبوتيلاميلين و N-

nitrosodipropylamine). شارك في هذا العمل وظائف الجرافيت الكهربائي والميكروويف بمساعدة تخليق وتجمد أكسيد التيتانيوم على كرات قشور الأرز نانوسيليكا عبر جل مائي الطرق. تم تقييم المحفز المانع والكاثود الوظيفي لفعالية وسرعة تدهور نيتروساميينيز في مياه حمام السباحة. كان تأثير المعايير التشغيلية الرئيسية التحقيق باستخدام التصميم المركب المركزي. في ظل الظروف المثلى ، وكفاءة تدهور N- وكان نيتروساميينيز في مياه حمام السباحة يصل إلى 100 ٪.

CHAPTER 1

INTRODUCTION

1.1 Background of the study

For any water authority, its primary concern is to maintain a safe water supply for human consumption. With the current rapid population growth, urbanization, industrialization, deforestation and pollution, most countries are experiencing the highest water deficit, and this has translated into appalling social and economic concern. Most countries have therefore envisioned water reuse as an alternative water reclamation mechanism. However, the major source of water for potential reuse is wastewater effluent. Water treatment is therefore mandatory in ensuring sustainable water quality. Recently, a new group of pollutants known as emerging contaminants (ECs) in aquatic environments have been receiving increased attention in the scientific community [1]. ECs are raising public concern because of their potential effect on public health, aquatic ecosystems and yet limited data regarding their fate, transport and occurrence is available [1]. ECs refer to anthropogenic unregulated chemicals that have been detected in wastewater effluent, surface water, foodstuffs, plants, soils, human and animal tissues in trace amounts throughout the world [2]. ECs result from the degradation and recombination of man-made chemicals from long term contaminated sites. They are non-biodegradable and are capable of changing the physiology of target receptors. Examples of ECs include, pharmaceuticals and disinfection by-products (DBPs) [3].

Most of these contaminants with their active metabolites and transformation products have continually being introduced into various aquatic systems through poorly treated and untreated sewage effluents and influents. Specifically, pharmaceutical active ingredients (PAI) and their metabolite have ended up in aquatic environments through excretion, improper disposal (of expired and unused drugs) or even from direct point sources as sewage effluents [4]. PAI metabolites pose serious side effects yet their concentrations in aquatic environments can sometimes exceedingly surpass that of their parent counterparts [5]. These ECs show some persistence in aquatic environments and some of them exhibit adverse effects on both terrestrial and aquatic organisms [6]. The disastrous effects of these ECs like beta-blockers on aquatic species is well documented [7,8]. Therefore, basing on ECs growing environmental and health concern, it is deemed right to reflect on their possibility for long time exposure effects to low level concentrations on terrestrial and aquatic ecosystems and the possibility of their removal [9]. Advanced Oxidation Processes (AOPs) and in particular oxidation based on Fenton's reagent offers a simple, effective and attractive technology for the degradation of multiple organic pollutants, utilizing non-toxic reagents and eventually leaves no residues [10]. This process is most effective at restricted pH near 3 [11]. Hence, search for AOPs that are less/not pH dependent is most desirable.

1.2 Problem statement

Continued improvement in analytical chemistry techniques to date, has allowed the continued detection and measurements of emerging contaminants (ECs) in various aquatic and terrestrial environments at very low concentrations.

When a parent organic pollutant enters an environmental matrix, it is more likely to undergo different processes such as dilution, absorption, adsorption, photolysis, biodegradation, hydrolysis, complexation, oxidation or volatilization [12]. The result are the emerging contaminants in form of parent organic contaminants, their metabolites or even transformation products. Noteworthy, ECs are often found in various environmental water matrices at reduced concentrations (µg to ng L^{-1}). It has been demonstrated in recent studies that despite the trace level (parts-per-billion levels) presence of ECs in the aquatic environments, they are of potential bionomic concern to wildlife and humans especially after a long-term exposure [13]. It is more likely that the toxicity of one ECs compound might synergistically be enhanced or antagonistically be eliminated by the presence of the other [14]. To this effect, significant environmental monitoring and risk assessments of ECs is being conducted to acquire in-depth knowledge that will prioritize them for possible regulation and monitoring. Because most of these compounds are unknown, the information about their potential interactive effects, biochemical and chemical properties in complex mixed environmental matrices is still scanty and unknown. For example, the identification, quantification and fate of metabolites/ transformation products of excreted ECs have received little attention. Owing to the high water demands to suit the global population increase and the continued detection of these refractory organic pollutants in aquatic environments, these micropollutants must be remediated from the municipal and industrial wastewater effluents before water reuse. Traditional wastewater treatment methods (like secondary biodegradation) can hardly remove many of these ECs at their trace level concentrations. Advanced treatment technologies like reverse osmosis and activated carbon are sought to be promising treatment alternatives leading to high water purity but only concentrate and transform pollutants from one level to the next, thus necessitating further remediation strategies to render them completely inert.

The combination of advanced analytical methods like Tandem mass spectrometry-based methods (LC/MS/MS) with electrochemical advanced oxidation techniques provides excellent means of insightful structure elucidation, and monitoring of trace level ECs, their metabolites and transformation products in complex mixed aquatic environments. Since, the analytical determination of ECs in aquatic environments are highly influenced by matrix effects and background interferences, appropriate sample preparation techniques are highly desirable [15]. The electrochemical advanced oxidation processes (EAOPs) represent better and promising alternatives to remove recalcitrant micro pollutants from complex aquatic environments through the use of in situ generated powerful and non-selective reaction oxygen species (H_2O_2, hydroxyl radical).

Also, EAOPs can provide effective water treatment technological solutions since they could be combined with traditional treatments thus decreasing the operation cost and creating a significant improvement in the effectiveness of the conventional treatment methods.

1.3 Justification of the study

The detection of trace level beta blockers (ß-blockers) and nitrosamines as emerging contaminants in surface drinking, ground and wastewater even after undergoing conventional water treatment, has aroused global scientific interest. Mixed ECs contamination present cumulative ecotoxicological effects to plants and aquatic organisms even at concentrations of ng L^{-1} to µg L^{-1}. Therefore, it is warranting to develop a potent degradation and monitoring approaches for complete removal of trace ECs with their metabolites during water treatment.

Most studies on ECs degradation in aquatic environments focus on gradual disappearance of parent analytes as a proof of degradation, neglecting their intermediate species/ metabolites that might even be more toxic. Moreover, the ECs concentration of (>15 mg/L), monitored in most reported literature, far exceeds the Maximum Contaminant Levels. A combination of electrochemical oxidation methods with advanced analytical instruments (LC-MS/MS and GC-MS), is asserted to offer a more appealing approach for monitoring the degradation pathways and intermediate product identification of trace level pollutants [16,17]. Electro-chemical advanced oxidation processes (EAOPs) have attracted significant interest in aquatic pollutant remediation, owing to their eco-friendliness, strong oxidation abilities, insignificant toxicities, technological simplicity, and higher degradation efficiencies [18,19].

1.4 General objectives

The primary objective of this thesis work is to bring a better fundamental understanding of the fate of trace level ECs in aquatic environments through design, fabrication and application of suitable EAOPs treatment methods in combination with advanced analytical systems to monitor the degradation/ removal of ECs in aquatic environments.

The initial study involves proper assessment of the potential formation/ presence of low concentration ECs in complex mixed environmental water matrices using advanced analytical methods. This is then followed by the design, fabrication and development of various EAOPs approaches to monitor their removal from the complex mixed aquatic environments using integrated approaches of both EAOPs and advanced analytical methods.

Since the efficiency of EAOPs is determined by their ability to electro generate reactive oxygen species (H_2O_2 and $^{\bullet}OH$). Much of our study was dedicated towards designing and fabricating electrolytic reactor systems, catalyst synthesis, electrode functionalization using sol-gel method and their critical assessment for enhanced ECs degradation efficiencies.

1.4.1 Specific Objectives

i) To assess the potential formation of ECs and in particular selected beta-blocker and nitrosamines in complex mixed aquatic environments.

ii) To design, fabricate and develop suitable low-cost electrolytic systems to enhance the electrochemical oxidation of (i) using (iii) and (iv)

iii) Synthesis, characterization and evaluation of suitable heterogeneous catalysts for improving the electrogeneration of reactive oxygen species.

iv) Functionalization of suitable electrode using sol-gel method for enhanced electrogeneration of reactive oxygen species and improved degradation efficiencies via;

(a) Anodic Oxidation (b) Electro-Fenton and, (c) Photo-Electro-Fenton

v) Performing kinetic studies on degradation of **(i)** and suggesting plausible pathways/ mechanisms.

Continued improvement in analytical chemistry techniques to date, has allowed the continued detection and measurements of emerging contaminants (ECs) in various aquatic and terrestrial environments at very low concentrations.

When a parent organic pollutant enters an environmental matrix, it is more likely to undergo different processes such as dilution, absorption, adsorption, photolysis, biodegradation, hydrolysis, complexation, oxidation or volatilization [12]. The result, are the emerging contaminants in form of parent organic contaminants, their metabolites or even transformation products. The presence of ECs in the aquatic environment is as a result of the transformation, degradation and persistence of each compound resulting from abiotic degradation, bioconversions that occur during water treatment [20]. As a result, ECs are often found in various environmental water matrices at reduced concentrations (µg to ng L^{-1}). It has been demonstrated in recent studies that despite their relative trace level presence in the aquatic environments, they are of potential bionomic concern to wildlife and humans especially after a long-term exposure [13]. Moreover, they exist in mixed environmental complex matrices, it is more likely that the toxicity of one compound might synergistically be enhanced or antagonistically be eliminated by the presence of the other [14]. Most of these compounds are still unknown and yet the information about their potential interactive effects in mixed environmental matrices remains scanty up-to-date. It is therefore desirable to effectively remediate these ECs from the treated water before reuse. Traditional wastewater treatment methods (like secondary biodegradation) can hardly remove most of these ECs in their trace level concentrations. While advanced treatment technologies like reverse osmosis and activated carbon are sought to offer promising treatment alternatives, however, they compromise the water quality by concentrating and transforming pollutants between treatment levels. This in turn increases the treatment costs as additional treatment will be required to render the pollutants completely unreactive. Electrochemical advanced oxidation processes (EAOPs) represent better and promising alternatives to remove recalcitrant micro pollutants from complex aquatic environments through the use of in situ generated powerful and non-selective reaction oxygen species (H_2O_2, hydroxyl radical).

Also, EAOPs can be combined with traditional treatments thus decreasing the operation cost and creating a significant improvement in the effectiveness of the conventional treatment methods.

CHAPTER 2

LITERATURE REVIEW

2.1 Introduction

The presence of emerging contaminants in various aquatic environment and their connection with potential hazards have increasingly attracted scientific attention. This concern emanates from the widespread detection of trace level refractory organic pollutants in the environmental waters using advanced analytical techniques. A growing body of scientific research reported measuring ECs at parts-per-trillion to parts- per-billion concentrations in aquatic systems [21]. With such much lower concentrations of these microcontaminants than the conventional contaminants, they are so difficult to remove especially in the presence of organic and inorganic matrices that are reported to be thousand to a million fold more abundant [22]. Biological treatment of wastewater [23] is the most widely used technology for elimination of "readily degradable" organics pollutants including ECs present in polluted water. However, with refractory organic pollutants "resistant to biological degradation", other types of treatment must be utilized. Alternative technologies include adsorption, solvent extraction for recovery, oxidation for destruction, chemical oxidation and volatilization. For the past three decades, research efforts have been directed towards development of potent technologies for complete removal of persistent organic pollutants from wastewaters [24].

In particular, advanced oxidation processes (AOPs) based on the in-situ production of highly reactive hydroxyl radicals (•OH) capable degrading highly recalcitrant compounds have acquired high relevance [25].

Recent research and development have demonstrated the attractive potential of electrochemical methods to offer promising alternative routes for treating wastewaters free of toxic/ recalcitrant organics [26]. The major advantages are simplicity, ease of control, increased efficiency and the possibility of building compact bipolar electrochemical reactors. Treatment of organic compounds in water is facilitated by both reduction and oxidation routes. Organic pollutants are oxidized to carbon dioxide (Equation 1) and to biocompatible organics that can easily be treated by conventional biological processes or even into non-toxic compounds.

$$C_mH_n + 2m\ H_2O \rightarrow m\ CO_2 + (n+4m)\ H^+ + (n+4m)\ e^- \quad \ldots\ldots 1$$

Advanced Oxidation Processes using functionalized electrodes have also been utilized for wastewater treatment. Key Advanced Oxidation Processes (AOPs) include homogeneous and heterogeneous photocatalysis based on solar visible irradiation or near-UV, anodic Oxidation (AO), wet oxidation, ozonation, Fenton's reagent and ultrasound. Among AOPs, oxidation based on Fenton's reagent offers a simple, effective and attractive technology for the degradation of multiple organic pollutants utilizing non-toxic reagents and eventually leaves no residues [10]. This process is most effective at a pH of ≤ 3 [11]. The degradation mechanism of organic pollutants by Fenton process follows the reactions given in equations (2-5) below;

$Fe^{2+} + H_2O_2 \rightarrow Fe^{3+} + HO^- + HO\bullet$……2

R-H (Organic molecule) + $HO\bullet \rightarrow R\bullet + H_2O$……..3

$R\bullet + Fe^{3+} \rightarrow R^+ + Fe^{2+}$……..4

$Fe^{2+} + HO\bullet \rightarrow Fe^{3+} + HO^-$…… ….5

Electrochemical advanced oxidation processes (EAOPs) based on Fenton's reaction chemistry are eco-friendly methods that have recently received renewed interest for water pollution control and remediation [27].

Electro-Fenton processes have advantages over the conventional Fenton processes like better process control and continuous generation of H_2O_2 that is supplied to the contaminated solution by equation 6 below.

$O_2 + 2H^+ + 2e^- \rightarrow H_2O_2$…… 6

The efficiency of electrochemical treatment processes as well as the potential formation of toxic by-products depends mainly on the judicious choice of the electrode material (the adsorptive properties of the electrode surface and O_2 overpotential) [15].

2.2 Parent compounds, transformation products and associated risks

Chemical substances can undergo different structural changes and be biotransformed in the environment by microorganisms or undergo structural change in human's body or even during an effluent treatment. Thus, the active molecules of ECs (ie parent structure of pharmaceutical active compound) undergoes several processes such as biodegradation, biotransformation, hydrolysis et cetera, resulting into several physico-chemical changes and with different pharmaceutical properties. Inside an animals/ human bodies, the PACs undergoes metabolic transformations via reductive, oxidative and hydrolytic pathways leading to various transformation products with different functional groups, hydrophobicity's and hydrophilicities, relative to unconjugated parent compound/metabolite. These compounds end up in various aquatic environments as ECs and are persistent to removal by conventional wastewater treatment technologies.

In most research studies related to the removal of ECs in aquatic environments, effective degradation/ removal efficiencies are determined by parent compound disappearance, and little attention is dedicated towards the monitoring and identification of transformation products during treatment.

Another challenge is the possibility of varied and mixed toxicities by mixed transformation products, parent and metabolites that are likely to exhibit synergistic toxic effects on the host organisms than a single compound. These compounds are present in aquatic environments at very low concentrations, however, even in their trace level concentrations, most of them exhibit potential prejudicial effects towards normal aquatic life development. Surprisingly, many of the ECs and metabolites have not been identified to date and hence it is challenging to assess collective and individual toxicities of metabolites and their parent compounds. Increased toxicities resulting from synergetic effect of mixed pharmaceutical contamination are asserted to change the physiology of host organism and lead to development of parasite-resistant strains [28]. Hence, it is warranting to monitor degradation efficiencies of individual parent organics with their transformation products as baseline for prioritizing which metabolites to consider during risk assessment, pollutant regulation and control. Consequently, the identification and toxicity evaluation of transformation products formed during water treatment processes and biodegradation of ECs has to be seriously taken into account.

2.3 Selected emerging contaminants for this study

2.3.1 Pharmaceutical (ß-blockers)

The recent advancement in sensitive, reliable and cost-effective analytical systems has led to the discovery and trace level detection of pharmaceuticals in river water [29], wastewater treatment plant effluents [30], ground water [31], as well as drinking water [32]. A lot more studies investigating the world wide occurrence of pharmaceuticals in aquatic environments are reported in literature [33].

Out of the many pharmaceutical compounds reported so far, a lot of strength is put on beta-blockers due to their inefficient removal by conventional water treatment processes, poor degradability and their intensive use for the treatment of various cardiovascular disorders, anxiety, hypertension, angina, glaucoma, and migraine [34]. β-blockers were detected cosmically in wastewater influents and with more in wastewater effluents to the tune of ng−μg L^{-1}, due to their partial elimination by traditional biological wastewater treatment methods [35]. They were found to affect heart rate of some invertebrates, vertebrates and also interfere with photosynthetic efficiency in aquatic plants (green algae) [7]. Hence, investigation of the environmental fate of β-blockers in the aquatic environments is highly desirable.

2.3.2 Disinfection Byproducts-Nitrosamines

Before water is declared safe for drinking, it undergoes disinfection as the last process to kill pathogens. However, during the disinfection process, the water quality is highly compromised by the generation of disinfection by-products (DBPs) originating from the reaction of disinfectants with anthropogenic contaminants, natural organic matter, iodides and bromides [36]. Apart from the

regulated DBPs (like haloacetic acids, bromate, chlorites and trihalomethanes), a lot more of the unregulated DBPs have been ascertained [37]. Nitrosoamines represent a class of novel DBPs that are potentially teratogenic, mutagenic and carcinogenic [38].

They have been classified as important environmental pollutants due to their typically low concentrations (nanogram per kilogram and nanogram per liter range) and ubiquitous presence in many environmental matrices [39]. These hydrophilic family of compounds are characterized by a nitroso group bonded to an amine with at least 300 previously documented congeners [40].

2.4 Management and removal of selected ECs in water treatment systems

With cognizance and evidence of ECs presence in aquatic environments, it is precautionary right to device mechanisms aiming at mitigating their release into the aquatic environment. Of all available options, incorporation of advanced wastewater treatment technologies in the conventional water treatment approaches offers cheap and most effective pollutant management strategies.

The advanced treatment technologies should be capable of completely removing ECs in wastewater during treatment.

2.4.1 Traditional water treatment methods and their challenges

The inadequacy of microorganisms in conventional treatment plants to completely remove persistent organic compounds during water treatment have resulted in detection of trace level ß-blockers in various aquatic environments in concentration ranges of ng/L to µ g/L [41].

A wastewater treatment plant constitutes a physicochemical treatment and bioreactor sections representing a primary and secondary system respectively.

All these systems are ineffective at removing recalcitrant organics and hence a lot more of these compounds remain in effluents and end up in ground and surface water and even drinking water. Tertiary water treatments involve biological systems, chemical precipitation, ion exchange, adsorption (on activated carbon), distillation for volatile organic compounds and advanced oxidation processes to remove toxic biorefactory organic compounds.

2.4.2 Advanced oxidation processes (AOPs)

Over the last three decades, AOPs have gained significant level of interest in both academics and industry for effective treatment of tertiary wastewater and drinking water free of refractory organic pollutants. They are characterized by the generation of highly reactive and non-selective reactive oxygen species (ROS) radicals ($OH^{\bullet}$, $O_2^{\bullet}$, $HO_2^{\bullet}$) which are strongly oxidizing in an aqueous medium. These ROS and most especially hydroxyl radicals ($^{\bullet}OH$) are potentially capable of oxidizing nearly all organic compounds to mineralization (water, carbon dioxide, and mineral salts) [25]. Some of the most important AOPs include homogeneous and heterogeneous photocatalysis based on solar visible radiation or near ultraviolet (UV), ozonation, the Fenton's reagent, electrolysis, wet air oxidation and ultrasound while less traditional but developing processes include ferrate agent method, ionizing radiation, pulsed plasma and microwaves. AOPs can be utilized alone or in combination with other biological or physicochemical methods basing on the properties of the waste stream to be treated. The stage is aimed at initially converting biorecalcitrant compounds in the pre-treatment stage to more readily biodegradable intermediates followed by biological post-treatment.

The treatment efficiencies of AOPs are generally assessed basing on their capability to completely destroy specific ECs in question though total mineralization which is at times not possible.

In AOPs scenarios where the degradation by-products/ transformation products are less toxic and more biodegradable than the parent substrate, a biological post-treatment may not be feasible [42]. The Fig. 1 below summarizes the AOPs used in water treatment.

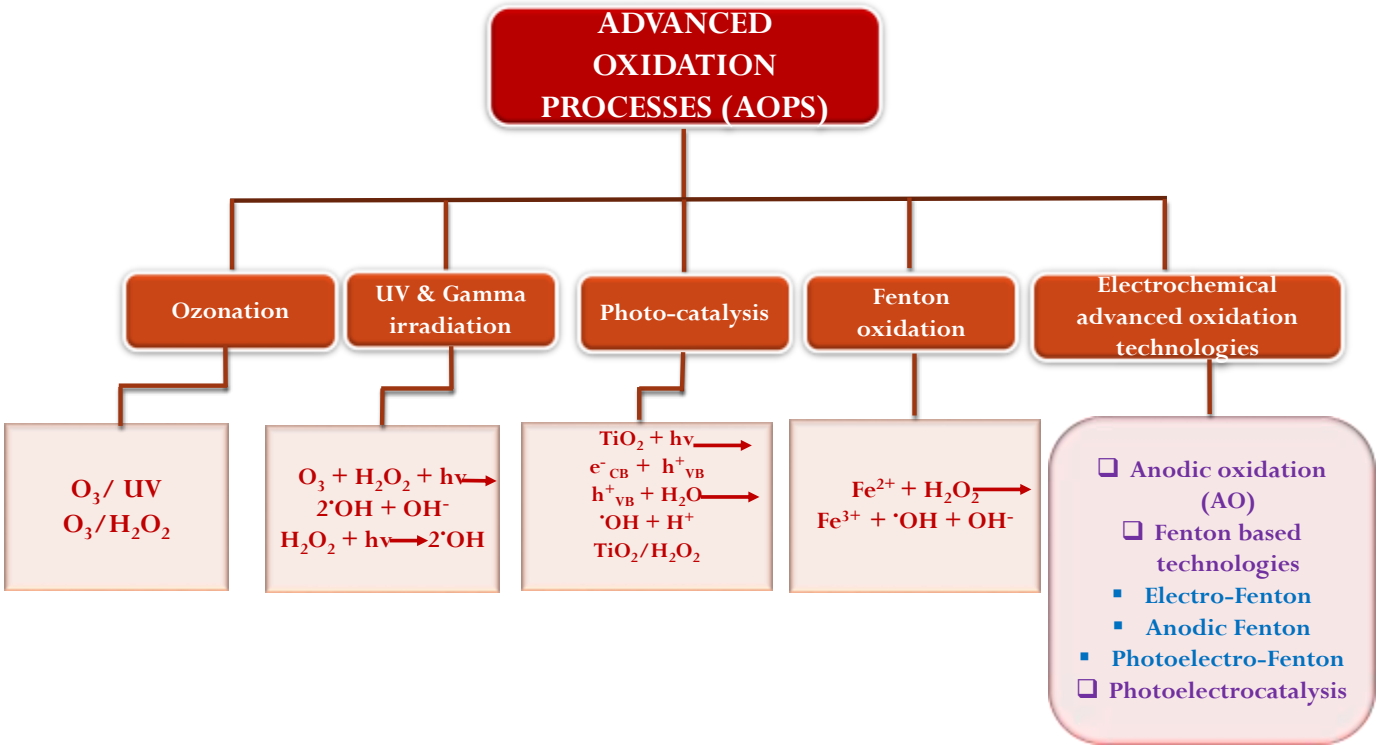

Figure 1: Main AOPs technologies involved in water treatment

2.5 Electrochemical advanced oxidation technologies (EAOPs)

Apart from the capability of EAOPs to completely remediate persistent organic pollutants, they also exhibit numerous key characteristics of environmental significance such as: (i) compact electrolytic reactors of smaller physical footprint that require lesser space requirement, (ii) mild operation conditions under ambient pressure and temperature (iii) no additional chemicals requirements, hence the storage and transportation of these chemicals are not essential, (iv) they can easily be incorporated in to conventional water treatment technologies for enhanced treatment efficiencies, (v) no secondary waste stream production and thus further treatment is not required (vi) allows full automatization and (vii) exhibit manageable operational costs. EAOPs include anodic oxidation (AO), anodic Fenton (AO-H_2O_2), electro-Fenton (EF), photo electro-Fenton (PEF) and solar electro-Fenton (SPEF) processes. Figure 2 reviews the main reaction that take place during EAOPs.

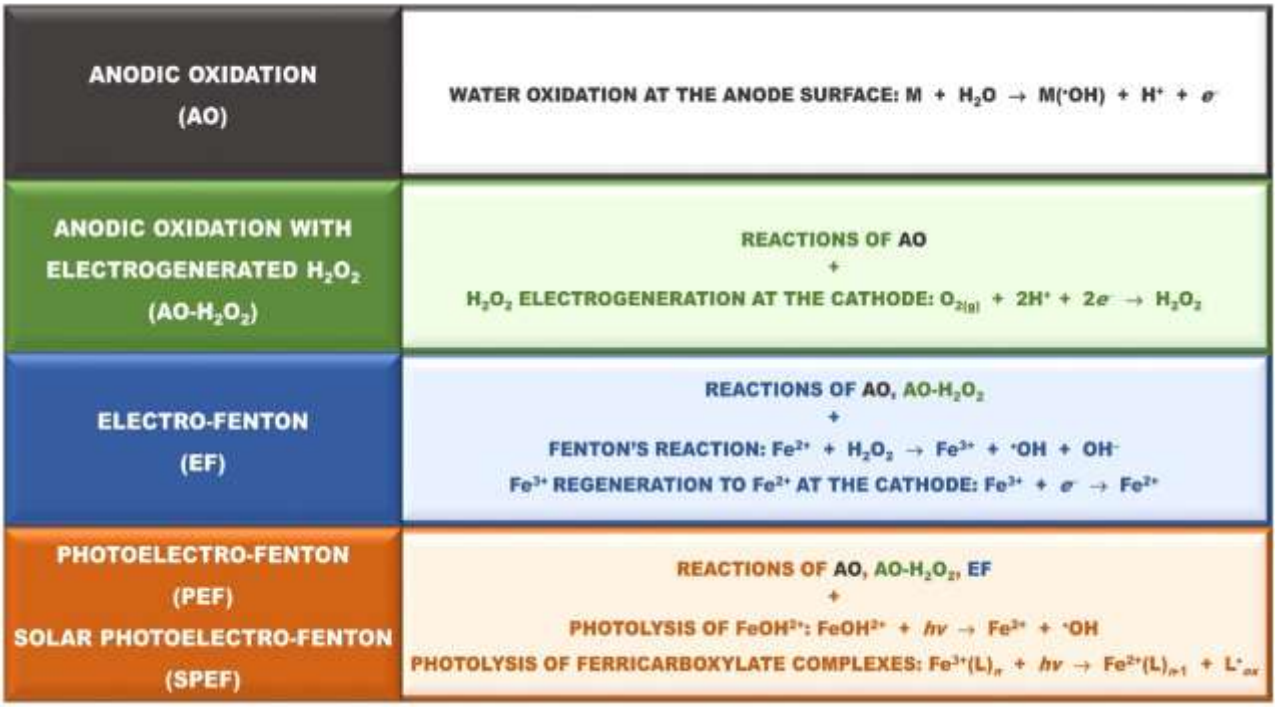

Figure 2: EAOPs technologies with their reactions involved in water treatment.

2.5.1 Anodic oxidation (AO) or electrochemical oxidation (EO)

AO is the most studied EAOPs since it is highly scalable and versatile [24]. The efficiency of AO in removing organic pollutants depends on its possibility of achieving partial degradation or complete mineralization. Hence the electrocatalytic properties of anodic materials selected and utilized, play a key role in the organic removal efficiency during AO operations. Hence, the oxidation of organic pollutants in an AO electrolytic reactor assumes two different pathways; namely (i) direct anodic oxidation, and (ii) indirect oxidation as shown in Fig.3 [43].

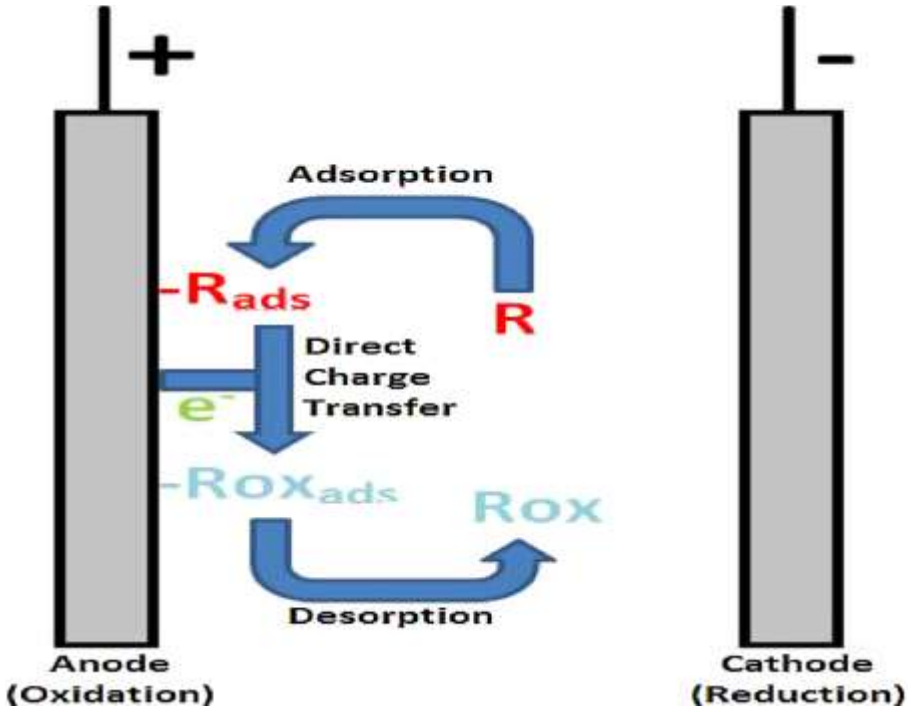

Figure 3: Scheme of direct electrolysis process in anodic oxidation.

Pollutant oxidation by anodic oxidation (AO) involves: (i) direct electron transfer to the anode surface M, (ii) production of heterogeneous reactive oxygen species (ROS) (M(•OH), H_2O_2, O_3) (equation 7-9) as a result of intermediates formed from water oxidation to oxygen, (iii) other weaker oxidant agents electrochemically produced from ions existing in the bulk [44]. Moreover the degradation efficiency by AO, entirely depends on the effective mass transfer of pollutant molecules from the bulk to the anode electrode surfaces [44]. Simultaneous oxidation of water and pollutants is achieved by application of high cell voltages while maintaining the anode activities. Hence type of anode material determines the anodic oxidation efficiency. And as such, anode materials for this process have been classified into "active", such as RuO_2, IrO_2 and Pt, and "non-active", like boron-doped diamond (BDD), PbO_2 and SnO_2 anodes as shown in Table 1.

$$M + H_2O \rightarrow M(\bullet OH) + H^+ + e^- \quad \ldots\ldots 7$$

$$2M(\bullet OH) \rightarrow 2MO + H_2O_2 \quad \ldots\ldots 8$$

$$3H_2O \rightarrow O_3 + 6H^+ + 6e^- \quad \ldots\ldots 9$$

To generate greater amounts of M(•OH) and avoid parasitic reactions, anodes with high overpotential for oxygen evolution reactions (OER) should be used to promote reaction (1) [45]. As a rule of thumb, the higher the potential for OER of the anode material, the weaker is the interaction of M(•OH) with the anode surface and the higher is the chemical reactivity toward organics oxidation [46]. According to anode classification Table 1, BDD anode is presented as most powerful "non-active" with high potential for oxygen evolution reaction and hence most suitable anode material for mineralization of persistent organic compounds in aquatic environments. The details for the mode of operation of anodic oxidation are well reported in reference [43].

When an electrochemical oxidation process (AO) is conducted alongside cathodic H_2O_2 electrogeneration, the process is referred to as anodic oxidation with H_2O_2 electrogeneration (AO-H_2O_2) [47]. The current efficiency and degradation rate of AO and AO-H_2O_2 processes are based on operational parameters such as sample pH, stirring rate, temperature, current density and substrate concentration, and all these parameters must be optimized to achieve best operations.

Table 1: Classification of anode materials based upon oxygen evolution potential

Anode material	Class	Oxygen evolution potential
RuO_2	1	1.47
IrO_2	1	1.52
Pt	1	1.60
Graphite	1	1.70
SnO_2	2	1.90
PbO	2	1.90
Boron Doped Diamond (BDD)	2	2.30

2.5.2 Electro-Fenton (EF) and photoelectro-Fenton (PEF)

To minimize the diffusion limitations typical of electrochemical oxidation processes, a simple Fenton reaction technology based on the heterogeneous generation of •OH radicals in the bulk solution was advanced for oxidation of organic pollutants. The traditional Fenton's reagent constitute both H_2O_2 and Fe^{2+}, discovered by Fenton that leads to the generation of the highly oxidizing •OH by the so-called Fenton's reaction under acidic conditions (equation 10) [27].

$Fe^{2+} + H_2O_2 \rightarrow Fe^{3+} + {}^{\bullet}OH + OH^{-}$……...10

However, its oxidation efficiency is highly constrained by numerous parasitic reactions involved during treatment. The key wasting reaction that consume both reagents and the generated •OH radicals are represented by equations 11 and 12.

$H_2O_2 + {\bullet}OH \rightarrow H_2O + HO_2^{\bullet}$……...11

$Fe^{2+} + {\bullet}OH \rightarrow Fe^{3+} + OH^{-}$……...12

The efficient operation of the classical Fenton process is limited by these major drawbacks;

(i) the risks and costs related to transportation, storage and application of H_2O_2,

(ii) the formation of iron sludge resulting from the use of high amounts of iron that must be removed after the treatment.

(iii) the requirement for restricted acidic pH (2.8-3.0), that requires subsequent neutralization at the end of the treatment

To overcome these limitations and improve removal efficiencies of organic pollutants, an electro-Fenton processes were developed [27,45].

EF is the most known and popular EAOP based on Fenton chemistry that lead to generation of reactive oxygen species responsible for oxidation of organic pollutants [27]. The acceptable mechanism constitutes;

(i) the in situ and continuous electrogeneration of H_2O_2 at a suitable cathode fed with pure oxygen or air (equation 13),

(ii) the addition of Fe^{2+} catalyst to the solution, and

(iii) the cathodic reduction of Fe^{3+} to Fe^{2+} (equation 14) with consequent continuous production of Fenton's reagent.

These processes lead to the catalytic decomposition of hydrogen peroxide into hydroxyl radical [27,45]. Basing on the catalytic activity of Fe^{3+}/Fe^{2+} couple, the effective operations of EF processes require optimal pH range of 2.8-3.0.

$Fe^{2+} + H_2O_2 + H+ \rightarrow Fe^{3+} + \bullet OH + H_2O$…….….13

$O_2\,(g) + 2H^+ + 2e^- \rightarrow H_2O_2$……...14

$Fe^{3+} + e^- \rightarrow Fe^{2+}$…….15

The EF process is usually conducted in an electrolytic reactor system fabricated to suit an undivided cell configuration or divided cell configuration system. For all EF application conducted in undivided reactor systems, the EF process is synergistically enhanced by additional ROS produced at the anode, mainly in form of M(•OH). Hence, the utilization of BDD anode electrodes significantly enhances the EF oxidation efficiency as shown in Figure 4.

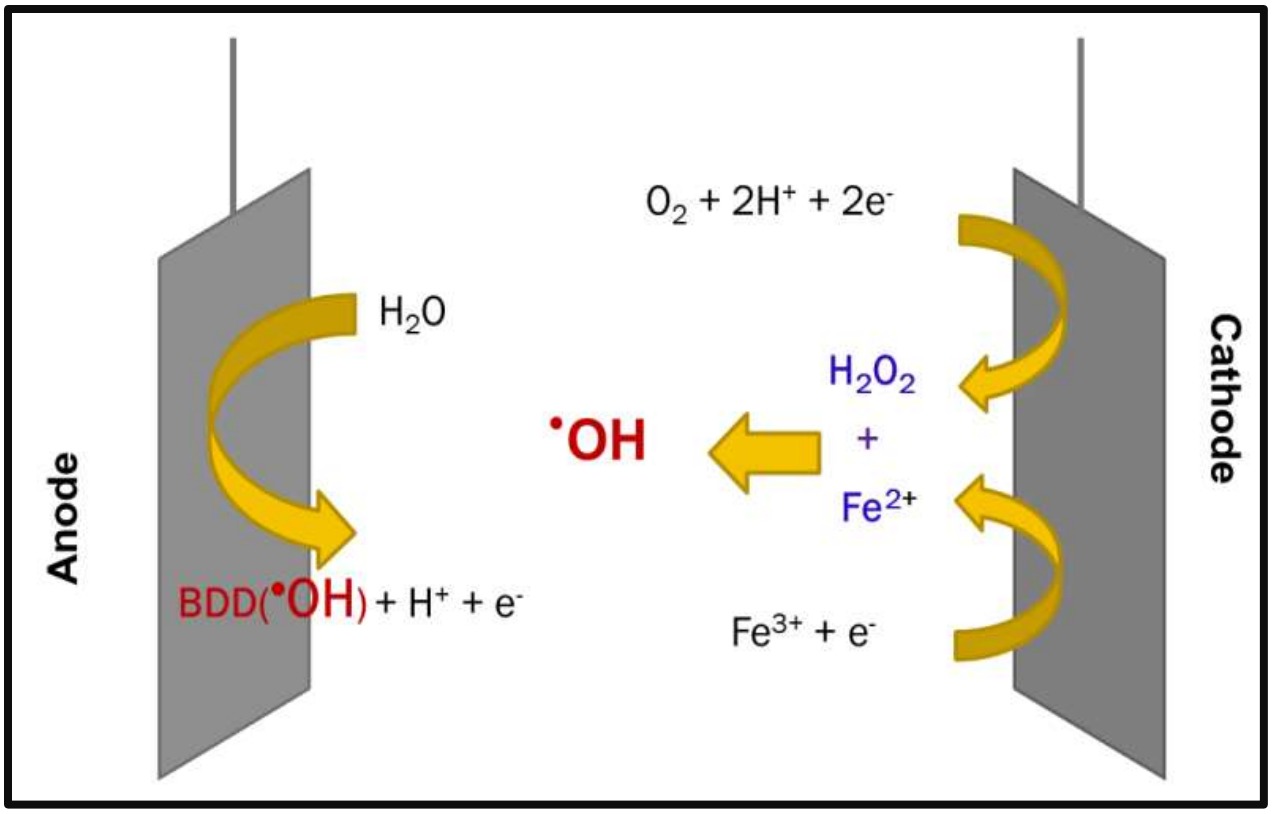

Figure 4: Generation of •OH during EF process using a BDD anode.

The photoelectron-Fenton (PEF) is a photo-assisted EF process that utilizes either solar/ visible light or ultra-violet (UVA and UVC) to photo-excite formed Fe^{2+} complexes during Fenton's reaction (Eq. (17) to produce both Fe^{2+} and hydroxyl radicals (Equation 18) hence helps to increase the degradation efficiency of the process through enhanced •OH regeneration. As a result, the photo-regenerated Fe^{2+} ion can thereafter catalyze the Fenton's reaction, forming more Fe^{3+}.

$Fe^{3+} + H_2O \rightarrow Fe\ (OH)^{2+} + H^+$ …….16

$Fe(OH)^{2+} + hv \rightarrow Fe^{2+} + \bullet OH$……17

$Fe(OOCR)^{3+} + hv \rightarrow Fe^{2+} + CO_2 + R^{\bullet}$……..18

CHAPTER 3

Development of a Liquid Chromatography Tandem Mass Spectrometry Method for Monitoring Trace-Level Beta Blockers in Complex Environmental Water Matrices

3.1 INTRODUCTION

The recent trend in environmental analysis is geared towards new approaches that simplify sample preparation procedures and make them green, cheaper, safer, faster and easier so as to generate precise results with low detection limits [48]. For the past few decades, there have been a multiplex increase in the effect of environmental chemical contamination due to worldwide use of pharmaceutically active compounds [49]. Among these compounds, the global presence of beta blockers (ß-blockers) as emerging contaminants in aquatic environments have aroused scientific interest in regard to their ambiguity in the environment and their adverse effects on non-target organisms (aquatic fauna and flora); even at trace level concentrations [3,4]. ß-blockers are commonly used drugs by clinician to treat myocardial infarctions [52]. They act by relaxing muscles thus directly slowing down the heart rate and as such, they have been abused by athletes that require high levels of mental endurance. Hence, have now been forbidden by the World Anti-Doping Agency [53].

Research has highlighted the ecotoxicity and undesirable effects associated with mixed ß-blockers on organisms even at low concentrations [54]. Hospitals are considered as an incontestable hot spot

and point source for some ß-blockers contamination [8-10]. Hospital wastewater (HWW) represents a complex matrix composed of contagious excretions, microorganisms, detergents, disinfectants, biological fluids, heavy metals and pharmaceutical compounds [56]. Owing to the poor degradability of ß-blockers, they escape treatment and end up in both surface and drinking water [55]. To date, there are many opportunities for screening various ultra-trace level analytes in complex matrices with highly sensitive and selective analytical instruments, but however, all require valid sample preparation protocols [57].

Sample preparation is aimed at elimination of sample interference effects, increasing the method's selectivity factor and thus leads to improved analyte enrichment [58].

In particular, the ability of liquid chromatography methods to avoid extra derivatization steps have been explored for sensitive environmental analysis of trace ß-blockers. However, their sensitivities are greatly compromised by matrix effects and hence require clean extracts [49]. In an effort to enhance sample throughput, recent research trend has focused on miniaturization and automation [59].

As such, numerous miniaturized extraction techniques have been reported for trace level determination of ß-blockers in aqueous matrices and these include dispersive micro-solid phase extraction [15,16], microextraction by packed sorbent [17,18], electrically enhanced microextraction [61], microwave assisted-solid phase extraction [62], stir bar sportive extraction [63], hollow fibre-protected liquid-phase microextraction [64] and electromembrane coupled with solid phase microextraction [65].

Micro-solid phase extraction (μ-SPE) method is miniaturized preparation technique that is applicable to different complex matrices analysis such as bio-analysis, wastewater, food analysis, and sewage sludge [17, 24]. The efficiency of the μ-SPE method depends on the wise choice of a sorbent [67].

Nano-composite sorbents offer unique and novel extraction phase qualities through their high functionalities that enhance numerous interactions of target analytes via electrostatic interactions [68]. Recently, silica-based mesoporous materials (MCM-14 and UVM-7) have widely been investigated as effective sorbents in trace preconcentration studies [69], however, their synthesis involve expensive and environmentally unappealing approach. Hydrolytic sol-gel modification of biogenic raw materials with metals offers tremendous opportunities in the design and fabrication of inexpensive and selective sorbents for adsorptive removal of organic pollutant [25, 28, 29].

Rice husk ash (RHA) is a cheap source of amorphous silica composite that provides sufficient support/surface area and naturally endowed functionalities for dispersion of any metal [70–72].

Additionally, RHA offers an excellent source of mesoporous silica (rice husk silica, RHS), hydroxyl-group-rich surface for anchoring metals, improving chemical stability and enhancing remarkable textural characteristics during synthesis of sorbents [30, 31]. Iron functionalized green nanosilica composite materials show great promise in adsorption of low-level pollutants in environmental waters. It is asserted that, the selectivity and improved extraction efficiency of iron supported RHS sorbents is enhanced by iron oxide [72–74].

Most practical research reports involving μ-SPE optimization rely on systematic study of one-factor-at-a-time in which all the factors are kept constant save the one being studied [15, 25, 32]. Such univariate approaches generate incomplete conclusions due to their failure to determine accurately, the interaction between variables [75].

Multivariate techniques based on design of experiments (DOE) are fast and efficient optimization approach. This is because they can potentially reduce the number of experimental runs, allow simultaneous optimization, and explain correctly the interaction effects [26, 34].

Out of these multivariate optimization techniques, FFD and CCD approaches, are more efficient towards judicious selection and optimization of the most significant parameters [76]. Usually, a desirability/ derringer function (DF) within CCD model is employed as a multi-criteria strategy to establish more accurately the numerical optimized values [77]. The aim of this study is to investigate the synergistic contribution of biogenic silica nanocomposite nanosorbent based µ-SPE technique with chemometric optimization of trace level ß-blockers in hospital wastewater. Fractional factorial design was used to screen the most significant parameters while central composite design with a desirability function was used as a multi response optimization strategy to achieve the best optimized experimental variables.

3.2 EXPERIMENTAL

3.2.1 Materials

All chemicals and reagents used in this experiment were of better analytical grade unless otherwise stated. All standards had a purity grade of more than 97%, adequate to LC-MS/MS analyses. Ferric nitrate, $Fe(NO_3)_3 \cdot 9H_2O$ (98.5%) was used as the iron precursor, sodium hydroxide, nitric acid, sulfuric acid, hydrochloric acid, sodium chloride, glycerol, acetone and cetyltrimethylammonium bromide (CTAB) were purchased from Sigma-Aldrich (St. Louis, USA).

Formic acid, methanol, and acetonitrile (LCMS grade) were secured from Fisher Scientific (Schwerte, Germany). Alprenolol hydrochloride-(ALP), (≥95%) atenolol (ATE), (99%), acebutolol hydrochloride (ACE) (≥98%), propranolol hydrochloride (PROP) (≥99%) and Pindolol (TLC powder, PIN) (≥98%), were purchased from Sigma-Aldrich (Deisenhofen, Germany) and used as received. Accurel (Q3/2, R/P) polypropylene sheet membranes (0.2-µm pore size, 157-µm thickness) were purchased from Membrana (Wuppertal, Germany). Rice husk was secured from a rice mill (Kerala, India) was used as biogenic silica precursor. Commercial sorbents: activated carbon, C_{18}, Porapak, Silica, C_{18}-porasil, Polysep- 4% divinybenzene and Polysep- 12% divinybenzene, were bought from Alltech (Deerfield, IL) and used without modification for µ-SPE comparison study. Plastic crimper vials, 0.2-mL (Landgraaf, The Netherlands) were used during ultrasonication. Ultrapure water obtained from Milli-Q system (Milford, MA, USA) was used throughout the experiments. Polyether sulfone syringe filters (pore size, 0.2 µm) were obtained from Sigma Aldrich. ß-blockers standard stock solutions (1000 mg L^{-1}) were each prepared in methanol while mixed drug working solutions were prepared weekly by appropriate dilutions of a series of low concentrations of standard solutions in MilliQ water. They were then stored at a temperature of 4^{o}C and were always brought to ambient temperature before use.

3.2.2 Instrumentation

All experiments were performed using a Shimadzu Nexera ultra high-performance liquid chromatograph coupled to a Triple Quadrupole Mass Spectrometer LCMS-8050 (Shimadzu). For data handling and quantification, Labsolutions (Shimadzu Corporation) was used. The liquid chromatography (LC) instrument included two pumps, Shimadzu (Kyoto, Japan), an auto sampler,

CTC-Pal (Analytics AG, Zwingen, Switzerland) and a 50 µL sample loop. Chromatographic separation of the analytes was carried out on an Ultra IBD column (100 x 2.1mm x 3µm particle size; Restek, Bellefonte, PA, USA). The injection volume was 10 µL. Gradient elution with solvent A (0.03% formic acid) and solvent B (methanol /acetonitrile, 25:75) at a flow rate of 0.3 mL/min was applied. The starting gradient was 10.0 % of mobile phase B with a hold of 0.5 min and then increased to 25 % at 3.0 min, then to 30 % at 3.5 min at a hold time of 0.5 min. From there, it was increased to 90 % for another 0.5 min then again to 10 % in another 0.5 min and 0.5 min was used for column equilibration and stability. The total run time was 6 min. The column oven temperature was set at 40 ◦C and the CTC-Pal tray temperature was set at 12 ◦C. Nitrogen was used as both drying and nebulizing gas and argon was used as collision gas. A neat ß-blockers mixed standard was directly infused in to the ion source to establish the precursor to product transitions for the target analyte.

Electrospray LC–MS/MS technique in multiple reaction monitoring (MRM) in positive ionization mode was used in quantification of the analytes. To achieve the best signals, the sensitivity of each individual compound was optimized by adjusting the values of collision energy (CE) entrance potential (EP), collision exit potential (CXP) and declustering potential (DP).

The optimized compound-dependent retention times, MRM transitions and MS-settings for the extraction of selected ß-blockers are summarized in Table I. The Brunauer-Emmett-Teller (BET) surface area, pore volume, and size, of the nanosorbent were measured on micromeritics and porosimetry analyzer (Micromeritics, ASAP2020, and USA) using liquid N_2 adsorption-desorption at −196 C by BET and Barrett-Joyner-Halenda methods. A field emission scanning electron microscope, (FESEM) (Tescan Lyla 3, USA) and energy-dispersive X-ray (EDX) (Tescan Lyla 3, USA) were used for identification of the surface morphology and elemental composition of the prepared nanosorbent.

Fourier Transform Infrared Spectroscopy (FT-IR spectra were recorded on Nicolet 6700 spectrometer (Thermo Electron, USA) equipped with a Deuterated triglycine sulfate detector, accumulating 64 scans at a spectral resolution of 2 cm^{-1} and using KBr method.

Table 2: Optimized target compound-dependent parameters for ß-blockers extraction

Compound	RT (min)	DP (V)	CXP (V)	EP (V)	$[M+H]^+$ (Da)	MRM-1 (Da)	MRM-2 (Da)	CE (V)
ATE	0.917	25	18	10	267	145.1	56	20
ALP	1.197	20	18	10	250	116.1	56	18
PIN	3.971	25	19	10	249	116.3	172.05	19
ACE	3.317	20	20	10	337	116.2	319.35	22
PROP	4.272	22	19	10	260	116	183.25	21

3.2.3 Collection of wastewater samples

Hospital wastewater was collected from King Fahd University of Petroleum and Minerals medical center. Samples were collected in grey glass bottles pre-rinsed with acetone, transported under cool conditions and refrigerated in the laboratory at 4 ^{o}C where they were analyzed without any further pretreatment.

3.2.4 Synthesis of nanosorbent by hydrolytic sol-gel method

40 g of milled rice husk was boiled (80 ^{O}C) for 3 h in 400 mL of 0.76 N H_2SO_4 under constant stirring followed by acid decantation. The solid residues were washed thoroughly with deionized water till neutral pH and then oven dried at110 ^{0}C. Subsequently, the dry residues were calcined in a muffle furnace at 700 ^{0}C for 8 h to obtain 15 % of the original material weight as RHA. RHA was mixed with 500 mL of 1M NaOH, stirred vigorously for 17 h to yield sodium silicate solution. The CTAB and glycerol (each 2 wt. %) dissolved in water/ethanol (1:1) solvent was added to sodium silicate solution and the mixture stirred at 60 ^{o}C till dissolution. Both CTAB and glycerol act as structure directing agents. Glycerol also acts as a capping agent ensuring stable nano-sized sorbent particles at high calcination temperature and enhances the increment of functional moieties on the RHS sol for anchoring loaded metals [78]. The resultant sodium silicate solution was then titrated slowly with 3.0 M HNO_3 or 3.0 M HNO_3 containing the appropriate mass of $Fe(NO_3)_3 \cdot 9H_2O$ (5, 15 and 20 (wt. %) of Fe) until pH 4.0.

The resulting solution (gel) was aged at room temperature for 48 h. The gel was recovered by centrifugation (Eppendorf centrifuge 5430, Hamburg, German) at 4000 rpm, washed thoroughly with distilled water and dried in an oven at 110 ^{0}C for 18 h. The nanosorbents were finally calcined for 5 h and at 700 ^{o}C to remove CTAB. The products (solids) obtained were ground and labeled as rice husk silica composite (RHS-0% Fe) or iron loaded rice husk silica composite (RHS-xFe, where x=0, 5, 15 and 20 (wt % of Fe). Zero signified no iron loading. These were then collected and stored in desiccators before further characterization and application as nanosorbents for µ-solid phase extraction of ß-blockers. Fig. 5 shows the schematic diagram for the hydrolytic sol-gel synthesis of biogenic silica composite sorbents (RHS-x%Fe).

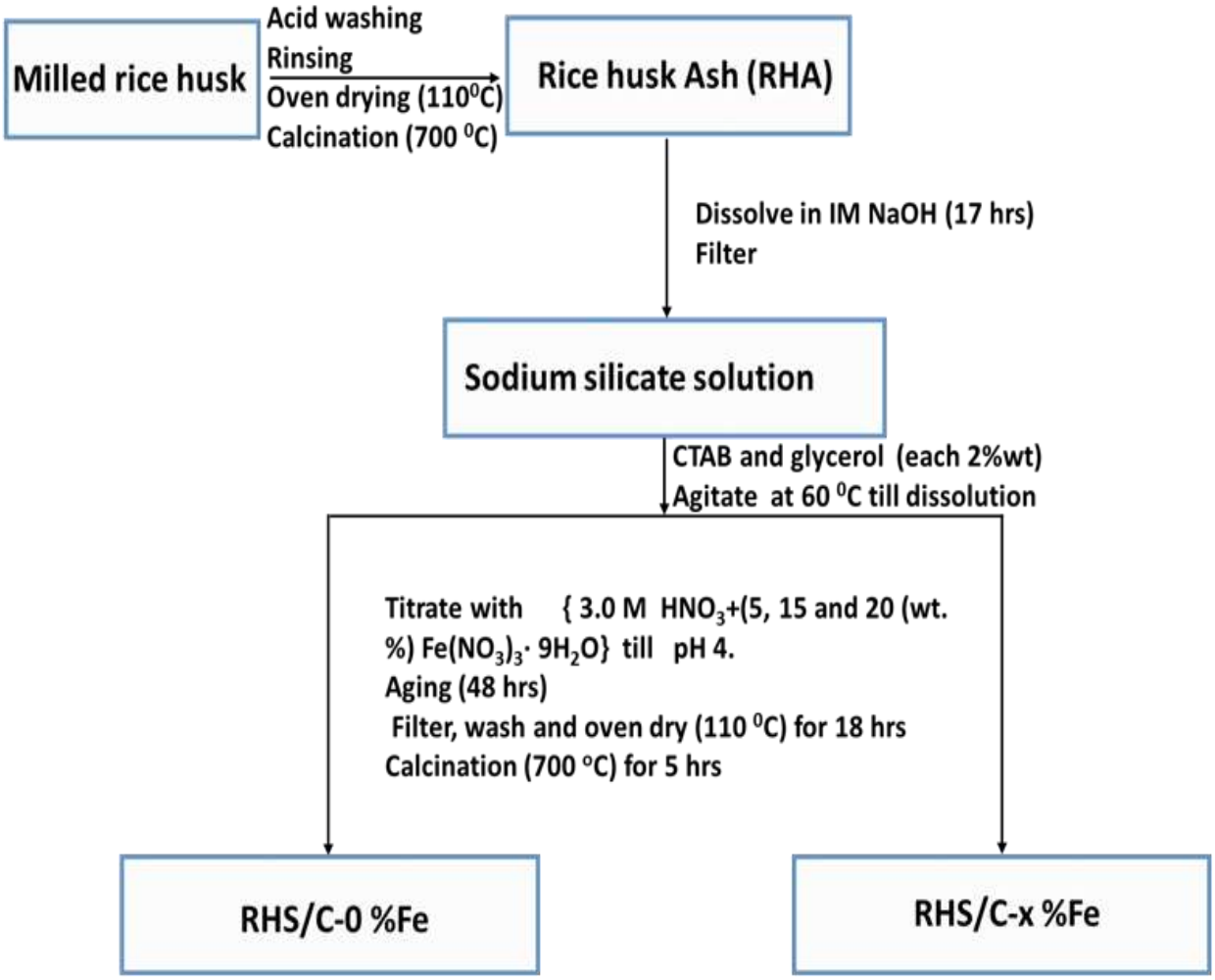

Figure 5: Schematic diagram for hydrolytic sol-gel synthesis of nanosorbents

3.2.5 µ-SPE fabrication and extraction procedure

The extraction procedure involved fabrication and packaging of the sorbent/ synthesized nanosorbents in to micro-solid phase extraction units followed by two successive steps, in which the target analytes were first extracted from the aqueous medium to the solid surface followed by desorption to the organic medium compatible with the LC-MS/MS instrument. Preparation of µ-SPE device is described earlier [67], briefly, the device is prepared by folding over a longer edge of a porous polypropylene membrane to a width of ~0.5 cm followed by heat sealing using an electrical sealer. The sealed section is then cut off from the membrane sheet. At this stage, a single envelope piece with dimensions (~ 0.5 cm x 1.0 cm) is cut out and one of the two open ends heat-sealed. A pre-weighed mass (35 mg) of the sorbent is then directed into a prepared membrane envelope through the remaining open end. The membrane envelope is heat-sealed to secure the sorbent material. Before, extraction, each µ-SPE device was conditioned in methanol and acetone for 10 min by ultrasonication and air dried before use. A µ-SPE device was then placed in 5 mL of a sample solution in an extraction glass bottle and the sample solution stirred at ~110 rad/s (1000 rpm; 1 rpm = 0.1047 rad/s) for 30 min. During extraction, the µ-SPE unit purled freely within the sample solution. After extraction, the device was removed from the sample solution using tweezers, and placed in a plastic crimper vial for analyte desorption. Using a suitable desorption solvent (300 µl) and for 20 min ultrasonication time, the analytes were desorbed from the µ-SPE device and later injected (3 µl) into the LC–MS/MS for analysis. The µ-SPE device was re-used after pre-cleaning with methanol and acetone.

3.2.6 Experimental design

To ensure technological feasibility of µ-SPE-LC-MS/MS extraction of ß-blockers in HWW, statistical experimental design was employed to offer a refined approach to accurately evaluate the influence of different operational parameters and their interactions with target analytes [73]. With this design, a second-degree polynomial model is fitted, that results into reduced experimental runs making the process cost effective. The second order polynomial model is represented by the equation 1;

$$Y = \beta_O + \sum_{i=A}^{E} \beta_i X_i + \sum_{i=A}^{E} \sum_{j=A \neq i}^{E} \beta_{ij} X_i X_j + \varepsilon \quad \ldots\ldots\ldots\ldots\ldots\ldots\ldots\ldots 1$$

Y is the predicted enrichment factor (%), $\boldsymbol{X_i}$ are the uncoded or coded values of the extraction variables, $\boldsymbol{\beta_i}$ are the main effect coefficients for each extraction variable, $\boldsymbol{\beta_O}$ is a constant, $\boldsymbol{\beta_{ij}}$ are the interaction effect coefficients, and $\boldsymbol{\varepsilon}$ represents the lack of fit. Minitab software (Minitab Inc., State College, PA, USA) was used in the construction of experimental designs (FFD and CCD), modeling of the data and in regression analysis. All the experiments were performed in triplicate with the mean values presented. An analysis of variance (ANOVA) was used in model evaluation. Fisher's test (F) and the coefficient of determination (R^2) values were used to statistically evaluate the significance, quality and adequacy of the polynomial model equation while the significance of the regression coefficients was tested using the Student's t-test. Three-dimensional response surface plots were utilized in graphical interpretation of interaction effects between optimized variables.

These optimum operating conditions are further validated using derringer/ desirability function (DF). DF value ensures that the values of the optimized factors satisfy the targeted response output. With DF, best optimized conditions for several responses are attained using a multiple response optimization approach [79]. Hence, simultaneous optimization of various responses maximizes the DF to a desirable value (0 to 1) [76]. It is important to note that attaining a desirability value equal to 1 is not the sole target for optimization procedure but to obtain a proper set of conditions that will constitute all the determined criteria [80]. A desired goal for each factor (ie within range, minimize, maximize, none and target) together with their respective lower and upper limits were set to obtain the numerical optimized parameters. The response factor enrichment factor was set as "maximize" for goal with highest importance. Lastly, using the optimized parameters, duplicate acceding experiments were performed to validate the results.

3.3 RESULTS AND DISCUSSION

3.3.1 Characterization of nanosorbent

The surface morphology, size distribution and homogeneity of the hydrolytic sol-gel synthesized silica loaded metal oxide sorbent materials depend on both reaction conditions and concentration of additives [81]. BET results (Table 2) showed specific surface area that decreased further with increasing iron loading and at calcination at 700 ^{o}C.

This is due to inter-particle condensation of free hydroxyl group at higher calcination temperatures that leads to rearrangement of silica spheres leading to faster collapse of pore structure [70]. This in turn lowers the specific surface area and increases the pore average diameter (Table 3).

Table 3: Surface parameters of RHS-0%Fe and RHS-15%Fe nanosorbents

Sample	BET surface area (m^2/g)	Micropore volume (cc/g)	Average diameter of pore (A^o)
RHS-0%Fe	98.66	0.0091	64.89
RHS-15%Fe	63.52	0.0027	124.93

On calcination the narrower pores are effectively closed resulting to a decrease in specific surface area. Figure 6a indicates a shift in the hysteresis loops to higher P/P^0 of N_2 adsorption–desorption isotherms as a result of increased iron loading on RHS. The N_2 adsorption–desorption isotherms of the nanosorbents (Fig. 6a) exhibit classical type IV isotherms with H3-type hysteresis loops under the IUPAC classification, which are typical of mesoporous compounds [82]. This is an indication of a well-defined pore structure as confirmed by the pore distribution in Fig. 6b. From the pore distribution curves, the pore volume decreases with increase in iron loading whereas the pore size reduces in a similar trend. The major pore range for all the sorbents displayed in Fig. 6b fall within the mesoporous range. The FESEM micrographs of RHS-0%Fe (Fig. 6c and d) and RHS-15%Fe (Fig. 6e and f) are represented at both low and high magnification. The FESEM micrographs show that the nanosorbents have well-resolved semi-spherical shapes characteristic of porous substance, however, (Fig.6c and d) reveal that RHS-0%Fe is more porous than RHS-15%Fe (Fig. 6e and f). These results are in agreement with the BET results (Table 3) in which specific surface area of RHS-0% Fe was relatively higher than that of RHS- 15% Fe.

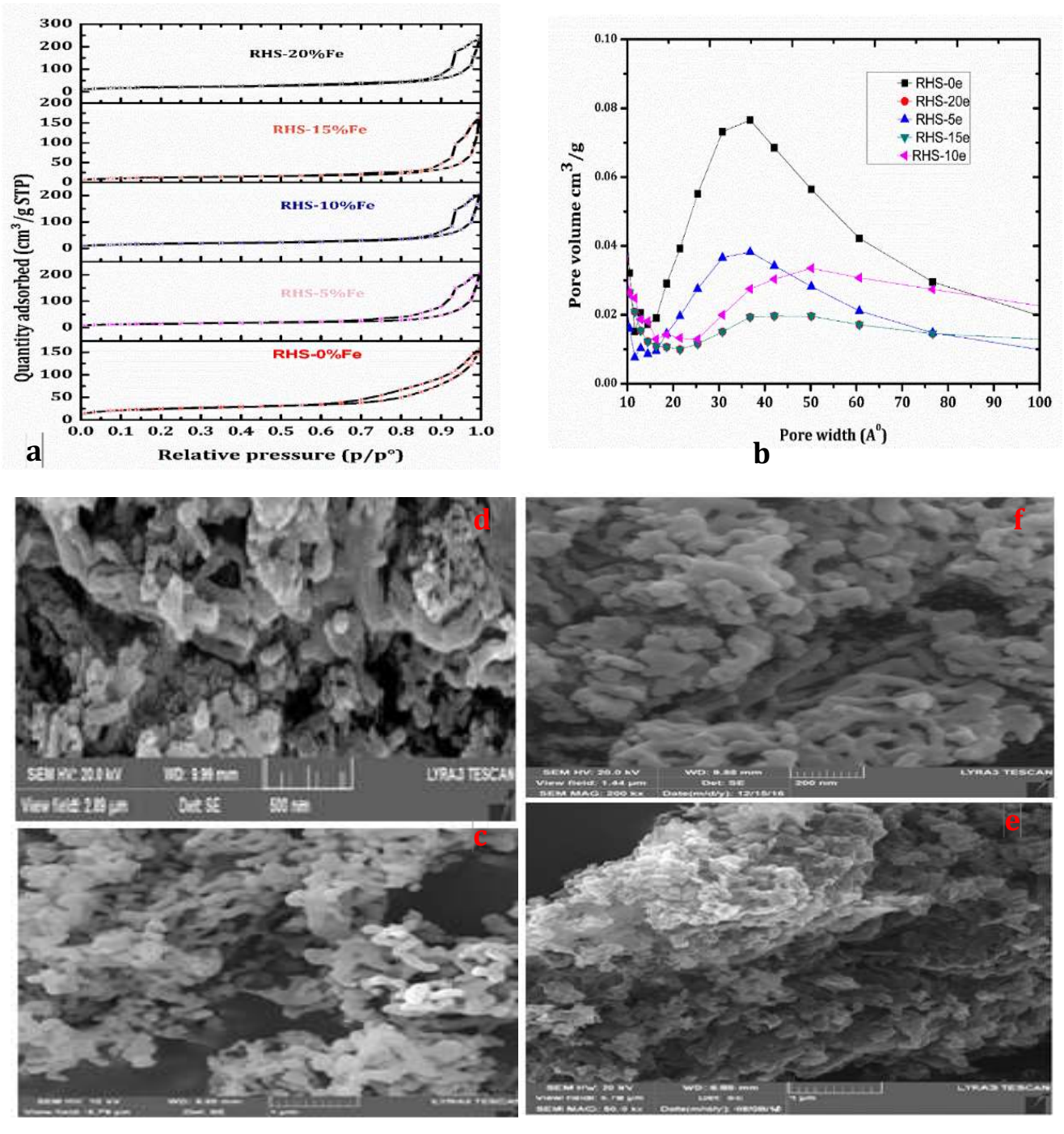

Figure 6: (a) N_2 sorption isotherms, (b) pore size distribution for RHS-x%Fe sorbents, (c) and (d) FESEM for RHS-0%Fe at low and high magnification, (e) and (f) FESEM for RHS-15%Fe at low and high magnification

The FESEM-EDS elemental mapping results represented by Fig.7a and b clearly show that carbon (C), silicon (Si) and oxygen (O) are the main components of the nanosorbents. The greater homogeneity of Fe in RHS-15%Fe is attributed to the fact that calcination at 700 ^{o}C removes the NO_3^- ions (through oxidation to gaseous nitrogen dioxides) and adsorbed water molecules from the pores which leaves the metal to be strongly bonded in the porous RHS matrix.

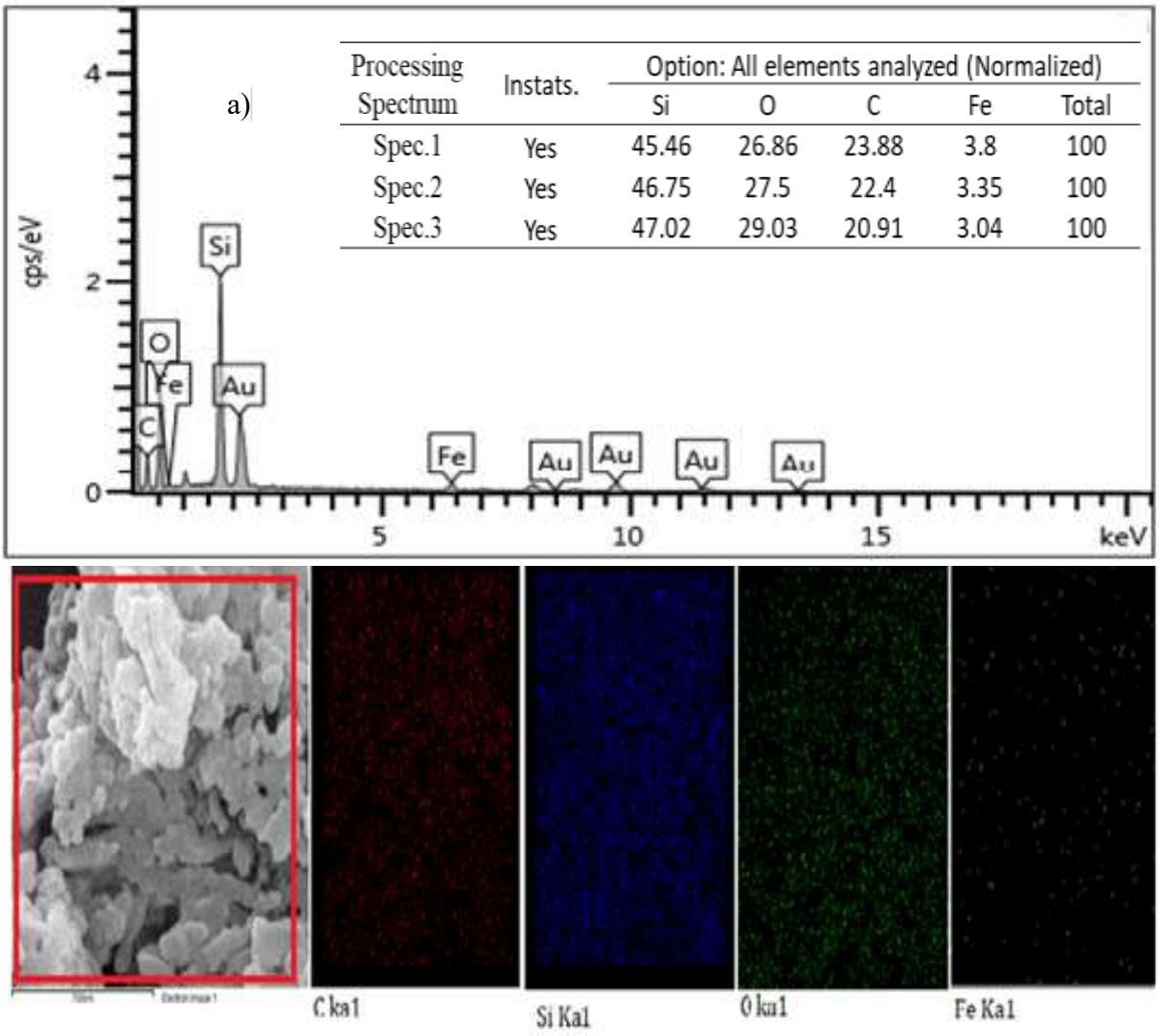

Figure 7: FESEM-EDS (a) elemental mapping results (b) sum spectra for RHS- 15% Fe

FTIR was used to establish the types of functional groups present in the synthesized nanocomposite sorbents. The FTIR spectrum (Fig. 8) shows the effect of iron and carbon loading on the silica support. The effect of metal loading to silica matrix is well reported [83,84]. In this study, two key features were identified; (i) the decrease in band intensity at 802 cm^{-1} signified the progressive Si-O-Fe bond formation resulting from incremental iron loading (0-20 wt.%) (ii) the band at 1095 cm^{-1} corresponded to Si–O–Si bond decreases in intensity and shifts towards low band values (red shift) due to iron loading (0 to 20 wt.%). The red shift for the band at 1095 cm^{-1} and the intensity decrease at 802 cm^{-1} confirm the Si–O–Fe bond structure formation [85]. The loading of iron decreased the availability of C-OH stretch (1095 cm^{-1}), OH stretch 3340 $cm^{-1,}$) oxygen and hydroxyl groups on the surface of the composite.

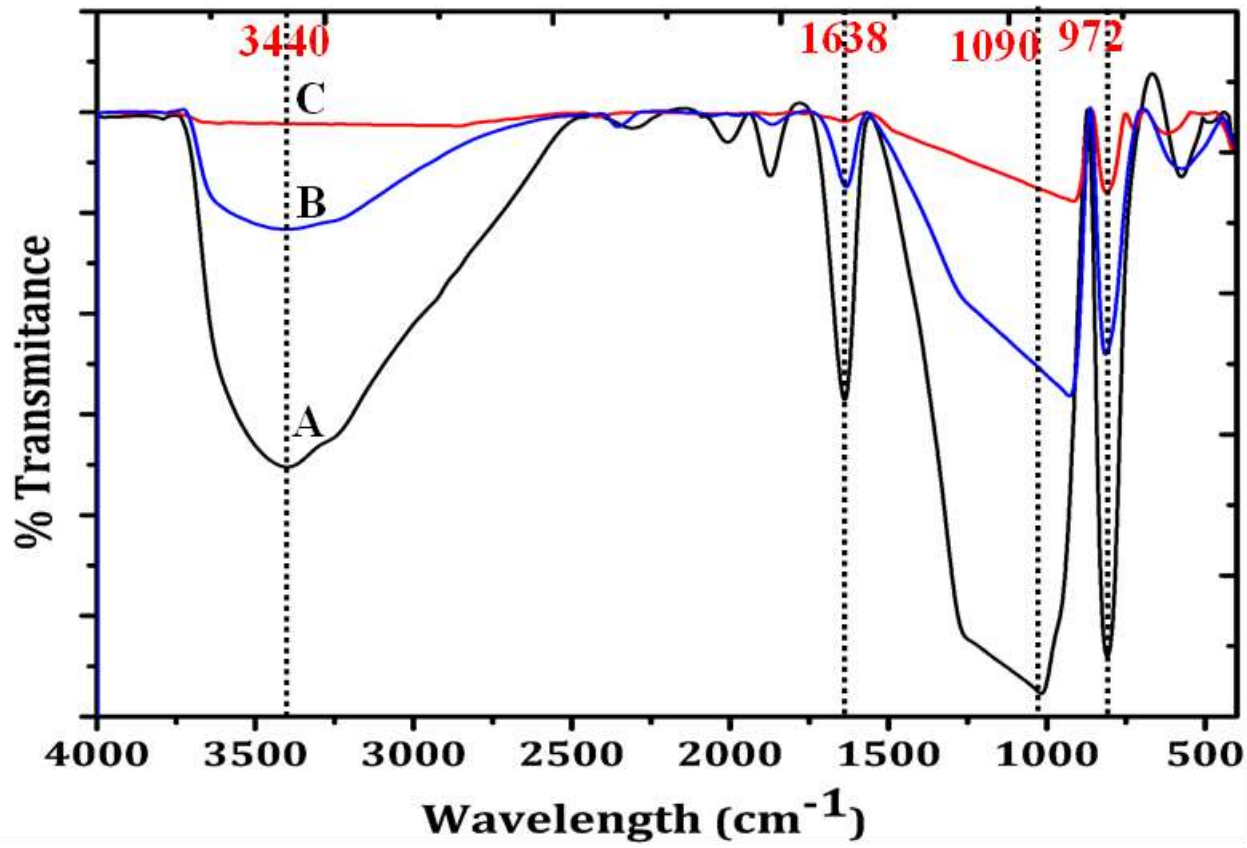

A-RHS-0%Fe, B-RHS-15%Fe, C-RHS-20%Fe

Figure 8: FTIR for the synthesized nanosorbents

3.3.2 Preliminary one factor at a time analysis

To achieve the best effectiveness and sensitivity of the extraction method, several variables were investigated and optimized. In the preliminary attempt, a univariate approach was applied to the µ-SPE experiments to select variables to be fixed during multivariate optimization. These were; suitable desorption solvent, type and amount of sorbent.

3.3.3 Selection of a suitable sorbent type

In our preliminary study, extraction efficiency of various percentage of iron functionalized rice husk silica composite sorbents (RHS-x%Fe, where x= 0, 5, 15 and 20) were investigated. Rice husk silica represent a cost effective porous template with many natural functional groups that facilitate the anchorage of metallic oxides [86]. From the trend in Fig.9a, there is a progressive increase in extraction efficiency from 0% up to 15%Fe, however at 20% Fe loading, the performance decreased. This is possibly due to pore blockage that lead to a significant decrease in surface area and reduced extraction functionality on the sorbent surface as a result of increasing iron loading as revealed by the FTIR (Fig.8).

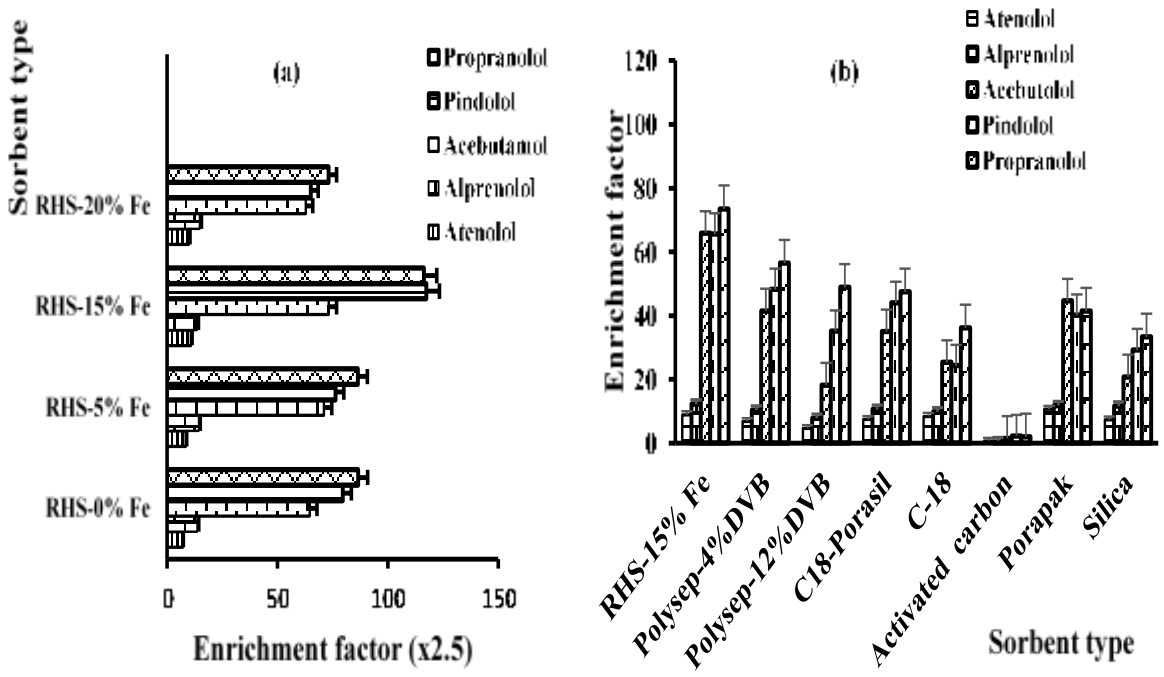

Figure 9: Comparing the extractability of synthesized RHS-15%Fe (a) with different iron loading (b) with purchased sorbents. Extraction conditions: concentration: 2.5 ng mL^{-1}; extraction time: 10 min; amount of salt: 0%; desorption solvent: Methanol; desorption

The extraction efficiency of the synthesized RHS-15%Fe was compared with that of other commercially available sorbents (activated carbon, C_{18}, porapak, silica, C_{18}-porasil, polysep- 4% divinybenzene and polysep- 12% divinybenzene) and results (Fig.9b) showed better performance of RHS-15%Fe sorbent. There are several possible interactions for drug molecule with the sorbent surface. The sorbent surface is composed of carbon and Fe_2O_3 on the silica moieties, which enhance strong electrostatic interaction with the drug molecule specifically by hydrogen bond and π-π interactions. The drug molecule is bound to the surface via cation-π interactions between the π-electrons of aromatic rings and surface cations (Fe^{3+}) giving a much stronger interactions. The intermolecular hydrogen bonds between the drug and the nanocomposite also play a significant role in the stability of the drug molecules. Additionally, the hydroxyl and amine groups in the drug molecule acts as electron donors to form hydrogen bond with the sorbent surface. Similarly, other functional groups such as carbonyl and ether moiety of drug molecules forms hydrogen bond with the sorbent surface. ß-blockers become significantly polar in aqueous medium and exhibit greater electrostatic interactions with the amorphous silica, carbon and Fe ion. Additionally, the amino groups on ß-blocker molecules exhibit stronger interaction with iron functionalized silica [41, 43].

Amount of sorbent for µ-SPE to obtain higher extraction efficiency was investigated (10, 20, 35 and 45 mg with volume of desorption solvent). From the results in (Fig. 10 a), the highest enrichment factor was obtained with 35 mg of sorbent and increased sorbent amount (45 mg), showed reduction in extraction efficiency. This might be due to the fact that when the amount of sorbent is increased, incomplete desorption was observed. For the 45 mg sorbent amount, more desorption solvent is required which further dilutes the enriched analytes on the µ-SPE.

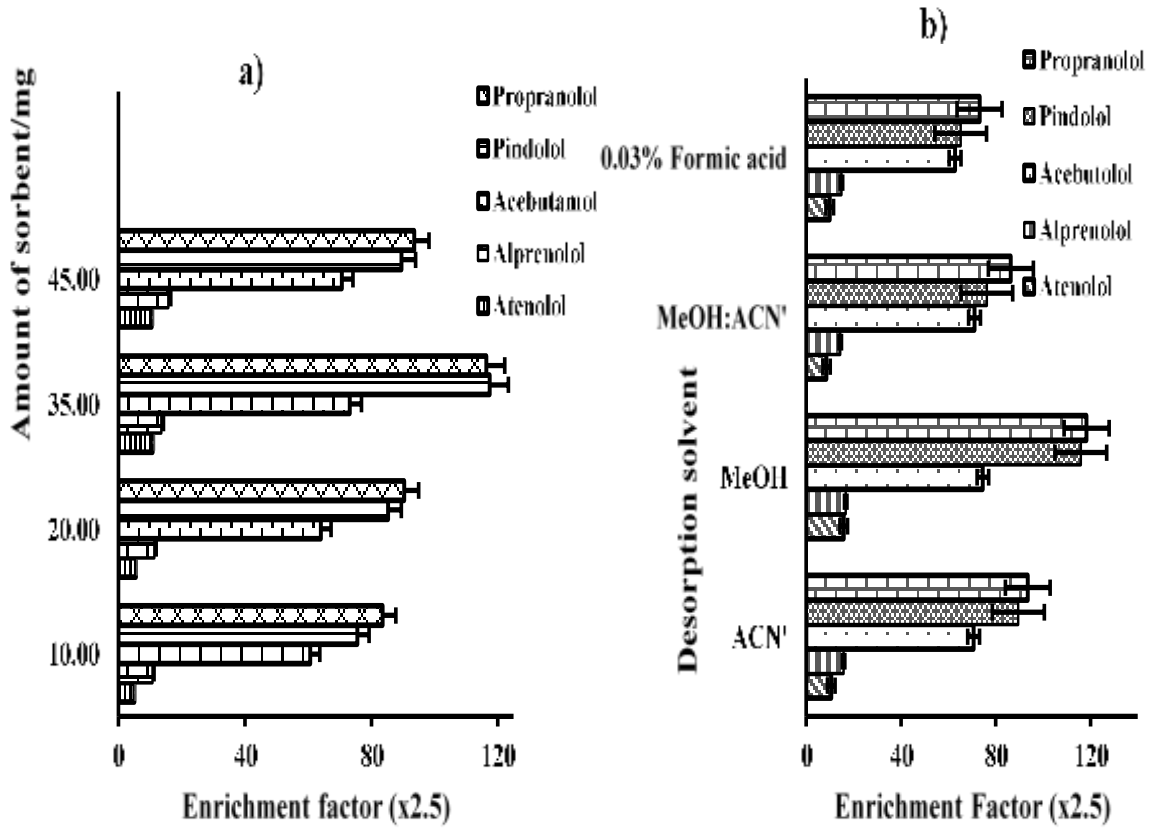

Figure 10: Preliminary; a)-best sorbent loading amount, b)- suitable desorption solvent used in extractability of ß-blockers from HWW by µ-SPE. Extraction conditions: concentration: 2.5 ngmL^{-1}; extraction time: 10 min; amount of added salt: 0%; desorption solvent

3.3.4 Selection of desorption solvent

In μ-SPE, the analytes are desorbed with a suitable solvent via ultra-sonication since they are always adsorbed to the sorbent material during extraction process [87]. Four solvents, namely, methanol (MeOH), acetonitrile (ACN), 0.03% Formic acid and Methanol: Acetonitrile (1:1) were tested as suitable desorption solvents. Results (Fig. 10b) showed that methanol was the best desorption solvent that facilitated complete analytes desorption. A reason for the excellent desorption performance of methanol is its higher solubility for ß-blockers and compatibility with LC conditions. Acetone was not a suitable eluting agent because it is too volatile. Hence, methanol was selected as a suitable desorption solvent for subsequent multivariate experiments.

3.3.5 Screening significant parameters using FFD

Fractional factorial design (FFD) including 18 experimental runs was randomly utilized in screening of the significant parameters affecting the recovery of ß-blockers from HWW. A FFD permits the extraction of information on main effects and low-order interactions by confounding the factorial into blocks and selecting one block to run [80]. A two level FFD, (2_{IV}^{5-1}) with the design parameters indicated in Table 4 was utilized in the screening of the significant variables and in the elimination of extraneous variables.

Basing on the preliminary experiments, five variables, namely sample pH, ionic strength (%w/v), extraction time (min), desorption time (min) and desorption volume (μL) were considered for screening.

To economize on the required number of runs, each factor in a fractional design is usually set at two levels and response measurements taken for only a fraction of the possible combinations of levels [80].

Table 4: The experimental factors and levels of the FFD (2^{5-1}) used in the extraction of ß-blockers by micro-solid phase extraction (µ-SPE).

Factor	**Key**	**Level**			
		Lower (-1)	**Upper (+1)**	**FFD Parameters (2_{IV}^{5-1})**	
Source phase pH	A	3.0	10	Factors	5
				Base	
Ionic strength (%w/v)	B	0.5	10	Design	4,16
Extraction time (min)	C	5.0	30		
				Center	
Desorption/Sonication time (min)	D	5.0	20	point	2
				Total	
Desorption volume (µL)	E	250.0	700	runs	18

The low and high levels assigned by (-) and (+) respectively were selected basing on prior experience and are represented by real values, results of which are indicated in Table 5.

Table 5: Fractional Factorial Design (FFD) (2_{IV}^{5-1}) responses (actual values) for CA-µSPE of ß-blockers with their average enrichment factors (n=3)

Run Order	A	B	C	D	E	Enrichment Factor					
						PROP	ACE	ATE	ALP	PIN	AVE
1	3	0.5	30	20	250	20.8	21.8	24.1	24.8	23.7	23.6
2	10	3	30	5	250	44.38	44.48	40.48	44.78	43.8	43.39
3	3	0.5	30	5	700	19	29	18.9	17.9	17.1	20.73
4	10	0.5	30	5	700	12.8	13.8	16.9	16.8	15.8	15.83
5	10	0.5	5	20	700	45.9	46	41.85	46.3	45.3	44.87
6	10	3	30	20	700	20.9	21	19.35	21.3	20.8	20.62
7	10	0.5	5	5	250	19.6	20.6	23	23.6	22.5	22.43
8	10	3	5	20	250	31.9	32	29.25	32.3	31.6	31.29
9	3	3	5	20	250	19	14	12.15	13.3	13.2	13.16
10	3	0.5	5	20	700	22.72	22.82	20.99	23.12	22.6	22.38
11	6.5	1.75	30	12.5	475	47	47.1	42.84	47.4	46.4	45.93
12	3	3	30	20	700	40	40.1	36.54	40.4	39.5	39.14
13	10	0.5	30	20	250	46.74	46.84	42.61	47.14	46.1	45.68
14	3	3	30	5	250	57.52	57.62	52.31	57.92	56.7	56.14
15	10	3	5	5	700	20.63	20.73	19.11	21.03	20.6	20.36
16	6.5	1.75	5	12.5	475	22.72	22.82	20.99	23.12	22.6	22.38
17	3	3	5	5	700	47	47.1	42.84	47.4	46.4	45.93
18	3	0.5	5	5	250	42.05	42.15	38.39	42.45	41.5	41.13

Pareto chart represented by Fig.11 shows the standardized effects of the FFD screening experimental results. The bar lengths in the Pareto chart are proportional to the enrichment factors while the vertical line serves as the reference line and represents the 95% confidence interval. Any effect caused by a factor that out match this reference line is considered significant with regard to enrichment factors. The Pareto chart of the standardized effects were deduced from ANOVA test results of the average enrichment factors of the ß-blockers.

The resultant Pareto chart (Fig. 11) indicates that the sample pH have the greatest significant effect on the average enrichment of ß-blockers from HWW. This was followed by extraction time, ionic strength and desorption volume in order of decreasing significance. The interaction effect between source phase pH with extraction time and ionic strength with extraction time were also found to have a significant effect on µ-SPE of ß-blockers. The significance of interaction effects on µ-SPE extraction is based on the fact that, to improve the extractability of ß-blockers in HWW, these analytes have to exist in their un-dissociated form. This is only achieved in alkaline conditions with (pH greater than their PKa) [51].

Since µ-SPE is an equilibrium based extraction procedure, the nanosorbent requires sufficient contact time with the sample. To construct a central composite design (CCD) for response surface optimization, the variables with a significant positive effect (sample pH, extraction time, ionic strength and desorption volume) on ß-blockers enrichment were evaluated further.

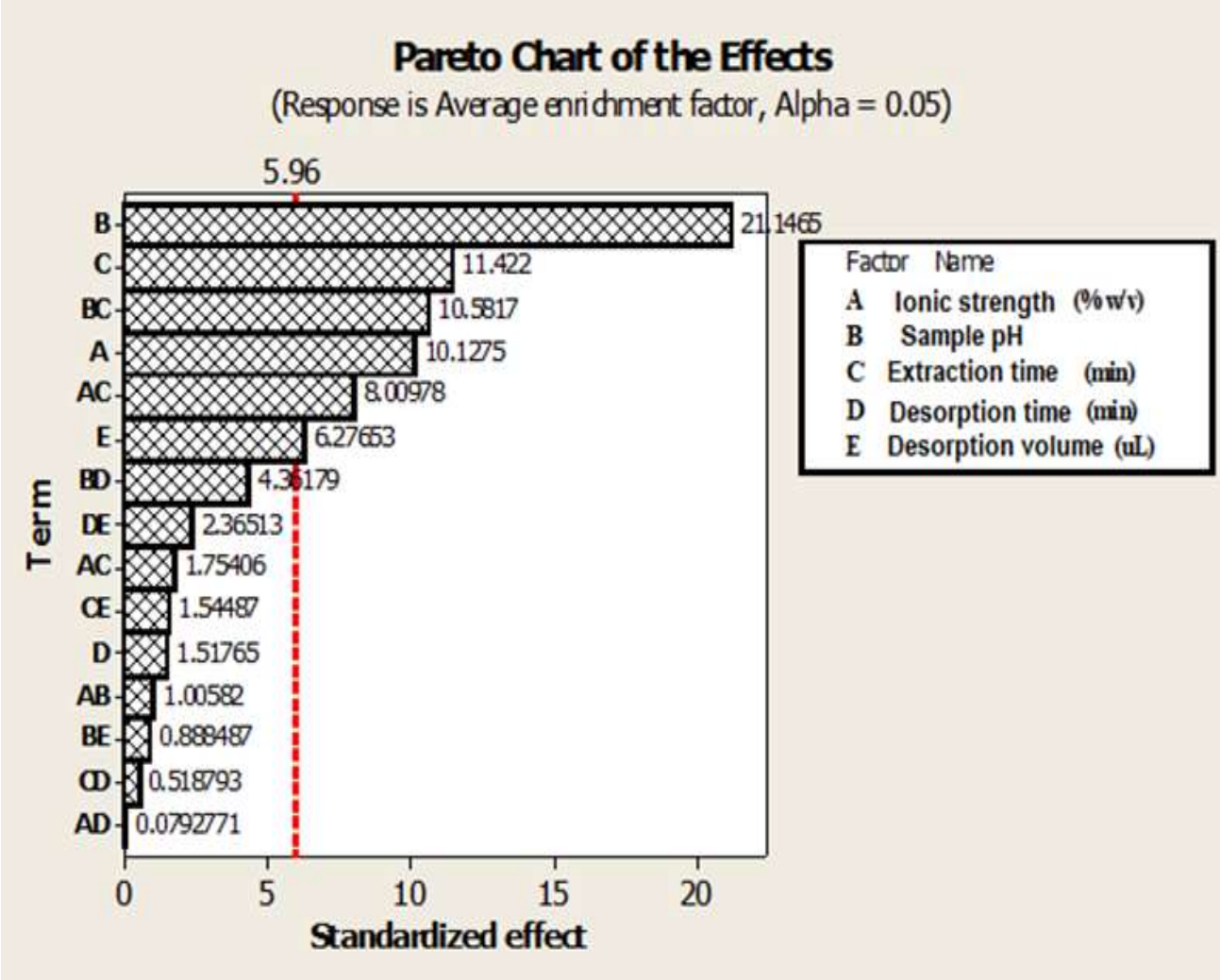

Figure 11: Pareto chart showing the selection of most significant factors affecting the extraction and preconcentration of beta blocker in hospital waste water

3.3.6 Optimization using central composite design with desirability function

On the basis of the significant factors generated from FFD experiments, a rotatable and orthogonal CCD was employed to improve and obtain the optimized conditions for µ-SPE extraction. The CCD design constitute factorial points ($N_f = 2$) (where f corresponds to number of factors), axial / star points ($N_a = 2f$), center points (C) and the response variables test results [80]. Equation 4 was used to determine the number of experiments conducted.

$$N = 2^K + 2K + C \qquad (4)$$

K signify number of variables/ factors used in the design.

In this study, the values for K and C were set at 4 and 6, respectively, generating 30 experimental runs. The CCD experimental design and variables involved in design are indicated in Table 6. It is logical to repeat center points so as to gain a better estimation of experimental error. The symbol α value is a representation of the orthogonality and rotatability of the design and can be calculated using Eq. (5). The axial points are positioned at distances +α and -α from the center of the experimental data [80].

$$\alpha = 2^{K/4} \qquad (5)$$

To minimize the effect of unexplained variability in the responses due to extraneous variables, 30 experiment combinations were randomly run. The rest of the parameters, such as sample amount, sorbent amount, sorbent type and desorption solvent were arbitrarily fixed using preliminary experiment results.

Table 6: The experimental factors and levels and ranges used in CCD optimization

Variables	Level Low (-1)	Central (0)	High (+1)	(-α)	(+α)	Randomized 2-level full Factorial CCD parameters	
Ionic strength (X_1) %w/v	0	15.0	30	7.50	22.50	Cube points	16
Source phase pH (X_2)	0	5.0	10	2.50	7.50	Center points	6
Extraction time (X_3) min	5	17.5	30	11.25	23.75	Axial Points	8
Desorption volume (X_4) (µL)	250	475.0	700	362.50	587.5		
						Number of runs*	30

'O'- in the design matrix indicates no factor adjustment

The CCD experimental design table and the corresponding responses are shown in (Table 7).

Table 7: Central Composite Design matrix (actual values) for µ-SPE extraction optimization and the response values.

Run order	Factors				EF-PROP	EF-ACE	EF-ATE	EF-ALP	EF-PIN	AVE.[a] EF
	X_1	X_2	X_3	X_4						
1	5.00	15.0	17.50	475.0	84.09	91.48	96.55	90.55	88.98	90.33
2	2.50	22.5	11.25	362.5	79.11	92.62	93.82	87.82	90.12	88.70
3	7.50	22.5	23.75	362.5	87.45	93.08	97.23	91.23	90.58	91.91
4	5.00	15.0	17.50	475.0	73.47	61.96	93.12	87.12	59.46	75.03
5	2.50	7.50	11.25	362.5	72.70	92.77	95.26	89.26	90.27	88.05
6	2.50	7.50	11.25	587.5	69.41	87.36	93.19	87.19	84.86	84.40
7	7.50	22.5	11.25	587.5	70.54	85.91	93.63	87.63	83.41	84.22
8	2.50	7.50	23.75	587.5	76.08	87.29	95.89	89.89	84.79	86.79
9	5.00	15.0	17.50	475.0	77.86	81.50	97.79	91.79	79.00	85.59
10	2.50	22.5	23.75	587.5	85.23	92.24	98.60	92.60	89.74	91.68
11	5.00	15.0	17.50	475.0	81.37	97.14	96.49	90.49	94.64	92.03
12	2.50	22.5	23.75	362.5	63.05	91.45	97.56	91.56	88.95	86.51
13	7.50	22.5	11.25	362.5	74.95	91.40	97.50	91.50	88.90	88.85
14	7.50	22.5	23.75	587.5	86.72	93.89	98.74	92.74	91.39	92.70
15	7.50	7.50	11.25	587.5	52.45	68.86	93.39	87.39	66.36	73.69
16	7.50	7.50	23.75	587.5	69.55	80.02	96.37	90.37	77.52	82.77
17	7.50	7.50	11.25	362.5	74.57	83.22	96.93	90.93	80.72	85.27
18	7.50	7.50	23.75	362.5	70.60	85.91	95.06	89.06	83.41	84.81
19	2.50	22.5	11.25	587.5	96.41	96.80	98.34	92.34	94.30	95.64
20	2.50	7.50	23.75	362.5	72.57	86.08	95.39	89.39	83.58	85.40
21	5.00	15.0	17.50	475.0	73.60	87.16	95.83	89.83	84.66	86.22
22	5.00	15.0	30.00	475.0	57.45	69.74	94.72	88.72	67.24	75.57
23	5.00	0.00	17.50	475.0	60.68	88.87	97.05	91.05	86.37	84.80
24	5.00	15.0	17.50	475.0	73.79	81.29	97.16	91.16	78.79	84.44
25	5.00	15.0	17.50	700.0	70.69	87.14	94.30	88.30	84.64	85.01
26	0.00	15.0	17.50	250.0	80.88	83.73	95.28	89.28	81.23	86.08
27	0.00	15.0	17.50	475.0	72.09	86.93	94.37	88.37	84.43	85.24
28	5.00	30.0	17.50	475.0	49.66	65.44	85.77	89.77	67.94	74.72
29	5.00	15.0	5.00	475.0	45.85	61.27	83.41	82.41	58.77	67.34
30	10.0	15.0	17.50	475.0	78.13	81.40	80.60	81.60	78.90	79.53

a- Average enrichment Factor (n=3)

Because the five ß-blockers have a similar aptness to vary in enrichment factors (EFs), average EFs were used to study the effect of the four factors. The experimental responses were analyzed by ANOVA and statistics to generate a second order polynomial model that was used to model the four factors represented in CCD experimental design. A polynomial model is a reasonable representation that compares the experimental response and model predictions using normal probability plots. To check the statistical adequacy of the model, ANOVA residuals and determination coefficients were analyzed and the regression results are presented in Tables (8 and 9). These results are used to evaluate the experimental results and investigate the significance of variable and their interactions. The CCD results were fitted to a quadratic polynomial with multiple regressions for the optimized parameters, leading to reduced quadratic equation 6.

$$Y \text{ (Ave. Enrichment Factor of ß-blockers)} = 79.3349 - (0.371*X_1) + (0.4499*X_2) + (2.0398*X_3) - (0.1518*X_4) + (0.0648*X_1*X_2) + (0.25*X_1*X_3) - (0.0151X_1*X_4) + (0.0042*X_2*X_4) \ldots\ldots 6$$

Table 8: Analysis of variance (ANOVA) for average extraction EF of ß-blockers

Source	Degree of freedom	Sum of Squares	Adj. Sum of Squares	Adj. Mean of Square	F-Value	P-Value
Regression Model	14	1864.83	1864.83	133.202	8.09	0.001
Linear	4	578.32	331.66	82.914	14.68	0.010
Square	4	148.80	148.80	37.200	3.31	0.057
Interaction	6	1137.72	1137.72	189.620	2.56	0.027
Residual Error	15	1826.28	1826.28	121.752		
Lack-of-Fit	10	1640.09	1640.09	164.009	7.40	0.073
Pure Error	5	186.20	186.20	37.240		
Total	29	3691.12				

'Source' signals the origin of variation from either factor, interaction or error. '**Total**' indicates the sum for all the sources. **'DF'** refers to degrees of freedom from each source. Since we had 30 observations (experimental runs), the total degrees of freedom is 29 corresponding to (n − 1). **'SS'** refers to the sum of squares within groups (error) and sum of squares between groups (factor), **'MS'** corresponds to mean squares (got by dividing the sum of squares by the degrees of freedom). **'F'** is obtained by dividing the MS (factor) by the MS (error). **'P'** is used use to determine the significance of a factor; by relating it with an alpha value of 0.05. P-values < 0.05 signify that the factor is significant

Table 9: Regression analysis for reduced quadratic model for the average extraction EF of ß-blockers

Term	Coef	SE Coef.	P-Value	Significance
Constant	79.3349	61.4896	0.0000	significant
X_1	-0.371	6.1166	0.0001	significant
X_2	0.4499	2.0389	0.0002	significant
X_3	2.0398	2.5997	0.0445	significant
X_4	-0.1518	0.1645	0.0371	significant
X_1^2	0.1941	0.2967	0.0523	insignificant
X_2^2	-0.0671	0.033	0.0600	insignificant
X_3^2	-0.1191	0.0475	0.0240	significant
X_4^2	0.0001	0.0001	0.0047	significant
X_1X_2	0.0648	0.1295	0.0062	significant
X_1X_3	0.2500	0.1554	0.0128	significant
X_1X_4	-0.0151	0.0086	0.0010	significant
X_2X_3	-0.0243	0.0518	0.6460	insignificant
X_2X_4	0.0042	0.0029	0.0016	significant
X_3X_4	0.0032	0.0035	0.3630	insignificant
R-squared	0.9471			
Pred. R-squared	0.8285			
Adj. R-squared	0.9064			
Prediction SS (PRESS)[a]	111.7581			

[a] represent the prediction sum of squares

The goodness-of-fitted model was examined using residual analysis (Fig. 12 A-D). The normalcy of the residuals in these plots signified error consistence with acceptable normal distribution, generating a completely randomized design.

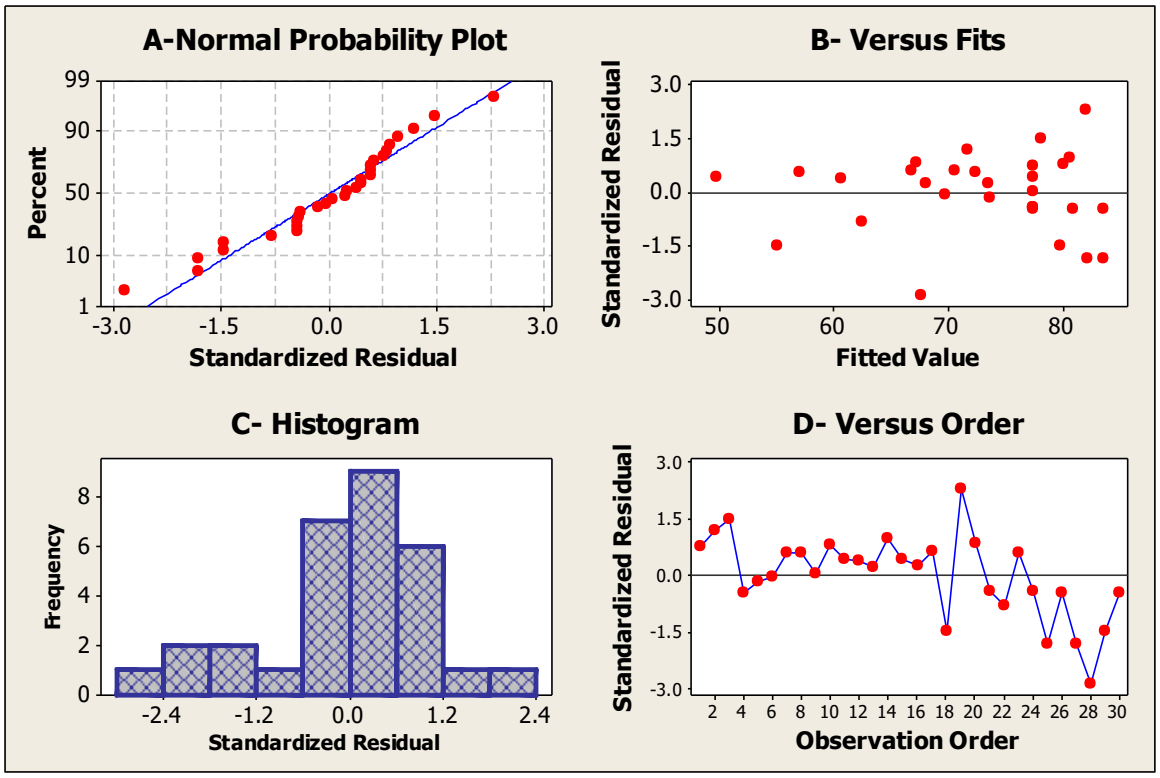

Figure 12: Residual Plots for average enrichment factor for extraction of Beta blockers

Only regression analysis parameters; sample pH (X_2), extraction time (X_2) and interaction between (X_1X_2, X_1X_3, and X_2X_4) (Table 8) showed positive linearity of a fitted model. The model's value of 'F' and "P" were 8.09 and 0.001(<0.05), respectively. These results confirm the significance of the model. P-values less than a significance level 0.05 is considered to be statistically significant, the lack-of-fit P-value > 0.05 implied that the model's lack of fit is insignificant relative to the pure error. A small P-value and large F-value for each term in the model signify the term's significant influence on the extractability of ß-blocker. The model's "lack of Fit" value was 0.073 (>0.05), implying that the "lack of Fit" was insignificant, an indication of model's good predictability. Also, the value of R^2 and "Prediction Sum of Squares (PRESS)" were 0.9471 and 111.7581, respectively. The model had good fitting between the calculated and observed results and the signal to noise ratio was desirable and adequate since the 'PRESS' value > 4. The coefficient of determination (R^2) of the regression equation is a measure of the overall variation in the data generated by the model. Hence, a good fit model based on acceptable data should have R^2 values closer to 1. The higher R^2 (94.71%) value meant that the model had a higher capacity to predict responses.

3.3.7 Interaction effects through response surface curves and DF optimization

Response surface methodology (RSM) was introduced as an easy way of optimizing the effects of source phase pH, ionic strength, extraction time and desorption time on the average EF of ß-blockers extractability from HWW. The 3D response surface plots (Fig.13) were used to predict the relationships between these factors (at different experimental levels) with their EF.

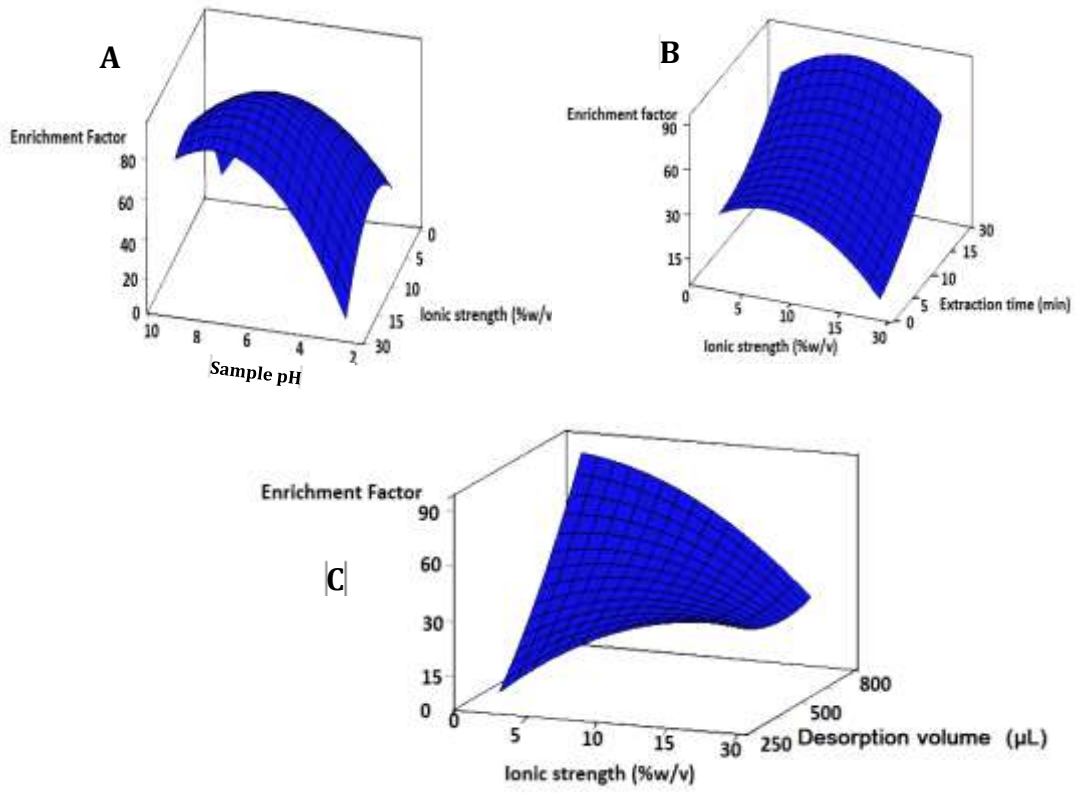

Figure 13: Response surfaces for the extraction of ß-blockers: (A) source pH vs ionic strength; (B) ionic strength vs extraction time; (C) ionic strength vs desorption volume

The possible interactions between these factors are indicated by the curvature in these response surface plots (Fig.13). Addition of salt in the microextraction process affects extraction efficiency by either reducing the solvation power towards the analytes and sorbent (enhanced extraction) or thickening of the Nernst diffusion layer (poor extraction) [60]. The surface charge of the extracting sorbent and 'analytes' ionization status is predominantly determined by the pH of the sample matrix. ß-blockers used in this experiment have pK_a values ranging from 8.8 to 9.6. At pH≤10 they become protonated on their amino group ($\sim NH_3^+$) and are rendered effective π-electron acceptor thus facilitating the π-π electron donor–acceptor interactions [51]. Results in Table 10, shows that the experimental optimized values for sample pH, ionic strength, and extraction time and desorption volume respectively were fairly closer to the predicted values (8.1, 0.0, 10.5 and 35.0). In this experiment, the effect of salt addition in the ranges of 0 to 30 %w/v was evaluated. The optimized value for the ionic strength (0 %w/v), meant that the sample wastewater samples did not require any salt adjustment before extraction.

Table 10: Applied versus predicted optimized extraction conditions.

	Optimal levels	
	Predicted	Experimental
Sample pH	8.1	8.0
Ionic strength (%w/v)	0.0	0.0
Extraction time (min)	10.5	10.0
Desorption volume (µl)	350	300
Predicted EF value	99.89	
Experimental EF value		97
% Relative standard deviation		4.3

'0' value indicate no parameter adjustment

3.4 Method Evaluation

The proposed RHS-15%Fe based μ-SPE-LC-MS/MS method was evaluated for matrix effect, linearity, recovery, sensitivity, accuracy, stability and precision under optimized conditions for HWW. Analytical figures of merit for this method, included dynamic linear ranges, relative standard deviations (RSD), correlation of determination (R^2), limits of detection (LODs) and quantification (LOQs), as listed in Table 11.

Table 11: Analytical figures of merit of RHS-15%Fe based µ-SPE-LC-MS/MS method.

Analyte	LDR[a] µg L^{-1}	R^2	LOD[b] ng L^{-1}	LOQ[c] ng L^{-1}	RSD[e] (%) Within-day			RSD (%) Between-day		
					0.25 µg L^{-1}	1.50 µg L^{-1}	2.50 µg L^{-1}	0.25 µg L^{-1}	1.50 µg L^{-1}	2.50 µg L^{-1}
PROP	0.02-5	0.9987	4.00	14.00	3.2(90.0)[d]	3.2(97.4)	3.00(96.0)	7.2	6.4	6.0
ACE	0.02-5	0.9973	6.40	19.00	5.3(94.0)	5.1(99.5)	4.80(97.0)	8.1	8.3	7.6
ALP	0.02-5	0.9954	6.00	18.00	6.0(93.3)	5.8(94.6)	5.50(95.0)	8.2	5.8	5.5
PIN	0.02-5	0.9981	5.00	16.00	3.0(92.0)	2.8(96.0)	2.60(95.0)	6.0	5.2	5.0
ATE	0.02-5	0.9982	4.20	13.00	2.6(83.3)	2.4(95.4)	2.34(94.0)	6.5	5.5	4.7

R^2 Coefficient of determination.

a Dynamic linear range.

b Limit of detection.

c Limit of quantification.

d Values in brackets represent relative recoveries (%RR).

e Intra-day and inter-day precision expressed as relative standard deviation (n = 5 samples for within day and n = 3 days for between day).

A signal to noise ratio of 3 and 10 were used to calculate the LODs and LOQs, respectively. Different concentrations of calibration ß-blocker standard mixtures (0.02, 0.05, 0.10, 0.50, 1.50, 2.50, 5.00 and 10.0 ng mL^{-1}) were used for generating calibration curves under the optimized extraction conditions. Good linearity, over a concentration range of 0.02-5.00 ng mL^{-1} with R^2 ranging from 0.9954 to 0.9987 was obtained. Reproducibility (between-days RSDs, n = 3 days),-and repeatability (within-day RSDs, n = 5 samples) were equal or less than 8.3% and 6.0%, respectively.

Results in Table 12 show that the relative recoveries (%) for all the HWW samples were in the acceptable ranges of 80.6 to 105.1% (RSDs in the range of 2.2-6.0). All the RR and RSDs are almost quantitative, an indication of good accuracy and precision of the proposed method.

Table 12: Analytical performance of proposed method for HWW samples.

Sample	Analyte	Spiking level (ng mL^{-1})	Recovery ±RSD (%)	Sample	Analyte	Spiking level (ng mL^{-1})	Recovery ±RSD (%)
S-1	ATE	2.50	84.5±4.8	S-3	ATE	2.50	85.6±4.7
		0.05	87.3±4.7			0.05	94.2±4.3
		0.00	ND[a]			0.00	ND
	ALP	2.50	80.4±6.0		ALP	2.50	81.7±5.4
		0.05	82.0±3.1			0.05	94.2±4.7
		0.00	ND			0.00	ND
	ACE	2.50	99.8±4.4		ACE	2.50	98.7±4.4
		0.05	94.2±4.7			0.05	94.2±5.7
		0.00	ND			0.00	ND
	PIN	2.50	89.8±3.4		PIN	2.50	91.2±3.4
		0.05	84.2±4.2			0.05	86.1±3.7
		0.00	ND			0.00	ND
	PROP	2.50	104.6±3.3		PROP	2.50	100.6±3.2
		0.05	100.2±5.5			0.05	102.4±4.1
		0.00	ND			0.00	ND
S-2	ATE	2.50	86.1±4.4	S-4	ATE	2.50	87.3±3.4
		0.05	85.2±3.7			0.05	94.2±4.7
		0.00	ND			0.00	ND
	ALP	2.50	80.6±4.4		ALP	2.50	81.2±3.4
		0.05	84.2±4.7			0.05	86.3±4.7
		0.00	ND			0.00	ND
	ACE	2.50	93.7±2.2		ACE	2.50	95.1±4.3
		0.05	90.1±3.8			0.05	94.2±3.1
		0.00	ND			0.00	ND
	PIN	2.50	86.3±4.4		PIN	2.50	89.5±3.4
		0.05	82.1±3.5			0.05	84.2±6.0
		0.00	ND			0.00	ND
	PROP	2.50	105.1±4.4		PROP	2.50	102.0±3.0
		0.05	100.2±3.7			0.05	99.8±3.7
		0.00	ND			0.00	ND

S-1 to S-4 are the different HWW samples used in this study.

ND- signifies below the quantification level

3.5 Re-usability and stability of the sorbent

To evaluate the performance of a synthesized sorbent, it is important to investigate it potential for reusability and stability. Following the procedure described in Section 2.5, the optimized conditions were employed to assess the re-usability and stability of the nanosorbent. Results in Fig.14 (a) reveals that the nanosorbent could be re-used up to 25 times without apparent decrease in the EFs for ß-blockers. Precision (%RSD) for the same device was$<$ 7.0. However, after 25th extraction time, the extraction efficiency of the µ-SPE device decreased drastically mainly due to the fact that the membrane envelope could have been damaged.

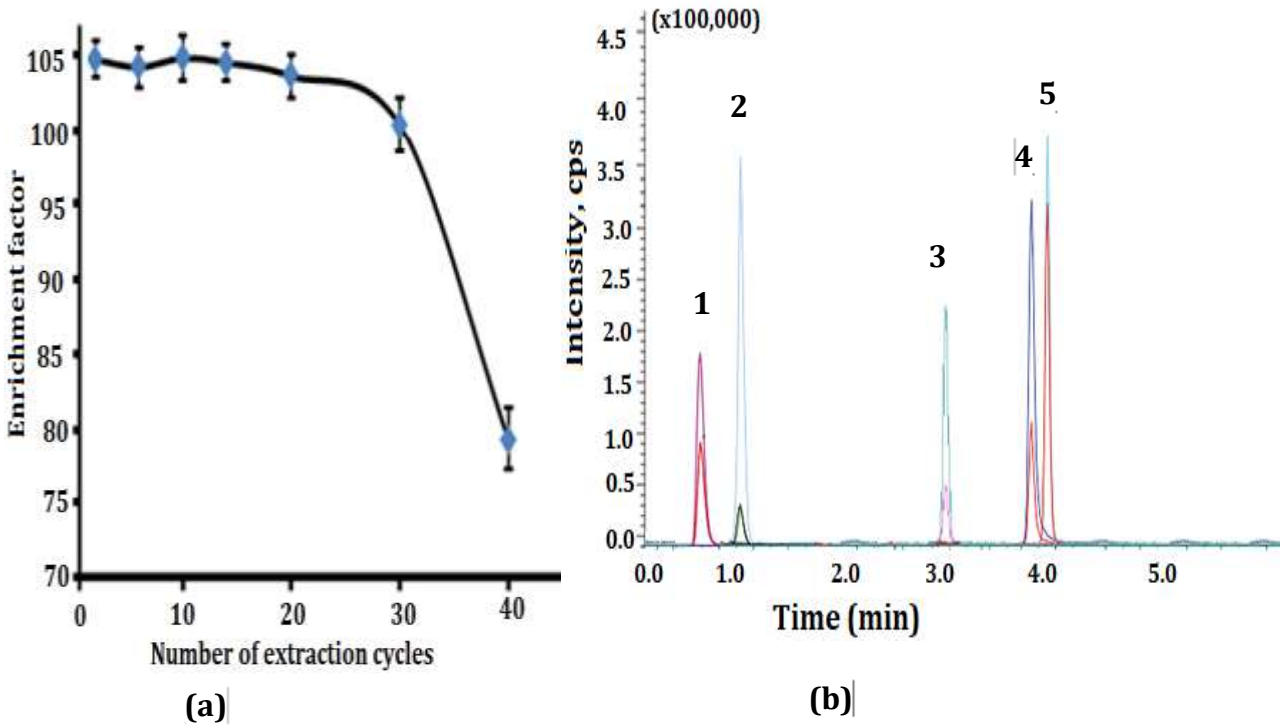

Figure 14: (a) Stability and reusability of a µ-SPE device, (b) Chromatogram of hospital waste water spiked at 0.05 ngL^{-1} of mixed ß-blockers after RHS-15%Fe based µ-SPE under optimal conditions. Peak identification; 1-Atenolol, 2-Alprenolol, 3-Acebutolol, 4-Pindolol

3.6 Analysis of real HWW sample and Comparison with other reported methods

The applicability of µ-SPE-LC-MS/MS for HWW samples were investigated. Un-spiked and spiked samples (spiking levels 0.05 and 2.5 $ngmL^{-1}$) were prepared. Four different HWW samples (represented by S-1 to S-4) were selected and analyzed. Results of the experiments in Table 12 shows that the ß-blockers drug concentrations in the blank HWW samples were below the method's LOQs. Recoveries and relative standard deviation (%RSD) were in the ranges of 80.4 to 105.2% with RSDs <6.0%, indicating that the complexity of the sample matrix does not significantly affect the µ-SPE extraction of trace ß-blockers. Figure 14 (b) shows a well separated chromatogram for spiked real samples after µ-SPE-LC-MS/MS analysis of ß-blockers in HWW samples. The analytical performance of µ-SPE-LC-MS/MS was compared with other microextraction methods reported in literature (Table 13). Results show that the proposed extraction method provides, a relatively wider and comparably better linearity ranges and lower detection limits when compared to other reported methods [17, 44-46].

Table 13: Comparison of the proposed method with reported literature.

Method, Instrument	Sample matrix	Extraction Time (min)	LOD (ng mL^{-1})	Accuracy (%R)	Precision (%RSD)	Ref
[a]Ppy-DBSNa/ZnO nanocomposite-US-D-SPE-HPLC-UV	Human plasma and urine samples	4.6	0.8-1.5	75.0–90.0	4.6-6.3	[60]
[b]Oasis HLB-SPE-UHPLC-UV	Human urine	f	13.8-28.8	81.2–99.6	4.4	[88]
[c]MIP-SPME-HPLC-UV	Human urine and plasma samples	60	3.8	75.2–88.8	8.5	[89]
[d]Carbon-XCOS-MEPS-LC-MS/MS	Human plasma	f	20 (nM)	80.0–90.0	14.4	[66]
[e]RHS-15%Fe-LC-MS/MS	Hospital wastewater	10	0.040-0.084	80.6-105.1	2.2-6.0	Current work

a- Ppy-DBSNa/ZnO nanocomposite-ultrasound promoted dispersive micro solid extraction-high performance liquid chromatography-ultraviolet detection.
b- Oasis HLB-solid-phase extraction-high performance liquid chromatography-ultraviolet detection.
c- Molecularly imprinted polymer-solid-phase microextraction-high performance liquid chromatography-ultraviolet detection.
d- Carbon-XCOS-microextraction by packed sorbent-liquid chromatography and tandem mass spectrometry.
e- Rice husk silica sol-gel loaded iron oxide sorbent based µ-solid phase extraction - tandem mass spectrometry.
f- No published data.

CHAPTER 4

A New Droplet-Flow Assisted Heterogeneous Electro-Fenton System for Degradation of Beta Blockers: Response Surface Optimization and Mechanism Elucidation

4.1 INTRODUCTION

The detection of trace level beta blockers (ß-blockers) as emerging pollutants in drinking, ground, waste and surface water, has evoked global scientific interest [50,51]. Mixed ß-blockers contamination present cumulative ecotoxicological effects to plants and aquatic organisms even at concentrations of ng L^{-1} to µg L^{-1} [28,90–92]. Therefore, it is warranting to develop a potent degradation and monitoring approach for complete degradation of trace level ß-blockers with their metabolites during water treatment. Most studies on ß-blockers degradation in aquatic environments focus on gradual disappearance of parent analytes as a proof of degradation [55,93,94], neglecting their intermediate species/ metabolites that might even be more toxic. Moreover, the ß-blockers concentration of (>15 mg/l) [55,93,94] monitored in most reported literature, far exceeds the Maximum Contaminant Levels.

A combination of electrochemical oxidation methods with liquid chromatography-tandem mass spectrometry (LC-MS/MS), is asserted to offer a more appealing approach for monitoring the

degradation pathways and intermediate product identification of trace level pollutants [16,17]. Electro-chemical advanced oxidation processes (EAOPs) have attracted significant interest in aquatic pollutant remediation, owing to their eco-friendliness, strong oxidation abilities, insignificant toxicities, technological simplicity, and higher degradation efficiencies [18,19]. Over the recent years, electro-Fenton (EF) process, a new EAOPs, has proven to be practical, effective and appealing water treatment technology for complete oxidation of refractory organic pollutants [95]. The EF process forfends potential risks associated with H_2O_2 transportation, handling and storage since H_2O_2 is electro-generated and electro-activated in-situ [95]. The EF process is classified as either homogeneous or heterogeneous EF depending on the type and nature of Fenton catalyst used [96].

With a homogeneous EF system, in situ H_2O_2 production and decomposition involve dissolved iron species (Fe^{2+}/ Fe^{3+}) and operates under acidic conditions (pH 2-3) [19,95]. Though, this technology involves simple, fast and efficient operations, its practical acceptance is limited by restrictive acidic pH ranges that are destructive to electrodes, iron sludge formation and non-catalyst re-usability [27]. To circumvent these drawbacks and ameliorate oxidation at a wider pH range, a hEF process is advanced as an efficient, ecofriendly, and highly promising water treatment technology [96,97]. A hEF utilizes heterogeneous/ solid catalysts to continuously decompose in situ electro-generated H_2O_2 to highly reactive hydroxyl radicals ($^{\bullet}OH$) [96,98]. The stepwise mechanism mainly involves; in-situ cathodic H_2O_2 production via oxygen reduction reaction (ORR) (equation 1), H_2O_2 decomposition to $^{\bullet}OH$ catalyzed by iron II species (Fe^{2+}) (equation 2) and continuous regeneration of Fe^{2+} (by reduction of Fe^{3+}) (equation 3) [97,99]. These highly reactive $^{\bullet}OH$ radicals non-selectively oxidize organic pollutants to non-toxic (CO_2 and H_2O) or even less toxic counterparts [100].

Carbon-based materials such as carbon/ graphite felt, carbon sponge and gas diffusion electrodes et cetera, are reported to offer low cost, stable and effective cathode materials for in-situ H_2O_2 electro-

generation [101,102]. Specifically, graphite felt electrode (GFE) is postulated to offer more mesoporous structures and high surface active sites for oxygen reduction reactions (ORR) [103]. Likewise, when a high–oxygen overvoltage anode (like boron doped diamond, BDD) is employed as an electrode in an EF process, highly reactive heterogeneous •OH radicals (BDD(•OH)) are formed at the anode (equation 4), that augment the effectiveness of the EF process [104].

$O_2 + 2H^+ + 2e^- \rightarrow H_2O_2$ …… (1)

$H_2O_2 + Fe^{2+} \rightarrow Fe^{3+} + {}^{\bullet}OH + OH^-$……..……... (2)

$Fe^{3+} + e^- \rightarrow Fe^{2+}$ ……..……... (3)

$BDD + H_2O \rightarrow BDD\ (\bullet OH) + H^+ + e^-$……. (4)

In addition to the cathode type requirement, the efficiency of a hEF system is highly dependent on reactor design and nature of a heterogeneous catalyst [105,106]. In an effort to overcome the limitations associated with batch reactors, such as limited mass transfer and inadequate treatment, continuous flow reactors have successfully been proposed [107,108]. The effectiveness of these flow systems is based on enhanced convective transfer of pollutant particles to exposed electrode surfaces [109] leading to more reactive oxygen species (ROS) (H_2O_2 and •OH). On the other hand, the utilization of Fe-C as an effective heterogeneous catalyst in hEF systems is well investigated [110,111]. It is postulated that when Fe-C composite material is added to an electrolytic solution, a multitude of micro-galvanic cells form in which iron serves as anode and carbon as cathode, leading to numerous Fe^{2+} regeneration [110,111]. With such hEF approach, the pollutant degradation efficiency can even extend to neutral pH conditions [98,109].

The choice of Fe-C as suitable hEF catalysts is based on their high catalytic activities for ORR, low cost, relative stability, eco-friendliness, ease of synthesis and abundancy of raw materials. The

popularity of the EF systems is highly compromised by high electrical energy demand that engender higher operational costs [45]. Hence, proper and adequate optimization of key parameters is averred to offer a practical solution [112]. Traditional univariate optimization probe one factor at a time while fixing the rest of the operational factors. This approach does not cater for the interactive effects of the main parameters, is expensive and time consuming for multi-parameter optimization [112]. Multivariate optimization techniques have therefore been introduced to merge process optimization of main variables with interaction effects; thereby maximizing the response output [80].

Out of the available response surface methodologies, central composite design (CCD) is the most flexible and efficient design capable of generating sufficient experimental data using fewer experimental runs [113].

In an effort to improve the in-situ generation of H_2O_2 and •OH, a simple and new droplet flow-assisted heterogeneous electro-Fenton (DFEF) reactor was fabricated and investigated for enhanced oxidation of trace level ß-blockers in hospital wastewater. The heterogeneous catalysts (Fe-C nanocomposite) used in this study, were synthesized from our previous work using hydrolytic sol-gel method and rice husk silica [114]. Herein, an extensive morphological characterization and evaluation of these catalysts for DFEF applications are provided. Two ß-blockers, denoted as PROP and ACE (propranolol and acebutolol) were selected as model pollutants. Response surface methodology based on CCD was used for both experimental design and optimization of the degradation efficiency. The degradation kinetics for both ACE and PROP were further investigated. The degradation process and intermediate species elucidation were followed using LC-MS/MS, from which plausible mechanisms were deduced.

4.2 EXPERIMENTAL

This study involved; (i) fabrication of a new DFEF reactor, (ii) synthesis, characterization of Fe-C catalysts and their evaluation for efficient DFEF operations at different pH conditions, (iii) CCD optimization of DFEF reactor, (iv) using optimized conditions to compare the degradation efficiency of DFEF reactor with other treatment modes, (V) degradation kinetic studies and, (vi) identification of degradation intermediates and mechanism elucidation.

4.2.1 Chemical and materials

Acebutolol hydrochloride (ACE) (≥98%) and propranolol hydrochloride (PROP) (≥99%) were purchased from Sigma-Aldrich. Ferric nitrate, $Fe(NO_{3)3}\cdot 9H_2O$ (99%), cetyltrimethylammonium bromide (CTAB), glycerol and high purity acids were purchased from Sigma-Aldrich. LC grade methanol, acetonitrile and formic acid were purchased from Fisher Scientific. In all experiments, 0.05 M Na_2SO_4 solution was used as a supporting electrolyte. Si/BDD electrode (2.75 µm BDD thin layer thickness (both sides) deposited on a conductive Si sheet, NeoCoat -Switzerland), graphite felt electrode (GFE) (5 mm thick PAN-based, Shanghai Qijie Limited Co., China). The pH of the sample solution was adjusted using 1M NaOH and H_2SO_4 (3 M). RHS/C.x%Fe composites were investigated as heterogeneous electro-catalysts. Rice husk used to produce biogenic silica was obtained from a rice mill in India. Double distilled water was used in this study. 0.2µm pores size syringe filters were purchased from Fisher Scientific. Hospital wastewater samples used for the degradation study were collected from the local medical center.

4.2.2 Synthesis of Fe-C nanocomposite (heterogeneous Fenton catalyst)

The detailed synthesis of Fe-C nanocomposites denoted as RHS/C-x%Fe from rice husk with different iron loading (5-20wt% Fe^{3+}) appears in our previous publication [114]. The synthesis explored the advantages of eco-friendly synthesis, waste management and utilization, and catalyst stability. The synthesis protocol involved the extraction of rice husk silica in form of sodium silicate that was used as a support for loading iron species (Fe^{3+}) and carbon. In brief, under constant stirring conditions, the silicate solution was titrated with either 3.0 M HNO_3 or 3.0 M HNO_3 containing appropriate amounts of Fe^{3+} in form of Fe $(NO_3)_3 \cdot 9H_2O$ (5, 10 and 20 wt. %) to pH 4.0. The result was either unmodified RHS/C-0%Fe or iron modified RHS/C-x%Fe sol-gel solutions. The resultant sol-gel solution was aged for 48 hours till gelation. The soft gel was recovered by centrifugation, washed clean with copious amount of deionized water and then oven dried (110 ^oC for 18 h). The dry gel was finally calcined at 700 ^oC for 5 h, ground into fine powder and labeled as RHS/C-xFe, where x denoted 0, 5, 10 15, and 20 wt% Fe^{3+}.

4.2.3 Catalyst characterization

Several physico-chemical techniques such as micromeritics and porosimetry analysis, field emission scanning electron microscopy, energy-dispersive X-ray analysis and Fourier Transform Infrared Spectroscopy were used to characterize the prepared catalysts. The details of these techniques were reported in our previous study [114].

In addition, X-ray Photoelectron Spectroscopy (XPS) (Thermo Scientific ESCALAB 250xi), was used to study the oxidation states and chemical composition of the elements present in the Fenton catalysts. Further, Transmission electron microscopy (TEM) was used to estimate the particle size and distribution within the Fenton catalysts. Selected Area Electron Diffraction (SAED) was used to study the phase composition of the catalysts which was confirmed by X-ray diffraction analysis at a continuous scan rate of 0.5^{o} /min, 0.02^{o} scan size and the Bragg's angle (2θ) range of 10-80°.

4.2.4 A new droplet-flow assisted heterogeneous electro-Fenton reactor (DFEF)

As shown in Fig.16, a novel DFEF reactor consisted of a fabricated 500 mL cylindrical continuous flow cell (Pyrex glass) designed to deliver fast droplet spray at the cathode electrode. Natural air was used as a nebulizing agent to deliver droplet spray of saturated air, catalyst and pollutant at the cathode electrode. The cell was equipped with GFE cathode and BDD anode electrodes (each with surface area of 4 cm^2) placed at a distance of 1 cm from the bottom of the reactor and 3 cm as inter electrode gap.

The reaction cell was powered by a direct current power source (Sargent Welch Scientific Ac/dc Power Supply, 0-22V, 4A) connected to a digital multimeter (auto range AC/DC voltage/ current, Fluke). With this kind of arrangement, highly enhanced cathodic ORR, Fe-C micro-electrolysis and Fe^{2+} regeneration led to fast production of ROS (H_2O_2 and $^{\bullet}OH$). Prior to every experiment, electrodes surfaces were cleaned and preconditioned with acetone and 35% HCl for 5 min and then rinsed with double distilled water.

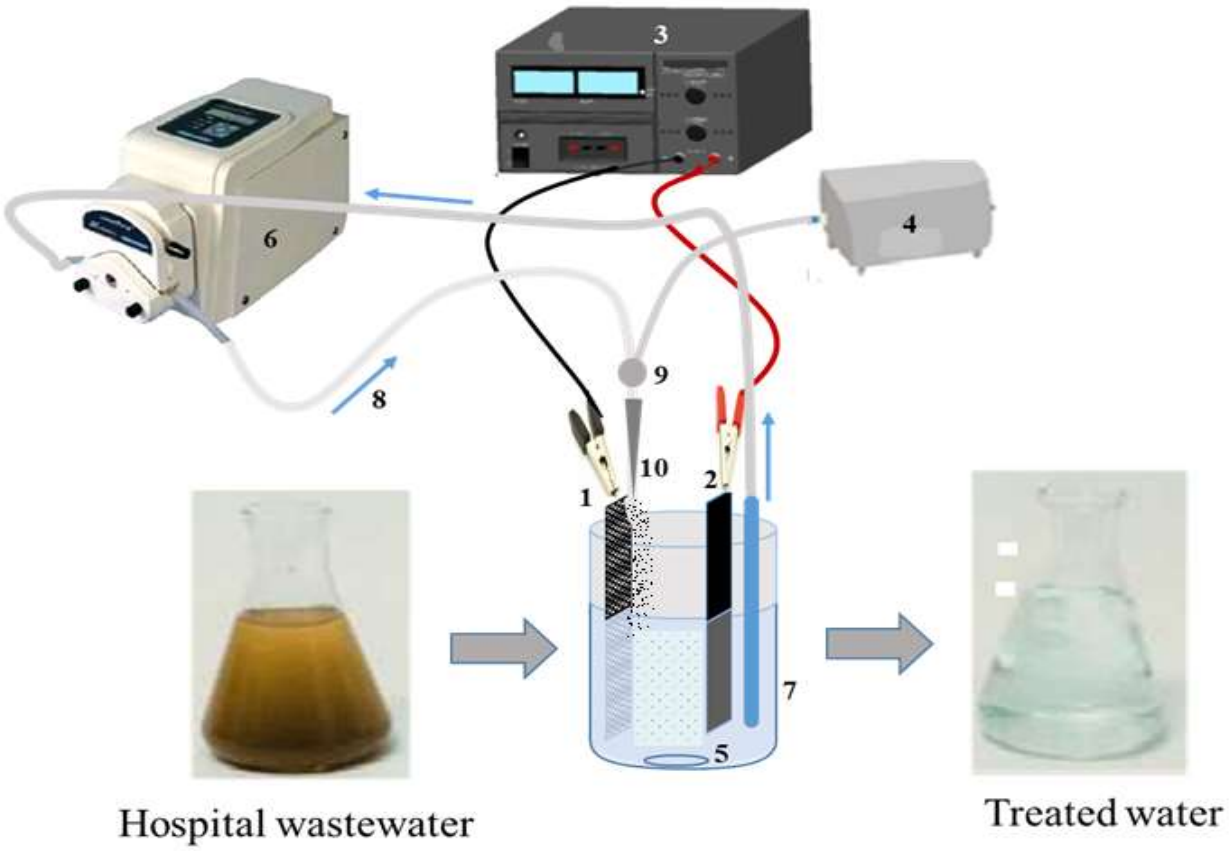

Figure 15: Schematic diagram of a droplet flow-assisted electro-Fenton reactor: (1) Graphite felt electrode acting as cathode, (2) Boron doped diamond electrode acting as anode, (3) DC power supply, (4) Air pump, (5) Magnetic stirrer, (6) Dual-headed peristaltic pump, (7) Electrolytic reactor, (8) Direction of sample flow (9) Junction for mixing natural air with untreated sample to form a droplet spray at cathode through (10)

4.2.5 Degradation and H_2O_2 evolution studies

Both degradation and H_2O_2 electro-generation experiments were conducted in the DFEF reactor (section 2.4) and at room temperature. For all the experiments, the sample solution was stirred magnetically. Prior to degradation studies, a working solution of 210 mL containing 0.05 M sodium sulfate (electrolyte) and defined amount of solid catalyst (Fe-C), were fed into the reactor. The resultant solution was then spiked with PROP/ACE standards at a predetermined concentration level based on the experimental design. The sample solution pH was initially left unadjusted and the reactor was allowed to operate for 30 min to allow the adsorption/ desorption equilibrium between the catalyst and sample at the cathode electrode surface to be established. 1 mL sample aliquots were continuously withdrawn from the electrolytic reactor at every 5 min time interval, filtered through polyether sulfone syringe filters (pore size, 0.2µm) before ultra-fast liquid chromatography tandem mass spectrometry, LC-MS/MS (LCMS-8050, Shimadzu, Japan) analysis. To evaluate the ß-blockers degradation efficiency (%), the concentrations of ACE and PROP in the sample solution before and after degradation were monitored using the developed LC-MS/MS method [114]. The degradation efficiency (% degradation) was calculated using equation 5.

$$Degradation\ efficiecy\ (\%) = \left(1 - \frac{A_t}{A_O}\right) x\ 100 \text{ ---------- (5)}$$

Where A_0 and A_t represent ß-blockers concentration at time (0) and (t) respectively.

Briefly, an ultra IBD column (100 x 2.1mm x 3µm particle size; Restek, USA) set at temperature of 40°C was used in separation of target analytes.

Gradient elution was carried out using solvent A (0.03% formic acid) and solvent B (methanol /acetonitrile, 25:75) and at a flow rate of 0.3 mL/min. The pump B gradient elution program followed: 0–40%, 0.01–1 min; 40–60%, 1–4 min; 100%, 4–5 min; and 20%, 5–7 min. Positive and negative electrospray ionization mode and multiple reaction monitoring (MRM) were used in acquiring mass spectra and quantification of all target analytes. Data acquisition and processing were controlled by LabSolutions software (LCMS Ver.5.91, Shimadzu). The potential of the proposed electrolytic reactor to electro-generate H_2O_2 was monitored using potassium titanium (IV) oxalate method [115]. Using this approach, the concentration H_2O_2 generated could be estimated on a Uv-vis spectrophotometer. Briefly, 1ml of filtered samples withdrawn from the electrolytic cell at regular time intervals were diluted with 1ml of deionized water (each) followed by addition of 4 ml titanium reagent (potassium titanium (IV) oxalate/ H_2SO_4). The sample mixture was mixed thoroughly for 5 min to allow the development of an intense yellow complex of pertitanic acid with H_2O_2. The samples were then analyzed using UV-vis spectrophotometric method at a wavelength of 400 nm.

4.2.6 Design of experiment using response surface methodology (RSM)

RSM is a statistical approach for practical model construction [105]. With this approach, fewer experimental runs can be used to evaluate the effect of independent parameters with their interactions on response through process optimization [79]. As a result, both time and resources are saved. The influence of independent variables on response can be statistically investigated and optimized by combining CCD to RSM [105].

Five parameters including initial ß-blocker concentration, [ß-blockers]$_0$ (X_1), catalyst dosage, Cat (X_2), current density, CD (X_3), electrolysis time, E.T (X_4) and sample pH (X_5) were selected as significant factors affecting the degradation efficiency of PROP and ACE.

Each parameter was evaluated at a five coded level standard (−2, −1, 0, +1, +2) with (–), (0) and (+) corresponding to low, center and high levels respectively. A CCD (2-level, half factorial, face centered) was applied to 5 variables resulting into 32 randomized experiments consisting of 10 axial, 16 cube and 6 replications at center point. The details of the CCD parameters, levels and ranges are presented in Table 14. All the experiments were performed in triplicate with the mean values presented. Minitab software (Version 17 Minitab Inc., USA) was used in CCD experimental design construction, data modeling, regression analysis and optimization. Three-dimensional (3-D) surface and two-dimensional (2-D) contour plots were used to illustrate the interaction between process variables and responses. The optimum operating conditions were established by CCD based on desirability function (DF) through fitted models and further validated through requisite experiments [79]. The DF value ensured that the process optimized variables satisfy the targeted response output.

Table 14: Factors, levels and ranges used for CCD construction

Variable	Ranges and levels				
	-2	-1	0	1	2
X_1(ng mL^{-1}) [ß-blocker conc.]$_0$	200	400	600	800	1000
X_2 (mg L^{-1}) Catalyst	23.8	71.4	119	166.7	214.3
X_3 (mA cm^{-2}) Current density	25	50	75	100	125
X_4 (min) Electrolysis time	5	10	15	20	30
X_5, pH	3	4	5	6	UN

4.3 RESULTS AND DISCUSSION

4.3.1 Heterogeneous Fenton catalyst characterization

The synthesized heterogeneous Fenton catalysts were characterized with different techniques.

4.3.1.1 TEM and SAED

TEM micrographs (Fig. 16a and 16 b) provided more insights into the effect of Fe^{3+} loading on microstructure of the synthesized RHS/C-10%Fe nanocomposite catalyst. Both samples demonstrated uniform and highly disordered microstructures with no evidence of agglomeration. SAED (inset in Fig. 16a and b) analysis confirmed the absence of crystalline material in both samples and confirmed their amorphous nature.

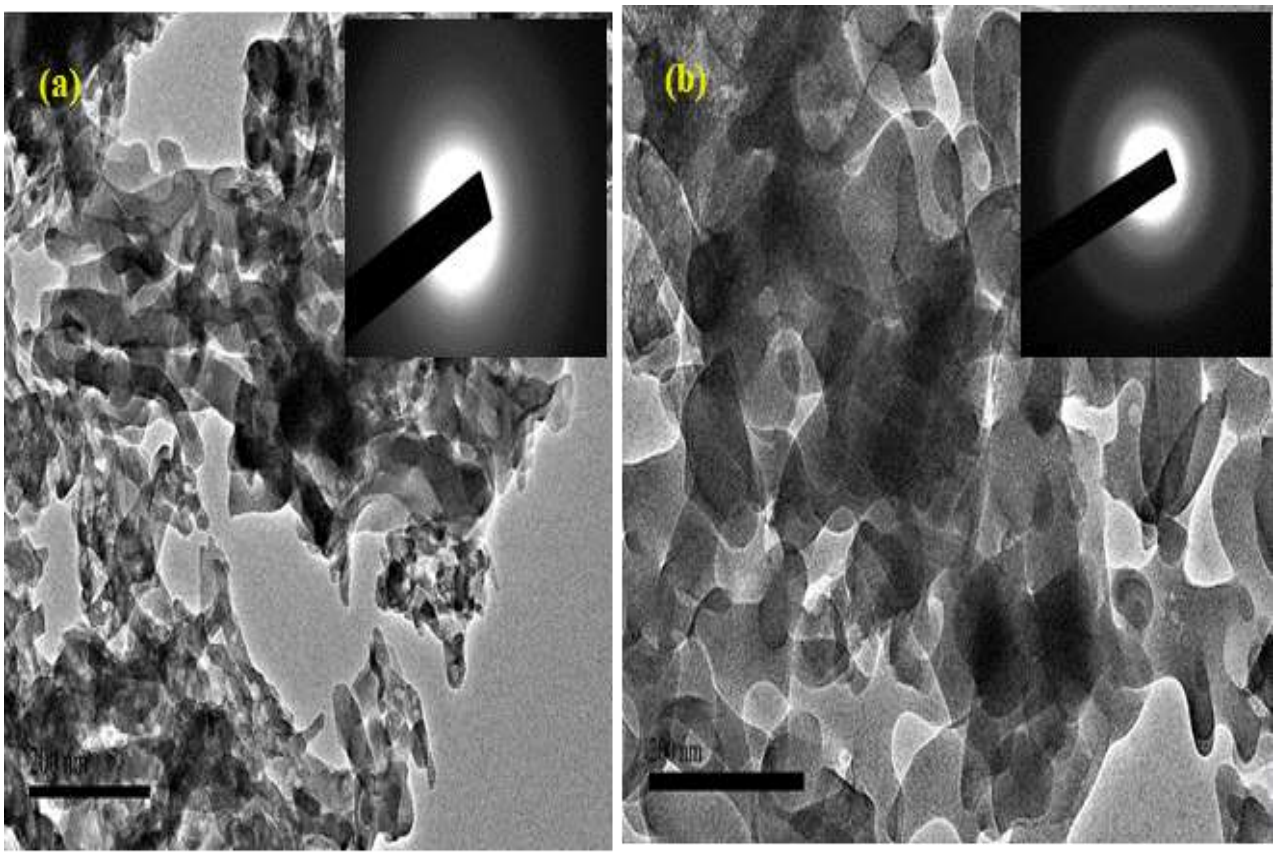

Figure 16: TEM micrographs; (a) RHS/C-0%Fe, (b) RHS/C-10 %Fe (inset the SAED images for a and b respectively)

4.3.1.2 XRD

These SAED results (Fig 16a and 16 (in-set) corresponded well with XRD spectral patterns (Fig.17) in which a broad peak, typical of amorphous structures was observed at around 23 ^{o}C, for both samples. XRD pattern (Fig. 167) confirmed the absence of crystalline metal/metal oxide phases in the synthesized nanocomposites even after metal loading.

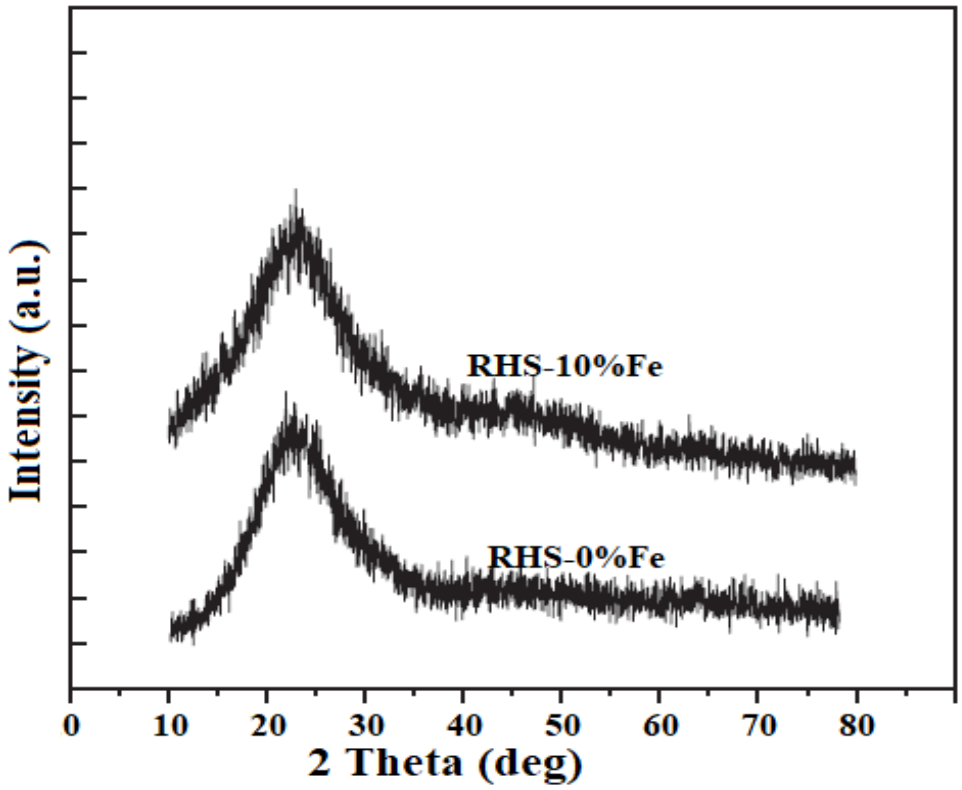

Figure 17: XRD patterns of synthesized of RHS/C-0%Fe and RHS/C-10 %Fe used as Fenton catalysts

4.3.1.3 XPS

XPS is a very valuable surface characterization technique used to ascertain elemental composition as well as oxidation states within sample of interest [116]. It provides insightful analysis of the electronic as well as chemical environments of the elements under study. The XPS spectra of the nanocomposites were measured (Fig. 18) and the survey (18 a) and high-resolution scans (18 c-f) for relevant core levels used in our study were recorded for metal free (RHS/C-0% Fe) and RHS/C-10% Fe nanocomposite catalyst respectively. Figure 18 (b) clearly revealed the results of the XPS elemental composition of the survey spectra as: C-1s, O-1s, Si-1s and Fe-2p in appropriate amounts for the two nanocomposite catalysts. They further indicate the presence of iron and carbon in the synthesized nanocomposites. Shown in Fig. 18 (f) is the Fe-2p spectrum of the RHS/C- 10%Fe. Due to spin-orbit coupling Fe-2p peak splits into two peaks Fe-$2p_{3/2}$ and Fe-$2p_{1/2}$ located at 712 eV and 726 eV, respectively. These Fe-2p peak details are in the ranges reported in literature [117]. X_3 and X_4 are shake-up satellite peaks characteristic of Fe_2O_3 lattice [117] while X_1 and X_2 are their respective spin-orbit components. Shown in Fig. 18 (e) is the C1s spectrum that was deconvulated into two peaks at 284.8 eV and 287.2 eV. The C 1s peak at 284.8 eV is due to graphitic carbon and is used as a reference line for any charging effect. The peak at 287.2 eV corresponds to carbon linked to the alcohol group. The deconvoluted spectra for silicon (Si-1s) and oxygen (O-1s) (Fig.18d and c) show binding energy peak at 102.5 eV assigned to Silicon while peaks at 529.2, 531.1 eV are assigned to O-1s and are typical of Fe_2O_3 and SiO_2 respectively.

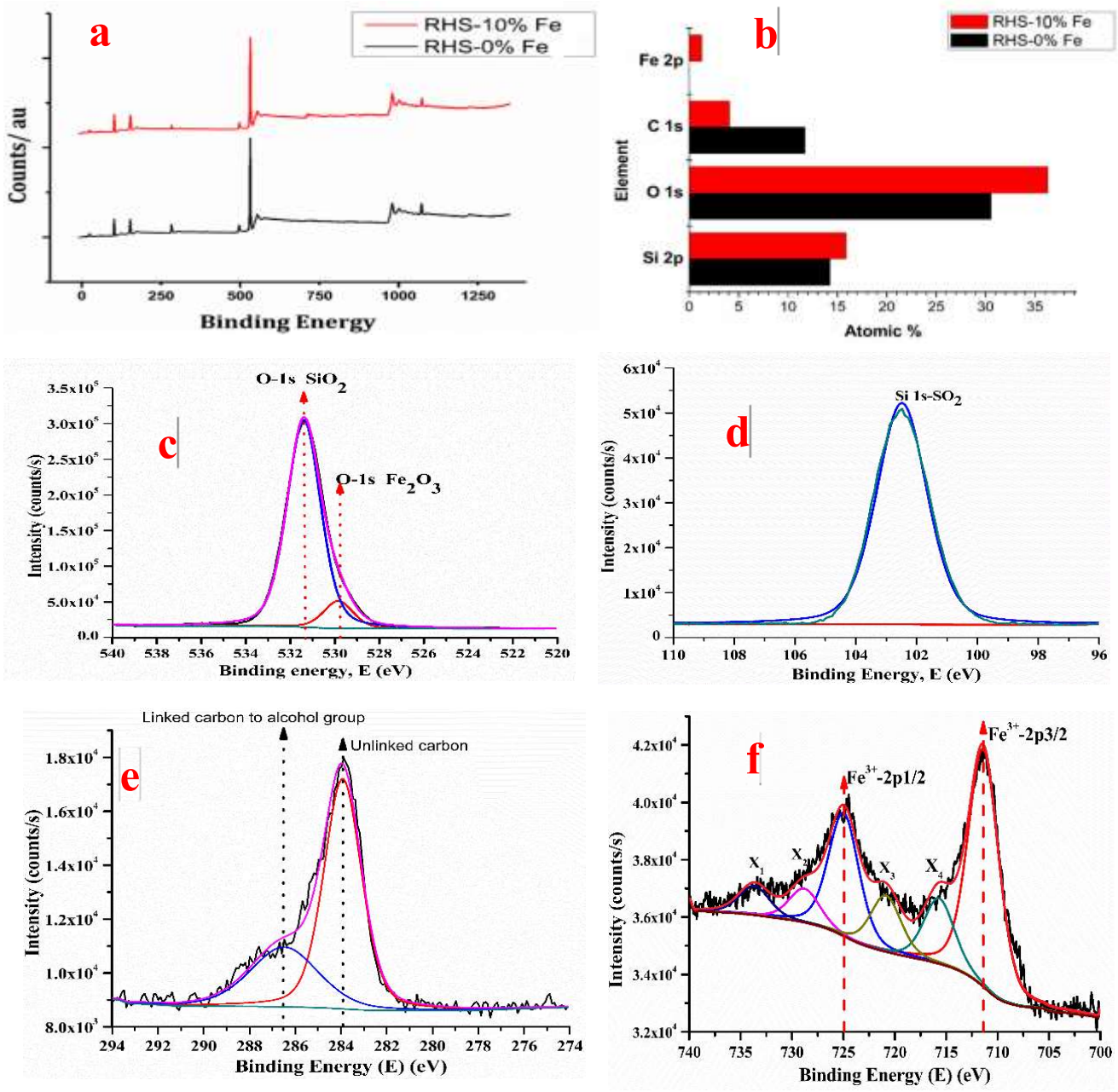

Figure 18: XPS investigation: (a) survey spectra's for RHS/C-0%Fe and RHS/C-10%Fe nanocomposites (b) elemental composition. Figure 18 (c-e) represent high resolution XPS spectras for; (c) oxygen (O 1s) (d) silicon (Si 1s) (e) carbon (C I s) (f) iron (Fe 2p)

4.3.2 Preliminary studies

4.3.2.1 Selection of a suitable Fenton catalyst for a DFEF reactor

In preliminary experiments, the synergetic contribution of the new DFEF reactor and the synthesized solid catalysts was evaluated for effective ß-blockers degradation at different iron loading and pH conditions. The oxidation power of an EF process is largely enhanced by the efficient Fe^{2+} regeneration [110]. Hence, proper iron loading in RHS/C matrix promotes effective degradation efficiency in a DFEF system. Fig. 19a, illustrate the results of ß-blockers degradation efficiencies at natural pH (without pH adjustment) using different catalysts with a current density of 75 mA/cm^2 and sample concentration of 200 µg/L. As clearly indicated, the rate of degradation increased with increase in iron loading up to 10% (RHS/C-10%Fe). However, beyond 10 % Fe loading, the degradation efficiency underwent a significant decrease due to $^{\bullet}OH$ scavenging effect of electro-generated $^{\bullet}OH$ with excess Fe^{2+} via reaction equation (7 and 8). The system's capacity to generate hydroxyl radical reduces gradually, resulting to a decrease in ß-blocker degradation efficiency. It is well illustrated in Fig. 19 (a) that the degradation efficiencies for both ACE and PROP followed a similar degradation pattern. This is supported by the fact that ß-blockers have nearly similar building blocks. Fig. 19 (b) depicts the decay profile of ACE at different iron loading for 60 min. As illustrated, when there was no iron loading (0%Fe), the degradation of ACE was very poor and could not be completed in even 60 minutes. This observation clearly supported the contribution of Fe^{2+} in the enhancement of ACE degradation efficiency. The major degradation process taking place at 0% Fe loading was anodic oxidation.

However, when a 5% Fe loading was used (RHS/C-5%Fe), there was a slight improvement in the degradation efficiency of ACE.

This could be explicated by the excessive H_2O_2 generation in the DFEF reactor system at very low Fe^{2+} ions concentration. At these conditions (low Fe^{2+} formation), less H_2O_2 is utilized in $^{\bullet}OH$ radical production, with the excess H_2O_2 preying on the already produced $^{\bullet}OH$ radicals to form less reactive $HO^{\bullet}_2$ (equation 6). When the % iron loading was doubled (RHS/C-10%Fe), the ACE degradation efficiency was greatly enhanced leading to fast and complete ACE degradation before 15 min of treatment. At a higher iron loading (RHS/C-20%Fe), the ACE degradation efficiency decreased tremendously due to scavenging effect of $^{\bullet}OH$ by excessively regenerated Fe^{2+} (equation 7 and 8). Because of the relatively low BET surface area of RHS/C-10%Fe composite catalyst [114], it was assumed that the contribution of catalyst adsorption of ß-blockers in HWW was negligible. The highly dispersed Fe-C nanoparticles, increased effectively the number of active sites on the nanocomposite catalyst at the cathode and the entire sample solution, leading to effective H_2O_2 catalytic activity activation.

$$H_2O_2 + {}^{\bullet}OH \rightarrow H_2O + HO_2^{\bullet} \quad \text{(6)}$$

$$Fe^{2+} + HO_2^{\bullet} \rightarrow Fe^{3+} + HO_2^{-} \quad \text{(7)}$$

$$Fe^{2+} + {}^{\bullet}OH \rightarrow Fe^{3+} + {}^{-}OH \quad \text{(8)}$$

Since some Fe^{2+} ions were regenerated at the cathode electrode and some from the micro-electrolytic cells within the sample solution, a 10%Fe loading (RHS-10%Fe) composite catalyst was selected for subsequent DFEF experiments.

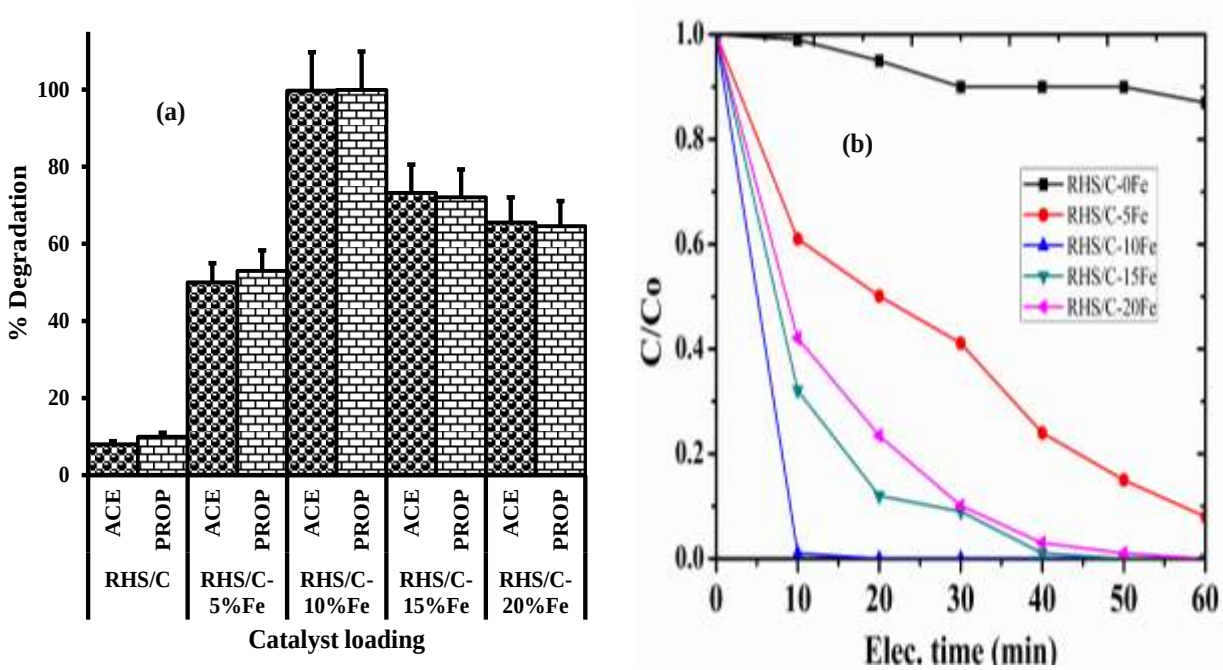

Figure 19: Selection of a suitable heterogeneous Fenton catalyst in a DFEF reactor: (a) degradation profile of both ACE and PROP for a sample solution (without pH adjustment) (b) degradation profile of ACE at varying electrolysis time. (200 µg/l ß-blocker spiking concentration, I= 75 mA/cm^2, $[Na_2SO_4]_0$ = 0.05 mol L^{-1}, 119 mg/L of RHS-x%Fe catalyst dosage and 60 min electrolysis time).

4.3.2.2 Evaluation of DFEF reactor for H_2O_2 electro-generation

The effectiveness of a hEF reactor depends on its high potential for in situ H_2O_2 electro-generation and $^{\bullet}OH$ radical production leading to enhanced pollutant oxidation [98]. The DFEF reactor system was investigated for H_2O_2 electro-generation and degradation efficiencies at various operating conditions; (1) under droplet flow mode and normal flow mode but without a Fenton catalyst, (2) at different current densities (0, 50, 75, 125 mA cm^{-2}). Fig. 20 (i) shows the H_2O_2 concentration produced on the graphite felt cathode electrode as a function of time while 20 (ii) depicts acebutolol degradation profile using a DFEF reactor at varying applied current. It is well reported in literature that the rate of cathodic H_2O_2 generation and decomposition is current dependent [118]. From Fig. 20 (i), it is observed that It is evident in Fig. 20 (ii) that ACE degradation efficiency under DFEF conditions increased with increase in current density from 0 to 75 mA/cm^2 and then decreased at a higher current density (125 mA/cm^2). This trend is ascribable to the proposed reactor design that facilitated an increase and fast generation of ROS (H_2O_2 and $^{\bullet}OH$) [105,111]. The progressive increase in H_2O_2 electro-generation is enhanced by the reactor design that allows a large surface area electrode to be in contact with the sample solution saturated with both air and Fenton solid catalyst. At high current density (125 mA/cm^2), the H_2O_2 electro-generation reduces greatly due to H_2O_2 loss resulting from its oxidation at the anode surfaces (equations 6 and 7) [18].

$$H_2O_2 \rightarrow HO_2^{\bullet} + H^+ + e^- \quad \text{(6)}$$

$$HO_2^{\bullet} \rightarrow O_2 + H^+ + e^- \quad \text{(7)}$$

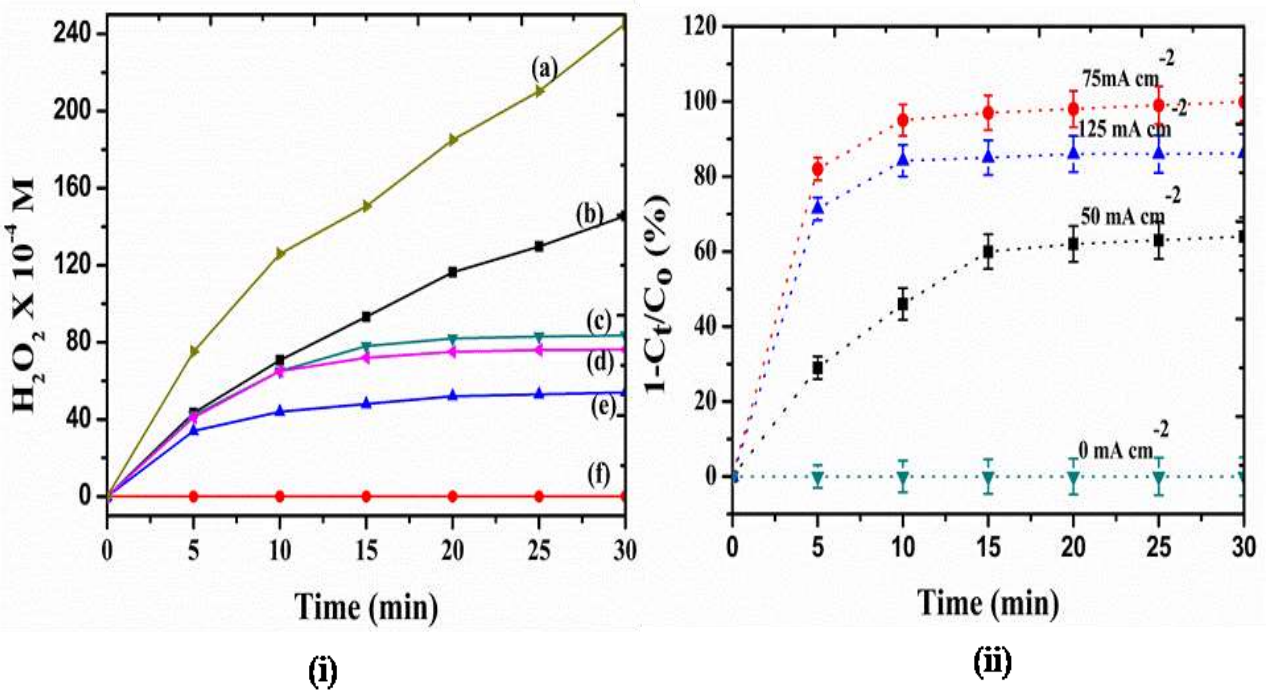

Figure 20: (i) H_2O_2 concentration generated as function of time for DFEF at various conditions; (a)- droplet flow mode (DFEF, no catalyst), (b) Normal flow- electro-Fenton (FEF, no catalyst), (c) DFEF at 75 mA cm^{-2}, (d) DFEF at 125 mA cm^{-2}, (e) DFEF at 50 mA cm^{-2}, (f) DFEF at 0 mA cm^{-2} (ii) DFEF degradation profile for acebutolol. $[Na_2SO_4]$ = 0.05 M, RHS/C-10%Fe dosage = 119 mg L^{-1} and sample pH = 3, spiking $[ACE]_0$ = 200 ng mL^{-1}. Current density for (i) a and b = 75 mA cm^{-2}

4.3.3 Statistical experimental design, analysis, validation and optimization

4.3.3.1 Development of a model's regression equation

CCD is capable of providing high-quality predictions over the entire design space using minimal experimental runs as compared to other design types [113]. The 5-variable CCD design matrix, experimental and predicted responses, resulting from percentage degradation of ß- blockers is presented in in Table 15. The average experimental ß- blockers DE (%) results ranged from 31.41 to 96.61 % while the calculated values ranged between 33.2 and 96.02 %.

Table 15: The CCD experimental design of independent test variables and design table of average ß-blocker degradation (%) in the DFEF reactor system.

Run	X_1	X_2	X_3	X_4	X_5	Experimental % degradation			Calculated % Degradation
						PROP	ACE	AVE	AVE
1	600	119	75	15	5	78.19	84.73	81.46	80.66
2	600	119	75	15	5	77.47	84.03	80.75	80.66
3	200	119	75	15	5	90.16	96.46	93.31	96.02
4	260	115	75	15	5	77.92	84.48	81.20	80.66
5	400	71.4	100	20	6	93.09	99.35	96.22	95.07
6	400	71.4	50	20	4	88.41	94.75	91.58	89.87
7	800	71.4	100	20	4	77.05	83.61	80.33	81.62
8	1000	119	75	15	5	85.43	91.83	88.63	85.88
9	600	119	25	15	5	62.13	68.99	65.56	68.81
10	600	214.3	75	15	5	58.57	65.51	62.04	57.16
11	800	71.4	50	20	6	68.38	75.12	71.75	70.33
12	800	71.4	50	10	4	33.03	40.47	36.75	35.50
13	600	119	125	15	5	90.28	96.58	93.43	90.13
14	400	166.7	50	20	6	78.15	84.69	81.42	81.06
15	600	119	75	5	8	27.64	35.18	31.41	33.20
16	800	71.4	100	10	6	58.36	65.30	61.83	61.13
17	400	166.7	50	10	4	53.69	60.73	57.21	57.02
18	600	119	75	15	5	76.50	83.08	79.79	80.66
19	600	23.8	75	15	5	31.11	38.59	34.85	39.68
20	600	119	75	15	3	75.90	82.50	79.20	77.02
21	600	119	75	15	UN	75.41	82.01	78.71	80.84
22	800	166.7	100	10	UN	54.92	61.92	58.42	61.23
23	600	119	75	15	5	76.02	82.60	79.31	80.66
24	800	166.7	50	20	4	79.16	85.68	82.42	84.50
25	400	166.7	100	20	4	88.28	94.62	91.45	93.81
26	400	71.4	50	10	6	42.81	50.05	46.43	42.73
27	400	166.7	100	10	6	68.18	74.92	71.55	71.92
28	800	166.7	50	10	6	54.93	61.93	58.43	58.53
29	800	166.7	100	20	6	83.21	89.65	86.43	89.07
30	600	119	75	15	5	78.14	84.68	81.41	80.66
31	400	23.8	100	10	4	48.41	55.55	51.98	51.00
32	600	119	75	30	5	93.49	99.73	96.61	94.77

UN-Un adjusted pH

Regression analysis (Table 16) was then used to compare and correlate responses with the independent parameters. This simplified to an empirical second order polynomial full equation (equation 8) that was used to predict responses.

$$Y(\text{coded value}) = 80.66 - 1.27[ß]0 + 2.18Cat + 2.6CD + 7.7ET + 0.48pH + 0.64[ß]_0^2 - 2.01Cat^2 - 0.07CD^2 - 1.04\ ET^2 - 0.11pH^2 + 0.31[ß]_0*Cat + 0.05[ß]_0*CD - 0.44[ß]_0*ET + 0.27[ß]_0*pH - 0.24\ Cat*\ CD - 0.73\ Cat*ET - 0.11\ Cat*pH - 0.28CD\ *\ ET + 0.68\ CD*pH - 0.69\ ET*pH \quad \ldots\ldots\ldots\ldots\ (8)$$

Where 'Y' is the average percentage ß-blocker degradation for both PROP and ACE, $[ß]_0$ = initial concentration of ß-blocker, Cat = catalyst dosage, CD = current density, ET for extraction time and pH for sample pH.

Table 16: CCD regression analysis table for DFEF degradation of ß-blocker (ACE and PROP) CCD regression analysis table for DFEF degradation of ß-blocker (ACE and PROP)

Term	Coef	SE coef[a]	T	P
Constant	80.6611	1.4886	54.184	<0.0001
$[ß]_0$, X_1	-2.535	0.7618	-3.327	0.007
Cat, X_2	4.3683	0.7618	5.734	<0.0001
C.D, X_3	5.3317	0.7618	6.998	<0.0001
E.T, X_4	15.3917	0.7618	20.203	<0.0001
pH, X_5	0.9558	0.7618	1.255	0.236
$[ß]_0$*$[ß]_0$	2.5714	0.6891	3.731	0.003
Cat * Cat	-8.0599	0.6891	-11.696	<0.0001
C.D * C.D	-0.2974	0.6891	-0.432	0.674
E.T * E.T	-4.1686	0.6891	-6.049	<0.0001
pH * pH	-0.4324	0.6891	-0.627	0.543
$[ß]_0$* Cat	1.2262	0.9331	1.314	0.216
$[ß]_0$* C.D	0.1937	0.9331	0.208	0.839
$[ß]_0$* E.T	-1.75	0.9331	-1.876	0.087
$[ß]_0$* pH	1.07	0.9331	1.147	0.276
Cat * C.D	-0.9675	0.9331	-1.037	0.322
Cat * E.T	-2.9237	0.9331	-3.134	0.01
Cat * pH	-0.4538	0.9331	-0.486	0.636
C.D * E.T	-1.1062	0.9331	-1.186	0.261
C.D * pH	2.7363	0.9331	2.933	0.014
E.T * pH	-2.74	0.9331	-2.937	0.014

A polynomial model provides a good fit that compares the experimental with the predicted results [113]. To assess and prove the reliability of the model, the predicted/ calculated values were plotted against the experimental/ actual degradation values (%) (Fig. 21) resulting to data points that lie closer to a straight line with coefficient of determination (R^2) values for average ß-blocker (ACE and PROP) = 0.9851. Such R^2 value closer to unity, fall within the desirability limit and hence the model is capable of capturing the relationship between the input parameters and output responses [80].

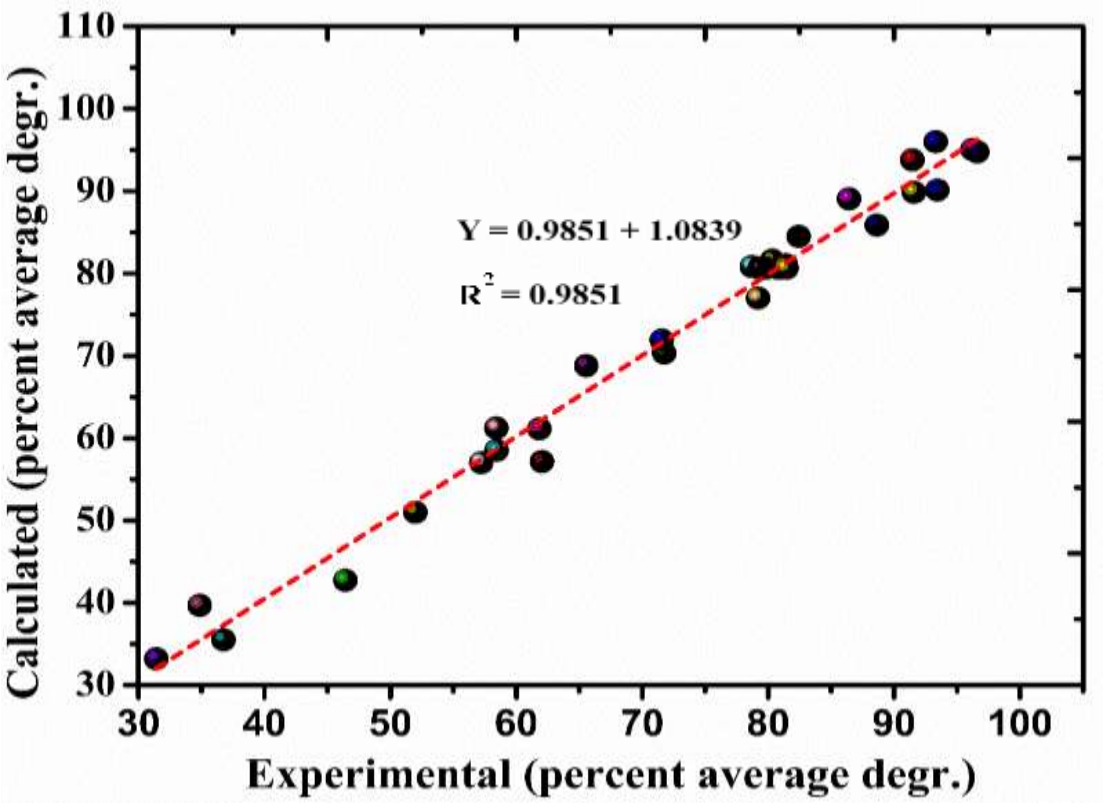

Figure 21: Calculated versus experimental percentage average degradation for ß-blockers.

4.3.3.2 Interpretation of ANOVA

ANOVA (Table 4) was used to test the adequacy and significance of the CCD model by comparing treatments and variations in random errors underlying response measurements [79]. This comparison is therefore affected using the F-value which is obtained by dividing the mean squares (MS) of the model by that of the residual error. The distant the F value is from the tabulated value (2.352 at significance of 95%), the stronger the confidence in the ability of a given model/ factor to explain adequately the existing variation [113]. From Table 17, the obtained F-value (36.43) was greater than the tabulated F-value and had P-value <0.0001, statistically signifying that, the existing variations could be well explained by the generated regression model equation [101]. In addition, the "P-values > F-values" and <0.05 (at 95% confidence level) indicate the significance of the terms, otherwise, terms with P-value >0.05 are insignificant [79]. The quadratic, square and linear term effects were found significant (their P-values were less than 0.05 at significance level of 95%). The interactions effects were generally identified basing on p-values < 5% of significance level that confirms their statistical significance. This meant that the selected factors for the CCD model had a pronounced contribution towards ß-blocker's degradation efficiency (%).The determination coefficient (R^2) is used to measure variation of the data generated from the model and R^2 values closer to 1 are prone to less errors [113]. The recorded responses for average ß-blocker degradation is well fitted to the mathematical model with a regression coefficient (R^2) of 0.9851 (>0.900). The higher R^2 values further demonstrated that the model's high capacity to predict responses. The lack of fit values were > 0.05, showing the insignificancy; an indication of good predictability of the model. Higher adjusted R^2 (95.81%) values closer to R^2 (98.51%) signify a desirable quality fit between the model and the experimental data.

Table 17: ANOVA for the degradation of ß-blockers by DFEF

Source of variation	DOF	% Degradation efficiency			
		Adj. SS	Adj. MS	F-value	P-value
Regression model	20	10148.00	507.40	36.43	<0.0001
Linear	5	7002.10	1400.41	100.54	<0.0001
Square	5	2639.50	527.89	37.90	<0.0001
Interaction	10	506.50	50.65	3.64	0.0220
Residual error	11	153.20	13.93		
Lack-of-fit	6	149.10	24.86	30.45	0.0010
Pure error	5	4.10	0.82		
Total	31	10301.30			
R-Squared (R^2)				98.51%	
Adjust R^2 (Adj R^2)				95.81%	
Predicted R^2 (Pred R^2)				88.03%	
Standard Deviation (SD)				0.829	

Since we had 32 observations (experimental runs), the DOF, total degrees of freedom is 31 corresponding to (n − 1). 'SS' refers to the sum of squares within groups (error) and sum of squares between groups (factor), 'MS' corresponds to mean squares (got by dividing the sum of squares by the degrees of freedom).

4.3.3.3 Interpretation of Residual plots for further validation of the CCD model

The CCD model was further examined and validated using residual analysis (Fig. 22 a-d). Residuals in Fig. 22 (a) lie along the straight line which proved normality of residual distribution. It is evident from the plot (Fig.22a) that the data used in the experiments were normally distributed. The normalcy of these residuals signified error consistence with acceptable normal distribution, generating a completely randomized design. The residual versus fitted value plot displayed in Fig.22b were nearly normally distributed and did not follow any definite pattern. This observation is characteristic of randomly and normally distributed residuals, hence typical of a good model. Fig.22c displays a histogram of symmetrically distributed residuals in which most measurements/ data were concentrated around the center. This suggests lack of outliers in a normally distributed data. The residuals versus observation order plot (Fig.22 d) indicated that the measurements were centered and closer to the central line (0.0), with no evidence of outliers in the observation order.

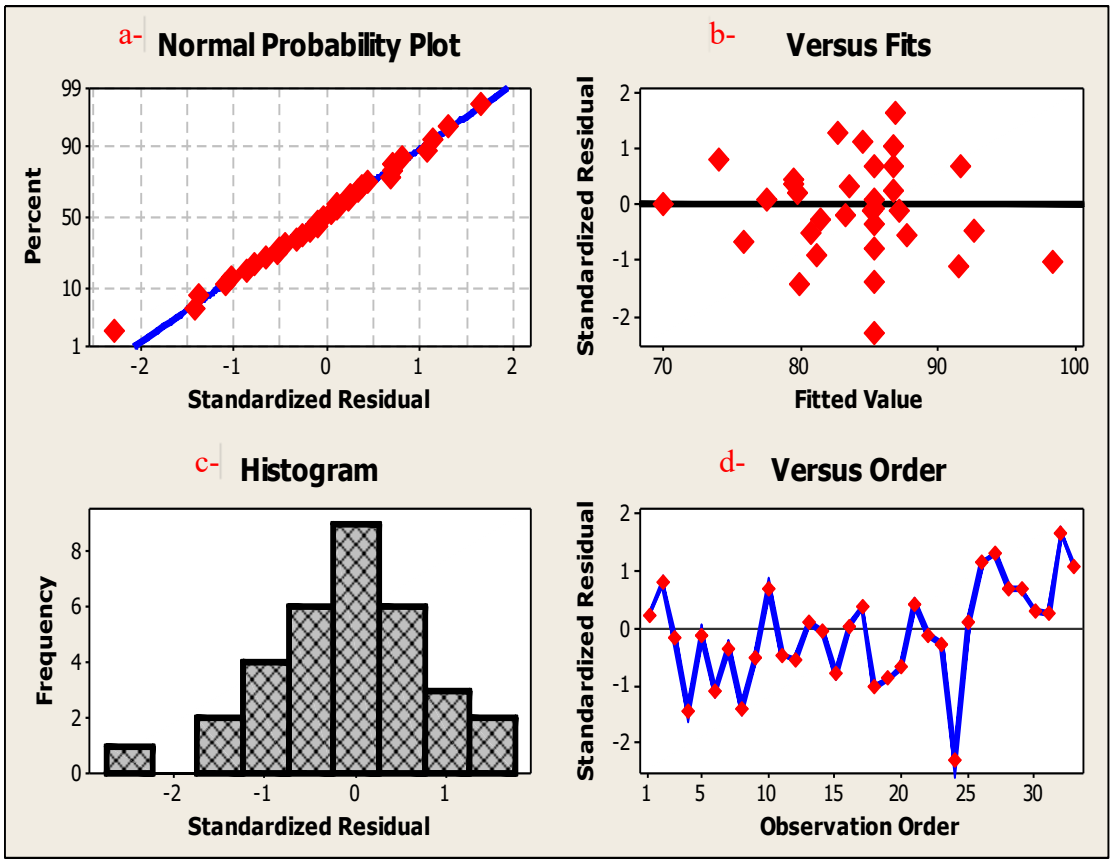

Figure 22: Residual plots for the percentage average ß-blockers (ACE and PROP) removal

4.3.3.4 Pareto chart analysis

The Pareto chart (Fig.23) was used in evaluating the level of significance of each variable/ combined effect, on the target response. It systematically analyses and presents the results of the regression analysis in a logical form. The terms/ effects on negative side of the Pareto chart signify antagonistic effects towards response, while those on the positive side signify synergistic effects [80]. The dominance of each term/effect on the Pareto chart is determined by the height of the corresponding bar. Accordingly, the electrolysis time (ET) was the most influential variable followed by current density (CD) and then catalyst dosage (Cat). These main variables displayed a pronounced synergistic effect while the effect of initial ß-blocker concentration $[ß]_0$ was antagonistic towards DE (%). In addition, the compounded effect of CD*pH, $[ß]_0$*$[ß]_0$, $[ß]_0$*Cat and $[ß]_0$*pH were synergistic while Cat*ET, ET*pH, Cat*Cat and ET*ET were found antagonistic.

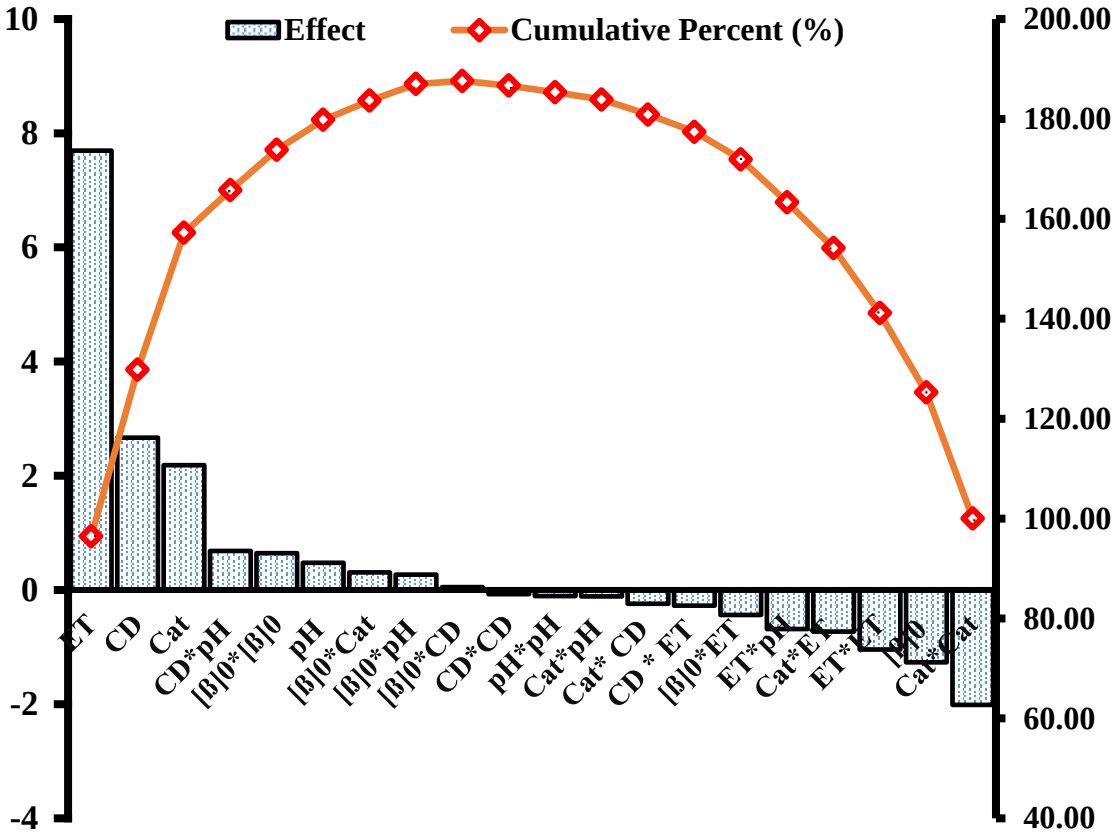

Figure 23: Pareto effects graphic analysis for the average degradation (%) of ß-blockers ACE and PROP

4.3.3.5 Effect of operational variables on ß-blockers DE (%)

3D-dimensional surface response plots (Fig. 24) were used to understand the contribution of main/ combined variables on degradation efficiency (%). Figure 24 (a) demonstrates the simultaneous effect of catalyst dosage (Cat) and electrolysis time (ET) on [ß-blocker]$_o$ degradation efficiency (%) at fixed [ß-blocker]$_o$ of 600 ng mL^{-1}, current density of 75 mA cm^{-2}, and electrolysis time of 15 min. As illustrated in plot (Figure 24 a), initial increase in both catalyst dosage and electrolysis time, increases degradation efficiency (%) up to optimum values and then decreases. Catalyst dosage (RHS/C-10%Fe) played an important role in enhancing the H_2O_2 decomposition rate to •OH radicals which in turn greatly improved the degradation efficiency. Initially, there was increased production of •OH from the increasing regeneration of Fe^{2+} ions (equation 2 and 3) for RHS/C-10%Fe composite catalyst, however, beyond the optimum value, the degradation efficiency reduced due to scavenging effects of Fe^{2+} (equations 9 and 10).

$Fe^{2+} + HO_2^{\bullet} \rightarrow Fe^{3+} + HO_2^-$……..... (9)

$Fe^{2+} + {}^{\bullet}OH \rightarrow Fe^{3+} + {}^-OH$…… (10)

Fig.24 (b) demonstrated the effect of combined variables (initial ß-blocker concentration and current density) on degradation efficiency. Initial increase in both ß-blockers concentration and current density improved DE (%) due to enhanced electro-generation of hydrogen peroxide and subsequent $^{\bullet}OH$ production [94].

These observations were in agreement with the weak synergistic cross interaction effects of [ß-blockers]$_0$ * CD of the Pareto chart.

As is illustrated in Fig.24 (c), the effect of electrolysis time and sample pH as a function of DE (%) at fixed [ß-blocker]$_0$ = 200 ng mL^{-1}, catalyst dosage (119 mg L^{-1}) and current density of 75 mA cm^{-1} is presented. As observed, the interaction effect of both pH and electrolysis time was antagonistic towards degradation efficiency (DE %). This observation is supported by the fact that the effective operation of the proposed DFEF reactor system with RHS/C-10%Fe is meant to cover a wider pH condition. Iron precipitation did not occur in such reactor system, and the effect of H_2O_2 decomposition at varying pH was unaffected because of its continuous H_2O_2 electro-generation and catalytic regeneration of Fe^{2+}.

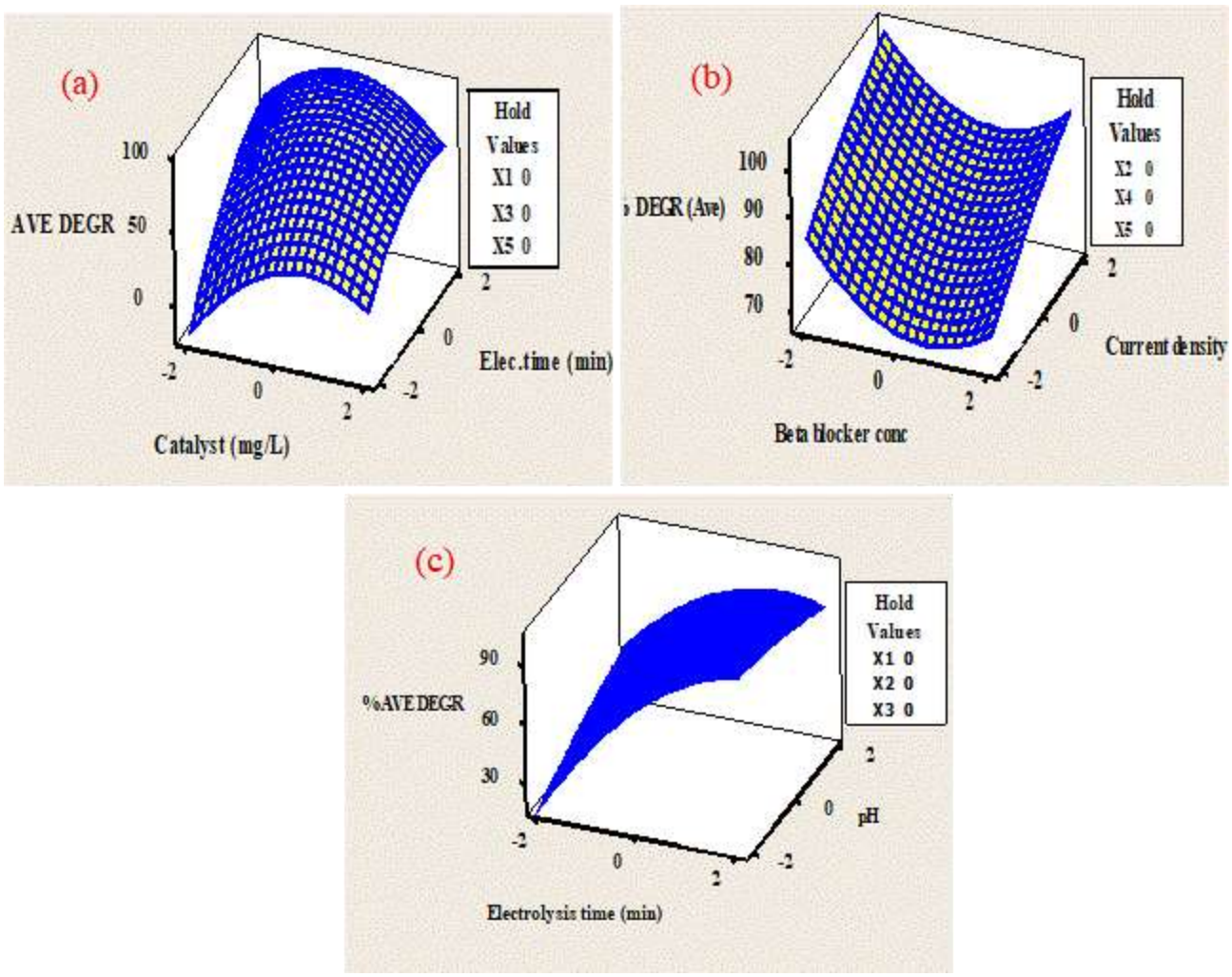

Figure 24: Response surface plots of the degradation efficiency (%) as the function of (a)- Catalyst dosage (mg L^{-1}) and reaction time (min), (b)- initial ß-blocker concentration [ß-blocker]0 and current density (mAcm-2) (c)-Electrolysis time (min) and pH.

4.3.3.6 Response optimization using desirability function (DF)

Response optimization based on desirability function [114] was used in identification of optimum conditions of the variables that resulted to maximum response. DF is a well-established approach for simultaneous determination of optimum values of input parameters with the aim of maximizing the performance levels of single or multiple responses. The stages involved in using DF to maximize response (s) is detailed in reference [119]. 100% was set as target value for the % ß-blocker degradation, a lower value of 31.41, and an upper value of 110 (since the upper value had to be > the target value. Finally, the importance and weight were both set to 1. The optimized conditions for degradation of ß-blockers with a composite desirability score of 0.99981 were catalyst dosage of 119 mg L^{-1}, current density of 75 $mAcm^{-1}$, electrolysis time of 15 min, sample pH=7 and $[ß\text{-blocker}]_0$ of 200 ng mL^{-1} to realize 99.99% degradation efficiency. Triplicate experiments were conducted at optimized degradation conditions resulting to complete degradation efficiency for both PROP and ACE.

4.4 Comparing the performance of DFEF with other treatment modes

At optimized conditions, the degradation efficiency of DFEF reactor was compared with other treatment modes (ie batch electro-Fenton (BEF), flow electro-Fenton and anodic oxidation (AO) as shown in Fig. 25. Similar experimental set-ups were used with some modifications to incorporate the mode used. With AO, the experiments were run in absence of RHS/C-10%Fe catalyst. Results obtained from the study clearly show the following trend of performance: AO > BEF > FEF > DFEF.

Highly improved ß-blockers degradation efficiency (%) by DFEF (Fig. 25) is due to combined enhancement effects leading to accelerated electro-generation of hydroxyl radicals.

The DFEF treatment mode, is highly favored by the synergistic degradation contributed by the droplets chemistry in the flow mode [109], micro-electrolysis from the iron-carbon nanocomposite [110]. For anodic oxidation, highly reactive •OH radicals are generated from the water oxidation and get adsorbed at the BDD electrode (Anode) while the E-Fenton equations (1-3) leading to bulk generation •OH radicals in sample solution, all contribute towards effective oxidation of ß-blockers.

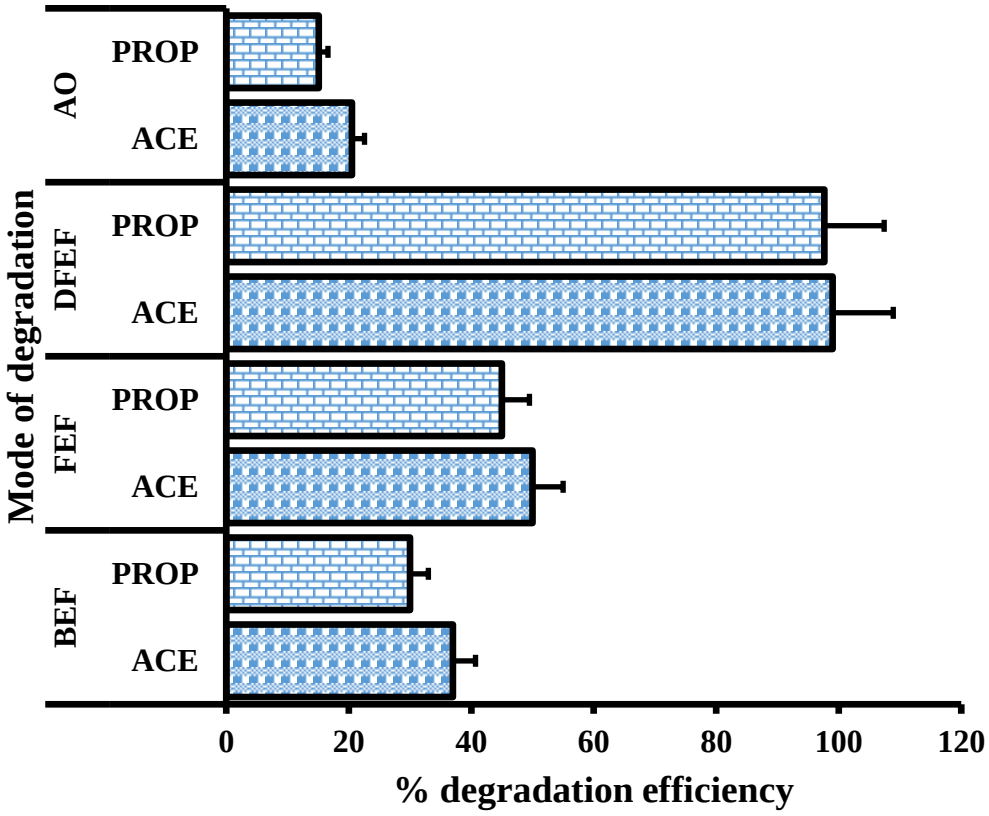

Figure 25: Degradation efficiency (%DE) for 200 µg L^{-1} ß-blockers sample solution at room temperature, I=75 $mAcm^{-2}$, pH =7, $[Na_2SO_4]_0$ = 0.05 $molL^{-1}$, 119 mg L^{-1} of RHS-15%Fe, AO-anodic oxidation, BEF-batch electro-Fenton, FEF- conventional flow assisted electro-Fenton, , DFEF-droplet- flow assisted electro-Fenton processes

4.5 Degradation kinetics studies

The decay kinetics of ß-blockers was studied at optimized DFEF conditions. The continuous electrogeneration of •OH in a heterogeneous EF process depends on the catalyst dosage [120]. The electrochemical degradation/decay of 200 $ngmL^{-1}$ ß-blocker (ACE) sample solution was therefore performed at different catalyst (RHS/C-10%Fe) dozing and at a fixed current density of 75 mA cm^{-2}. The degradation trend illustrated in Fig.26 was attributed to a compounded effect of anodic oxidation, DFEF and micro-electrolysis arising from Fe-C in the composite catalyst (RHS/C-10%Fe). As depicted in Fig.26, poor degradation of ACE was realized without catalyst loading (RHS/C-10%Fe catalyst).

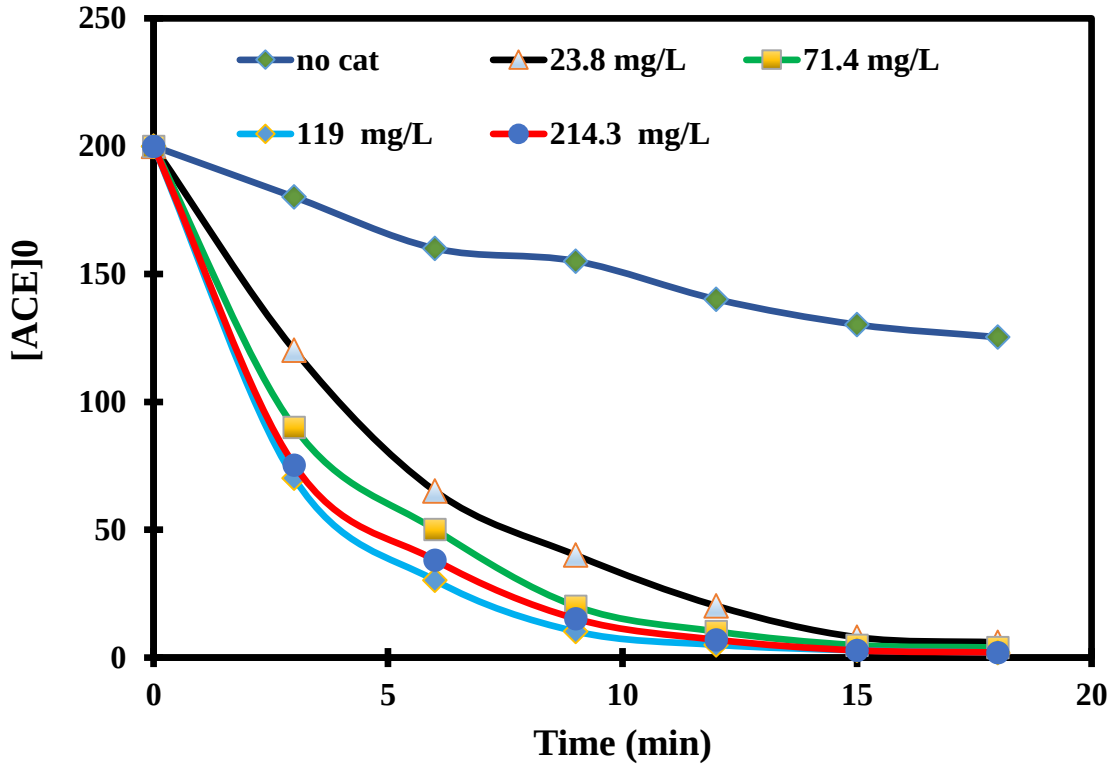

Figure 26: Representative decay plots of ACE under different RHS/C-10% Fe catalyst loading

The fastest and almost complete degradation of ACE was achieved using a catalyst loading of 119 mg/L and within 15 min of DFEF treatment. The degradation ß-blockers (ACE) in the DFEF system therefore, depends majorly on the electro-generation of bulk •OH radicals in the entire sample solution via Fenton reaction and the adsorbed hydroxyl radicals ($•OH_{ads}$) at BDD anode. These radicals are capable of degrading ß-blockers and even other micro-pollutants present in the sample solution to total mineralization using reaction 9 and 10.

ß-blocker + $•OH_{bulk}$ +$•OH_{ads}$→ byproducts…… (9)

byproducts + $•OH_{bulk}$ +$•OH_{ads}$→ $CO_2 + H_2O$…… (10)

The exponential decrease of the initial ß-blockers concentrations (ACE and PROP) with time demonstrated that the degradation by •OH radicals followed pseudo-first order reaction kinetics assuming quasi-static concentration of •OH radicals. This trend in behavior is similar to what was reported in literature in regard to oxidative degradation of organic pollutants with strongly oxidizing hydroxyl radicals [111,120,121]. The following equations (reaction equations 11-14) were utilized in determining the pseudo first-order rate constants (k_{obs}). (c is the concentration of ß- blocker at t time and C_0 is the 200 ng mL^{-1} as the initial ß-blockers concentration: two kinds of radicals react with ß- blocker at different reaction rates denoted as k_a and k_b respectively.

$$\frac{-d[ß-blocker]}{dt} = (k_a\,[\ \bullet OH_{bulk}] + k_b\,[\bullet OH_{ads}])[ß - blocker]0 \quad \ldots\ldots\ldots\ldots\ldots (11)$$

$$= k_{observed}[ß - blocker]0 \ldots\ldots\ldots\ldots\ldots\ldots\ldots\ldots\ldots\ldots\ldots\ldots (12)$$

$$-\frac{dC}{dt} = k_{observed}\,C, hence,\ lnC = -k_{observed}t + \ln C_o \ldots\ldots\ldots\ldots\ldots\ldots\ldots\ldots\ldots\ldots (13)$$

(t=0, C=C_o)

Therefore, $\ln\left(\frac{C_O}{C}\right) = K_{observed}t$ ... ... (14)

Plotting ln (c_0/c) against *t* resulting from the degradation of varied amounts of ß-blockers solution with various initial catalyst amounts (RHS/C-10%Fe composite) generated results presented in Table 18. The observed rate constant (pseudo first-order, k_{obs}) values were calculated from linear regression analysis and the k_{obs} values with their corresponding regression coefficients (linear R^2) are tabulated in Table 18.

Regression coefficient (R^2) values higher than 0.98 for both ACE and PROP indicated that the degradation process was well fitted to a pseudo first-order kinetics. There was a great increase in the observed rate constant ($_{kobs}$) for both ß-blockers in the ranges of (0.19-2.72 x 10^{-2}) for ACE and (0.16-2.54 x 10^{-2}) for PROP at increasing catalyst loading (RHS/C-10%Fe) from 0-119 mg L^{-1}. This observed kinetic behavior indicated that the degradation of ß-blockers was majorly by $\bullet OH_{bulk}$ attributed to E-Fenton process than $\bullet OH_{adsorbed}$ for anodic oxidation. However, increasing the amount of catalyst beyond 119 mg L^{-1} (ie to 166.7 mg L^{-1}) decreased the $K_{observed}$ to 2.34 x 10^{-2} and 2.16 x 10^{-2} for ACE and PROP respectively mainly due to quenching effect of •OH caused by excess Fe^{2+} present. Fast reaction rates ($K_{observed}$) of 3.62 x 10^{-2} and 3.57 x 10^{-2} min^{-1} for ACE and PROP were realized when the initial ß-blocker concentration was halved to 100 ng mL^{-1}, however on doubling the initial concentration to 400 ng mL^{-1}, the $K_{observed}$ decreased to 1.53x 10^{-2} and 1.39 x 10^{-2} min^{-1} for ACE and PROP respectively. Different byproducts are formed by the reaction between •OH radicals and the ß-blockers, when the concentration is increased, the available •OH radicals compete with the increased formation of ß-blockers degradation byproducts leading to a decrease in reaction rate.

Table 18: Pseudo first-order rate constants and regression coefficients for ß-blockers degradation.

$[ß\text{-blocker}]_0$ ng mL^{-1}	RHS-10%Fe (mg L^{-1})	K_{obs} (ACEx10^{-2}) (min^{-1})	K_{obs} (PROPx10^{-2}) (min^{-1})	R^2 (ACE)	R^2 (PROP)
200	0.0	0.19	0.16	0.9856	0.9776
200	23.8	2.06	1.90	0.9932	0.9952
200	71.4	2.23	2.05	0.9924	0.9944
200	119.0	2.72	2.54	0.9954	0.9964
200	166.7	2.34	2.16	0.9947	0.9987
100	119.0	3.62	3.57	0.9973	0.9953
400	119.0	1.53	1.39	0.9933	0.9953

4.6 Identification of degradation by-products

In view with the data obtained from LC–MS/MS line spectra studies of each degradation product, a degradation pathway of both ß-blockers ACE and PROP were established. Their degradation pathways are shown in Fig. 27 along with their proposed structures. To avoid fast degradation of ß-blockers intermediates, a low current density of 50 mA cm^{-2} during 10 min and higher ß-blocker concentration of 1000 ng mL^{-1} were utilized. Under these weak oxidation conditions, most stable carboxylic acids and aromatics are realized. The electrochemical degradation pathway of ß-blockers follows two main routes, namely; the side chain cleavage resulting to amino-diol and hydroxylation of the aromatic ring followed by formation of keto-derivatives after the ring opening. Both ACE and PROP contain two main active sites during the reaction with •OH, aromatic groups and aliphatic chains with amine, amide and ether groups. The primary step during the reaction of •OH with PROP include oxidative C-H insertion of •OH followed by the cleavage of C-O bond that resulted in 1-naphtol and aliphatic group. Competing reaction with the previous one is the oxidative cleavage of C-N bond as well as the oxidative hydroxylation of aromatic group that results in poly hydroxylated naphthol derivatives. Further oxidation of the resultant byproducts by •OH generated relatively stable highly oxidized small molecular weight carboxylic acid derivatives such as malic, oxalic, oxamic acids. Schematic representation of the degradation mechanism of PROP and ACE can be summarized as shown in Figure 27.

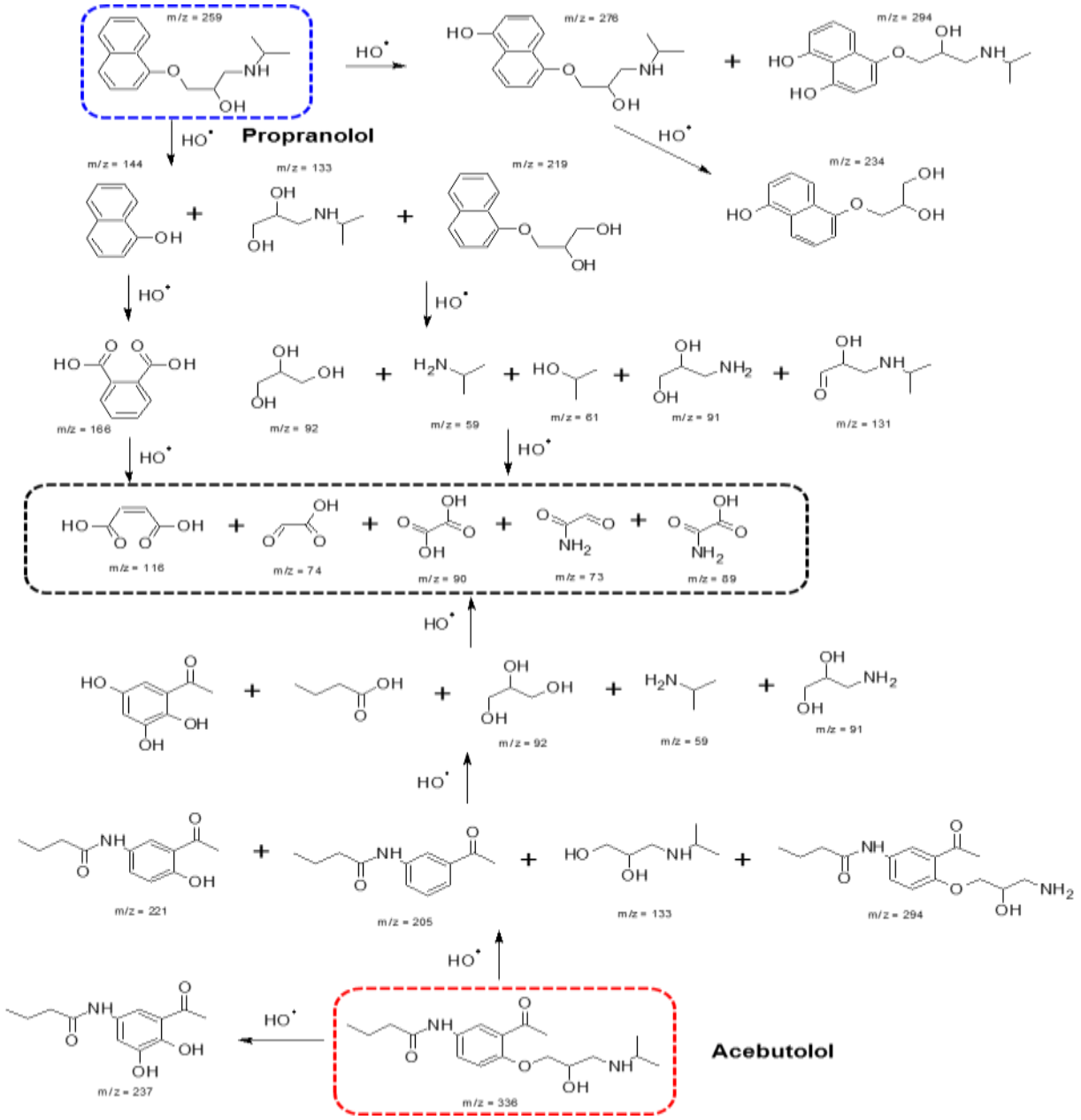

Figure 27: Proposed reaction scheme for the degradation of propranolol and acebutolol upon treatment with •OH

Similar reaction sequence for ACE can be observed during the treatment of •OH. First oxidative cleavage of C-O bond takes place to generate phenol derivative and the alkyl group followed by the cleavage of C-N bond (Fig. 26). Oxidative hydroxylation of the phenyl group also takes place despite having electron withdrawing acetyl group, although in lesser extent compared to the naphthol group of the propranolol [96].

CHAPTER 5

Response Surface Optimization of an Enhanced Beta-Blockers Degradation Method Using Copper-Boron-Ferrite Supported Graphite Electrodes and Continuous Droplet Flow-Assisted Electro-Fenton Reactor

5.1 INTRODUCTION

Advanced oxidation processes (AOPs) based on homogeneous Fenton reaction, are sought to be eco-friendly, non-selective and appealing wastewater treatment options [122] for refractory organic pollutants. They involve catalytic decomposition of externally added hydrogen peroxide (H_2O_2) by homogenous ferrous iron (Fe^{2+}) to highly reactive hydroxyl radicals (•OH) at low pH ranges [27,123]; with the aim of non-selective oxidization of recalcitrant and non-biodegradable organic pollutants to mineralization [123]. The challenges associated with these approaches are; narrow acidic pH working ranges (~2-3), need for careful chemical handling, storage, transportation and Fenton dozing optimization [124,125]. To overcome these constraints, electrochemical advanced oxidation processes (EAOPs) based on Fenton reaction chemistry (electro-Fenton and related

methods) were advanced as inexpensive, simple, environmentally benign and effective wastewater treatment options [27,45].

In particular, the EF process; under controlled applied current, utilizes an in-situ generated H_2O_2 and Fenton catalyst (Fe^{2+} in catalytic quantity), to continuously generate highly reactive •OH radicals and regenerate Fenton catalyst (Fe^{2+}) as shown in reaction equations (1-3) [27,45].

$$O_2 + 2H^+ + 2e^- \rightarrow H_2O_2 \quad (1)$$

$$Fe^{2+} + H_2O_2 + H^+ \rightarrow Fe^{3+} + H_2O + {}^{\bullet}OH \quad (2)$$

$$Fe^{3+} + e^- \rightarrow Fe^{2+} \quad (3)$$

The classical EF processes are highly constrained by high operational costs related to maintenance of optimally low working pH ranges (2.5-3.5), non-catalyst recyclability and need to neutralize the acidic effluent after treatment [27]. Moreover, the effectual acidic pH conditions typical of classical EF operations can potentially destroy electrodes during long time treatment.

To circumvent these limitations, heterogeneous-EF (hEF) methods, utilizing solid catalyst sources to facilitate H_2O_2 decomposition to •OH, have thoroughly been investigated [96,103,126–128]. Such techniques favor effective degradation of organic contaminants from multi-variant effluents without pH restrictions, as is common with traditional EF systems [96]. The probable mechanism for successful hEF operations are: (i) pH self-regulation mode in which a heterogeneous catalyst in O_2 presence accumulate H^+ ions that lower the sample solution pH to acceptable EF ranges, (ii) catalytic H_2O_2 decomposition to •OH at the surface of solid heterogeneous catalyst [96]. The resultant •OH radicals react non-selectively with organic pollutants through electron transfer, dehydrogenation, and electrophilic addition reactions till complete remediation [122]. Other key advantages of a hEF

system include; ease of catalyst recyclability, re-usability and possibility of electrode fabrication to permit simultaneous Fenton catalyst and oxygen reduction reaction (ORR) activities [96,129,130]. The recent trend in research is aimed at fabricating flow hEF reactors equipped with functionalized cathodes/ solid catalysts to improve ORR activities, Fenton catalyst electro-generation, re-use, and with subsequent reduction in operational costs [96,103,128]. Notwithstanding, hEF experiments are conducted in fabricated electrolytic flow reactors with the aim of improving mass transfer kinetics and space-time treatment efficiency of target pollutant molecules [107,131]. Most hEF studies on wastewater treatment have focused on the synthesis and applications of suspended heterogeneous Fenton catalysts in enhancing ORR across a wider pH window, and with greater potential for catalyst recyclability [98,120,132–134]. Alternatively, when a Fenton catalyst is immobilized on a cathode electrode in a hEF system, the resultant integrated cathode serve a simultaneous role of both Fenton catalyst and recyclable electrocatalyst [128,130]. This extends the hEF operations across wider pH ranges [128], promotes electrode re-use [132] and prevents continuous catalytic additions and removal during treatment [96]. As shown in equation 1, the in situ H_2O_2 electro-generation is determined by adequate oxygen/air supply and adsorption at an appropriate cathode material [27]. A presaging multifunctional cathode electrode in a hEF reactor should be capable of fast H_2O_2 production as well as high •OH radical formation [128]. Most reported methods for cathode electrode modification in hEF systems are by chemical, thermal and hybrid coatings (composite). Specifically, composite cathode electrodes like Fe_3O_4/Fe/Fe_3C on porous carbon nanofiber [129], Fe_3O_4 on graphite felt [135], and Fe_3O_4/Fe_2O_3 on activated carbon aerogel [136] are asserted to show simultaneous H_2O_2 productivities and effective Fenton activities during hEF operations. The practical and longtime application of these composite cathode electrodes are limited by their complex fabrication procedures, porosity blockage during fabrication, agglomeration and catalyst leaching

[137]. Still, the formation of iron oxides on these electrode surfaces during modification is reported to increase the electrode charge transfer resistance, decrease the electrode longevities and limit their electrical conductivities [138]. Electrode surface functionalization with transition metals is averred to enhance its efficiency for simultaneous H_2O_2 electro-generation, decomposition to $^{\bullet}OH$ radicals and Fe^{2+} regeneration [25,128]. During hEF process, many competing reactions that consume $^{\bullet}OH$ radicals occur [139], hence appropriate cathodic modification will not only enhance the H_2O_2 production, but will prevent the formation of such parasitic reactions [140]. Particularly, graphite electrodes utilized in many EF degradation studies as cathode electrodes, exhibit unique advantages such as low-cost, availability, non-toxicity, high stability, and high conductivity [141–144]. However, the large-scale utilization of graphite cathode electrodes for long electrolytic treatment times is limited by their low specific surface area, poor chemical stability and electrode fouling [141–144]; especially during re-use. Hydrolytic sol-gel chemistry is a well-established protocol for fabricating electrodes with enhanced surface characteristics like improved conductivity, chemical stability, enhanced surface area, surface particle homogeneity and corrosion protection [145]. With this approach, metallic ions can easily be incorporated into the fabrics of hybrid materials using very low-cost sources [146]. Bimetallic (Fe-Cu) catalysts have been advanced as stable and efficient hEF catalysts than single supported iron catalysts [128]. Likewise, incorporation of boron into the oxygen lattice vacancies during electrode modification, highly improves the electrode thermal stability, recycling stability and conductivity [147]. Model pollutants selected for this study were pharmaceutical beta blockers atenolol (ATE) and propranolol (PROP). They are considered toxic, pseudo-persistent, resistant to removal by conventional wastewater treatment technologies and are now measured in various aquatic environments at trace level concentrations [28,90–92]. Several parameters are reported to influence the efficient operation of an EF degradation process, and hence

proper optimization is averred to improve the systems degradation efficiency [27]. Response surface methodology (RSM) in combination with desirability function (DF) is the most widely used optimization approach [148]. This combinatory statistical approach yields competent optimization and variable-variable interaction studies at the minimum working time and solvent consumption [149].

In this study, copper-boron-ferrite (Cu-B-Fe) supported graphite electrodes, were investigated for the first time as efficient integrated cathode electrodes for flow assisted heterogeneous electro-Fenton (DFEF) degradation of trace level beta-blockers in hospital wastewater. The Cu-B-Fe composites were immobilized on treated graphite electrodes via rice husk silica-based hydrolytic sol-gel method. To tap into the outstanding benefits of droplet flow chemistries [150,151], the synergistic contribution of DFEF system and the prepared integrated cathode electrodes were investigated for fast and continuous electro-generation of H_2O_2 and quicker production of •OH radicals. The effects of operating parameters on degradation efficiencies were evaluated and optimized using response surface methodology based on a central composite design and desirability function. Considerable attention was put on the stability of the newly integrated cathode electrode for multiple re-uses. A combination of DFEF system with liquid chromatography-tandem mass spectrometry (LC-MS/MS) analysis offered new opportunities for monitoring, prediction, and identification of trace level degradation pathways in hospital wastewater.

5.2 EXPERIMENTAL

This work includes hydrolytic sol-gel immobilization of Cu-B-Fe composites on treated graphite electrodes and characterization. The electrodes are then investigated as suitable cathodes for ORR via H_2O_2 electro-generation and degradation efficiency (%) using a fabricated DFEF system. RSM based on central composite design with desirability function are used in both experimental design and optimization.

5.2.1 Sol-gel electrode modification and characterization

5.2.1.1 Graphite electrode modification with Cu-B-Fe via hydrolytic sol-gel method

Analytical grade chemicals were used as received in this study. High purity graphite plate electrodes (100 mm x 100 mm x 4 mm, Shanghai Qijie Limited Co., China) were used as catalyst support.

The graphite plate was cut into rectangular plates of dimensions 2.0 cm x 2.0 cm, polished with ultrafine grit emery sheet and then dipped in 3.0 M sulfuric acid (at 100 ^oC) for 3 hours. This improved the electrodes porosity and introduced some oxygen functionalities on the electrode surface. The electrodes were then rinsed in ultrapure water till neutral pH and then ultra-sonicated in acetone for 10 minutes to ensure no adhesive remained attached.

They were then oven dried at 100 ^oC for 5 hours to prepare them for sol-gel modification. The sulfonated graphite electrodes were denoted as SGE. Meanwhile a typical sol-gel synthesis

procedure for preparing Cu-B-Fe composite from rice husk silica prior to graphite electrode functionalization is mentioned elsewhere in reference [114] but with some modification.

Briefly, milled rice husk (50 g) collected from Kerala, India was washed in 500 mL acid solution (3.0 Wt. % sulfuric) at 80 ^{o}C for 3 hours under constant stirring. This was followed by filtration and rinsing in deionized water till neutral pH and then oven drying (110 ^{o}C) for 8 hours. The samples were then calcined in a muffle furnace (700 ^{0}C) for 5 hours to obtain rice husk ash (RHA). RHA (2.0 g) was then dissolved in 250 mL NaOH (I.0 M at 80 ^{0}C) under constant stirring for 5 hours, undissolved residues sieved out to obtain clear sodium silicate (Na_2SiO_3) solution. To the aliquot of Na_2SiO_3 solution (15 mL) was added glycerol and cetyltrimethylammonium bromide (CTAB) as surface directing reagents (each 3 wt. %) and then stirred at 60 ^{o}C till dissolution.

Glycerol and CTAB further increased the functional moieties in the silicate solution for anchoring loaded metals and boron. Under constant stirring conditions, the resultant solution was slowly titrated with 3.0 M HNO_3 containing the appropriate proportions of iron (III) nitrate nonahydrate (10, 20 and 30 (wt. % of iron)), copper-II-nitrate trihydrate (10 wt. % of copper) and boric acid (5 wt. % of Boron) until gelation (pH 3.0). These loading ratios were established from our preliminary experiments. The samples were aged in an oven (60 ^{0}C) for 5 hours.

This was then followed by centrifugation, thorough rinsing with copious amounts of double distilled water and finally dispersed into 150 mL of double distilled water. This was followed by dipping and drying of the already treated SGE (oven drying at 100 ^{o}C for 10 min after every dipping). Basing on our preliminary results, the electrode dipping and drying cycles were repeated 3 times before final annealing for 2 hr (muffle furnace at 450 ^{o}C).

The modified electrodes were marked as BGE for bare graphite electrode, 10-SMGE for 10% Fe^{3+} of Cu-B-Fe loading on BGE; 20-SMGE for 20% Fe^{3+} of Cu-B-Fe loading on BGE and 30-SMGE for 30% Fe^{3+} of Cu-B-Fe loading on BGE. The graphite plate electrode fabrication procedure is depicted in Fig. 28.

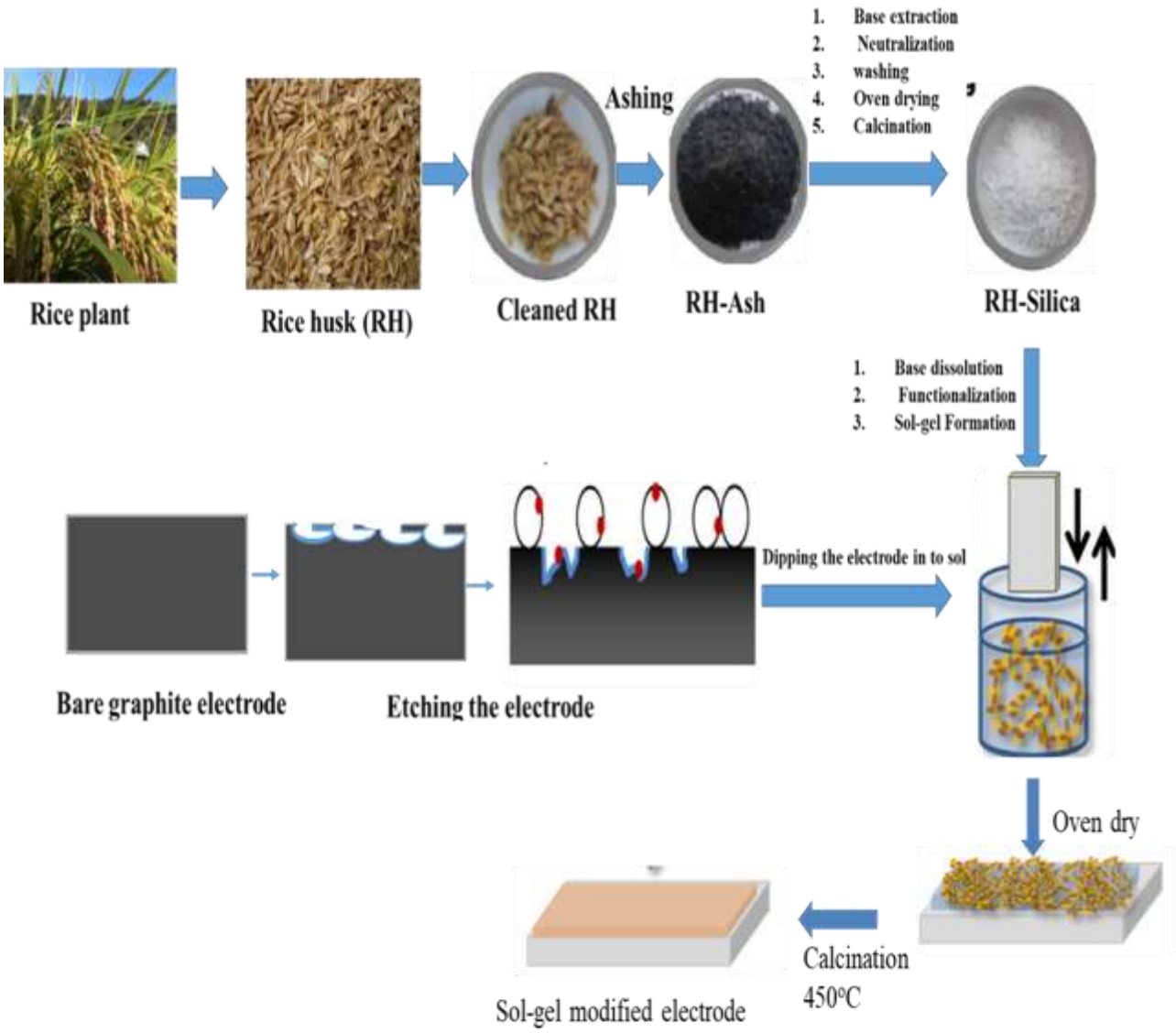

Figure 28: Fabrication steps of Cu-B-Fe graphite plate electrodes by sol-gel method

5.2.1.2 Electrode characterization methods

The electrochemical performance of the modified electrodes was evaluated using cyclic voltammetry (CV) at a scan rate of 0.1 mV s^{-1}, 0-1V, room temperature) using an electrochemical workstation (CHI1140A, CH Instruments Inc., Austin, TX, USA). A three-electrode system consisting of graphite plate (1 cm^2) electrode (bare or modified) as working electrode, a platinum wire as auxiliary electrode and an Ag/AgCl (in 3MKCl) as reference electrode constituted the electrochemical cell. The supporting electrolyte was 10 mM $K_4Fe(CN)_6$ in 1.0 M KNO_3. A graphite plate (1 cm^2) was used as the substrate electrode for sol-gel deposition.

The electrodes surface texture was analyzed using AFM/Scanning probe microscopy in contact mode. The tip used had the following specifications, silicon nitride probes, r = 20 - 60 nm and a manufacturer force specified constant (K) of 0.12 N/m. The electrodes friction coefficient (before and after modification) were done using a linear micro-scratch tester (MCTX-S/N: 01-04300). The contact load settings ranged between 0.0025- 0.1 N. Other analysis parameters included a 0.01 N/s loading rate, 5 mm/min scanning speed and 1 mm scratch depth.

Lab Ram HP Evolution Raman spectrometer LabRAM HR Evolution Raman spectrometer equipped with an internal HeNe (< 20 mW) laser at an excitation wavelength of 633 nm was used to record the Raman spectra. The microscope objective lens of 10x supported on a spectrograph of focal length 800 mm and 600 gr/mm grating was applied to focus the laser beam. The signal was detected on 1024 x 256 pixels –TE-Cooled CCD detector for UV–Vis-NIR with an acquisition time of 25 s and accumulation of 2 s.

The electrodes surface morphological features resulting from multifunctional hybrid sol-gel immobilization were monitored using scanning electron microscope (SEM, JEOL JSM-6610 LV) and energy dispersive X-ray spectroscope (EDX) at 20.0 kV.

X-ray photoelectron spectroscopy (XPS) was used to investigate the chemical composition of the multifunctional sol-gel deposition on the graphite electrodes. Thermo Scientific Escalab 250Xi spectrometer employing monochromatic Al Ka (1486.6 eV) x-ray source and operating at a resolution of 0.5 eV was used in the analysis. A takeoff angle of 45 ^{o}C and spot size of 200 µm were used for all the measurements. Clean gold surfaces with $Au4f_{7/2}$ at 83.98 eV were used in calibrating the binding energy scale of the system. Carbon core level peak (C 1s) at 284.5 eV$\pm$0.2 eV was used as a reference peak for all the measurements.

5.2.2 Catalytic evaluation of the prepared cathode electrodes in a DFEF reactor

The degradation efficiency of a hEF system is dependent on its potential for fast and continuous production of highly oxidizing •OH radicals [128]. However, the quantification of •OH radicals during EF operations is limited by their short life time (3.7×10^{9}s). Hence, for proper •OH radicals monitoring, the measurement of both H_2O_2 generation and degradation efficiencies (%) is considered an indirect technique for •OH radicals' determination. In view of the above observation, the H_2O_2 electro-generation studies were conducted in a continuous flow mode reactor designed to suit a droplet flow-assisted heterogeneous electro-Fenton system (DFEF) as shown in Fig. 29. It was composed of a 0.5 L undivided cylindrical shaped glass cell, a peristaltic pump and air pump.

An air pump connected to a continuous sample flow system ensured continuous air-saturation at the cathode electrode in form of droplet spray. The system was first run for 5 minutes prior to electrolysis experiments.

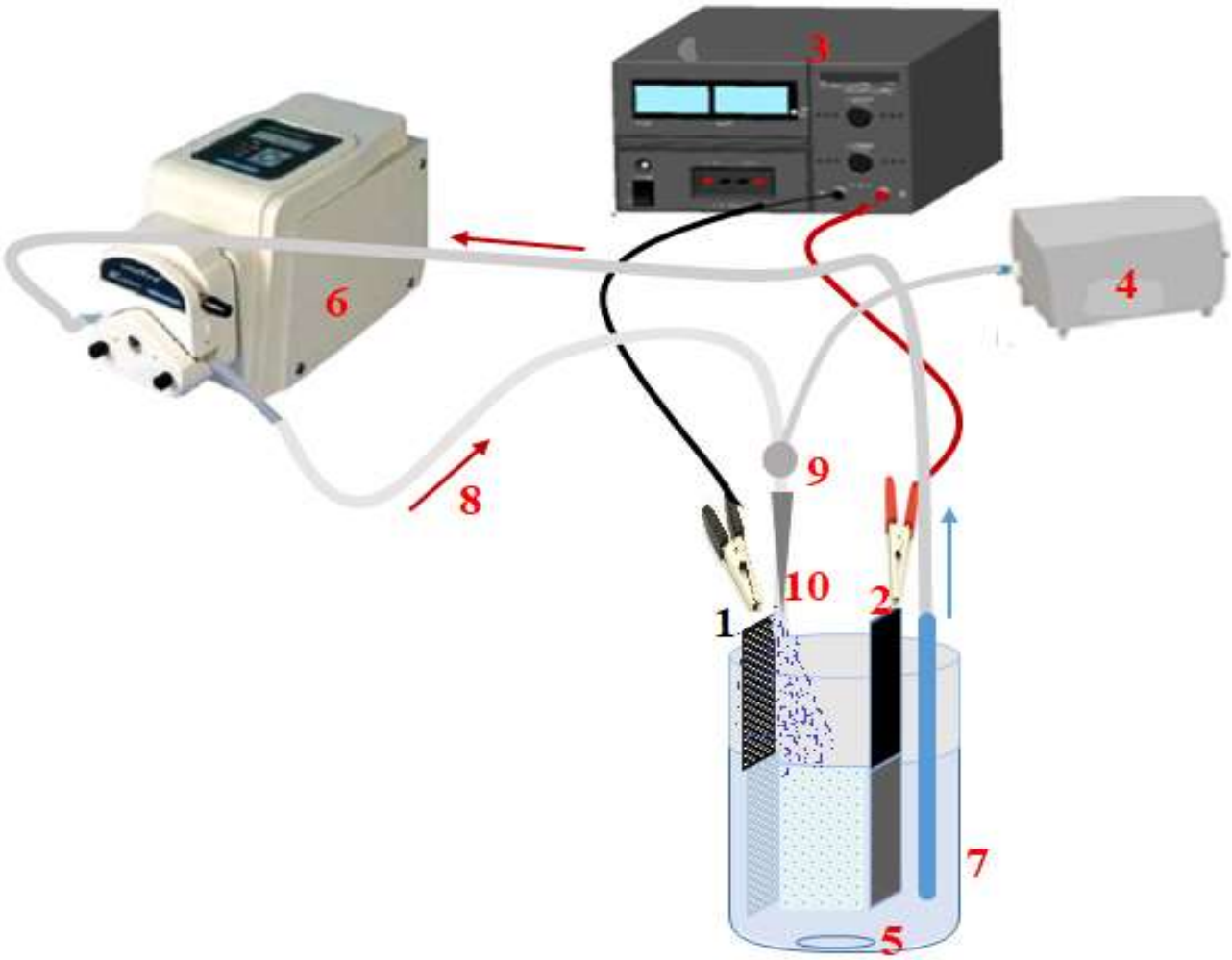

Figure 29: Schematic diagram of a droplet flow-assisted electro-Fenton (DFEF) reactor: (1) Sol-gel modified graphite cathode electrode (SMGE) (multifunctional cathode) (2) Bare graphite electrode acting as anode, (3) DC power supply, (4) Air pump, (5) Magnetic stirrer, (6) Dual-headed peristaltic pump, (7) Electrolytic reactor, (8) Direction of sample flow (9) Junction for mixing natural air with untreated sample to form a droplet spray at cathode through (10)

The graphite cathode electrodes used in this study were denoted as BGE, 10-SMGE, 20-SMGE, 30-SMGE (each with surface working area of 4 cm^2). Boron doped diamond 2.75 µm BDD thin layer, Si/BBD, NeoCoat-Switzerland) was used as anode electrode. The inter electrode gap was maintained at 2 cm while a 1 cm distance was reserved from the bottom of the reactor. A reactor contained a 0.21 L sample solution containing 0.02 M sodium sulfate, as an inert supporting electrolyte. The sample solution pH was adjusted using sulfuric acid (3 M) and sodium hydroxide (1 M). Electric field was supplied and monitored by a DC power source (Sargent Welch Scientific) equipped with a digital multimeter (Fluke). To evaluate the ß-blockers (ATE and PROP) removal efficiencies, a spiking concentration of 200 ng mL^{-1} was used while H_2O_2 evolution experiments were conducted in absence of ß-blockers standards. Samples were always periodically withdrawn from the electrolytic reactor at predefined times, filtered (using polyether sulfone syringe filters, pore size, 0.2µm) prior to LC-MS/MS analysis. To identify the degradation intermediates, 210 mL sample solution with 200 mg L^{-1} of mixed ß-blockers standard solution was saturated with Na_2SO_4 and degraded (25 ^{0}C) for I hour and at 100 mA. ATE and PROP purchased from Sigma-Aldrich (St. Louis, USA) were used to prepare 1000 mg L^{-1} of standard stock solution using methanol and was later stored in at −4◦C in freezer. Hospital wastewater used in this study was collected from a medical facility at KFUPM.

5.2.3 Analysis methods

The degradation of ß-blockers ATE and PROP were conducted using the experimental set-up depicted in section 2.2. It was anticipated that as a result of the cathode modifications in a DFEF system, the cathodic oxygen electro-reduction reactions (ORR) and Fenton activity would simultaneously be enhanced leading to improved ß-blockers degradation efficiencies.

The EF degradation efficiency (%) was evaluated using the sample concentration of ATE and PROP as measured before and after degradation. Equation (4) was used to monitor the degradation process.

$$Degradation\ efficiency = \left(1 - \frac{B_i}{B_O}\right) x\ 100 \text{ ---------- (4)}$$

Where B and B_0 represent ß-blockers concentration at time (t) and (0) respectively.

The degradation process for trace ß-blockers in HWW was monitored on an ultra-high-performance liquid chromatograph triple quadrupole mass spectrometry (LCMS-8050, Shimadzu) using method developed in reference [114]. Data manipulation was carried out using LabSolutions (LCMS Ver.5.91, Shimadzu-Kyoto, Japan) and an Ultra IBD column (100 x 2.1mm x 3µm particle size, PA, USA) was used in chromatographic separation. The column temperature was set at 40 $\pm$ 1 ^{0}C while the injection volume was 10 µL. Gradient elution program at a flow rate of 0.3 mL/min was executed using 0.03% formic acid (Solvent A) and methanol /acetonitrile, 25:75 (solvent B); 7 minutes analysis time; nitrogen as a desolvation gas (flow rate = 800 L/h); argon (99.9995 % pure) as collision gas; dissolvation temperature 400 ^{o}C and source temperature of 150 ^{o}C. The target analytes were detected and quantified in multiple reaction monitoring, MRM (positive/ negative ionization) mode using electrospray LC–MS/MS technique.

For reaction intermediates identification, a total ion scan was first conducted (scan mass range m/z 100-600) followed by product scan (for each identified reaction intermediate) and was finally subjected to multiple reaction monitoring mode.

Hydrogen peroxide electro-generation was monitored on UV-vis spectrophotometer using potassium titanium (IV) oxalate method [115]. Prior to the analysis, 2 mL of the withdrawn sample (containing the anticipated H_2O_2) was shaken with 1 mL of titanium (iv) oxysulfate-sulfuric acid (27-31% H_2SO_4, Sigma Aldrich).

The development of an intense yellow complex of pertitanic acid complex was monitored at wavelength of 400 nM. The current efficiency for H_2O_2 electro-generation [152] was calculated using equation (5).

$$CE\ (\%) = \frac{nFC_{H_2O_2}V}{\int_0^t Idt} x\ 100 \quad \text{.....(5)}$$

CE is the current efficiency, C_{H2O2} is the concentration of generated H_2O_2 (mol L^{-1}), F represents the Faradays constant (96486 C mol^{-1}), n is the number of electrons transferred (O_2 reduction to H_2O_2), V is the volume of the working solution (L), t is the time (s) and I is the current in A.

5.2.4 Experimental design using response surface methodology

Minitab 17 (Minitab Inc., State College, PA, USA), was used in statistical experimental design, data modelling, analysis and optimization of the DFEF system. Experimental design is an effective technique aimed at estimating experimental error, eliminating systematic errors and reducing the number of experiments so as to optimize the process. With this approach, the relative significance of various factors can easily be estimated even in presence of complex interactions. Central composite design (CCD) based on response surface methodology (RSM) was used in designing DFEF process experiments and selection of suitable operational parameters. Basing on the reported literature, central composite design (CCD) is asserted to offer adequate second-order RSM for construction of five level fractional factorial designs (-α, -1, 0, +1, +α) [105,153]. For this study, four factors were selected namely; sample pH, electrolysis time (min), applied current (mA) and beta blocker concentration [ß-blocker]$_0$, as they were the significant parameters affecting the degradation efficiency. The corresponding CCD design matrix, levels, ranges, are presented in Table 19.

The levels and ranges used were based on the results obtained from our previous experiments. As a result, 30 experimental runs were randomly generated for this study comprising of 6 center point replications, 8 axial points and 16 cube points. Equation (6) was used in coding independent variables (X_i) and these were represented as x_i for statistical calculations.

$$x_i = \left(\frac{X_i - X_o}{\delta X}\right) \quad \text{.....(6)}$$

Where δX is the step change while X_o is the amount of X_i at the center point.

The dependent variables (% degradation efficiencies (%DE) and independent variables were correlated using a second order polynomial equation (7).

$$\%DE = b_o + \sum_{i=1}^{k} b_i X_i + \sum_{i=1}^{k} b_{ii} X_i^2 + \sum_{1 \le i \le j}^{k} b_{ij} X_i X_j \text{.....(7)}$$

Where in the above equation, the linear, squared and interaction regression coefficients are respectively represented as b_i, b_{ii} and b_{ij}. %DE is the response variable representing percentage degradation efficiency and the coded variable experimental levels are represented by x_i.

Table 19: CCD design matrix for DFEF degradation experiments

Variable	Code Level	Values of coded levels				
		-2	**-1**	**0**	**1**	**2**
[ß-blocker] ng/mL	X_1	100	200	400	800	1000
Current (mA)	X_2	50	100	200	300	400
Electrolysis time (min)	X_3	10	20	30	40	60
pH	X_4	3	5	7	8	10

The experimental response values were reported as mean values of the three repeated experiments for each data entry. Analysis of variance (ANOVA) was used in testing the CCD models adequacy and significance while Pareto analysis was used in identifying variables that present the highest cumulative effect on response [118]. Multivariate desirability function was utilized to establish more accurately the optimized parameter conditions. This multi-criterion approach simultaneously maximizes the ß-blockers degradation efficiency and minimize the energy consumption, a requirement for an effective wastewater treatment technology. The desirability function used in this study was reported in reference [148]. The overall desirability, D, is determined using the geometric mean of all the individual desirability functions as indicated in equation (8).

$$D = (d_1 d_2 d_3 \ldots\ldots d_k)^{(1/k)} \quad \ldots\ldots (8)$$

Where k corresponds to number of responses.

5.3 RESULTS AND DISCUSSION

5.3.1 Effect of Cu-B-Fe sol-gel modification on H_2O_2 electro-generation, current efficiencies and ß-blockers removal

The effect of sol-gel cathode modification on; (i) H_2O_2 generation (ii) current efficiencies and ß-blockers degradation efficiency was investigated as shown in Fig. 30 (a), (b) and (c). Basing on the results of our preliminary experiments, the concentration of iron in the composite was varied while that of boron and copper were kept constant.

As depicted in Fig. 30 (a), the concentration of H_2O_2 obtained after 60 minutes treatment using BGE, 10-SMGE, 20-SMGE and 30-SMGE cathode electrodes were 10.6, 9.4 1.8 and 6.2 mM respectively. Decreasing H_2O_2 electro-generation with sol-gel cathode modification signified the positive influence of modification on H_2O_2 decomposition. As illustrated in Fig. 30 (a), the concentration of H_2O_2 electro-generated at the bare graphite electrode (BGE) was almost six times greater than that of the modified electrode (20-SMGE). The presence of Fe and Cu in the surface matrix of the graphite electrode enhances the quicker reduction of H_2O_2 to •OH radicals while boron improves electrode stability, porosity and conductivity. Lack of linearity in the [H_2O_2] versus time plots for BGE was due to subsequent H_2O_2 loss resulting from its oxidation to O_2 as reflected in equations (9) and (10).

$H_2O_2 \rightarrow HO_2\bullet + H^+ + e^-$……. (9)

$HO_2\bullet \rightarrow O_2 + H^+ + e^-$……. (10)

On assumption that only reaction (1) took place at the cathode electrode, current efficiencies for H_2O_2 evolution (after 60 min) were determined as displayed in Fig. 30 (b). The current efficiencies for BGE, 10-SMGE, 20-SMGE and 30-SMGE under DFEF operations fell within acceptable ranges of 60 to 85 %.

It was observed that the current efficiencies generally decreased with sol-gel modification. The decreased current densities for modified electrodes as compared to bare graphite electrode meant that the modified surfaces had better catalytic activities for ORR and H_2O_2decomposition. These results are explicitly explained by the reactor design (continuous O_2 rich droplets at the cathode electrode) and the surface chemistry characterization techniques of the modified cathode depicting a relatively increased surface area, increased surface roughness and formation of nanoscale pores. Such flow reactor modification and porous electrode configurations ensure faster O_2 diffusion, mass transfer

kinetics and a highly efficient H_2O_2 production system. Hence, it is clearly supported that Cu-B-Fe modified BGE electrodes are good cathode materials for H_2O_2 electro-generation.

As is illustrated in Fig.30 (c), the modified graphite electrodes (x-SMGE) displayed higher ß-blockers (atenolol) degradation efficiencies at all pH conditions while the BGE showed reduced degradation efficiencies under all pH conditions. Propranolol degradation (Figure not shown) showed a similar trend as atenolol.

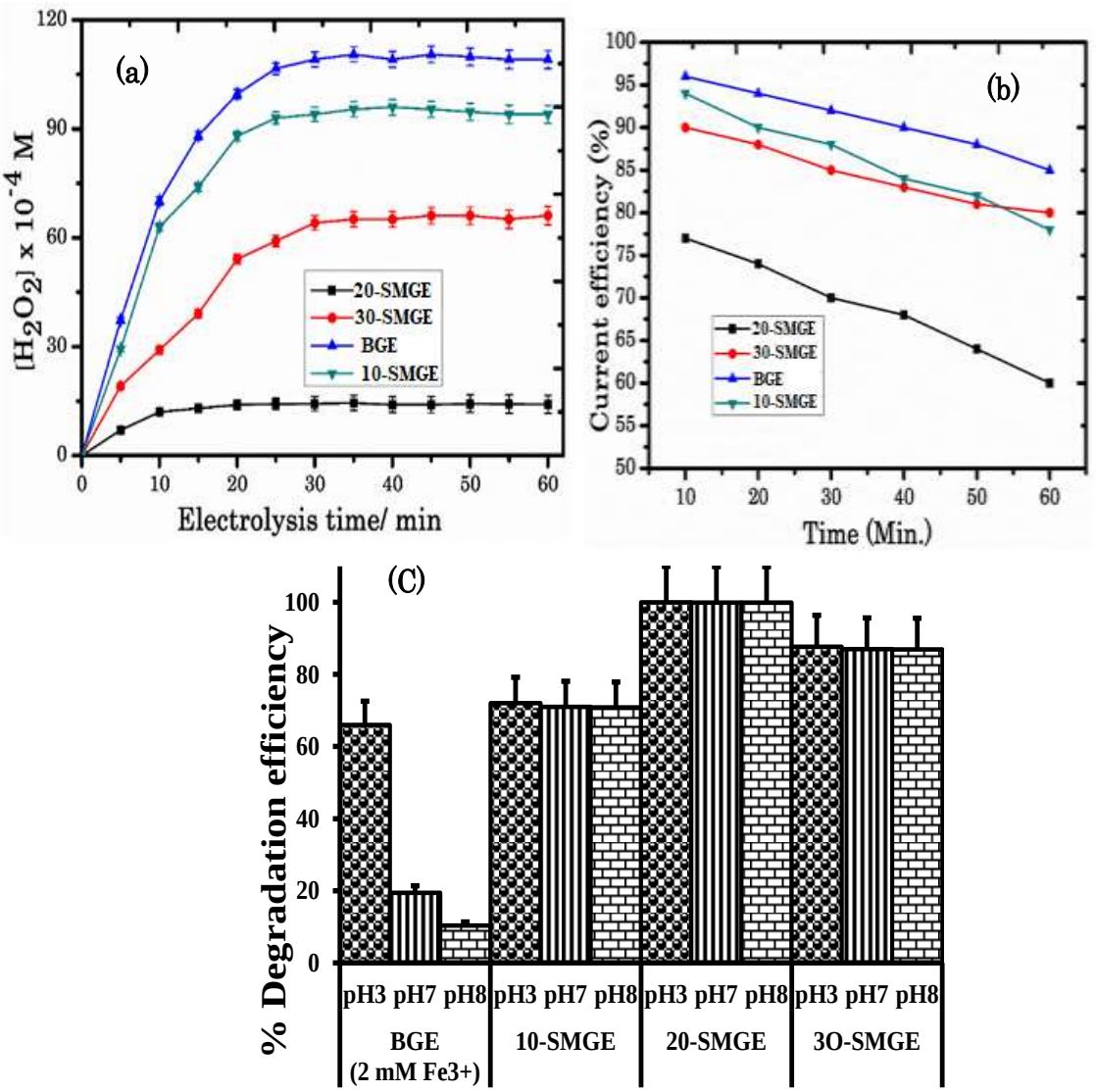

Figure 30: The effect of Cu-B-Fe sol-gel coating to bare graphite electrode on (a) H2O2 electro-generation and (b) current efficiency (c) degradation efficiency of 200 ng mL-1 of atenolol. I= 100 mA, [Na_2SO_4] = 0.02 M.

5.3.2 Electrode characterization

5.3.3 Electrochemical behavior

To investigate the observed results of H_2O_2 production and current efficiencies in section 3.1, cyclic voltammetry (CV) was conducted on both BGE and sol-gel modified electrodes as illustrated in Fig. 31. All the modified electrodes displayed well defined redox peaks resulting from forward and reverse scans of the redox couples of $Fe(CN)_6^{3-/4-}$. The redox peaks were significantly enhanced with increase in immobilization. The region for the positive current indicate anodic oxidation while that for the negative region represent cathodic reduction [154]. The modified/ treated electrodes exhibited almost rectangular shaped voltammograms which confirm their high potential for increased electron transfer at the electrode surfaces [155]. The sulfuric acid treated electrode (SGE) and sol-gel modified electrodes exhibited highly enhanced current responses towards oxygen reduction reactions (ORR) and increasing negative hydrogen evolution potentials than the bare graphite electrode. According to equations 1, the ORR is proton consuming and hence competes with the hydrogen evolution reaction at the cathode. Hence, the occurrence of ORR at less negative potentials resulting from cathode modification suppresses hydrogen evolution reaction. The enhancement of ORR at less negative potentials after electrode modification is a clear manifestation of fast electron transfer kinetics at the cathode electrode [156].

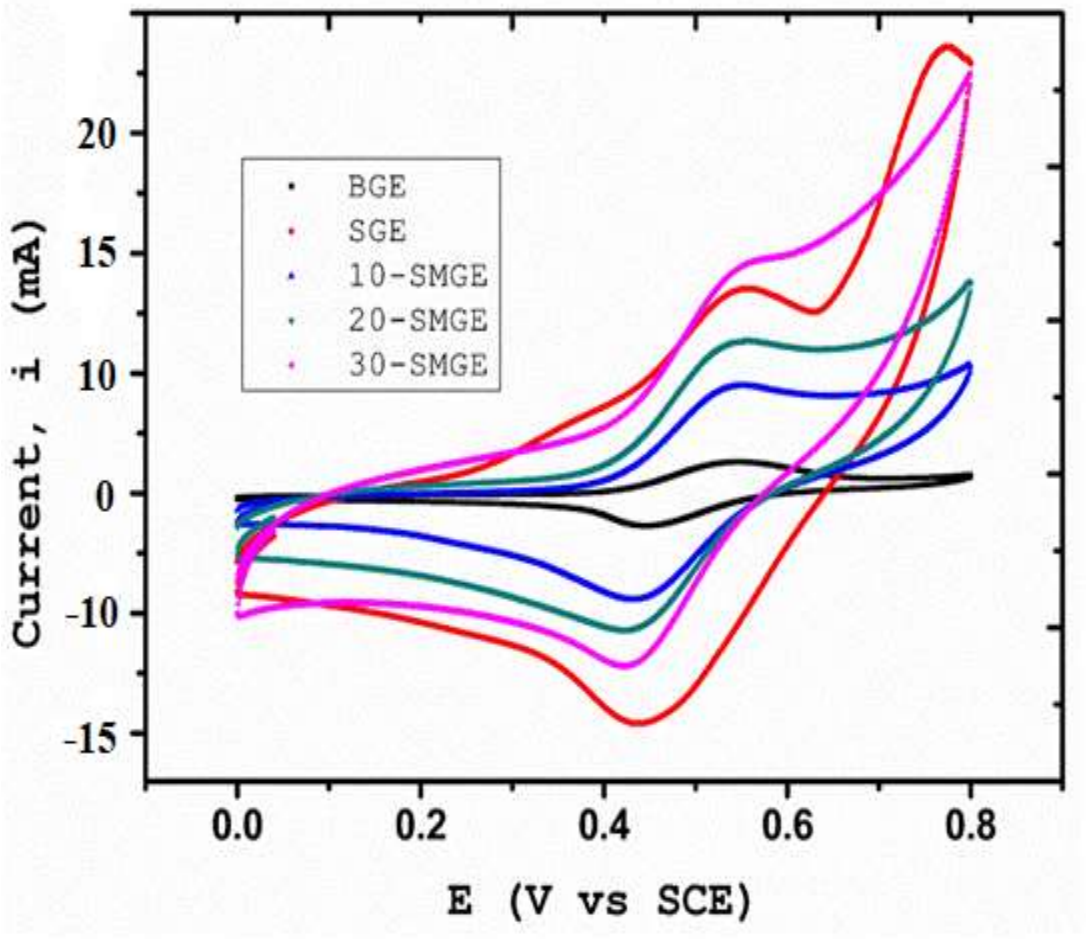

Figure 31: Cyclic voltammograms of BGE, SGE, 10-SMGE, 20-SMGE, 30-SMGE; Conditions scanning potential range 0-1 V.

5.3.4 Surface and structural characterization

The enhancements in H_2O_2 production on modified graphite electrodes was attributed to incorporation of nano-pore structures and increased electroactive surface area resulting from both etching and sol-gel modification. The SEM micrographs of bare graphite and 20-SMGE are presented in Fig. 32 (a) and (b). As depicted in Fig. 32 (a) bare graphite electrode shows some relatively smooth surface morphology, however, after etching and sol-gel modification, the smooth surfaces developed some ridges and nanoscale roughness. There are some observable spherical shapes resulting from the nano-doping in the 20-SMGE with approximate diameters of 15-75 nM.

To gain insight into the surface composition, SEM-EDX results in Fig. 32 (a) and (b) (insets) were used to clearly confirm the successful incorporation of Cu, B and Fe on the graphite surface after sol-gel treatment. Zhao et al in his electro-catalytic studies postulates that loading copper and iron ions into carbon matrix improves porosity [128]. Sulfuric acid etching roughened and introduced some surface functionalities (hydrophilic surfaces) on the BGE that were used to anchor loaded metals ions and improve surface area for ORR.

Molecular structures for both BGE and 20-SMGE are represented by the Raman spectras as shown in Fig. 32 (c). Both electrodes (before and after modification) present typical graphite sp^2 hybridization Raman characteristic peaks at 1352 and 1584 cm^{-1} corresponding to D and G bands respectively. Another D^I band appeared at 1626 cm^{-1}. The D band represents disordered phase reflecting grain and vacancies boundaries while the G band represent E2g phonon first order scattering of the of the *sp*2 carbon-carbon bond in the graphitic carbon phase. Additional D^I bands appeared at 1626 cm^{-1}. This implied that the graphite structure was retained even after sol-gel modification.

The degree of disorderliness resulting from BGE sol-gel surface functionalization was assessed using the ratio of integrated D and G band intensities (I_D/I_G) as an evidence for the level of functionalization. The I_D/I_G ratio increased from 0.76 to 0.94 demonstrating the presence of more surface defects and disorderliness attributed to Cu-B-Fe composite doping atoms. These observations are key towards enhanced cathodic ORR. The uniform distribution of the loaded metal atoms (Cu-B-Fe) was confirmed by SEM- elemental mapping results represented in Fig.32 (d).

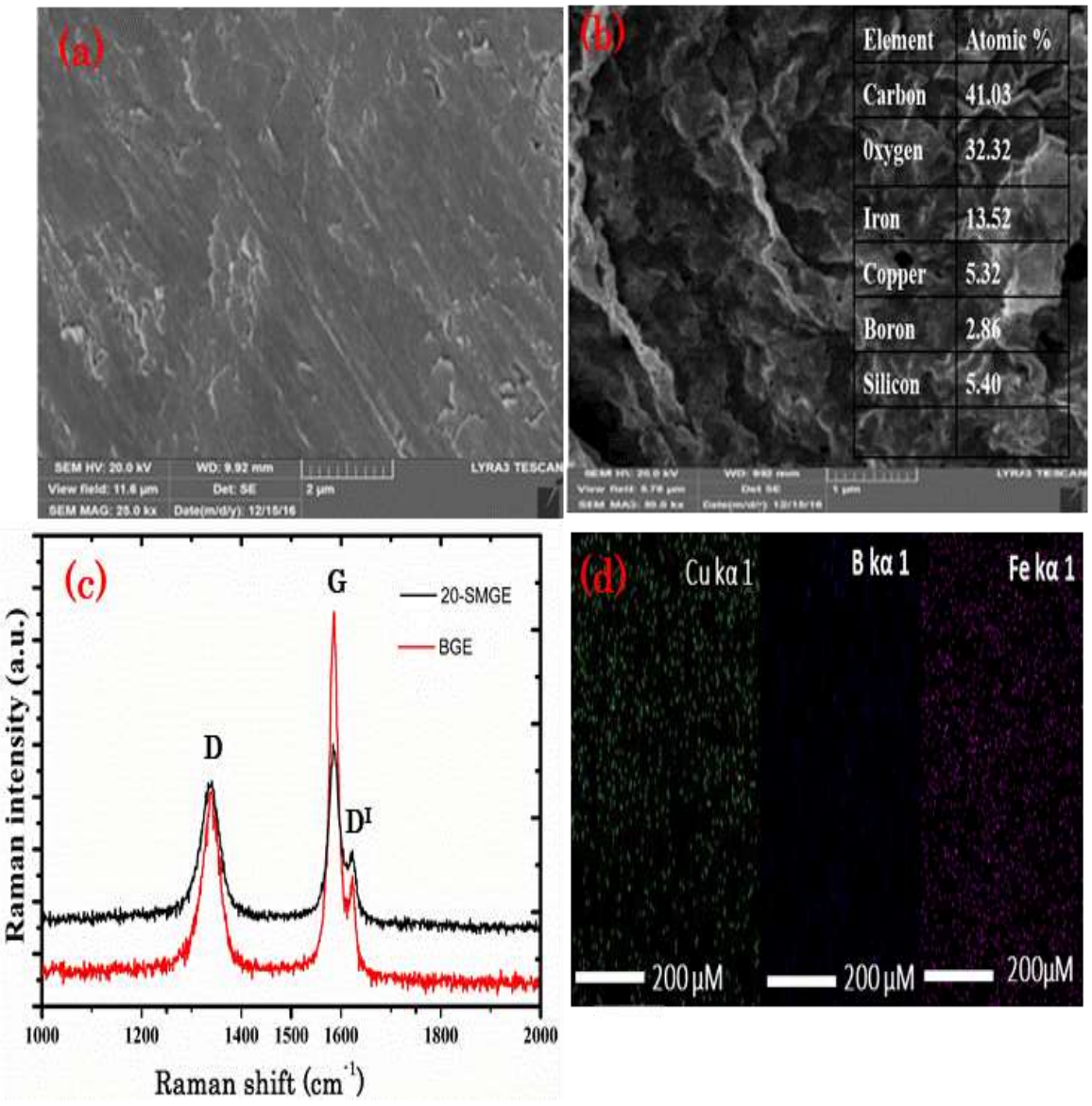

Figure 32: SEM image with EDS composition (inset) of (a) BGE (b) 20-SMGE (c) surface-enhanced Raman spectra's of BGE and 20-SMGE (d) elemental mapping of 20-SMGE.

Topographical 3D AFM represented by Figure 33 (a) and (b) for both BGE and 20-SMGE samples reveal that sol-gel modification creates well distributed porous valleys and hills structures on 20-SMGE electrode surface. These results are consistent with SEM characterization. They reflect an increase in active surface area that will enhance O_2 surface diffusion and fast H_2O_2 electro-generation.

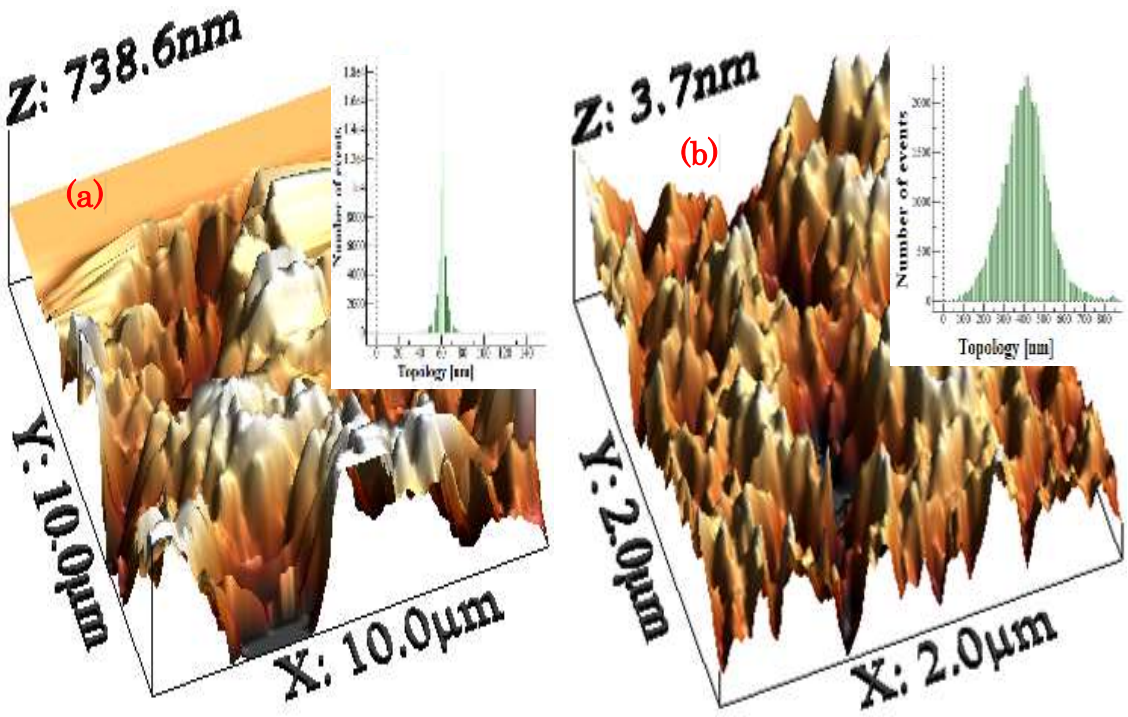

Figure 33: 3D topographical AFM images (inset-surface roughness distribution) of (a) BGE and (b) 20-SMGE.

XPS characterizations of BGE before and after modification were studied to establish further the surface elemental composition and functional groups. With XPS analysis, an insightful analysis of an elemental electronic with its chemical environment is availed and this explores further its probable oxidation states [116]. From the results of the XPS survey scan (Fig.34 a), BGE shows only the presence of carbon and oxygen while 20-SMGE shows incorporation of boron, iron and copper. These XPS elemental results correspond well with the SEM-EDX results above.

High resolution scans for relevant core levels for Fe2p (Fig.34 b) displayed two peaks at binding energies of 712.1 and 725.4 eV respectively. These were identified as spin orbit splitting of Fe^{3+} in Fe_2O_3 and were assigned to Fe^{3+} $2p_{3/2}$ and Fe^{3+} $2p_{1/2}$ respectively. Similar Fe2p binding energies (within the range) have been reported elsewhere [117]. Similar scan for Cu2p (Fig.34c) resulted to peaks at 933.9 eV and 953.3 eV and were separated by a distance of 19.9 eV. These peaks were finally assigned to Cu^{+}2p3/2 and Cu^{+}2p1/2 respectively and were attributed to monovalent Cu^{+} [157] in the modified sample. In addition, two high resolution spectral peaks located at 934.9 eV and 955.0 eV and assigned to Cu^{2+}2p3/2 and Cu^{2+}2p1/2 respectively were ascribed to bivalent Cu^{2+} spin-orbit splitting [158]. High resolution scans for both Carbon and B1s (Figures not included) showed incorporation of boron in carbon lattice.

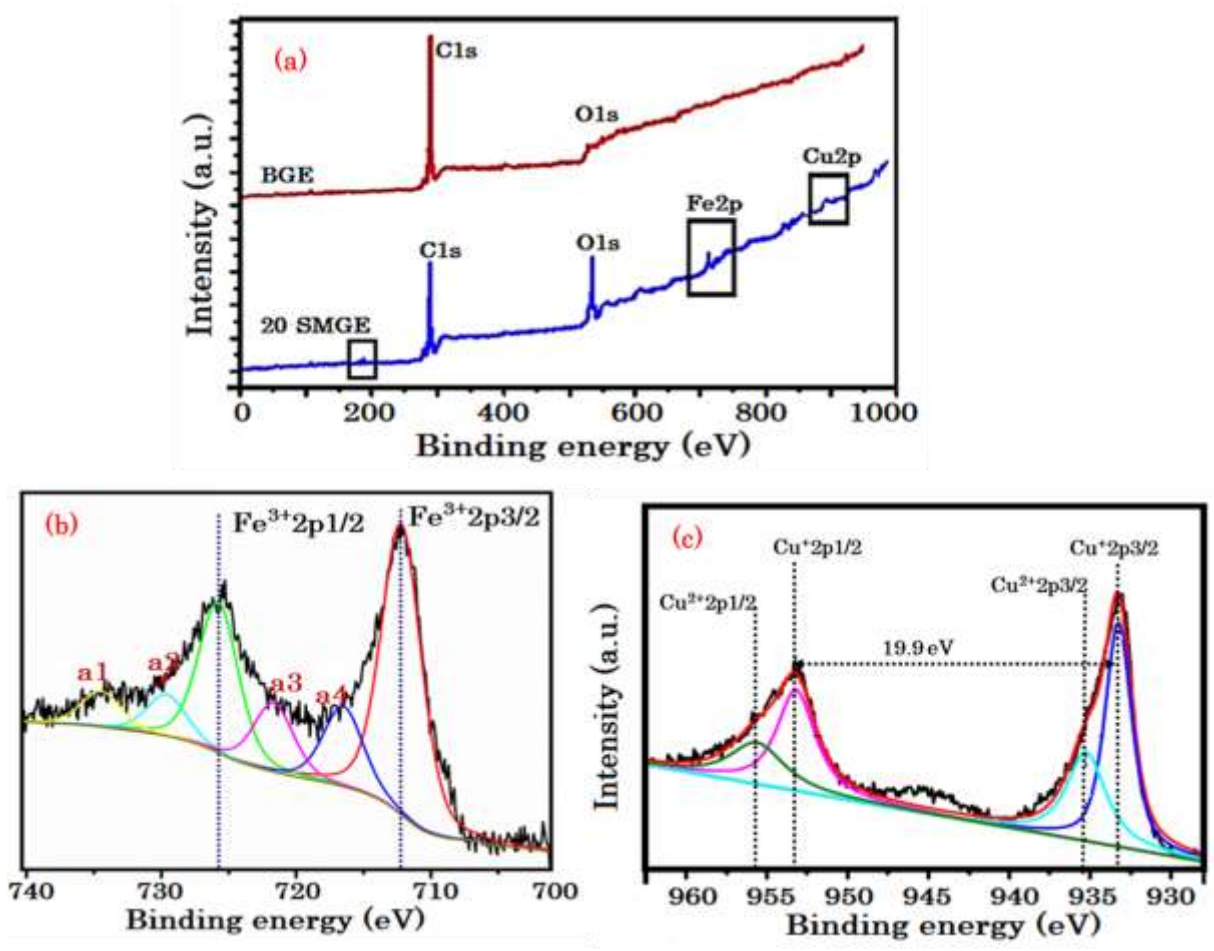

Figure 34: (a) XPS survey spectra for both BGE and 20-SMGE and high-resolution spectra for 20-SMGE in terms of (b) Fe2p (c) Cu2p.

5.3.5 Experimental design

5.3.6 Regression model development

The results of the 4-factors CCD design matrix with both experimental and predicted values are presented in Table 20. The experimental average removal values range from 59.05 to 95.43% while the predicted percentage average removal is between 57.61 and 97.40%. From the Minitab 17 software, and using a face centered CCD, a full second order quadratic polynomial model equation (%Y) (equation 11) expressing an empirical relationship between the predicted response (%Y) and independent parameters was deduced.

$$Y = 75.453 - 5.728 X_1 + 3.738 X_2 + 5.551 X_3 + 4.880 X_4 - 0.745 X_{12} + 0.940 X_{22} - 0.015 X_{32} + 2.018 X_{42} - 0.139 X_1*X_2 - 0.284 X_1*X_3 + 0.154 X_1*X_4 + 0.969 X_2*X_3 - 1.539 X_2*X_4 + 0.096 X_3*X_4 \quad \ldots\ldots(11)$$

Where the coefficients are statistically accepted values and X_1, X_2, X_3, X_4 represent the coded values for beta blockers concentration ([ß-blocker]$_{o,}$ ng/mL), applied current (mA), electrolysis time (min) and pH respectively. The negative and positive terms in the regression equation indicate unfavorable and favorable effects on respective degradation efficiencies.

Table 20: CCD design matrix table with results for DFEF degradation of ATE and PROP

EXP.No.	X_1	X_2	X_3	X_4	PROP	ATE	EXPR. % AVE. DEGR.	PRED. % AVE. DEGR.
1	2	0	0	0	58.9	59.2	59.05	61.02
2	0	0	2	0	90.49	90.79	90.64	86.49
3	-2	0	0	0	86.11	86.41	86.26	83.93
4	0	-2	0	0	72.17	72.47	72.32	71.74
5	0	0	0	2	94.02	94.32	94.17	93.29
6	0	0	0	-2	73.1	73.4	73.25	73.77
7	0	0	0	0	75.74	76.04	75.89	75.45
8	0	2	0	0	86.32	86.62	86.47	86.69
9	0	0	0	0	72.78	73.08	72.93	75.45
10	0	0	-2	0	60.36	60.66	60.51	64.29
11	0	0	0	0	78.65	78.95	78.80	75.45
12	1	-1	1	-1	65.05	65.35	65.20	66.95
13	1	-1	-1	1	71.42	71.72	71.57	70.50
14	1	1	1	-1	78.06	78.36	78.21	78.17
15	1	1	-1	1	74.02	74.32	74.17	72.68
16	-1	-1	-1	1	80.98	81.28	81.13	80.80
17	1	-1	1	1	78.05	78.35	78.20	79.29
18	0	0	0	0	76.13	76.43	76.28	75.45
19	-1	1	-1	-1	78.67	78.97	78.82	77.36
20	1	1	-1	-1	66.77	67.07	66.92	65.89
21	1	1	1	1	84.94	85.24	85.09	85.35
22	1	-1	-1	-1	59.68	59.98	59.83	57.55
23	-1	-1	1	-1	76.74	77.04	76.89	78.01
24	-1	1	-1	1	83.53	83.83	83.68	83.54
25	0	0	0	0	74.28	74.58	74.43	75.45
26	-1	-1	1	1	88.93	89.23	89.08	90.73
27	-1	-1	-1	-1	67.96	68.26	68.11	68.47
28	0	0	0	0	74.36	74.66	74.51	75.45
29	-1	1	1	-1	88.95	89.25	89.10	90.76
30	-1	1	1	1	95.28	95.58	95.43	97.34

Using a deduced second-order polynomial equation (equation 10), calculated values were graphically compared to experimental (Fig.35) resulting to correlation coefficient (R^2) of 0.968 (>0.900) and closer to unity. This confirms that the observed values were in good agreement with the calculated values and this supports the model's capability and reliability to predict responses (%Y).

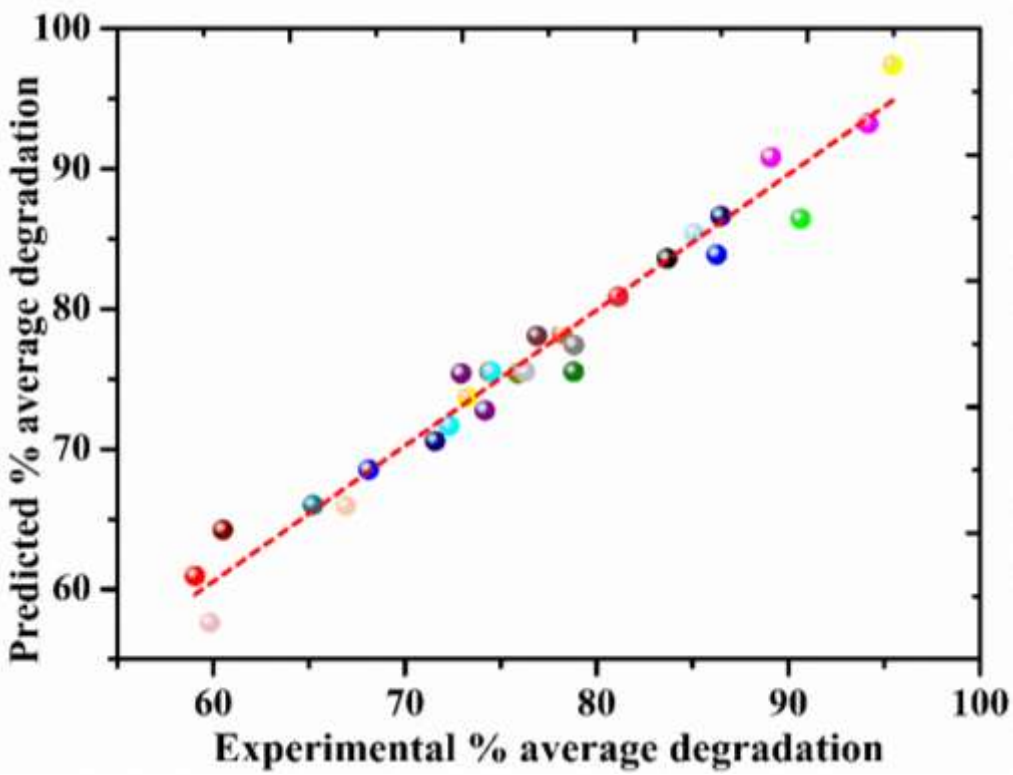

Figure 35: Predicted versus experimental degradation response plot.

5.3.7 Regression analysis

The regression results generated from the regression model analysis are presented in supplementary Table 3. The significance of the regression coefficients was determined using student's t-test. Table 21 depicts the relevant variables, student's t-distribution alongside their variable estimates whose significances are tested using the corresponding p-values. A parameter coefficient is considered significant when the magnitude of its t-value is larger and its corresponding p-value is smaller ($\leq$0.05). Precisely, the statistical significance of the model terms are signified by their corresponding p-values (Prob > F $\leq$ 0.05). The statistical insignificancy of the models terms are indicated by the p-values >0.1 while the p-value Prob > F $\leq$ 0.1 indicate borderline significance at 95%confidence limit [80]. Therefore, given the variable estimates with their accompanying p-values, the test variables with the highest significance (Table 19) suggested that initial beta blockers concentration (X_1), applied current (X_2), electrolysis time (X_3) and pH (X_4) were highly significant. Likewise, the linear relations between X_2*X_2 and X_4*X_4 and quadratic relations between X_{2*3} and X_{2*4} were found to be highly significant ($p \leq 0.0001$). Residual analysis plots were used to test the model's adequacy and normality.

Table 21: Regression coefficients estimates with their corresponding t and P-values from the central composite design data obtained during DFEF experiments

Coefficient	Parameter estimate	Standard error	t-value	P-value
Intercept	75.4527	1.0288	73.340	0.0001
X_1	-5.7279	0.5081	-11.273	0.0001
X_2	3.7379	0.5081	7.357	0.0001
X_3	5.5513	0.5081	10.926	0.0001
X_4	4.8796	0.5081	9.604	0.0001
X_{11}	-0.7453	0.4753	-1.568	0.1390
X_{22}	0.9397	0.4753	1.977	0.0012
X_{33}	-0.0153	0.4753	-0.032	0.9750
X_{44}	2.0184	0.4753	4.247	0.0001
X_{12}	-0.1394	0.6223	-0.224	0.8260
X_{13}	-0.2844	0.6223	-0.457	0.6550
X_{14}	0.1544	0.6223	0.248	0.8080
X_{23}	0.9694	0.6223	1.558	0.0002
X_{24}	-1.5394	0.6223	-2.474	0.0001
X_{34}	0.0956	0.6223	0.154	0.8800

As is shown in normal probability plot of “studentized” residuals (Fig. 36), the residuals lie along the straight line, a proof of normal residual distribution and good data correlation with the model. The residuals normalcy meant that the error within the model were consistent with the acceptable normal distribution, signifying a completely randomized design.

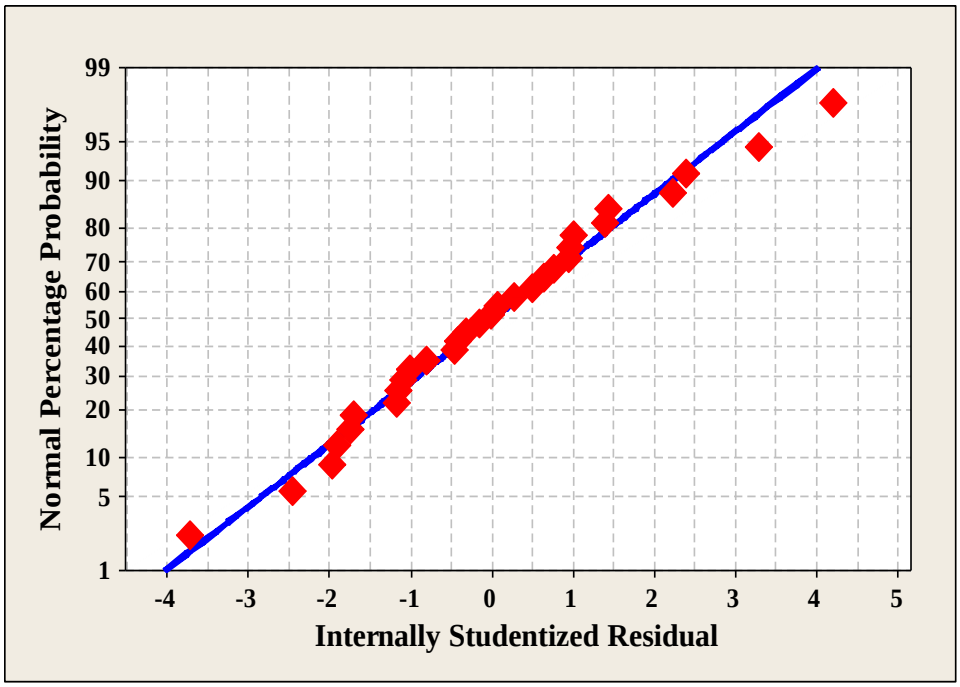

Figure 36: Model's normal probability plot of studentized residuals

5.3.8 Statistical ANOVA analysis

The statistical relevance and adequacy of the developed quadratic model to predict ß-blockers degradation efficiency was tested using analysis of variance (ANOVA). ANOVA is a key statistical tool used in testing the adequacy and relevancy of the generated models [79]. The P-values, a Fisher variation ratio (F-values), coefficient of variance, lack of fit F-value, coefficient of determination (R^2) and adjusted R^2 were some of the parameters assessed towards models accuracy and validity [105]. Based on ANOVA results (Table 22), an F-value of 30.55 greater than the tabulated F (2.352) at significance level 95% and at very low probability value ($P_{model} > F = 0.001$), was an indication that the current model was highly significant [101]. The lack of fit (LOF) of 1.64 (F-value < $F_{Critical}$ =4.7725) and p-value of 0.3340 (P-value > 0.05) demonstrated further, the adequacy of the obtained model in predicting ß-blockers degradation efficiency. All the R^2 and adj. R^2 represented in Table 22 were closer to unity; a justification of model's accuracy.

Table 22: Summary of Analysis of variance (ANOVA) to fit droplet-assisted flow electro-Fenton degradation of ß-blockers using CCD design.

Source	DF	Sum of squares	Adjusted mean square	F	P
Regression	14	2649.83	189.27	30.55	<0.0001
Residual Error	14	86.74	6.19		
Lack-of-Fit	10	69.76	6.97	1.64	0.3340
Pure Error	4	2.98	0.75		
Total	29	2736.57			
S.D	2.49%				
R^2	96.83%	R^2-(pred)	80.63%	R^2-(adj)	95.43%

S.D = standard deviation

5.3.9 Pareto Chart analysis

By calculating the effect of each variable/interaction on the response, the Pareto chart analysis provides an in-depth result treatment [118]. The Pareto analysis (Fig.37) clearly indicates the cumulative effect of each parameter/ interaction on response; with those on negative exhibiting antagonistic effects, while those on the positive side are synergistic towards responses [80]. The strength and significance of each variable/ interaction is measured by its length. The relatively significant parameters/ interactions are the ones with the longest bars. It is clearly seen that all the four selected factors are statistically significant, however, the order of significance was ET > pH > $[\text{ß-blocker}]_o$ > Applied current (Curr.). In particular $[\text{ß-blocker}]_o$ was antagonistic while the rest of the factors exhibited synergistic effects towards ß-blockers degradation efficiency. Also, the interaction effects of pH*pH, Curr.*ET and Curr.^2 were synergistic while the interaction effects of Curr.*pH, $[\text{ß-blocker}]_o^2$ and $[\text{ß-blocker}]_o$*ET demonstrated negatively (antagonistic) towards the degradation efficiency. Based on the above analyses, electrolysis time, pH and applied current were the most influential positive variables towards DFEF degradation efficiency of ß-blockers.

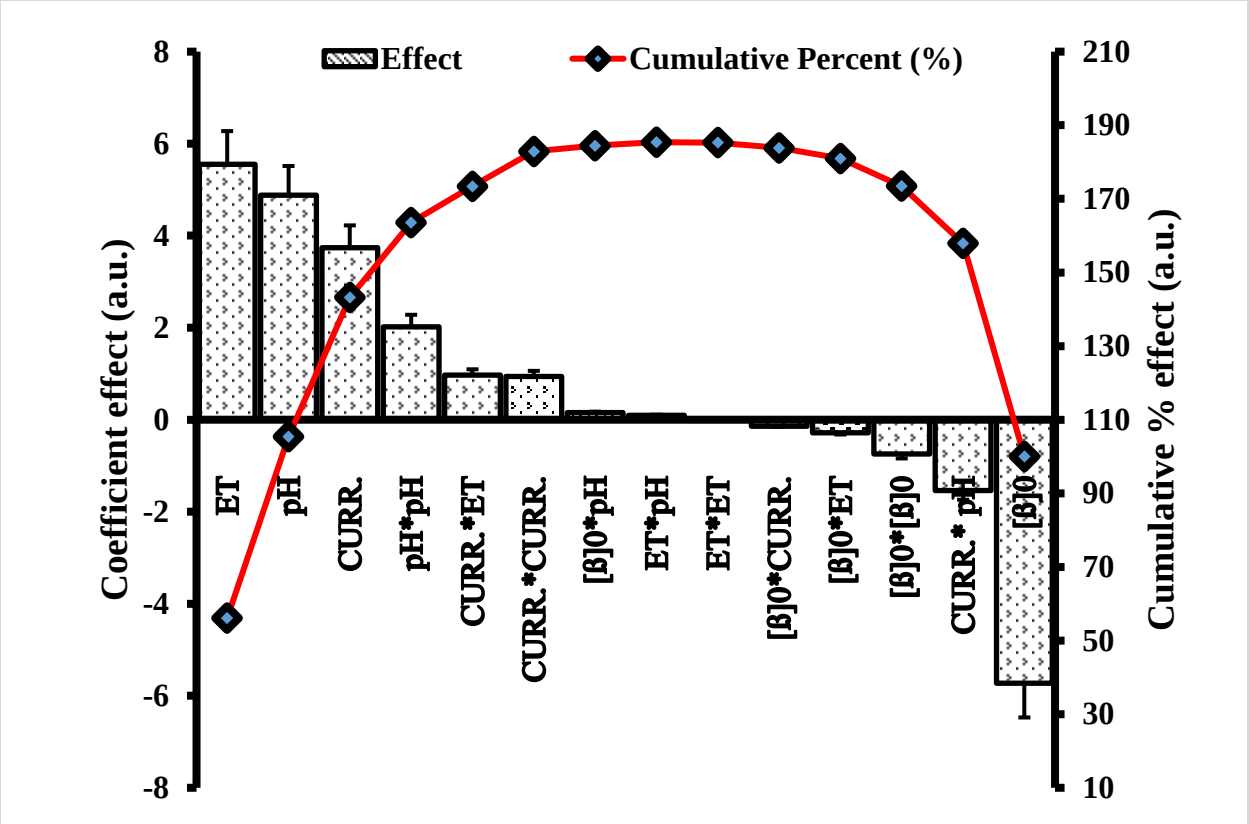

Figure 37: Pareto chart representation analysis level of significant variables and interactions affecting the ß-blockers degradation efficiency.

5.3.10 3D response surface and 2D contour plots

The simultaneous effects of two of the operational variables on ß-blockers degradation efficiency (% D.E) were represented by 2D contour and 3D response surface plots. This was made possible by maintaining some variables constant (at optimum level) while varying the rest of the variables over the experimental range. These graphical representations depict the significance of mutual interaction between the variables and as a result, useful information about the systems operation within the design (experimental) can be extracted. Fig. 38 (a) and (b) show the impacts of the interaction of the initial ß-blocker concentration ($[ß]_0$) and current (mA) on degradation efficiency (% DE). As depicted in Fig. 38 (a) and (b), the ß-blocker degradation efficiency (%DE) in the DFEF system was current-dependent and found to initially increase with an increase in applied current. When the applied current was increased from 100 mA towards 500 mA), a noteworthy trend in ß-blockers degradation efficiency was realized (Fig. 38 (b)). The results clearly indicate that a more rapid ß-blockers degradation can be attained upon increasing the applied current to a certain optimum value. This trend is majorly attributable to faster H_2O_2 production and faster regeneration of Cu^+ /Cu^{2+} and Fe^{2+} at relatively increased current that lead to increased production of •OH; all of which contribute to enhanced degradation efficiency. The probable reason for this behavior is that, with the graphite electrode surface modification, more surface particle electrodes become polarized with increasing applied current leading to enhanced surface redox process. However, the decrease in degradation efficiency at high applied current is mainly due to the onset of parasitic reactions. These results are attributable to the fast and increased •OH generation from Fenton's reaction [27] resulting from the cathode electrode modification [23], reactor design [20, 47] and anodic oxidation.

The DFEF experimental set-up allows a large electrode surface area to be in contact with the sample solution. Increase in applied current therefore leads to increase in the number of polarized particle surface electrodes. This enhances the surface redox processes leading to increased H_2O_2 production at the cathode which in presence of immobilized heterogeneous catalytic particles results into electro-generation of more •OH radicals. As a result, improved ß-blockers degradation efficiency is guaranteed. Since a BDD anode was used, there is also continuous and increased •OH production in form of BDD $(•OH)_{ads}$, which in turn also generates H_2O_2.

However, as the applied current increase to high values (500 mA) and with increased electrolysis time, there occurs a marked decrease in H_2O_2 electro-generation due to H_2O_2 oxidation at the anode electrode as represented in equations (9) and (10). As current is increased, time is reached when a 4-electron ORR (equation 12) supplants the 2-electron ORR (equation 1) resulting to greater reduction in H_2O_2 production. High applied current is also asserted to aggravate parasitic side reactions that are not favorable for continuous H_2O_2 production (equation 13-16) [139,140].

$$O_2 + 4H^+ + 4e^- \rightarrow 2H_2O \quad \text{.....(12)}$$

$$2H^+ + 2e^- \rightarrow H_2 \quad \text{.....(13)}$$

$$Fe^{2+} + HO• \rightarrow Fe^{3+} + OH^- \quad \text{.....(14)}$$

$$2HO• \rightarrow H_2O_2 \quad \text{.....(15)}$$

$$H_2O_2 + HO• \rightarrow H_2O + HO_2• \quad \text{.....(16)}$$

The performance of most AOPs is greatly influenced by the pH of the sample solution.

The effective operation of heterogeneous AOPs cover a wider pH range while transition metal ion activated homogeneous AOPs operate under restrictive acidic conditions [95]. Fig. 38 (c) and d)

illustrates the synergistic effect of current and pH on DE% for initial ß-blockers concentration of 400 ng/mL and electrolysis time of 10 min. method. As shown, DE% is greatest at pH 3 and remains almost constant (> 90 %) over a wider pH range of 4-7 and then decreases when the pH tends to 8. These observations reveal that the DFEF system with the Cu-B-FE composite cathode can effectively work under wider pH ranges spanning from 3-7.

Hydrogen peroxide catalytic decomposition for •OH production is favored by the presence of Fe^{3+} at low acidic conditions and is enhanced by Cu^{2+} at increasing pH on account of the deprotonated form of H_2O_2 (HO^{2-}, as the major electron donor for reduction of Cu^{2+}), appearing at pKa of nearly 11.6 [159].

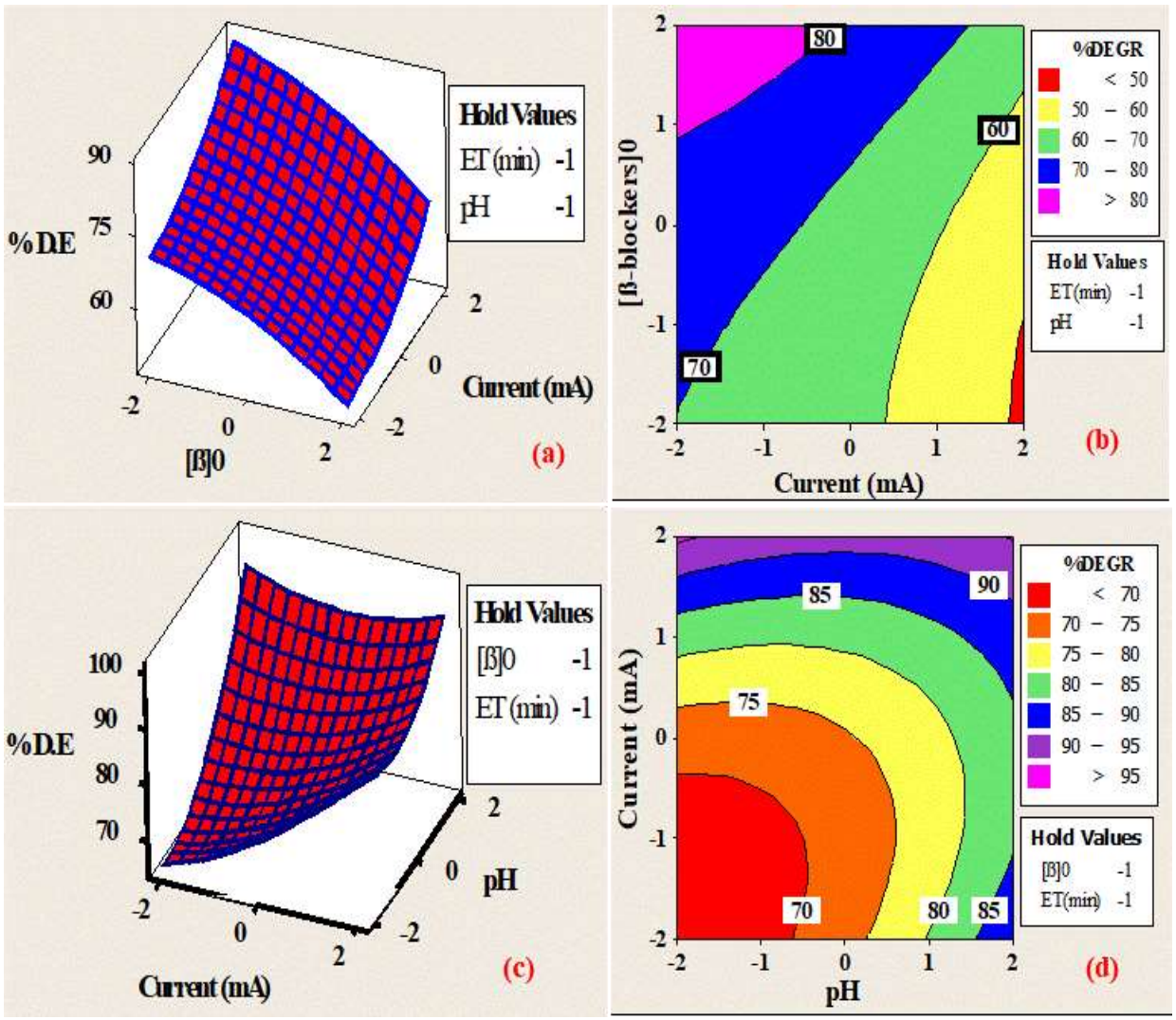

Figure 38: The 3D response surface and 2D contour plots of the effects of the interaction of (a) initial ß-blocker concentration ([ß]0 with (b) pH and between (c) applied current (mA) and (d) pH on ß-blocker removal efficiency (%DE).

5.3.11 Response optimization and validation

The 4-parameters influencing the ß-blockers degradation efficiencies (%DE) were optimized using response optimization approach. With this approach, optimal parameter values that result to maximum ß-blockers degradation efficiency are identified. 100% was set as the target value for the ß-blockers %DE while the lower value was set at 55. Since the upper value has to be greater than the target value, it was set at 110 while the weight and importance were all set to 1. Table 23 shows the results of the optimization and validation. The model was able to predict 99.9978% ß-blockers degradation efficiency and with an excellent composite desirability of 0.98995. The optimized conditions were then validated on both ACE and ATE using three consecutive experiments (V_1-V_3). Since the optimum pH for effective degradation was 7.0 while the pH of the sample solution was 6.8, the validation experiments were conducted without pH adjustment. The obtained %DE efficiencies for all the pollutants (ATE and PROP) were $\geq$99.9 %.

Table 23: Optimization conditions, prediction and composite desirability of the model

	[ß-Blockers]$_0$	I (mA)	ET (min)	pH	Composite Desirability	Predicted% degradation
1	200	100	10.00	7.0	0.98995	99.9978
	Validation of optimized conditions				%Ave.(PROP)	%Ave.(ATE)
V_1	200	100	10.00	UN	99.987	99.977
V_2	200	100	10.00	UN	99.979	99.959
V_3	200	100	10.00	UN	99.956	99.921

UN-meant without pH adjustment (the measured pH of hospital wastewater was 6.8). Each measurement is average of the triplicate reading.

5.4 Electrode reusability and stability studies

Electrode stability takes precedence, if it's to be considered for practical applications. Under identical optimized conditions, the same electrode was repetitively used in DFEF of ATE and ATE as illustrated in Fig. 39 (a). For all the degradation cycles (20 cycles), the degradation efficiencies for both ACE and ATE were maintained at $\geq$ 99 %. No significant change in ß-blockers removal efficiencies even after the 20^{th} cycle. Both ATE and ACE had the pseudo first order degradation rate constants of 0.016 and 0.014 min^{-1} respectively after one cycle of treatment. However, after 20 cycles of repeated degradation experiments, the average degradation rate constants for both ATE and ACE were 0.013 and 0.012 min^{-1} respectively which fall within the same order of magnitude as the rate constants in one cycle of treatment. This therefore demonstrate that the prepared integrated cathode electrode is stable and reusable for sequential DFEF degradation experiments at nearly neutral pH. The aforementioned observations are further supported by the electrodes Raman spectra's before and after 20 cycles of DFEF degradation studies as shown in Fig. 39 (b). The characteristic D, G and D^1 Raman bands for the 20-SMGE electrodes before degradation were at 1352, 1584 and 1626 cm^{-2} respectively, and, there was a slight peak shifting to 1354, 1590 and 1630 cm^{-1} after 20 cycles of degradation. These slight differences in band positions suggesting that the band positions fall within acceptable ranges and thus the 20-SMGE is stable even after 20 cycles treatment time.

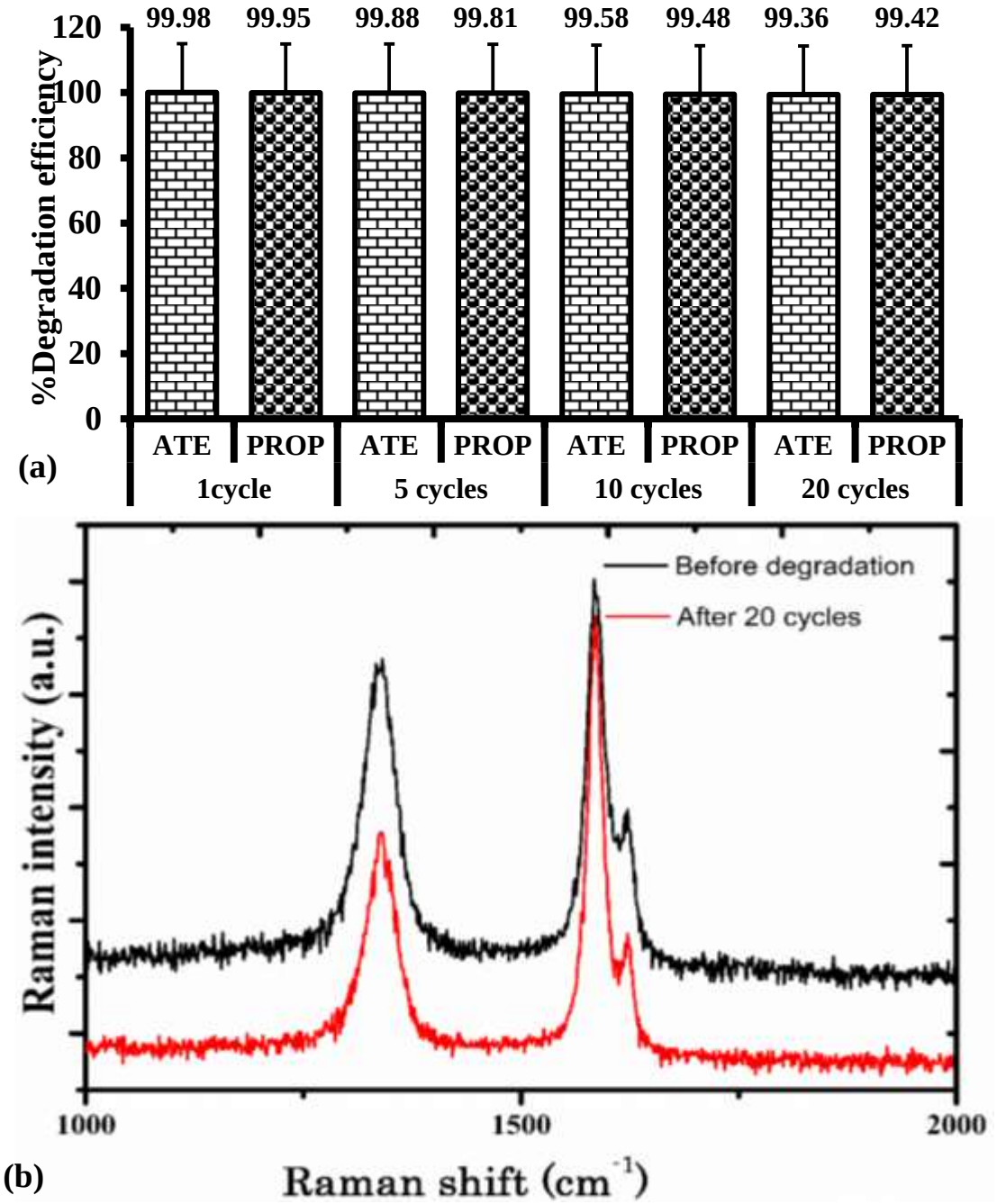

Figure 39: (a) Electrode reusability study using 20-SMGE in the DFEF degradation of ATE and PROP (At optimized conditions, in the beginning and end of 20 cycles) (b) Surface enhanced Raman spectra of 20-SMGE before degradation and after 20 cycles of electrode reuse in DFEF system

5.5 Mechanism of degradation on the modified electrodes

In establishing the possible degradation mechanism, on BGE functionalized Cu-B-Fe cathode electrode under a DFEF system, the degradation efficiency of both ATE and PROP were monitored at different conditions as depicted in Fig.40. The effect of different types of radical scavengers on ß-blockers degradation is shown in Fig. 40. After adding •OH scavenger (TBA or ethanol), there was a tremendous decrease in the degradation efficiency for both ATE and PROP. This demonstrates the great contribution of the generated •OH radicals in the DFEF system towards ß-blockers degradation.

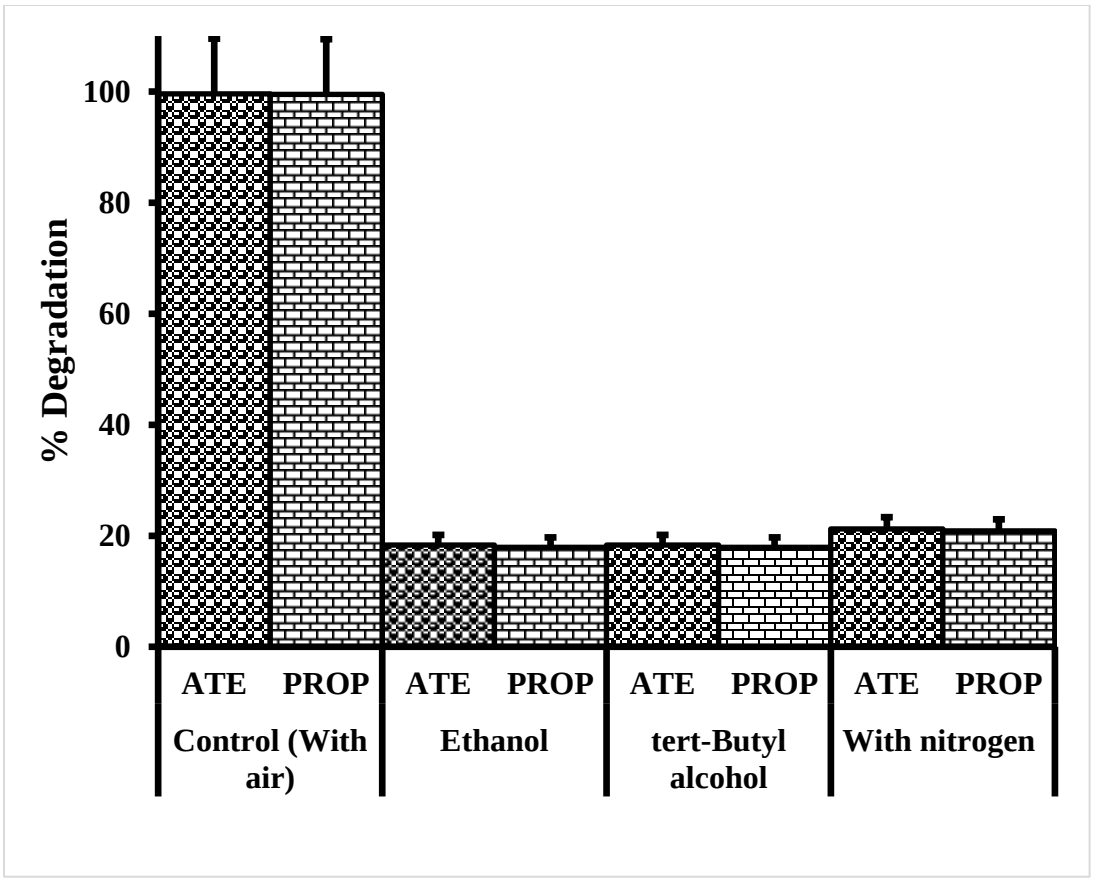

Figure 40: Effect of radical scavengers and nitrogen on DFEF degradation efficiency of (ATE and PROP). Ethanol (1/10, v/v, •OH scavenger), TBA (1/10, v/v, •OH scavenger) and Nitrogen assisted Flow-EF). (At optimized conditions)

Hence the probable EF oxidation mechanism on the 20-SMGE involves; (i) continuous adsorption and diffusion of air on the modified electrode, (ii) continuous electro-catalytic conversion of O_2 to H_2O_2 via 2-electron oxygen reduction reactions (equation 1), (iii) subsequent decomposition of H_2O_2 to •OH radicals by Fe^{2+} in the Cu-B-Fe bound on pretreated graphite electrode using (equations 2 and 4 and 17). In this case, copper serves a promoter role to facilitate the reduction of Fe^{3+} to Fe^{2+} (iv) the •OH radicals the oxidizes the ß-blocker (electron-rich), (v) in the process, Fe^{3+} is continuously regenerated via equation 3. In this case, the treated graphite electrode provides an excellent support for the Fenton catalyst as well as favorable surface (active sites) for ORR via a 2-electron pathway. Through the graphite network enriched with boron atoms, Fe^{3+} gets the electrons and serves the Fenton role of in situ generation of •OH radicals via reversible redox reactions. The generation of mainly •OH radicals in the DFEF system oxidizes the ß-blocker pollutants. The DFEF reactor improves the systems oxygen saturation at the cathode electrode and enhances the mass transfer kinetics of pollutant molecules during treatment. The proposed overall degradation mechanism on a 20-SMGE is depicted in Fig. 41.

$Fe^{3+} + Cu^{+} \rightarrow Fe^{2+} + Cu^{2+}$ ……..……...(17)

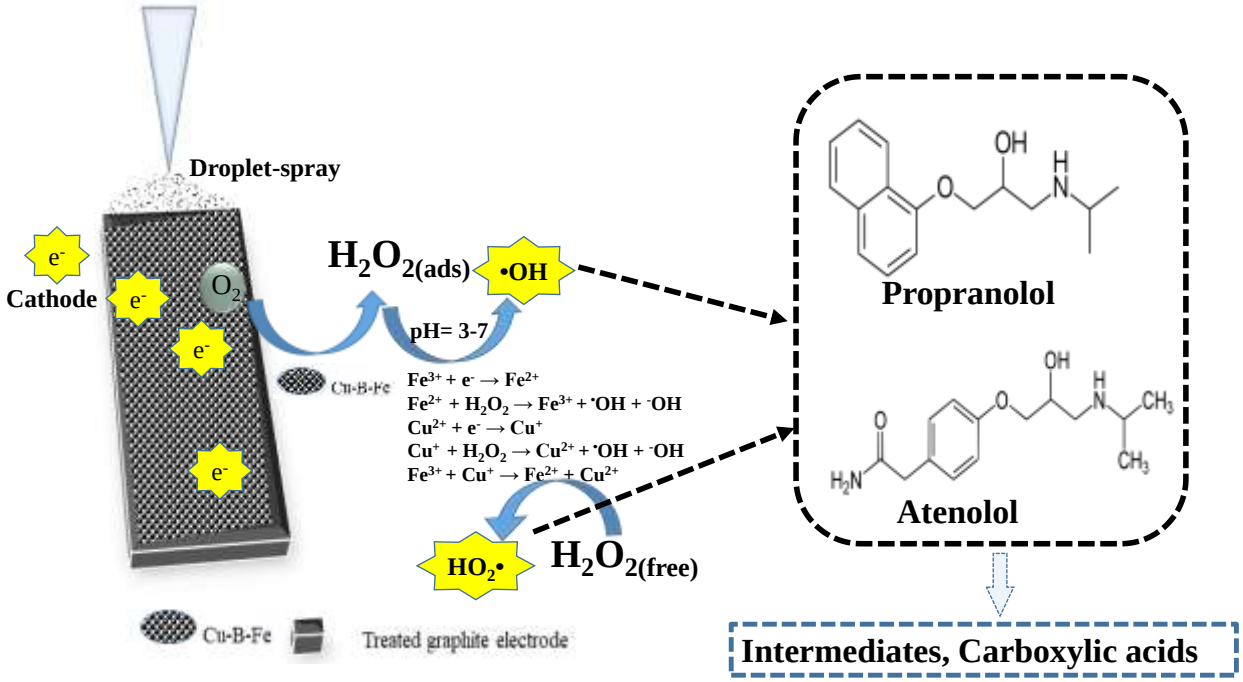

Figure 41: Proposed electrode surface mechanism for ß-blockers degradation in DFEF system.

CHAPTER 6

Combining Photoelectron-Fenton and Photocatalytic Methods for Enhanced Degradation of Nitrosamines in Swimming Pool Water

6.1 INTRODUCTION

Great concern has been raised about nitrosamines; the emerging disinfection byproducts of chloramination, chlorination, ozonation and industrial byproducts, owing to their surmised mutagenicity, carcinogenicity, and widespread distribution in various aquatic environments [160–164]. They are continuously formed through complex pathways, majorly determined by the disinfectant type and composition of the treated water [160,165]. Five N-nitrosamines have been included on US-EPA Contaminant Candidate List 4 [166]. Prominent among them are N-nitrosodiethylamine (NDEA) and N-nitrosodimethylamine (NDMA)) which are considered highly carcinogenic even at extremely low concentrations [161]. Literature has linked N-nitrosamines formation to household products, pharmaceuticals and personal care products since they constitute precursor sources such as quaternary or tertiary amines [167–170]. These compounds are discharged into the aquatic environment in form of wastewater effluents and because of inadequate treatment, they end up in domestic water supplies [169,171]. Some additional precursors including sunscreen products, urine, and human sweat; typical components of swimming pool waters, have been linked to nitrosamines formation [172]. Most of these emerging refractory contaminants are toxic and

cannot be completely remediated by conventional physico-chemical and microbiological treatment, hence, search for potent remediation methods. Advanced oxidation processes (AOPs) are asserted to provide ultimate remediation alternative and have received appealing relevance in water treatment systems [122,160,165,173–175]. AOPs are characterized by in-situ production of highly oxidizing reactive oxygen species (ROS) mainly hydroxyl radicals (•OH) capable of oxidizing most organic pollutants including recalcitrant counterparts [173,174]. Since most organic pollutants are electron rich compounds, they are rapidly and non-selectively attacked by electrophilic •OH radicals till mineralization [176]. Since •OH radicals are short-lived and easily annihilated (self) from the water treatment systems [177], there is a strong need for their fast and continuous generation. Numerous and innovative AOPs including but not limited to photoelectrochemical, electrochemical, photochemical and chemical methods are asserted to offer versatile •OH generation pathways that match particular treatment needs [178]. Coupling AOPs during treatment enhances degradation efficacies and decreases the degradation time [179] thus reducing the operational costs. Over the years, heterogeneous photocatalysis (PC), as a form of AOP involving semiconductor materials and UV-light irradiation, has gained significant importance in degradation of aquatic organic pollutants [180–183]. Different semiconductor materials like SnO_2, WO_3, ZnO, ZnS, CdS, and $SrTiO_3$ have been utilized, however TiO_2 nanoparticles, especially in their anatase phase have been preferred and their mode of action is reported elsewhere [176]. The beneficial properties of TiO_2 as a photocatalyst include: natural abundancy, low cost, low toxicity, high photocatalytic efficiency, chemical and physical stability [184–187]. However, lower solar energy conversion efficiency, low adsorption ability, and wider band gap renders undoped TiO_2 ineffective and with limited practical photocatalytic applications [188]. In photocatalytic degradation of most pollutants in aquatic environments, TiO_2 is used in its suspended mode, thus registering increased surface UV-light illumination efficiency [189].

The use of mesoporous silica as a TiO_2 support towards degradation of organic pollutants has extensively been studied [190]. The use of porous supports in Titania synthesis prevents particle agglomeration, promotes homogeneous dispersion and help in controlling TiO_2 size and shape [191]. Such mesoporous silica orientations offer unique surfaces with highly enhanced surface area, functionalizable surface, uniformly distributed mesopores and excellent thermal and chemical stabilities [191,192]. Microwave assisted sol-gel routes have been reported as novel and interesting synthesis methods for binary oxide nanoparticles owing to its eco-friendliness, faster reaction kinetics and higher energy efficiency [190,193]. On the other hand, electrochemical advanced oxidation processes (EAOPs) like electro-Fenton (EF), photoelectro-Fenton (PEF) and anodic oxidation (AO) have been approved as versatile, eco-friendly and highly effective technologies for on-site degradation of organic pollutants [27,194,195]. In particular, Fenton-based EAOPs, like EF, Hetero-EF (hEF) and Hetero-PEF processes (hPEF), have received greater attention in remediation of wide varieties of recalcitrant organic pollutants from aquatic environments [196–198]. Typically, such EAOPs utilizes both AO and electrogenerated H_2O_2 (EO-H_2O_2) which in presence of a heterogeneous/ homogeneous Fenton catalyst generates highly reactive $^{\bullet}OH$ radicals [199] key in un-selective mineralization of organic pollutants. These reactive oxygen species (H_2O_2, $^{\bullet}OH$) are formed either in the entire sample (bulk) solution via Fenton reaction chemistry (equation 2) or at the anode surface through water oxidation (equation 1) [27,177,195] especially if high O_2 evolution overpotential anodes (B) like boron doped diamond are used [200].

$B(H_2O) \rightarrow B(^{\bullet}OH) + H^+ + e^-$ .... (1)

$Fe^{2+} + H_2O_2 + H^+ \rightarrow Fe^{3+} + {}^{\bullet}OH + H_2O$ .... (2)

Organic pollutants degradation efficiencies majorly depend on reactor design, nature and type of the electrodes used [201]. In an effort to fabricate an efficient hEF electrolytic reactor, its ability for fast and effective H_2O_2 electro-generation is considered a key selection factor [202].

Nowadays, new and different electrode surfaces with enhanced surface properties for H_2O_2 electro-generation during hEF processes, are being developed by different researchers [178,199]. Notably, recent research trend is aimed at fabricating stable, eco-friendly and efficient hEF and Hetero-PEF systems capable of mitigating Fenton catalyst agglomeration, fall-off, dissolution as well as multi-step catalyst synthesis/ electrode functionalization [199].

Carbon based electrodes are widely used electrodes in EF studies, however, to date a great deal of research effort is dedicated towards their modifications for stable and efficient heterogeneous EF applications [199]. Also, the utilization of hetero-EF systems as reusable and recyclable Fenton catalysts over an extended pH range during water treatment [178,199,201] cannot go un-noticed. When the heterogeneous EF process is simultaneously irradiated with UV-light in a hPEF reaction, three determining reactions occur [199]; (i) enhanced Fe^{2+} regeneration with more •OH production from photolysis of $Fe(OH)^{2+}$ species as shown in equation (3).

$$Fe(OH)^{2+} + hv \rightarrow Fe^{2+} + {}^{\bullet}OH \quad \ldots\ldots\ldots\ldots\ldots\ldots\ldots\ldots\ldots\ldots\ldots\ldots\ldots\ldots\ldots\ldots 3$$

(ii) photo-decomposition of generated Fe(III)-carboxylate complexes as shown in equation 4 [176].

$$Fe(OOCR)^{2+} + hv \rightarrow Fe^{2+} + CO_2 + R^{\bullet} \quad \ldots\ldots\ldots\ldots\ldots\ldots\ldots\ldots\ldots\ldots\ldots\ldots\ldots\ldots 4$$

(iii) homolytic cleavage of H_2O_2 leading to additional ${}^{\bullet}OH$ production as indicated in reaction equation 5.

$$H_2O_2 + hv \rightarrow 2{}^{\bullet}OH \quad \ldots\ldots\ldots\ldots\ldots\ldots\ldots\ldots\ldots\ldots\ldots\ldots\ldots\ldots\ldots\ldots\ldots\ldots 5$$

Like in the case of EF processes, the nature and type of cathode plays a cardinal role in PEF experiments since it determines H_2O_2 electrogeneration, Fenton catalyst electroreduction, in addition $^{\bullet}OH$ generation and pollutants degradation [177]. For such processes, to achieve excellent catalytic activities, the contact between water, reactants and the electrode need to be maximized and as such different electrolytic reactor designs have been investigated [203].

The high operational costs typical of most AOPs technologies are associated with high electrical energy demand which can be minimized through logical optimization. The classical optimization technique of changing one variable at a time to study the effects of variables on a given response is time consuming and expensive, especially for multivariable optimization [204]. Moreover, this approach does not account for interaction effects between different variables. Statistical experimental design based on central composite design (CCD) offers utile techniques for extracting valuable and statistical experimental information using minimal number of experimental runs [204]. `

The present study investigates the efficiency of a coupled flow-assisted heterogenous photoelectron-Fenton system and TiO_2 immobilized rice husk silica for the treatment of two N-nitrosoamine compounds in swimming pool water. This study involves fabrication of graphite electrode with Cu-B-Fe composite and loading TiO_2 on rice husk nanosilica spheres via microwave-assisted sol-gel routes. The efficiency of this approach is assessed through effects analysis on various operating parameters with the aim of selecting the most suitable and adequate operating parameters. The target N-nitroso compounds used in this study were N-nitrosodi-n-propylamine (NDPA) and N-nitrosodi-n-butylamine (NDBA). Lastly, a response surface methodology approach based on central composite design was used in experimental design and parameter optimization.

6.2 EXPERIMENTAL

This work involves microwave assisted sol-gel synthesis of rice husk silica coated TiO_2 and hydrolytic sol-gel immobilization of Cu-B-Fe composites on treated graphite electrodes. By using a continuous flow-assisted electro-Fenton system designed to suit photoelectron-Fenton reactor and central composite design optimization, the prepared materials were evaluated for effective degradation efficiency of N-nitrosamine in swimming pool water via coupled PEF/photocatalysis.

6.2.1. Chemicals

All the chemicals used in this study were of analytical/ HPLC grade from Sigma-Aldrich, Panreac and Merck. Tetra-n-butyl titanate (Ti(OBu)4), reagent grade 97.0% obtained from Sigma-Aldrich. Graphite plate electrodes (high quality, 100 mm x 100 mm x 4 mm) were secured from Shanghai Qijie Limited Co., China. Nitrosamines containing N-nitroso-di-n-propylamine (NDPA) and N-nitroso-di-n-butylamine (NDBA (all 99.9% purity) were secured from Supelco (Bellefonte, PA, USA). Stock standard solutions of NAs (1000 mg/L concentrations of each) were prepared in amber-colored bottles using methanol (LC–MS-grade) and stored in the freezer at -23 oC. All the synthetic solutions were prepared using double distilled water.

6.2.2. Swimming pool water

The swimming pool water samples were collected from nearby swimming pool facilities. Disposable polypropylene bottles (500 mL) covered with aluminum foil were used to collect water samples. This

was done to avoid effects of sun-light pollutant evaporation. After collection, the samples were preserved in a refrigerator at 4^{o}C and used in the following two weeks.

6.2.3. Immobilization of TiO_2 on rice husk nanosilica spheres

Rice husk nanosilica sphere coated TiO_2 was prepared from rice husk silica, $Ti(OBu)_4$ and co-solvents via microwave-assisted sol-gel synthesis. In a typical synthesis, 45g of milled rice husk (RH) was first washed with 10% hydrochloric acid and then 30% sulfuric acid solutions (500 mL at 60 ^{o}C) for 5 hours under constant stirring conditions. This was aimed at removing metallic impurities. After acid-drain off, the rice husk was rinsed with distilled water till neutral pH. The acid-leached rice husk was oven dried at 110 ^{o}C overnight. The dry RH samples were then placed in a muffle furnace and calcined at 750 ^{o}C for 5 h to obtain rice husk ash (RHA). About 3.0 g of RHA was dissolved in NaOH (250mL, 1.0 M and at 80 ^{0}C) under constant stirring for 5 hours. The resultant solution was then sieved to obtain clear sodium silicate (Na_2SiO_3) solution. The prepared Na_2SiO_3 solution was labelled M. To obtain pure RHS, 15 mL of Na_2SiO_3 solution was titrated with 1.0M HCl till gel formation (pH<5). The resultant solution was labeled "Y". Meanwhile a TiO_2 precursor was prepared separately as follows. To 25.0 ml of $Ti(OBu)_4$ was added 1.0 ml of acetylacetone and 20.0 ml of ethanol and then ultrasonicated for 1 h. This was then followed by addition of 4.0 ml of distilled water and 0.4 ml of concentrated hydrochloric acid with a 0.5 min ultrasonication time. This solution was labelled as "N". Solution N was added drop wise to 15 mL of solution M with simultaneous stirring till gel-formation. The resultant gel solution was labelled "X". The gel-solution of X, Y and N were subjected to Microwave Digestion/Extraction system of (Anton Paar Synthos 3000, Graz, Austria) at operating conditions of; 800 W, 1.0 MPa, 80 min processing time (100 ^{o}C) and 100 ^{o}C constant heating (30

min). The resultant microwave synthesized samples were then centrifuged at 7000rpm for 3 min, washed with distilled water and ethanol, oven dried at 150 ◦C for 5 h. It was then finally ground into powders (mortar-pestle) and calcined in a muffle furnace at 550 ◦C for 8 h.

6.2.4. Functionalization of graphite electrodes

Several graphite plates of dimensions (4.0 cm^2 for each plate) were first polished using ultrafine grit emery sheet and then sulfonated with 3.0 M sulfuric acid (100 ^oC, 3.0 h). This was aimed at improving electrode porosity and adding oxygen-related functionalities to the electrodes. This stage was followed by electrode rinsing and oven drying (100 ^oC, 5 h) to prepare them for sol-gel modification. The sulfonated graphite electrodes were at this stage denoted as 'SGE'. Meanwhile, to 25 mL of Na_2SiO_3 solution (rice husk based) prepared in section 2.3 was added pre-dissolved glycerol and cetyltrimethylammonium bromide (CTAB), (2% each), as surface directing and capping agents respectively (each 3 wt. %). Under constant stirring conditions, a prepared acidic solution (3 M HNO_3, 10 wt. % Cu^{2+}, 20% Fe^{3+} and 5 wt. % of boron) was added to Na_2SiO_3 solution dropwise till gel formation (pH 3.0). The precipitated gel was aged at 60 ^oC in an oven for 2 h and then washed clean with copious amount of double distilled water using a centrifuge. The clean aged samples were then dispersed in 200 mL of double distilled water from which the previously sulfonated electrodes (SGE) were subsequently dipped (3-cycles of repeated dipping) and then oven drying at 150 ^oC for 10 min after each dipping cycle. The dip-coated electrodes were finally annealed in a muffle furnace at 450 ^oC for 2.0 h.

6.2.5. Characterization techniques

Several characterization techniques were used to characterize the fabricated electrodes and synthesized photocatalyst. Characterization details of Cu-B-Fe functionalized graphite electrodes used in this study appear in the previous chapter (chapter 5). More characterization for RHS-TiO_2 characterization is presented in this chapter alongside some few characterizations of the modified graphite electrodes. The crystallographic nature and phase-identification of the RHS-TiO_2 were investigated using X-Ray diffraction (Rigaku Miniflex, diffractometer). The analysis was carried out using Cu Kα X-Ray source (λ = 1.5418 A^o) operating at 45 kV with a scan rate of 2 $^o min^{-1}$. The intensity of the diffracted X-ray was plotted as a function of diffraction angle (2θ) in ranges of 20 to 80 ^{o}C. The microstructures, morphologies, and elemental mapping of the RHS-TO_2 samples were characterized using Scanning electron microscope (SEM, JEOL JSM-6610 LV) and energy dispersive X-ray spectroscope (EDX) at 20.0 Kv. The electrochemical properties of the modified electrodes were evaluated using cyclic voltammetry (CV) (electrochemical workstation, CHI1140A, CH Instruments Inc., Austin, TX, USA).

6.2.6. Combined hetero-photoelectro-Fenton and hetero-photocatalytic degradation studies

The electrolytic reactor system used in degradation study constituted a flow-assisted heterogeneous electro-Fenton system suited to incorporate both heterogeneous PEF and heterogeneous photocatalytic degradation simultaneously. As depicted in Fig.42, this reactor system consisted of five parts: Electrolytic cell (0.5 L), current source, peristaltic pump, air pump and light source (MAX-

350, Xenon Light Source 300W Asahi Spectra USA Inc). An air pump ensured continuous supply (inflow) of both air and reactant species to the cathode electrode in form of droplet spray while the peristaltic pump ensured continuous sample flow. Both the anode and the cathode were 20-SMGE. A distance of 1cm was maintained between the electrodes. Constant DC supply was supplied and monitored by a variable DC power supply (Sargent Welch Scientific) equipped with a digital multimeter (Fluke). The sample solution was illuminated by UV-VIS-light source from the side of the cathode electrode and the system was covered by an aluminium foil as shown in Fig. 42 to direct light to the reactants. 0.05M Na_2SO_4 (210 mL) was used as supporting electrolyte while 3 M, H_2SO_4 or 1M NaOH was used to adjust the sample pH. The sample solutions were stirred vigorously with a magnetic bar to maintain suitable movements of reactant molecules from/towards both electrodes. Before the degradation experiments, the experiment was allowed to run for 10 minutes to prevent electrode sorption effects and improve sample aeration. In every experimental run, 210 mL of swimming pool water spiked with 250 ng mL^{-1} of nitrosamines were directed into the reactor system. The applied current was initially set at 100 mA and sample pH maintained at 3. Both the visible light source and the DC power supply were switched on. Both experimental conditions and operational variables of each experimental trial is provided in Table 24. At specific time intervals (as reflected in the experimental design), the samples were withdrawn, extracted and analyzed using GC-MS in terms of degradation efficiency (%DE) following equation (6).

Degradation efficiency=$(1- C_i/C_O)x\ 100$ ---------- (6)

Where C and C0 represent ß-blockers concentration at time (t) and (0), respectively.

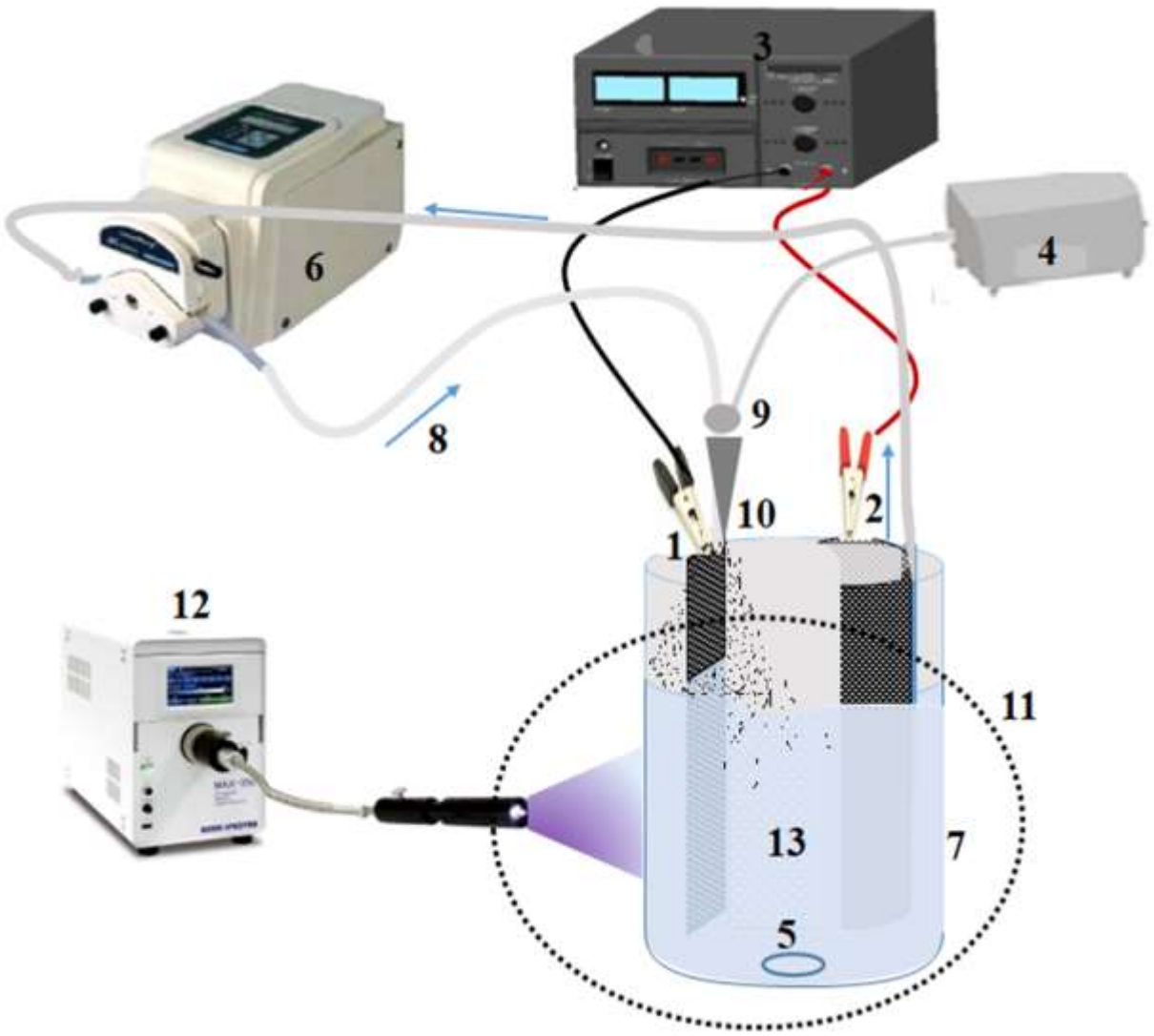

Figure 42: Sketch diagram of a photoelectron-Fenton reactor designed in form of droplet flow-assisted electro-Fenton (DFEF) system: (1) Sol-gel modified graphite anode electrode (20-SMGE) (2) Cathode electrode (3) Variable DC power supply, (4) Air pump, (5) Magnetic stirrer, (6) Dual-headed peristaltic pump, (7) Electrolytic reactor, (8) Direction of sample flow (9) Junction for mixing natural air with untreated sample to form a droplet spray at cathode electrode through (10) (11) part covered with aluminium foil during treatment (12) Xenon Light Source.

6.2.7. Extraction procedure and GC-MS analytical parameters

The target analytes were extracted using dispersive liquid-liquid extraction as follows. To a 5 mL sample solution was added 1.5 mL methanol (dispersant) and 25 µL carbon tetrachloride, followed by ultrasonication for 2 minutes to form a cloudy solution. The nitrosamines were extracted in the cloudy solution as fine droplets of dispersed CCl_4.This was followed by 5 min centrifugation (5000 rpm) with the extraction solvent settling at the bottom of the conical tube. By using a micro syringe, about 16 µL was transferred to micro vials ready for injection into the GC–MS. Analyses was performed on a GC–MS (Shimadzu technologies, QP 2010 ultra-system) equipped with split–split less injection port and an inert ion source. The analysis was made using high purity helium (>99.999%) as a carrier gas operating at constant flow rate of 1.0 mL min^{-1}. Chromatographic separation was achieved on a stationary phase column with the injection volumes of 3µL. An injection port, interface, and ion source temperatures used were 230 ºC, 250 ºC and 200 ºC in the split less mode. The GC-temperature program used in the analyses was: initial column temperature of 70 ◦C held for 3 min and then increased to 140 ◦C at 15◦C min^{-1}, then to 200 ◦C at 5◦C min^{-1} and finally to 250 at 10 ◦Cmin^{-1}. Selected ion monitoring (SIM) mode was used in analyte quantification using both target ion and qualifier ions (Table 25) while the scan mode was operated from m/z 30 to 200.

Table 24: Experimental ranges and levels of the independent test variables.

	Ranges and levels				
Variables	-2	-1	0	1	2
[N-nitrosamine] $_o$ (ng/mL) (X_1)	50	100	150	200	250
RHS-TiO_2 dosage (g/L) (X_2)	0.50	1.25	2.00	2.15	2.50
Applied current (mA) (X_3)	100	200	300	400	500
Electrolysis time (min) (X_4)	5	10	30	40	60

6.2.8. Experimental design

A response surface methodology based on central composite design (CCD) was used to optimize of combined effect of Droplet-flow-photoelectro-Fenton with photocatalytic process towards degradation of β-blockers. Four main factors were selected to evaluate the effect of operating variables on degradation efficiencies of N-nitrosamines (NDPA and NDBA) in swimming pool water. These included; [N-nitrosamine] $_o$ (ng/L) (X_1), RHS-SiO_2 dosage (g/L) (X_2), applied current (mA) (X_3) and electrolysis time (min) (X_4). Using Minitab 17 software, thirty-one (31) randomly distributed experimental runs including 16 cube points, 7 center point replications and 8 axial points were generated and used in experimental design and analysis. The test variables (X_i) were coded as x_i in the statistical calculations according to the relationship below.

$$x_i=\frac{X_i-X_o}{\delta x} \quad \text{.....5}$$

where δx represent a step change while X_0 is the value of X_i at the center point [203,204]. The experimental levels and ranges are presented in Table 24 while the design matrix based on coded values is presented as Table 26. Both NDPA and NPBA had very closer DE% values and as a result, the average value for the two N-nitrosamines was considered for statistical analysis.

Table 25: Target analyte, their retention time and qualifier ions (in SIM mode).

Retention time (min)	Target compound	Abbreviation	Selected target ions
10.55	N-nitrosodipropylamine	NDPA	42, 43, 70
13.5	N-nitrosodibutylamine	NDBA	41, 57, 84

Table 26: Randomized design matrix used in DF-PEF-RHS/TiO2 degradation of N-nitrosamines

StdOrder	X_1 (ng/mL)	X_2 (g/L)	X_3 (mA)	X_4 (min)
5	-1	-1	1	-1
14	1	-1	1	1
3	-1	1	-1	-1
19	0	-2	0	0
22	0	0	2	0
20	0	2	0	0
13	-1	-1	1	1
11	-1	1	-1	1
28	0	0	0	0
30	0	0	0	0
23	0	0	0	-2
12	1	1	-1	1
21	0	0	-2	0
4	1	1	-1	-1
6	1	-1	1	-1
17	-2	0	0	0
10	1	-1	-1	1
31	0	0	0	0
26	0	0	0	0
2	1	-1	-1	-1
24	0	0	0	2
7	-1	1	1	-1
8	1	1	1	-1
25	0	0	0	0
15	-1	1	1	1
29	0	0	0	0
1	-1	-1	-1	-1
16	1	1	1	1
18	2	0	0	0
9	-1	-1	-1	1
27	0	0	0	0

6.3 RESULTS AND DISCUSION

6.3.1 Characterization

XRD patterns of microwave-assisted sol-gel synthesized rice husk silica (RHS), TiO_2 and titanium oxide immobilized RHS (RHS-TiO_2) were presented in Fig. 43. As it is shown, the amorphous phase of pure rice husk silica and crystalline structure of microwave assisted synthesized TiO_2 were demonstrated for comparison purposes. The XRD patterns of pure TiO_2 and after its immobilization on rice husk silica (RHS-TiO_2) revealed the existence of anatase TiO_2 (JCPDS No. 21-1272). The key diffraction peaks for pure TiO_2 appeared with 2θ values of 25.3^o, 37.8^o, 48.0^o, 53.9^o and 55.1^o. These were ascribed to pure TiO_2 anatase phase formation with respective miller indices of 101, 004, 200, 105, and 211 [205]. Similar major diffraction peaks for pure TiO_2 (anatase) were depicted in the XRD patterns for RHS-TiO_2. The intense and sharp peak at 25.3^o in pure anatase phase suggested the formation of a well-crystalline single anatase phase that is key in performance and conductivity of a photocatalyst. The presence of the diffraction peaks of TiO_2 on RHS silica is a clear demonstration of sample crystallization.

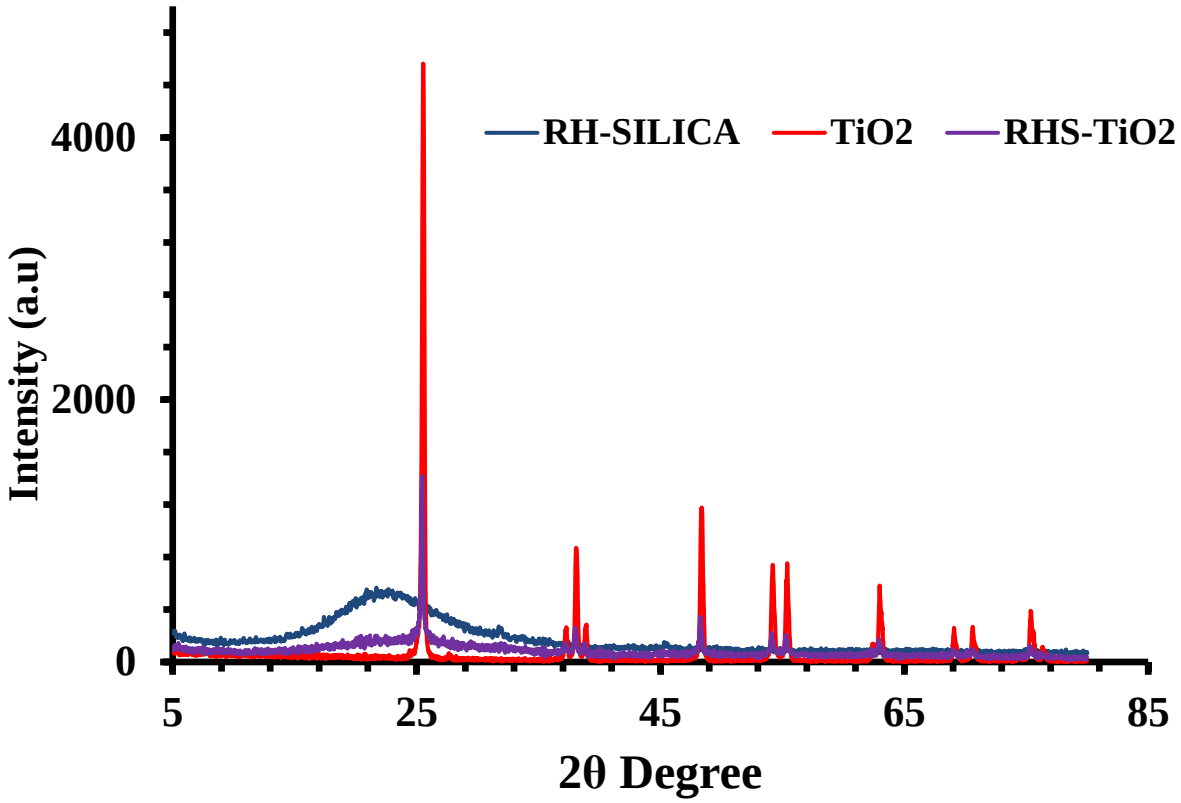

Figure 43: XRD Patterns of powdered samples of RHS, TiO_2 and RHS-TiO_2.

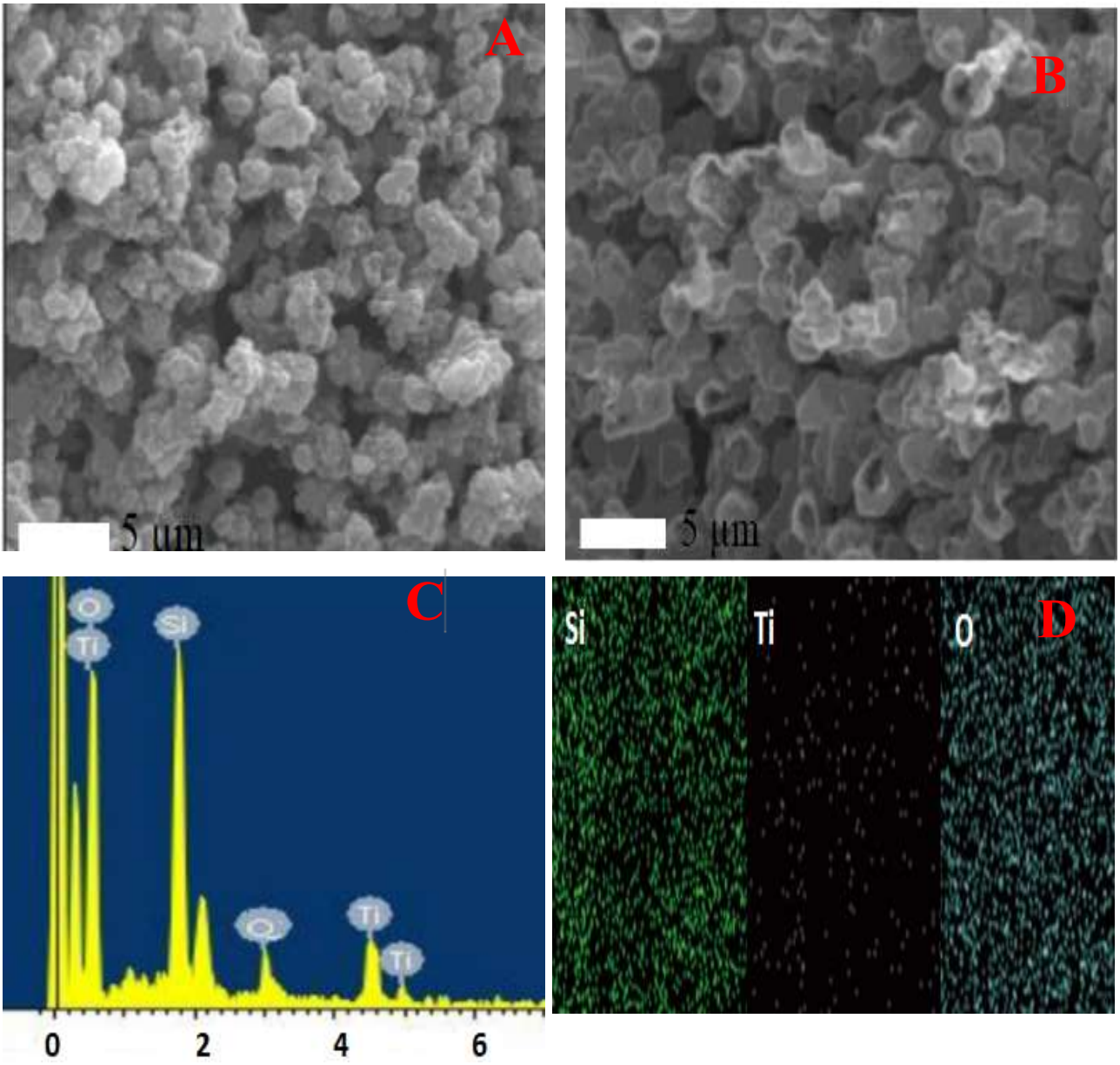

Figure 44: SEM micrographs of microwave-synthesized (a) RHS, (b) RHS-TiO_2, (c) EDS of RHS-TiO_2 (d) elemental mapping of RHS-TiO_2

Figure 44 a and b shows morphologies for rice husk SiO_2, and RHS-TiO_2. Rice husk silica shows spherical particles with uniform spherical and smooth surface morphologies. However, the immobilization of TiO_2 on SiO_2 made the smoother surface appear rough. Still, there is some marked increment in porosity after immobilization. Moreover, the EDS analysis in Fig. 44c clearly indicated the presence Ti, Si and O in the composite matrix. These results were further supported by the EDX elemental mapping composition (Fig.44d) with evidence of elemental particle homogeneity in the composite matrix. The electrochemical properties resulting from Cu-B-Fe modification of the bare graphite electrode (BGE) were demonstrated using cyclic voltammetry as illustrated in Fig.45. Fig. 45 depicts well-defined redox peaks typical of forward and reversed scans of $Fe(CN)_6^{3-/4-}$ redox couples. It is clear that the Cu-B-Fe immobilization on BGE enhanced the redox peaks significantly. The anodic and cathodic regions are indicated by the respective positive and negative regions on the voltammogram [154]. The nanoparticle morphologies resulting from electrode modification are characteristic of the observed electrodes electrochemical properties. Its reported in several studies that nanoparticle electrode modification highly improves the catalytic and electron transfer kinetics at the electrode surfaces [206]. The nearly rectangular shaped voltammogram exhibited by the 20-SMGE modified electrode is a clear manifestation that the electrode has higher potential for enhanced electron transfer on the electrode surfaces [155]. Compared to BGE, 20-SMGE displayed a highly enhanced current response towards oxygen reduction reactions (ORR) and increasing negative hydrogen evolution potentials

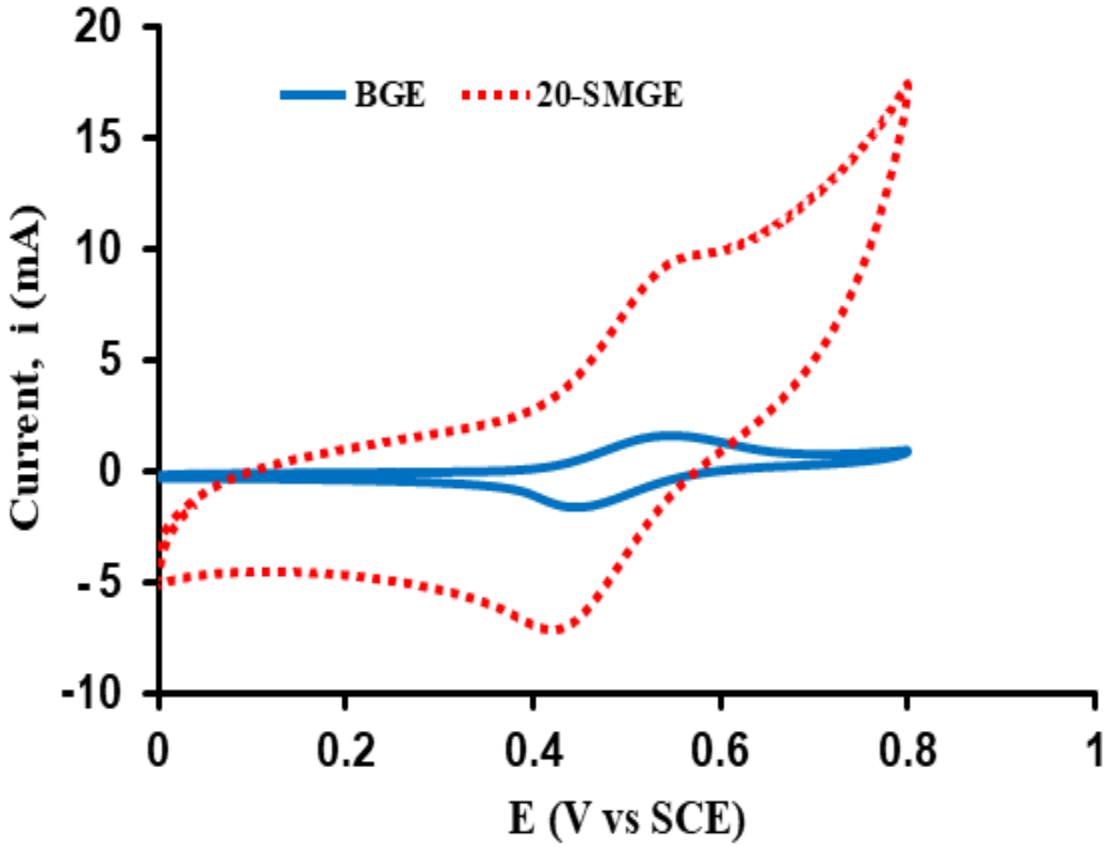

Figure 45: Cyclic voltammograms of BGE and 20-SMGE

6.3.2 Central composite design (CCD) model

A second-order polynomial equation (8) was used to express the empirical relationship between the response and independent variables basing on the generated experimental results. Both NDPA and NPBA had very closer DE% values and as a result, the average value for the two N-nitrosamines was considered for statistical analysis.

$$DE\ (\%) = 83.86 - 0.89X_1 + 0.30X_2 + 5.68X_3 + 3.04X_4 + 0.86X_{11} - 0.179X_{22} + 0.15X_{33} - 2.05X_{44} + 0.59X_{12} + 0.33X_{13} - O.72X_{14} - 0.041X_{23} - 1.01X_{24} - X_{34} \quad \ldots\ldots(8)$$

Equation (8) was used to predict the degradation efficiencies (DE (%). These results indicated that both the predicted and experimental values were in good agreement and with correlation coefficient (R^2) of 92.65% and with closer Adj-R^2 of 86.76% value The models adequacy and significance were further tested using analysis of variance (ANOVA) (Table 27) [204]. The total variation is subdivided by ANOVA in to two components; models' variation and experimental errors variation and this is further tested for significance. The Fishers value (F-value), the ratio between the mean square of the model and the residual error is used to assess the comparison. If a models F-value is greater than the tabulated F-value at a given level of significance for a certain number of degrees of freedom, then the model is confirmed fit and adequate [203]. Accordingly, the obtained F-value was 7.76 far greater than the tabulated F-value (2.352 at 95% significance). The model used was then confirmed to be adequate and fit. The student's t distribution with their parameter estimates and corresponding values are depicted in Table 28. The results in Table 28 were used to check the significance of each coefficient in relation to the obtained P-values, which information is key to understanding the pattern of mutual interactions between the test parameters. The greater the student's t-test value and smaller P-value, the more significant is the corresponding coefficient [204].

Table 27: Analysis of variance (ANOVA) for fitting the DE (%)

Source of variation	Sum of squares	Degree of Freedom	Adjusted mean square	F-Value	P-value
Model	8527.55	14	609.11	7.76	<0.001
Residual	1256.36	16	78.52		
Total	9783.91	30			
R^2	92.65%				
Adj-R^2	86.76%				

The normal probability plot of “studentized” residuals is presented in Fig.46. Accordingly, most residuals lie along the straight line, a proof of good data correlation and normal residual distribution with the model. This meant that the error within the model was consistent with the acceptable normal distribution. Hence signifying a completely randomized design.

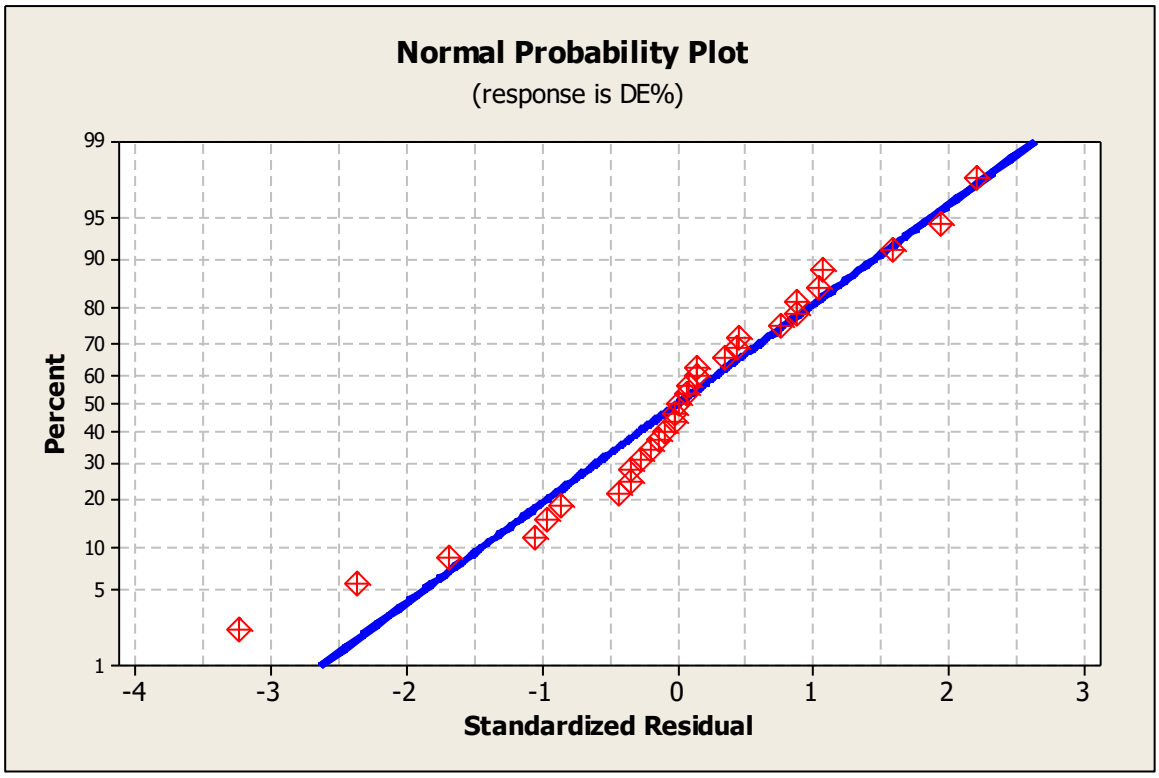

Figure 46: Normal probability plot of standardized residuals

Table 28. Estimated regression coefficients with corresponding t and P values

Coefficient	Parameter estimate	Standard error	t-value	P-value
b_0	83.864	3.3493	25.04	0.000
b_1	-0.89	0.9044	-0.984	0.340
b_2	0.295	0.9044	0.326	0.749
b_3	5.6775	0.9044	3.365	0.004
b_4	3.0438	0.9044	6.278	0.000
b_{11}	0.8637	0.4143	2.085	0.033
b_{22}	-1.794	0.4143	-4.33	0.001
b_{33}	0.1465	0.4143	0.354	0.072
b_{44}	-2.053	0.4143	-4.955	0.000
b_{12}	0.5894	0.5538	1.064	0.303
b_{13}	0.3313	0.5538	0.598	0.558
b_{14}	-0.72	0.5538	-1.301	0.212
b_{23}	0.0413	0.5538	0.074	0.942
b_{24}	-1.013	0.5538	-1.83	0.086
b_{34}	-0.56	0.5538	-1.011	0.320

The Pareto analysis [207] provides substantial information about the effect of each variable/ interaction on response. This is calculated in terms of percentage effect of each parameter/ interaction on response. The Pareto graphic analysis is represented by Fig. 47. As illustrated, the effects on the positive side of the Pareto graphic chart are synergistic towards response while those on the negative side are antagonistic towards response. Results in Figure 47 show that applied current (AC) and electrolysis time (ET) and RHS-TiO_2 were statistically significant main parameter while the significant compounded effects were ET*A.C, [N-amine] *ET and [N-amine] *RHS-TiO_2. In the DF-PEF-RHS-TiO_2 process, the rate of $^{\bullet}OH$ production is determined by applied current, photocatalyst in a defined time (electrolysis) under UV-illumination.

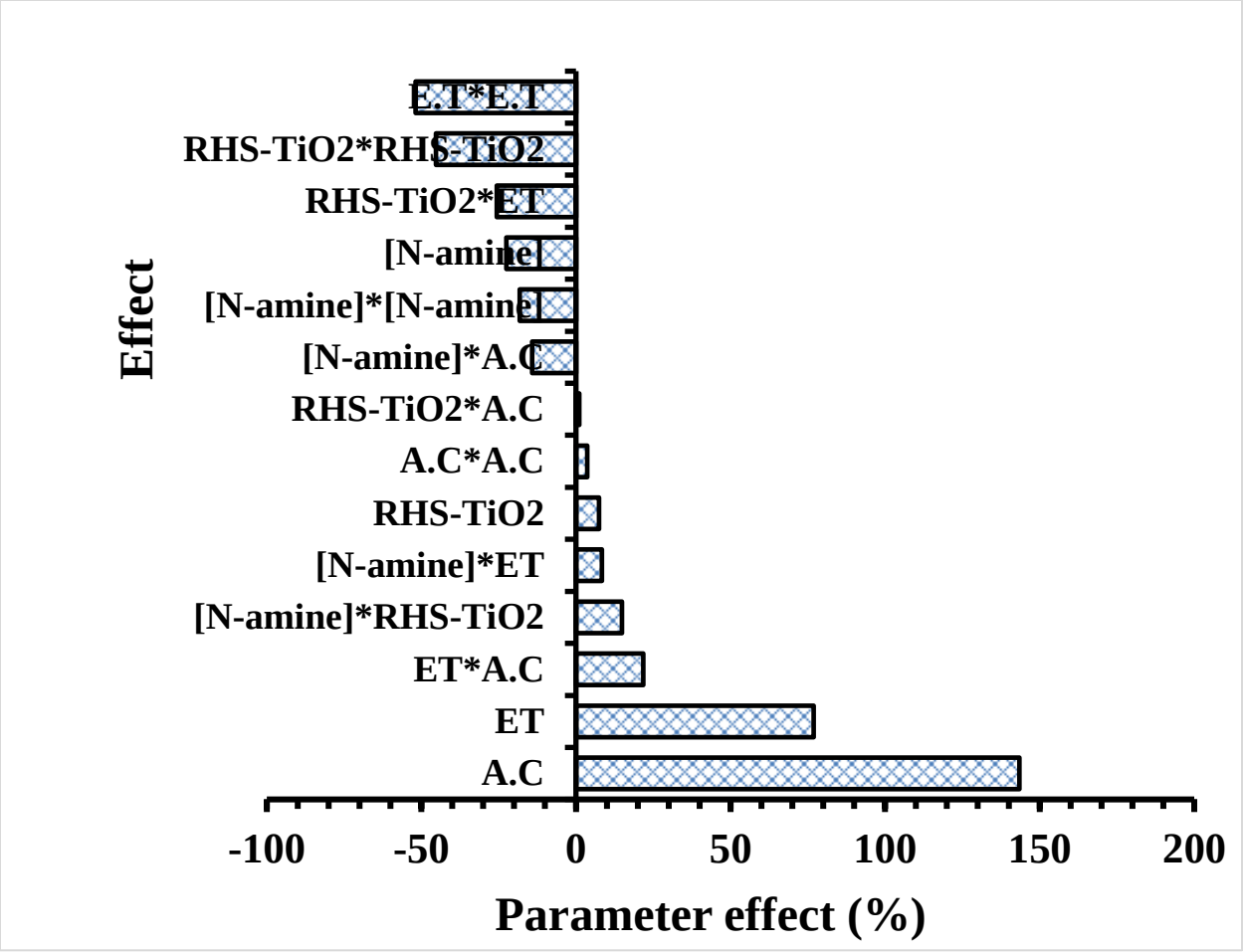

Figure 47: Pareto graphic analysis.

6.3.3 Interaction effects of variables on response

Figs. 48 (a–d) show typical response surface profiles among the main factor's; treatment time (under both electrolysis and UV-illumination), N-nitrosamine concentration, applied current and RHS-TiO_2 dosage, drawn using MINITAB software. Analysis of the response curves at the chosen experimental field show that the maximum (DE %) was obtained where the treatment time and the applied current are increased. It is noted that N-nitrosamine DE (%) is marginally affected by both increased applied current and RHS-TiO_2 catalysts. This implies that appreciably less photocatalyst dosage and applied current are enough to realize high DE (%).

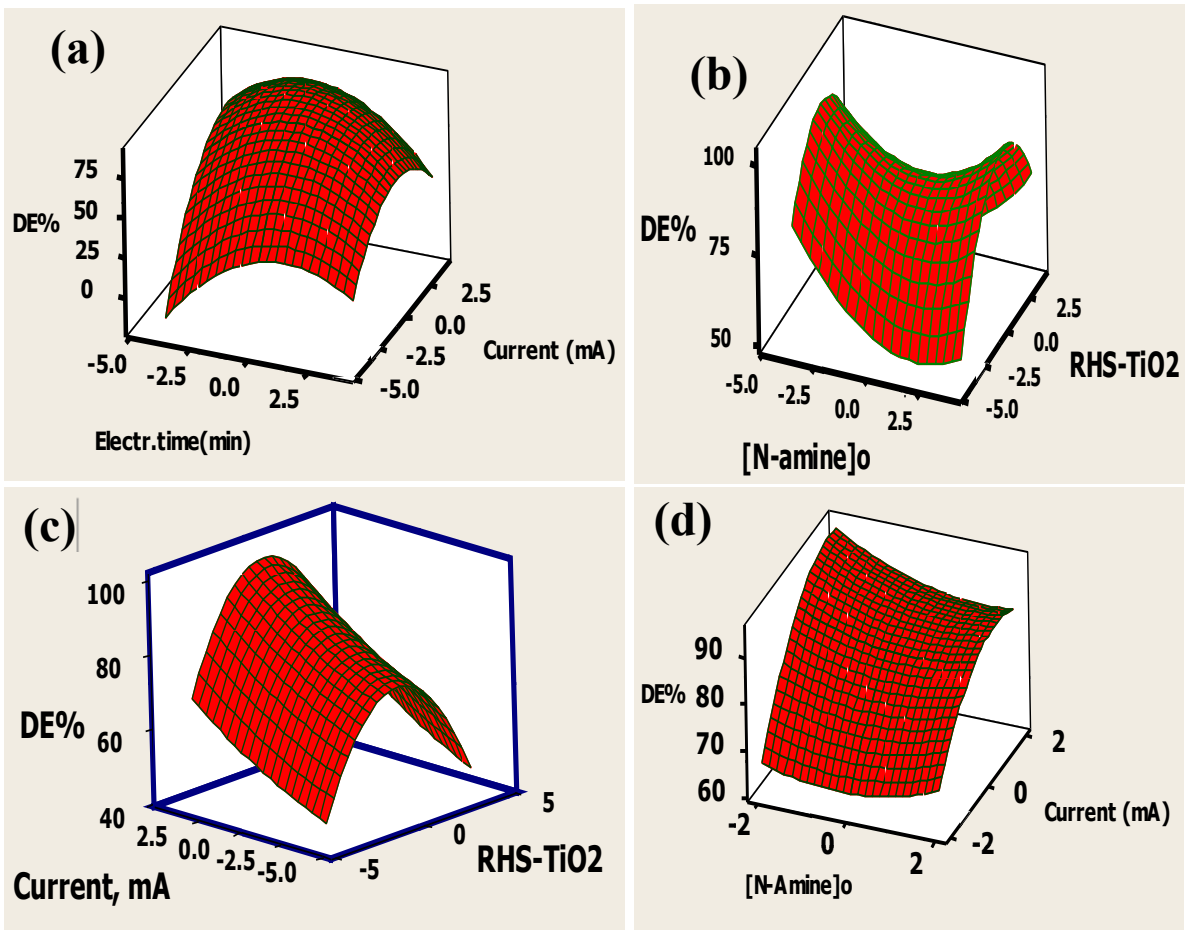

Figure 48: Effects of variable interactions as response surfaces

6.3.4 **Determination of optimal conditions for degradation of N-nitrosamines**

The major aim of optimization was to obtain optimum values for maximizing DF-PEF-UV-RHS/TiO_2 degradation process. Using desirability function approach, the desired goal was defined in term of DE (%) and set as "maximize" to achieve highest degradation efficiency. As a result, the optimum values of 10 min as the electrolysis time, 200 ng/mL as concentration of N-nitrosamine, 1.25 g/l RHS-TiO_2 catalyst dosage and the applied current of 200 mA were generated, tested and verified.

6.3.5 **Comparison studies**

At optimum conditions, degradation efficiency of N-nitrosamines using droplet flow assisted photoelectro-Fenton/photocatalytic (DF-PEF/ RHS-TiO_2) was compared with photocatalysis (UV-RHS/TiO_2), droplet flow assisted electro-Fenton (DF-EF), droplet flow assisted photoelectro-Fenton (DF-PEF, without a photocatalyst) as illustrated in Fig 49. The experiments were conducted using similar experimental apparatus but with some modification to suite a degradation technique under investigation. It is well-illustrated that the highest degradation efficiency was registered using PEF/UV/RHS-TiO_2 degradation technique. The results also showed that N-nitrosamine 10 min degradation follows the decreasing order: DF-PEF/UV/TiO_2 > DF-PEF > DF-EF > UV/RHS-TiO_2. Moreover, the N-nitrosamines were degraded quickly during the first 10 min of DF-PEF/UV/TiO_2 process, yielding up to 99.99% for both N-nitrosamine, while other degradation techniques DF-PEF, DF-EF and UV/RHS/TiO_2 processes results were up to 91.85%, 86.44% and 14.80% degradation efficiency. These results suggest the compounding effect of both DF-PEF with photocatalytic process (UV/RHS-TiO_2) to effectively enhance N-nitrosamine degradation efficiency.

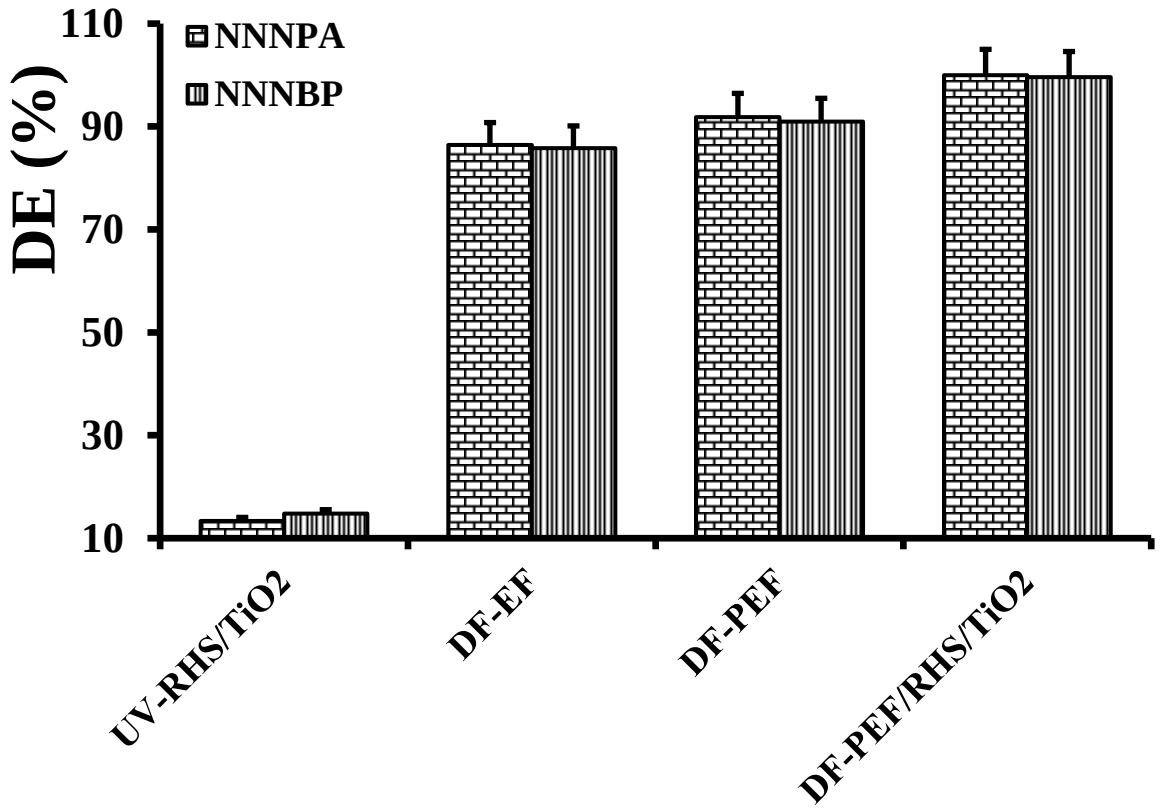

Figure 49: Comparing different degradation techniques with DF-PEF/RHS-TiO_2 method

CHAPTER 7

General Conclusions and Future Works

In the first part of this this work, rice husk silica-based nanocomposite sorbents were synthesized via hydrolytic sol-gel method and investigated as effective sorbents for micro-solid phase extraction (µ-SPE) of ß-blocker in hospital wastewater followed by Liquid chromatography tandem mass spectrometry (LC-MS/MS) analysis. Coupling chemometrics to µ-SPE-LC/MS/MS, the following advantages were realized;

- Improved extraction efficiencies resulting from the synergistic contribution of carbon, silica and iron oxide in the synthesized nanocomposite sorbent.
- Decreased number of experiments with effective optimization using fractional factorial design and central composite design (CCD) with desirability function.
- Less extraction time, low detection limits, high enrichment factors, acceptable repeatability's and improved LC-MS/MS sensitivity are the key attributes of this method.

In the second part of this thesis work, a new droplet-flow assisted heterogeneous electro-Fenton (DFEF) process catalyzed by rice husk silica supported iron-carbon composite catalysts was successfully utilized in effective degradation of ß-blockers in hospital wastewater. The following advantages were identified for this "green" approach: (i) the synergistic contribution of droplet-impingement at the cathode resulting to fast kinetics in H_2O_2 production, (ii) use of low cost yet re-usable biogenic silica composite catalyst as an iron-carbon source, (iii) the system's ability to perform the EF process without pH confinement of <3 (i.e. at natural pH) since the biogenic iron composite source provided a suitable acidity for the Fenton's reaction and

(iv) incorporation of CCD based response surface methodology providing adequate process optimization at minimal experimental runs. The experimental data was in good agreement with the predicted values as demonstrated in the validation step. A comparison study clearly revealed that; the degradation efficiencies exhibited by the proposed DFEF mode were many orders of magnitude higher than that of conventional flow-assisted EF and even other treatment modes. The concentration decay of both pharmaceutical β-blockers (propranolol, PROP and acebutolol, ACE) followed pseudo-first-order kinetics with complete degradation achieved within 15 min. Hence this treatment approach can be applied to any real wastewater effluent without prior pH adjustment.

The third part of this thesis work involving the degradation of pharmaceutical ß-blockers (ACE and ATE) was demonstrated using novel Cu-B-Fe supported graphite electrodes as integrated cathode electrodes and droplet flow-assisted heterogeneous electro-Fenton reactor. Different Cu-B-Fe composites were synthesized and immobilized on the treated graphite electrodes (X-SMGE) via rice husk silica based hydrolytic sol-gel method. SEM-EDS and XPS analysis results depicted success loading of Cu-B-Fe composite on the graphite electrode surfaces. Through the SEM-EDS elemental mapping composition, it was demonstrated that the C, B and Fe were highly dispersed in surface matrix of the graphite electrode. The prepared electrodes were then evaluated for ß-blockers degradation in in terms of reactive oxygen species generation and degradation efficiency (%). Highest degradation efficiency was achieved when 20-SMGE was used in a DFEF reactor. The effect of influencing parameters was investigated using CCD and desirability function approaches. At optimized conditions, a 99.99% degradation efficiency with a significant desirability value of 0.999 was warranted even at neutral pH (pH=7).

Since the sample pH was closer to 7.0, all validation experiments were conducted without pH adjustment and resulted to $\geq$99.9% degradation efficiency for both β-blockers (ACE and ATE).

The modified graphite electrodes possessed more active surface characteristics for simultaneous in situ H_2O_2 electro-generation, •OH production and catalyst regeneration. The enhancement in ß-blockers degradation efficiencies was due to a synergistic contribution of DFEF reactor, prepared cathode electrode and anodic oxidation of BDD. The reusability and stability of the integrated cathode electrode was also assessed and displayed a high degradation efficiency even after the 20^{th} cycle of consecutive reuse. A cleaner and efficient droplet-flow assisted EF system with automatic sample pH regulation was demonstrated.

In the last part of thesis work, the degradation efficiencies of selected N-nitrosamines (N-nitrosodipropylamine, N-nitrosodibutylamine) in swimming pool water were investigated using a combined treatment of droplet-flow assisted photoelectro-Fenton process (DF-PEF/UV/RHS-TiO_2) with Cu-B-Fe functionalized electrode as cathode and photocatalytic process utilizing an RHS immobilizedTiO_2 nanoparticles. The combined DF-PEF/UV/RHS-TiO_2 process could be conducted under UV-light irradiation, not only due to the formation of degradable iron-copper and RHS-TiO_2 complexes with electrogenerated H_2O_2. The nitrosamines were quickly degraded in the first 10 minutes of combined treatment, yielding ≥99.99% of DE (%). Simultaneously, droplet flow assisted photoelectro-Fenton (DF-PEF), convention droplet flow assisted electro-Fenton (DF-EF) and photocatalytic (UV/RHS-TiO_2) treatment processes yielded 91.85%, 86.44% and 14.80% DE (%) respectively. Analysis of variance demonstrated a higher R^2 = 92.65%, that ensured acceptable statistical regression model predictions with the experimental data.

References

[1] S.D. Richardson, T.A. Ternes, Water Analysis: Emerging Contaminants and Current Issues, Water. 75 (2005) 3809–3836. doi:10.1021/ac500508t.

[2] Y. Picó, D. Barceló, Emerging contaminants in biota, Anal. Bioanal. Chem. 404 (2012) 2525–2526. doi:10.1007/s00216-012-6311-1.

[3] D. Fatta-Kassinos, C. Michael, Wastewater reuse applications and contaminants of emerging concern, Environ. Sci. Pollut. Res. 20 (2013) 3493–3495. doi:10.1007/s11356-013-1699-5.

[4] P. Bottoni, S. Caroli, Presence of residues and metabolites of pharmaceuticals in environmental compartments , food commodities and workplaces : A review spanning the three-year period 2014 – 2016, Microchem. J. 136 (2018) 2–24. doi:10.1016/j.microc.2017.06.016.

[5] N. Collado, S. Rodriguez-mozaz, M. Gros, A. Rubirola, D. Barceló, J. Comas, I. Rodriguez-roda, G. Buttiglieri, Pharmaceuticals occurrence in a WWTP with signi fi cant industrial contribution and its input into the river system, 185 (2014) 202–212. doi:10.1016/j.envpol.2013.10.040.

[6] M. Taheran, M. Naghdi, S.K. Brar, M. Verma, R.Y. Surampalli, Emerging contaminants: Here today, there tomorrow!, Environ. Nanotechnology, Monit. Manag. 10 (2018) 122–126. doi:10.1016/j.enmm.2018.05.010.

[7] L. Bittner, E. Teixido, B. Seiwert, B.I. Escher, N. Klüver, In fl uence of pH on the uptake and toxicity of β -blockers in embryos of zebra fi sh , Danio rerio, 201 (2018) 129–137.

doi:10.1016/j.aquatox.2018.05.020.

[8] B. Khan, R.M. Burgess, S.A. Fogg, M.G. Cantwell, D.R. Katz, K.T. Ho, Chemosphere Cellular responses to in vitro exposures to b -blocking pharmaceuticals in hard clams and Eastern oysters, Chemosphere. 211 (2018) 360–370. doi:10.1016/j.chemosphere.2018.07.156.

[9] M. Cleuvers, Initial risk assessment for three b -blockers found in the aquatic environment, 59 (2005) 199–205. doi:10.1016/j.chemosphere.2004.11.090.

[10] P. V. Nidheesh, R. Gandhimathi, Trends in electro-Fenton process for water and wastewater treatment: An overview, Desalination. 299 (2012) 1–15. doi:10.1016/j.desal.2012.05.011.

[11] J. Kochany, E. Lipczynska-Kochany, Utilization of landfill leachate parameters for pretreatment by Fenton reaction and struvite precipitation-A comparative study, J. Hazard. Mater. 166 (2009) 248–254. doi:10.1016/j.jhazmat.2008.11.017.

[12] S. Mompelat, B. Le Bot, O. Thomas, Occurrence and fate of pharmaceutical products and by-products, from resource to drinking water, Environ. Int. 35 (2009) 803–814. doi:10.1016/j.envint.2008.10.008.

[13] M. Taheran, M. Naghdi, S.K. Brar, M. Verma, R.Y. Surampalli, Emerging contaminants: Here today, there tomorrow!, Environ. Nanotechnology, Monit. Manag. 10 (2018) 122–126. doi:10.1016/j.enmm.2018.05.010.

[14] R. Altenburger, H. Walter, M. Grote, What contributes to the combined effect of a complex mixture?, Environ. Sci. Technol. 38 (2004) 6353–6362. doi:10.1021/es049528k.

[15] R. Andreozzi, A.. Fallis, M.E.H. Bergmann, a. S. Koparal, T. Iourtchouk, M.H. Park, M.H. Park, M. Sala, M.C. Guti??rrez-Bouz??n, I. Sirés, N. Oturan, M.A. Oturan, R. Naidu, M.H.

Wong, B.J. Vanderford, J.E. Drewes, A. Eaton, Y.C. Guo, A. Haghani, C. Hoppe-Jones, M.P. Schluesener, S.A. Snyder, T. Ternes, C.J. Wood, L. Feng, Q. Dai, J. Zhou, X. Meng, D. Feng, C. Wu, J. Chen, J. Radjenovic, D.L. Sedlak, H. Li, J. Ni, X. Chen, G. Chen, F. Gao, P.O.L. Yue, C. Engineering, T.H. Kong, High-Performance Ti / BDD Electrodes for Pollutant Oxidation, Water Res. 44 (2013) 51–59. doi:10.1017/CBO9781107415324.004.

[16] U. Jurva, L. Weidolf, Electrochemical generation of drug metabolites with applications in drug discovery and development, TrAC - Trends Anal. Chem. 70 (2015) 92–99. doi:10.1016/j.trac.2015.04.010.

[17] W. Lohmann, U. Karst, Biomimetic modeling of oxidative drug metabolism : SStrategies, advantages and limitations, Anal. Bioanal. Chem. 391 (2008) 79–96. doi:10.1007/s00216-007-1794-x.

[18] E. Isarain-Chávez, R.M. Rodríguez, J.A. Garrido, C. Arias, F. Centellas, P.L. Cabot, E. Brillas, Degradation of the beta-blocker propranolol by electrochemical advanced oxidation processes based on Fenton's reaction chemistry using a boron-doped diamond anode, Electrochim. Acta. 56 (2010) 215–221. doi:10.1016/j.electacta.2010.08.097.

[19] F.C. Moreira, R.A.R. Boaventura, E. Brillas, V.J.P. Vilar, Electrochemical advanced oxidation processes: A review on their application to synthetic and real wastewaters, Appl. Catal. B Environ. 202 (2017) 217–261. doi:10.1016/j.apcatb.2016.08.037.

[20] D. Huerta, B., Rodríguez-Mozaz, S., Barceló, Critical Review Pharmaceutical metabolites in the environment : Analytical Challenges and Ecological Risks, 28 (2009) 2473–2484. doi:10.1897/09-173.1.

[21] E. Gracia-Lor, M. Martínez, J. V. Sancho, G. Peñuela, F. Hernández, Multi-class determination of personal care products and pharmaceuticals in environmental and wastewater samples by ultra-high performance liquid-chromatography-tandem mass spectrometry, Talanta. 99 (2012) 1011–1023. doi:10.1016/j.talanta.2012.07.091.

[22] C. Jung, A. Son, N. Her, K.-D. Zoh, J. Cho, Y. Yoon, Removal of endocrine disrupting compounds, pharmaceuticals, and personal care products in water using carbon nanotubes: A review, J. Ind. Eng. Chem. 27 (2015) 1–11. doi:10.1016/j.jiec.2014.12.035.

[23] D. Pant, A. Adholeya, Biological approaches for treatment of distillery wastewater: A review, Bioresour. Technol. 98 (2007) 2321–2334. doi:10.1016/j.biortech.2006.09.027.

[24] F.C. Moreira, R.A.R. Boaventura, E. Brillas, V.J.P. Vilar, Applied Catalysis B : Environmental Electrochemical advanced oxidation processes : A review on their application to synthetic and real wastewaters, "Applied Catal. B, Environ. 202 (2017) 217–261. doi:10.1016/j.apcatb.2016.08.037.

[25] M.A. Oturan, J.-J. Aaron, Advanced Oxidation Processes in Water/Wastewater Treatment: Principles and Applications. A Review, Crit. Rev. Environ. Sci. Technol. 44 (2014) 2577–2641. doi:10.1080/10643389.2013.829765.

[26] C. a. Martínez-Huitle, E. Brillas, Decontamination of wastewaters containing synthetic organic dyes by electrochemical methods: A general review, Appl. Catal. B Environ. 87 (2009) 105–145. doi:10.1016/j.apcatb.2008.09.017.

[27] E. Brillas, I. Sirés, M. a. Oturan, Electro-fenton process and related electrochemical technologies based on fenton's reaction chemistry, Chem. Rev. 109 (2009) 6570–6631.

doi:10.1021/cr900136g.

[28] B.I. Escher, N. Bramaz, R.I.L. Eggen, M. Richter, In Vitro Assessment of Modes of Toxic Action of Pharmaceuticals in Aquatic Life, Environ. Sci. Technol. 39 (2005) 3090–3100. doi:10.1021/es048590e.

[29] B.J. Vanderford, R. a Pearson, D.J. Rexing, S. a Snyder, Analysis of Endocrine Disruptors, Pharmaceuticals, and Personal Care Products in Water Using Liquid Chromatographyrrandem Mass Spectrometry, Anal. Chem. 75 (2003) 6265–6274.

[30] R. Andreozzi, R. Marotta, N. Paxéus, Pharmaceuticals in STP effluents and their solar photodegradation in aquatic environment, Chemosphere. 50 (2003) 1319–1330. doi:10.1016/S0045-6535(02)00769-5.

[31] D.W. Kolpin, E.T. Furlong, M.T. Meyer, E.M. Thurman, S.D. Zaugg, L.B. Barber, H.T. Buxton, Pharmaceuticals , hormones , and other organic wastewater Contaminants in U . S . Streams , 1999 - 2000 : A National Reconnaissance, Environ. Sci. Technol. 36 (2002) 1202–11. doi:10.1021/es011055j.

[32] M.A.K. Silveira, S.S. Caldas, J.R. Guilherme, F.P. Costa, B.D.S. Guimarães, M.B.R. Cerqueira, B.M. Soares, E.G. Primel, Quantification of pharmaceuticals and personal care product residues in surface and drinking water samples by SPE and LC-ESI-MS/MS, J. Braz. Chem. Soc. 24 (2013) 1385–1395. doi:10.5935/0103-5053.20130176.

[33] J. Xu, L. Wu, A.C. Chang, Degradation and adsorption of selected pharmaceuticals and personal care products (PPCPs) in agricultural soils, Chemosphere. 77 (2009) 1299–1305. doi:10.1016/j.chemosphere.2009.09.063.

[34] A. Jouyban, M.H. Sorouraddin, M.A. Farajzadeh, M.H. Somi, R. Fazeli-Bakhtiyari, Vortex-assisted liquid–liquid extraction combined with field-amplified sample injection and sweeping micellar electrokinetic chromatography for improved determination of β-blockers in human urine, Talanta. 149 (2016) 298–309. doi:10.1016/j.talanta.2015.11.046.

[35] Y. Chen, X. Lu, L. Liu, D. Wan, H. Chen, D. Zhou, V.K. Sharma, Oxidation of B-blockers by birnessite: Kinetics, mechanism and effect of metal ions, Chemosphere. 194 (2018) 588–594. doi:10.1016/j.chemosphere.2017.12.015.

[36] S.D. Richardson, Disinfection by-products and other emerging contaminants in drinking water, TrAC - Trends Anal. Chem. 22 (2003) 666–684. doi:10.1016/S0165-9936(03)01003-3.

[37] S.D. Richardson, M.J. Plewa, E.D. Wagner, R. Schoeny, D.M. DeMarini, Occurrence, genotoxicity, and carcinogenicity of regulated and emerging disinfection by-products in drinking water: A review and roadmap for research, Mutat. Res. - Rev. Mutat. Res. 636 (2007) 178–242. doi:10.1016/j.mrrev.2007.09.001.

[38] B. Xu, Z. Chen, F. Qi, J. Ma, F. Wu, Rapid degradation of new disinfection by-products in drinking water by UV irradiation: N-Nitrosopyrrolidine and N-nitrosopiperidine, Sep. Purif. Technol. 69 (2009) 126–133. doi:10.1016/j.seppur.2009.07.004.

[39] A.J. Gushgari, R.U. Halden, Critical review of major sources of human exposure to N-nitrosamines, Chemosphere. 210 (2018) 1124–1136. doi:10.1016/j.chemosphere.2018.07.098.

[40] S.S. Hecht, Approaches to Cancer Prevention Based on an Understanding of N-Nitrosamine Carcinogenesis, Exp. Biol. Med. 216 (1997) 181–191. doi:10.3181/00379727-216-44168.

[41] M. Ramil, T. El Aref, G. Fink, M. Scheurer, T.A. Ternes, Fate of beta blockers in aquatic-

sediment systems: Sorption and biotransformation, Environ. Sci. Technol. 44 (2010) 962–970. doi:10.1021/es9027452.

[42] M. Klavarioti, D. Mantzavinos, D. Kassinos, Removal of residual pharmaceuticals from aqueous systems by advanced oxidation processes, Environ. Int. 35 (2009) 402–417. doi:10.1016/j.envint.2008.07.009.

[43] S. Garcia-Segura, J.D. Ocon, M.N. Chong, Electrochemical oxidation remediation of real wastewater effluents—A review, Process Saf. Environ. Prot. 113 (2018) 48–67. doi:10.1016/j.psep.2017.09.014.

[44] M. Panizza, G. Cerisola, Direct and mediated anodic oxidation of organic pollutants, Chem. Rev. 109 (2009) 6541–6569. doi:10.1021/cr9001319.

[45] I. Sirés, E. Brillas, M.A. Oturan, M.A. Rodrigo, M. Panizza, Electrochemical advanced oxidation processes: today and tomorrow. A review, Environ. Sci. Pollut. Res. 21 (2014) 8336–8367. doi:10.1007/s11356-014-2783-1.

[46] C. Barrera-Díaz., P. Cañizares, F.J. Fernández, R. Natividad, M.A. Rodrigo, Electrochemical Advanced Oxidation Processes:, J. Mex. Chem. Soc. 58 (2014) 256–275. http://www.scielo.org.mx/scielo.php?script=sci_arttext&pid=S1870-249X2014000300003.

[47] P.E. Acta, P. Llu, Wastewaters by Electrochemical Advanced Oxidation Processes Using a BDD Anode and Electrogenerated H2O2 ... Wastewaters by Electrochemical Advanced Oxidation, 26 (2015) 15–46. doi:10.4152/pea.200801015.

[48] M. Krawczyk, E. Stanisz, Ultrasound-assisted dispersive micro solid-phase extraction with nano-TiO2 as adsorbent for the determination of mercury species, Talanta. 161 (2016) 384–

391. doi:10.1016/j.talanta.2016.08.071.

[49] S. Zorita, B. Boyd, S. Jönsson, E. Yilmaz, C. Svensson, L. Mathiasson, S. Bergström, Selective determination of acidic pharmaceuticals in wastewater using molecularly imprinted solid-phase extraction, Anal. Chim. Acta. 626 (2008) 147–154. doi:10.1016/j.aca.2008.07.051.

[50] K. Fent, A.A. Weston, D. Caminada, Ecotoxicology of human pharmaceuticals, Aquat. Toxicol. 76 (2006) 122–159. doi:10.1016/j.aquatox.2005.09.009.

[51] M. Serrano, T. Chatzimitakos, M. Gallego, C.D. Stalikas, 1-Butyl-3-aminopropyl imidazolium-functionalized graphene oxide as a nanoadsorbent for the simultaneous extraction of steroids and β-blockers via dispersive solid-phase microextraction, J. Chromatogr. A. 1436 (2016) 9–18. doi:10.1016/j.chroma.2016.01.052.

[52] W. Gong, S. Feng, X. Wang, J. Fan, A. Li, S. ping Nie, Beta-blockers reduced the risk of cardiac rupture in patients with acute myocardial infarction: A meta-analysis of randomized control trials, Int. J. Cardiol. 232 (2017) 171–175. doi:10.1016/j.ijcard.2017.01.035.

[53] G.J. Murray, J.P. Danaceau, Simultaneous extraction and screening of diuretics, beta-blockers, selected stimulants and steroids in human urine by HPLC-MS/MS and UPLC-MS/MS, J. Chromatogr. B Anal. Technol. Biomed. Life Sci. 877 (2009) 3857–3864. doi:10.1016/j.jchromb.2009.09.036.

[54] G.A.K. Anquandah, V.K. Sharma, V.R. Panditi, P.R. Gardinali, H. Kim, M.A. Oturan, Ferrate(VI) oxidation of propranolol: Kinetics and products, Chemosphere. 91 (2013) 105–109. doi:10.1016/j.chemosphere.2012.12.001.

[55] M.L. Wilde, W.M.M. Mahmoud, K. Kümmerer, A.F. Martins, Oxidation-coagulation of Beta-

blockers by K2FeVIO4 in hospital wastewater: Assessment of degradation products and biodegradability, Sci. Total Environ. 452–453 (2013) 137–147. doi:10.1016/j.scitotenv.2013.01.059.

[56] C. Boillot, C. Bazin, F. Tissot-Guerraz, J. Droguet, M. Perraud, J.C. Cetre, D. Trepo, Y. Perrodin, Daily physicochemical, microbiological and ecotoxicological fluctuations of a hospital effluent according to technical and care activities, Sci. Total Environ. 403 (2008) 113–129. doi:10.1016/j.scitotenv.2008.04.037.

[57] E. Boyaci, Á. Rodríguez-Lafuente, K. Gorynski, F. Mirnaghi, É.A. Souza-Silva, D. Hein, J. Pawliszyn, Sample preparation with solid phase microextraction and exhaustive extraction approaches: Comparison for challenging cases, Anal. Chim. Acta. 873 (2015) 14–30. doi:10.1016/j.aca.2014.12.051.

[58] M.M. Moein, M. Javanbakht, M. Karimi, B. Akbari-adergani, M. Abdel-Rehim, Three-phase molecularly imprinted sol–gel based hollow fiber liquid-phase microextraction combined with liquid chromatography–tandem mass spectrometry for enrichment and selective determination of a tentative lung cancer biomarker, J. Chromatogr. B. 995–996 (2015) 38–45. doi:10.1016/j.jchromb.2015.05.005.

[59] Z. Altun, M. Abdel-Rehim, Study of the factors affecting the performance of microextraction by packed sorbent (MEPS) using liquid scintillation counter and liquid chromatography-tandem mass spectrometry, Anal. Chim. Acta. 630 (2008) 116–123. doi:10.1016/j.aca.2008.09.067.

[60] M. Hemmati, M. Rajabi, A. Asghari, Ultrasound-promoted dispersive micro solid-phase extraction of trace anti-hypertensive drugs from biological matrices using a sonochemically

synthesized conductive polymer nanocomposite, Ultrason. Sonochem. 39 (2017) 12–24. doi:10.1016/j.ultsonch.2017.03.024.

[61] S. Seidi, Y. Yamini, M. Rezazadeh, Electrically enhanced microextraction for highly selective transport of three ß-blocker drugs, J. Pharm. Biomed. Anal. 56 (2011) 859–866. doi:10.1016/j.jpba.2011.07.029.

[62] S.E. Evans, P. Davies, A. Lubben, B. Kasprzyk-Hordern, Determination of chiral pharmaceuticals and illicit drugs in wastewater and sludge using microwave assisted extraction, solid-phase extraction and chiral liquid chromatography coupled with tandem mass spectrometry, Anal. Chim. Acta. 882 (2015) 112–126. doi:10.1016/j.aca.2015.03.039.

[63] I. Aparicio, J. Martín, J.L. Santos, J.L. Malvar, E. Alonso, Stir bar sorptive extraction and liquid chromatography–tandem mass spectrometry determination of polar and non-polar emerging and priority pollutants in environmental waters, J. Chromatogr. A. 1500 (2017) 43–52. doi:10.1016/j.chroma.2017.04.007.

[64] W. Liu, L. Zhang, Z. Wei, S. Chen, G. Chen, Analysis of β-agonists and β-blockers in urine using hollow fibre-protected liquid-phase microextraction with in situ derivatization followed by gas chromatography/mass spectrometry, J. Chromatogr. A. 1216 (2009) 5340–5346. doi:10.1016/j.chroma.2009.05.040.

[65] M. Rezazadeh, Y. Yamini, S. Seidi, B. Ebrahimpour, Electromembrane surrounded solid phase microextraction: A novel approach for efficient extraction from complicated matrices, J. Chromatogr. A. 1280 (2013) 16–22. doi:10.1016/j.chroma.2013.01.034.

[66] T. Abuzooda, A. Amini, M. Abdel-Rehim, Graphite-based microextraction by packed sorbent

for online extraction of ß-blockers from human plasma samples, J. Chromatogr. B Anal. Technol. Biomed. Life Sci. 992 (2015) 86–90. doi:10.1016/j.jchromb.2015.04.027.

[67] H. Nsubuga, C. Basheer, Determination of haloacetic acids in swimming pool waters by membrane-protected micro-solid phase extraction, J. Chromatogr. A. 1315 (2013) 47–52. doi:10.1016/j.chroma.2013.09.050.

[68] A. Asfaram, M. Ghaedi, A. Goudarzi, Optimization of ultrasound-assisted dispersive solid-phase microextraction based on nanoparticles followed by spectrophotometry for the simultaneous determination of dyes using experimental design, Ultrason. Sonochem. 32 (2016) 407–417. doi:10.1016/j.ultsonch.2016.04.009.

[69] T. Khezeli, A. Daneshfar, Development of dispersive micro-solid phase extraction based on micro and nano sorbents, TrAC - Trends Anal. Chem. 89 (2017) 99–118. doi:10.1016/j.trac.2017.01.004.

[70] E.F. Vansant; P.Van Der Voort; K.C.Vrancken, Chapter 8 Chemical modification of silica: applications and procedures, in: Stud. Surf. Sci. Catal., 1995: pp. 149–192. doi:10.1016/S0167-2991(06)81516-8.

[71] Y. V. Larichev, P.M. Yeletsky, V.A. Yakovlev, Study of silica templates in the rice husk and the carbon-silica nanocomposites produced from rice husk, J. Phys. Chem. Solids. 87 (2015) 58–63. doi:10.1016/j.jpcs.2015.07.025.

[72] Y.Y. Hsieh, Y.C. Tsai, J.R. He, P.F. Yang, H.P. Lin, C.H. Hsu, A. Loganathan, Rice husk agricultural waste-derived low ionic content carbon–silica nanocomposite for green reinforced epoxy resin electronic packaging material, J. Taiwan Inst. Chem. Eng. 78 (2017) 493–499.

doi:10.1016/j.jtice.2017.06.010.

[73] F. Gandolfi, L. Malleret, M. Sergent, P. Doumenq, Parameters optimization using experimental design for headspace solid phase micro-extraction analysis of short-chain chlorinated paraffins in waters under the European water framework directive, J. Chromatogr. A. 1406 (2015) 59–67. doi:10.1016/j.chroma.2015.06.030.

[74] B.H. Fumes, M.R. Silva, F.N. Andrade, C.E.D. Nazario, F.M. Lanças, Recent advances and future trends in new materials for sample preparation, TrAC - Trends Anal. Chem. 71 (2015) 9–25. doi:10.1016/j.trac.2015.04.011.

[75] J.M. Leca, A.C. Pereira, A.C. Vieira, M.S. Reis, J.C. Marques, Optimal design of experiments applied to headspace solid phase microextraction for the quantification of vicinal diketones in beer through gas chromatography-mass spectrometric detection, Anal. Chim. Acta. 887 (2015) 101–110. doi:10.1016/j.aca.2015.06.044.

[76] L. Vera Candioti, M.M. De Zan, M.S. Cámara, H.C. Goicoechea, Experimental design and multiple response optimization. Using the desirability function in analytical methods development, Talanta. 124 (2014) 123–138. doi:10.1016/j.talanta.2014.01.034.

[77] W. Setyaningsih, I.E. Saputro, C.A. Carrera, M. Palma, C.G. Barroso, Multiresponse optimization of a UPLC method for the simultaneous determination of tryptophan and 15 tryptophan-derived compounds using a Box-Behnken design with a desirability function, Food Chem. 225 (2017) 1–9. doi:10.1016/j.foodchem.2016.12.034.

[78] X. Da, X. Chen, B. Sun, J. Wen, M. Qiu, Y. Fan, Preparation of zirconia nanofiltration membranes through an aqueous sol-gel process modified by glycerol for the treatment of

wastewater with high salinity, J. Memb. Sci. 504 (2016) 29–39. doi:10.1016/j.memsci.2015.12.068.

[79] M.A. Bezerra, R.E. Santelli, E.P. Oliveira, L.S. Villar, L.A. Escaleira, Response surface methodology (RSM) as a tool for optimization in analytical chemistry, Talanta. 76 (2008) 965–977. doi:10.1016/j.talanta.2008.05.019.

[80] G.W. Oehlert, A first course in design and analysis of experiments, W.H.Freeman & Co Ltd, New York, United States, 2000.

[81] N. Casado, D. Perez-Quintanilla, S. Morante-Zarcero, I. Sierra, Current development and applications of ordered mesoporous silicas and other sol-gel silica-based materials in food sample preparation for xenobiotics analysis, TrAC - Trends Anal. Chem. 88 (2017) 167–184. doi:10.1016/j.trac.2017.01.001.

[82] S.J. Gregg, K.S.W. Sing, Adsorption, Surface Area and Porosity, Acad. Press London. (1982) 1–313.

[83] F. Adam, K. Kandasamy, S. Balakrishnan, Iron incorporated heterogeneous catalyst from rice husk ash, J. Colloid Interface Sci. 304 (2006) 137–143. doi:10.1016/j.jcis.2006.08.051.

[84] F. Adam, J. Andas, I.A. Rahman, A study on the oxidation of phenol by heterogeneous iron silica catalyst, Chem. Eng. J. 165 (2010) 658–667. doi:10.1016/j.cej.2010.09.054.

[85] J.S. Choi, S.S. Yoon, S.H. Jang, W.S. Ahn, Phenol hydroxylation using Fe-MCM-41 catalysts, Catal. Today. 111 (2006) 280–287. doi:10.1016/j.cattod.2005.10.037.

[86] M.R.M. Chaves, E.R. Dockal, R.C.R. Souza, P.M. Büchler, Biogenic modified silica as a sorbent of cadmium ions: Preparation and characterization, Environ. Technol. 30 (2009) 663–

671. doi:10.1080/09593330902854160.

[87] M. Sajid, Porous membrane protected micro-solid-phase extraction: A review of features, advancements and applications, Anal. Chim. Acta. 965 (2017) 36–53. doi:10.1016/j.aca.2017.02.023.

[88] I. Baranowska, S. Magiera, J. Baranowski, UHPLC method for the simultaneous determination of β-blockers, isoflavones and their metabolites in human urine, J. Chromatogr. B Anal. Technol. Biomed. Life Sci. 879 (2011) 615–626. doi:10.1016/j.jchromb.2011.01.026.

[89] X. Hu, J. Pan, Y. Hu, G. Li, Preparation and evaluation of propranolol molecularly imprinted solid-phase microextraction fiber for trace analysis of β-blockers in urine and plasma samples, J. Chromatogr. A. 1216 (2009) 190–197. doi:10.1016/j.chroma.2008.11.064.

[90] R. Varga, Z. Eke, K. Torkos, Identification of phase i metabolites of cardiovascular and anti-ulcer drugs in surface water samples with liquid-chromatography-mass spectrometry methods, Talanta. 85 (2011) 1920–1926. doi:10.1016/j.talanta.2011.07.020.

[91] J. Rivera-Utrilla, M. Sánchez-Polo, M.Á. Ferro-García, G. Prados-Joya, R. Ocampo-Pérez, Pharmaceuticals as emerging contaminants and their removal from water. A review, Chemosphere. 93 (2013) 1268–1287. doi:10.1016/j.chemosphere.2013.07.059.

[92] M. Cleuvers, Initial risk assessment for three β-blockers found in the aquatic environment, Chemosphere. 59 (2005) 199–205. doi:10.1016/j.chemosphere.2004.11.090.

[93] M.L. Wilde, S. Montipó, A.F. Martins, Degradation of Beta-blockers in hospital wastewater by means of ozonation and Fe2+/ozonation, Water Res. 48 (2014) 280–295. doi:10.1016/j.watres.2013.09.039.

[94] S.O. Ganiyu, N. Oturan, S. Raffy, G. Esposito, E.D. van Hullebusch, M. Cretin, M.A. Oturan, Use of Sub-stoichiometric Titanium Oxide as a Ceramic Electrode in Anodic Oxidation and Electro-Fenton Degradation of the Beta-blocker Propranolol: Degradation Kinetics and Mineralization Pathway, Electrochim. Acta. 242 (2017) 344–354. doi:10.1016/j.electacta.2017.05.047.

[95] E. Brillas, I. Sire, M.A. Oturan, I. Sirés, M.A. Oturan, Electro-Fenton Process and Related Electrochemical Technologies Based on Fenton ’s Reaction Chemistry, Chem. Rev. 109 (2009) 6570–6631. doi:10.1021/cr900136g.

[96] S.O. Ganiyu, M. Zhou, C.A. Martínez-huitle, Heterogeneous electro-Fenton and photoelectro-Fenton processes: A critical review of fundamental principles and application for water/wastewater treatment, "Applied Catal. B, Environ. (2018). doi:10.1016/j.apcatb.2018.04.044.

[97] N. Barhoumi, N. Oturan, S. Ammar, A. Gadri, M.A. Oturan, E. Brillas, Enhanced degradation of the antibiotic tetracycline by heterogeneous electro-Fenton with pyrite catalysis, Environ. Chem. Lett. 15 (2017) 689–693. doi:10.1007/s10311-017-0638-y.

[98] I. Ouiriemmi, A. Karrab, N. Oturan, M. Pazos, E. Rozales, A. Gadri, M.Á. Sanromán, S. Ammar, M.A. Oturan, Heterogeneous electro-Fenton using natural pyrite as solid catalyst for oxidative degradation of vanillic acid, J. Electroanal. Chem. 797 (2017) 69–77. doi:10.1016/j.jelechem.2017.05.028.

[99] T.X. Huong Le, R. Esmilaire, M. Drobek, M. Bechelany, C. Vallicari, D.L. Nguyen, A. Julbe, S. Tingry, M. Cretin, Design of a novel fuel cell-Fenton system: a smart approach to zero energy depollution, J. Mater. Chem. A. 4 (2016) 17686–17693. doi:10.1039/C6TA05443A.

[100] A.R. Khataee, V. Vatanpour, A.R. Amani Ghadim, Decolorization of C.I. Acid Blue 9 solution by UV/Nano-TiO2, Fenton, Fenton-like, electro-Fenton and electrocoagulation processes: A comparative study, J. Hazard. Mater. 161 (2009) 1225–1233. doi:10.1016/j.jhazmat.2008.04.075.

[101] A.R. Khataee, M. Safarpour, M. Zarei, S. Aber, Combined heterogeneous and homogeneous photodegradation of a dye using immobilized TiO_2 nanophotocatalyst and modified graphite electrode with carbon nanotubes, J. Mol. Catal. A Chem. 363–364 (2012) 58–68. doi:10.1016/j.molcata.2012.05.016.

[102] N. Oturan, J. Wu, H. Zhang, V.K. Sharma, M.A. Oturan, Electrocatalytic destruction of the antibiotic tetracycline in aqueous medium by electrochemical advanced oxidation processes: Effect of electrode materials, Appl. Catal. B Environ. 140–141 (2013) 92–97. doi:10.1016/j.apcatb.2013.03.035.

[103] V. Poza-Nogueiras, E. Rosales, M. Pazos, M.Á. Sanromán, Current advances and trends in electro-Fenton process using heterogeneous catalysts – A review, Chemosphere. 201 (2018) 399–416. doi:10.1016/j.chemosphere.2018.03.002.

[104] F. Sopaj, N. Oturan, J. Pinson, F. Podvorica, M.A. Oturan, Effect of the anode materials on the efficiency of the electro-Fenton process for the mineralization of the antibiotic sulfamethazine, Appl. Catal. B Environ. 199 (2016) 331–341. doi:10.1016/j.apcatb.2016.06.035.

[105] A. Xu, K. Wei, Y. Zhang, W. Han, J. Li, X. Sun, J. Shen, L. Wang, A facile-operation tubular electro-Fenton system combined with oxygen evolution reaction for flutriafol degradation: Modeling and Parameters optimizing, Electrochim. Acta. 246 (2017) 1200–1209. doi:10.1016/j.electacta.2017.06.133.

[106] S. Rahim Pouran, A.A. Abdul Raman, W.M.A. Wan Daud, Review on the application of modified iron oxides as heterogeneous catalysts in Fenton reactions, J. Clean. Prod. 64 (2014) 24–35. doi:10.1016/j.jclepro.2013.09.013.

[107] G. Ren, M. Zhou, M. Liu, L. Ma, H. Yang, A novel vertical-flow electro-Fenton reactor for organic wastewater treatment, Chem. Eng. J. 298 (2016) 55–67. doi:10.1016/j.cej.2016.04.011.

[108] I.M.S. Pillai, A.K. Gupta, Performance analysis of a continuous serpentine flow reactor for electrochemical oxidation of synthetic and real textile wastewater: Energy consumption, mass transfer coefficient and economic analysis, J. Environ. Manage. 193 (2017) 524–531. doi:10.1016/j.jenvman.2017.02.046.

[109] L. Ma, M. Zhou, G. Ren, W. Yang, L. Liang, A highly energy-efficient flow-through electro-Fenton process for organic pollutants degradation, Electrochim. Acta. 200 (2016) 222–230. doi:10.1016/j.electacta.2016.03.181.

[110] C. Zhang, M. Zhou, G. Ren, X. Yu, L. Ma, J. Yang, F. Yu, Heterogeneous electro-Fenton using modified iron-carbon as catalyst for 2,4-dichlorophenol degradation: Influence factors, mechanism and degradation pathway, Water Res. 70 (2015) 414–424. doi:10.1016/j.watres.2014.12.022.

[111] M.S. Çelebi, N. Oturan, H. Zazou, M. Hamdani, M.A. Oturan, Electrochemical oxidation of carbaryl on platinum and boron-doped diamond anodes using electro-Fenton technology, Sep. Purif. Technol. 156 (2015) 996–1002. doi:10.1016/j.seppur.2015.07.025.

[112] S. Mohajeri, H.A. Aziz, M.H. Isa, M.A. Zahed, M.N. Adlan, Statistical optimization of process

parameters for landfill leachate treatment using electro-Fenton technique, J. Hazard. Mater. 176 (2010) 749–758. doi:10.1016/j.jhazmat.2009.11.099.

[113] C.M.A.-C. Raymond H. Myers, Douglas C. Montgomery, Response Surface Methodology: Process and Product Optimization Using Designed Experiments, Fourth Edi, John Wiley & Sons, Inc., New york, 2016.

[114] H. Nsubuga, C. Basheer, M.B. Haider, R. Bakdash, Sol-gel based biogenic silica composite as green nanosorbent for chemometric optimization of micro-solid-phase extraction of beta, J. Chromatogr. A. 1554 (2018) 16–27. doi:10.1016/j.chroma.2018.04.044.

[115] R.M. Sellers, Spectrophotometric determination of hydrogen peroxide using potassium titanium(IV) oxalate, Analyst. 105 (1980) 950. doi:10.1039/an9800500950.

[116] S.J. Gerber, E. Erasmus, Electronic effects of metal hexacyanoferrates: An XPS and FTIR study, Mater. Chem. Phys. 203 (2018) 73–81. doi:10.1016/j.matchemphys.2017.09.029.

[117] T. Yamashita, P. Hayes, Analysis of XPS spectra of Fe2+ and Fe3+ ions in oxide materials, Appl. Surf. Sci. 254 (2008) 2441–2449. doi:10.1016/j.apsusc.2007.09.063.

[118] A.R. Khataee, M. Zarei, L. Moradkhannejhad, Application of response surface methodology for optimization of azo dye removal by oxalate catalyzed photoelectro-Fenton process using carbon nanotube-PTFE cathode, Desalination. 258 (2010) 112–119. doi:10.1016/j.desal.2010.03.028.

[119] M.A. Islam, V. Sakkas, T.A. Albanis, Application of statistical design of experiment with desirability function for the removal of organophosphorus pesticide from aqueous solution by low-cost material, J. Hazard. Mater. 170 (2009) 230–238. doi:10.1016/j.jhazmat.2009.04.106.

[120] S. Ben Hammouda, F. Fourcade, A. Assadi, I. Soutrel, N. Adhoum, A. Amrane, L. Monser, Effective heterogeneous electro-Fenton process for the degradation of a malodorous compound, indole, using iron loaded alginate beads as a reusable catalyst, Appl. Catal. B Environ. 182 (2016) 47–58. doi:10.1016/j.apcatb.2015.09.007.

[121] Y. Li, J. Han, B. Xie, Y. Li, S. Zhan, Y. Tian, Synergistic degradation of antimicrobial agent ciprofloxacin in water by using 3D CeO2/RGO composite as cathode in electro-Fenton system, J. Electroanal. Chem. 784 (2017) 6–12. doi:10.1016/j.jelechem.2016.11.057.

[122] J.J. Pignatello, E. Oliveros, A. MacKay, Advanced oxidation processes for organic contaminant destruction based on the fenton reaction and related chemistry, Crit. Rev. Environ. Sci. Technol. 36 (2006) 1–84. doi:10.1080/10643380500326564.

[123] B.C. Hodges, E.L. Cates, J.-H. Kim, Challenges and prospects of advanced oxidation water treatment processes using catalytic nanomaterials, Nat. Nanotechnol. 13 (2018) 642–650. doi:10.1038/s41565-018-0216-x.

[124] C.K. Duesterberg, T.D. Waite, Process Optimization of Fenton Oxidation Using Kinetic Modeling, Environ. Sci. Technol. 40 (2006) 4189–4195. doi:10.1021/es060311v.

[125] J.M. Peralta-Hernández, Y. Meas-Vong, F.J. Rodríguez, T.W. Chapman, M.I. Maldonado, L.A. Godínez, In situ electrochemical and photo-electrochemical generation of the fenton reagent: A potentially important new water treatment technology, Water Res. 40 (2006) 1754–1762. doi:10.1016/j.watres.2006.03.004.

[126] H. Zhang, F. Zhang, Y. Lin, G. Li, B. Liu, Y. Wei, D. Liu, Enhanced degradation of ibuprofen by heterogeneous electro-Fenton at circumneutral pH, Chemosphere. 209 (2018) 998–1006.

doi:10.1016/j.chemosphere.2018.06.164.

[127] R. Jinisha, R. Gandhimathi, S.T. Ramesh, P. V. Nidheesh, S. Velmathi, Removal of rhodamine B dye from aqueous solution by electro-Fenton process using iron-doped mesoporous silica as a heterogeneous catalyst, Chemosphere. 200 (2018) 446–454. doi:10.1016/j.chemosphere.2018.02.117.

[128] H. Zhao, L. Qian, Y. Chen, Q. Wang, G. Zhao, Selective catalytic two-electron O2reduction for onsite efficient oxidation reaction in heterogeneous electro-Fenton process, Chem. Eng. J. 332 (2018) 486–498. doi:10.1016/j.cej.2017.09.093.

[129] S.H. Yoo, D. Jang, H.I. Joh, S. Lee, Iron oxide/porous carbon as a heterogeneous Fenton catalyst for fast decomposition of hydrogen peroxide and efficient removal of methylene blue, J. Mater. Chem. A. 5 (2017) 748–755. doi:10.1039/c6ta07457j.

[130] S.O. Ganiyu, T. Xuan, H. Le, M. Bechelany, G. Esposito, E.D. Van Hullebusch, M.A. Oturan, M. Cretin, modi fi ed carbon-felt cathode for heterogeneous, (2017) 3655–3666. doi:10.1039/C6TA09100H.

[131] Y. Zhang, S. Zuo, M. Zhou, L. Liang, G. Ren, Removal of tetracycline by coupling of flow-through electro-Fenton and in-situ regenerative active carbon felt adsorption, Chem. Eng. J. 335 (2018) 685–692. doi:10.1016/j.cej.2017.11.012.

[132] M.Á. Fernández de Dios, E. Rosales, M. Fernández-Fernández, M. Pazos, M.Á. Sanromán, Degradation of organic pollutants by heterogeneous electro-Fenton process using Mn-alginate composite, J. Chem. Technol. Biotechnol. 90 (2015) 1439–1447. doi:10.1002/jctb.4446.

[133] B. Lai, Y. Zhou, P. Yang, J. Yang, J. Wang, Degradation of 3,3’-iminobis-propanenitrile in

aqueous solution by Fe0/GAC micro-electrolysis system, Chemosphere. 90 (2013) 1470–1477. doi:10.1016/j.chemosphere.2012.09.040.

[134] P. V. Nidheesh, Heterogeneous Fenton catalysts for the abatement of organic pollutants from aqueous solution: a review, RSC Adv. 5 (2015) 40552–40577. doi:10.1039/C5RA02023A.

[135] K. V. Plakas, S.D. Sklari, D.A. Yiankakis, G.T. Sideropoulos, V.T. Zaspalis, A.J. Karabelas, Removal of organic micropollutants from drinking water by a novel electro-Fenton filter: Pilot-scale studies, Water Res. 91 (2016) 183–194. doi:10.1016/j.watres.2016.01.013.

[136] Q. Peng, H. Zhao, L. Qian, Y. Wang, G. Zhao, Applied Catalysis B : Environmental Design of a neutral photo-electro-Fenton system with 3D-ordered macroporous Fe 2 O 3 / carbon aerogel cathode : High activity and low energy consumption, "Applied Catal. B, Environ. 174–175 (2015) 157–166. doi:10.1016/j.apcatb.2015.02.031.

[137] H. Zhao, L. Qian, X. Guan, D. Wu, G. Zhao, Continuous Bulk FeCuC Aerogel with Ultradispersed Metal Nanoparticles: An E ffi cient 3D Heterogeneous Electro-Fenton Cathode over a Wide Range of pH 3 − 9, (2016). doi:10.1021/acs.est.6b00265.

[138] G. Bhattacharya, G. Kandasamy, N. Soin, R.K. Upadhyay, S. Deshmukh, D. Maity, J. McLaughlin, S.S. Roy, Novel π-conjugated iron oxide/reduced graphene oxide nanocomposites for high performance electrochemical supercapacitors, RSC Adv. 7 (2017) 327–335. doi:10.1039/c6ra25630a.

[139] A. Da Pozzo, P. Ferrantelli, C. Merli, E. Petrucci, Oxidation efficiency in the electro-Fenton process, J. Appl. Electrochem. 35 (2005) 391–398. doi:10.1007/s10800-005-0801-1.

[140] A. Khataee, S. Sajjadi, S. Rahim Pouran, A. Hasanzadeh, Efficient electrochemical generation

of hydrogen peroxide by means of plasma-treated graphite electrode and activation in electro-Fenton, J. Ind. Eng. Chem. 56 (2017) 312–320. doi:10.1016/j.jiec.2017.07.024.

[141] P. V. Nidheesh, R. Gandhimathi, Textile Wastewater Treatment by Electro-Fenton Process in Batch and Continuous Modes, J. Hazardous, Toxic, Radioact. Waste. 19 (2015) 04014038. doi:10.1061/(ASCE)HZ.2153-5515.0000254.

[142] S.J. George, R. Gandhimathi, P.V. Nidheesh, S.T. Ramesh, Electro-fenton oxidation of salicylic acid from aqueous solution: Batch studies and degradation pathway, Clean - Soil, Air, Water. 42 (2014) 1701–1711. doi:10.1002/clen.201300453.

[143] G. Santana-Martínez, G. Roa-Morales, E.M. Del Campo, R. Romero, B.A. Frontana-Uribe, R. Natividad, Electro-Fenton and Electro-Fenton-like with in situ electrogeneration of H2O2and catalyst applied to 4-chlorophenol mineralization, Electrochim. Acta. 195 (2016) 246–256. doi:10.1016/j.electacta.2016.02.093.

[144] L. Labiadh, M.A. Oturan, M. Panizza, N. Ben Hamadi, S. Ammar, Complete removal of AHPS synthetic dye from water using new electro-fenton oxidation catalyzed by natural pyrite as heterogeneous catalyst, J. Hazard. Mater. 297 (2015) 34–41. doi:10.1016/j.jhazmat.2015.04.062.

[145] M. del M. Cordero-Rando, J.L. Hidalgo-Hidalgo de Cisneros, E. Blanco, I. Naranjo-Rodríguez, The sonogel-carbon electrode as a sol-gel graphite-based electrode, Anal. Chem. 74 (2002) 2423–2427. doi:10.1021/ac010782u.

[146] D. Ghime, P. Ghosh, Heterogeneous Fenton degradation of oxalic acid by using silica supported iron catalysts prepared from raw rice husk, J. Water Process Eng. 19 (2017) 156–

163. doi:10.1016/j.jwpe.2017.07.025.

[147] J. Liu, S. Wang, Z. Ding, R. Zhou, Q. Xia, J. Zhang, L. Chen, W. Wei, P. Wang, The Effect of Boron Doping on Structure and Electrochemical Performance of Lithium-Rich Layered Oxide Materials, ACS Appl. Mater. Interfaces. 8 (2016) 18008–18017. doi:10.1021/acsami.6b03056.

[148] L. Vera Candioti, M.M. De Zan, M.S. Cámara, H.C. Goicoechea, Experimental design and multiple response optimization. Using the desirability function in analytical methods development, Talanta. 124 (2014) 123–138. doi:10.1016/j.talanta.2014.01.034.

[149] K. Cruz-González, O. Torres-Lopez, A.M. García-León, E. Brillas, A. Hernández-Ramírez, J.M. Peralta-Hernández, K. Cruz-Gonzalez, O. Torres-Lopez, A.M. Garcia-Leon, E. Brillas, A. Hernandez-Ramirez, J.M. Peralta-Hernandez, Optimization of electro-Fenton/BDD process for decolorization of a model azo dye wastewater by means of response surface methodology, Desalination. 286 (2012) 63–68. doi:10.1016/j.desal.2011.11.005.

[150] S. Mashaghi, A. Abbaspourrad, D.A. Weitz, A.M. van Oijen, Droplet microfluidics: A tool for biology, chemistry and nanotechnology, TrAC - Trends Anal. Chem. 82 (2016) 118–125. doi:10.1016/j.trac.2016.05.019.

[151] A.M. Nightingale, T.W. Phillips, J.H. Bannock, J.C. De Mello, Controlled multistep synthesis in a three-phase droplet reactor, Nat. Commun. 5 (2014) 1–8. doi:10.1038/ncomms4777.

[152] L. Zhou, M. Zhou, Z. Hu, Z. Bi, K.G. Serrano, Chemically modified graphite felt as an efficient cathode in electro-Fenton for p-nitrophenol degradation, Electrochim. Acta. 140 (2014) 376–383. doi:10.1016/j.electacta.2014.04.090.

[153] I. Mangili, M. Lasagni, K. Huang, A.I. Isayev, Modeling and optimization of ultrasonic

devulcanization using the response surface methodology based on central composite face-centered design, Chemom. Intell. Lab. Syst. 144 (2015) 1–10. doi:10.1016/j.chemolab.2015.03.003.

[154] A.G. Akerdi, Z. Es, S.H. Bahrami, M. Arami, Journal of Environmental Chemical Engineering Comparative study of GO and reduced GO coated graphite electrodes for decolorization of acidic and basic dyes from aqueous solutions through heterogeneous electro-Fenton process, J. Environ. Chem. Eng. 5 (2017) 2313–2324. doi:10.1016/j.jece.2017.04.028.

[155] J. Wang, P. Yang, M. Cao, N. Kong, W. Yang, S. Sun, Y. Meng, J. Liu, A novel graphene nanodots inlaid porous gold electrode for electrochemically controlled drug release, Talanta. 147 (2016) 184–192. doi:10.1016/j.talanta.2015.09.020.

[156] Z.H. Sheng, L. Shao, J.J. Chen, W.J. Bao, F. Bin Wang, X.H. Xia, Catalyst-free synthesis of nitrogen-doped graphene via thermal annealing graphite oxide with melamine and its excellent electrocatalysis, ACS Nano. 5 (2011) 4350–4358. doi:10.1021/nn103584t.

[157] O.A. Zelekew, D.H. Kuo, Facile synthesis of SiO2@CuxO@TiO2heterostructures for catalytic reductions of 4-nitrophenol and 2-nitroaniline organic pollutants, Appl. Surf. Sci. 393 (2017) 110–118. doi:10.1016/j.apsusc.2016.10.016.

[158] Z. Xu, Y. Yu, D. Fang, J. Liang, L. Zhou, Simulated solarlight catalytic reduction of Cr(VI) on microwave-ultrasonication synthesized flower-like CuO in the presence of tartaric acid, Mater. Chem. Phys. 171 (2016) 386–393. doi:10.1016/j.matchemphys.2016.01.037.

[159] J.F. Marco, N. Escalona, Microporous and Mesoporous Materials Preparation and characterization of bimetallic Fe e Cu allophane nanoclays and their activity in the phenol

oxidation by heterogeneous electro-Fenton reaction, 225 (2016) 303–311. doi:10.1016/j.micromeso.2016.01.013.

[160] Y. Ji, R. Guo, S.F. Lee, S.F.Y. Li, Rapid determination of trace level N-nitrosamine precursors in secondary-treated wastewater by using two dimensional-ion chromatography, J. Hazard. Mater. 368 (2019) 452–458. doi:10.1016/j.jhazmat.2019.01.074.

[161] W. Wang, J. Wang, Y. Guo, C. Zhu, F. Pan, R. Wu, C. Wang, Removal of multiple nitrosamines from aqueous solution by nanoscale zero-valent iron supported on granular activated carbon: Influencing factors and reaction mechanism, Sci. Total Environ. 639 (2018) 934–943. doi:10.1016/j.scitotenv.2018.05.214.

[162] W. Wang, J. Yu, W. An, M. Yang, Occurrence and profiling of multiple nitrosamines in source water and drinking water of China, Sci. Total Environ. 551–552 (2016) 489–495. doi:10.1016/j.scitotenv.2016.01.175.

[163] M. Krauss, P. Longrée, F. Dorusch, C. Ort, J. Hollender, Occurrence and removal of N-nitrosamines in wastewater treatment plants, Water Res. 43 (2009) 4381–4391. doi:10.1016/j.watres.2009.06.048.

[164] M. Eichholzer, F. Gutzwiller, Dietary nitrates, nitrites, and N-nitroso compounds and cancer risk: a review of the epidemiologic evidence., Nutr. Rev. 56 (1998) 95–105. http://www.ncbi.nlm.nih.gov/pubmed/9584494.

[165] H. Mestankova, K. Schirmer, S. Canonica, U. von Gunten, Development of mutagenicity during degradation of N-nitrosamines by advanced oxidation processes, Water Res. 66 (2014) 399–410. doi:10.1016/j.watres.2014.08.012.

[166] US EPA, Chemical contaminants - CCL 4 [WWW document]., 2014. www.epa.gov/ccl/chemical-contaminants-ccl-4.

[167] J.M. Kemper, S.S. Walse, W.A. Mitch, Quaternary amines as nitrosamine precursors: A role for consumer products?, Environ. Sci. Technol. 44 (2010) 1224–1231. doi:10.1021/es902840h.

[168] J. Le Roux, H. Gallard, J.P. Croué, Chloramination of nitrogenous contaminants (pharmaceuticals and pesticides): NDMA and halogenated DBPs formation, Water Res. 45 (2011) 3164–3174. doi:10.1016/j.watres.2011.03.035.

[169] W.A. Mitch, D.L. Sedlak, Characterization and Fate of N-Nitrosodimethylamine Precursors in Municipal Wastewater Treatment Plants, Environ. Sci. Technol. 38 (2004) 1445–1454. doi:10.1021/es035025n.

[170] T. Zeng, W.A. Mitch, Contribution of N-Nitrosamines and Their Precursors to Domestic Sewage by Greywaters and Blackwaters, Environ. Sci. Technol. 49 (2015) 13158–13167. doi:10.1021/acs.est.5b04254.

[171] M.G. Anderson, J. Mcdonnell, C. Ximing, S. a Cline, W.W. Balance, J. Rockstrom, G.C. Daily, P.R. Ehrlich, C. a Reidy, M. Dynesius, C. Revenga, L. Dams, E. Reichel, M.A. Global, P. Green, J. Salisbury, R.B. Lammers, S. Kanae, T. Oki, a Y. Hoekstra, P. Eichert, K.C. Abbaspour, a B. Zehnder, A. Kitoh, M. Hosaka, K. a Dunne, a V Vecchia, C. Valeo, K. Heal, I. Science, M. Bengtsson, Y. Agata, H. Kim, E. Science, The Challenge of Micropollutants in Aquatic System, Science (80-.). 313 (2006) 1072–1077. doi:10.1126/science.1127291.

[172] S.D. Richardson, Water Analysis: Emerging Contaminants and Current Issues, Anal. Chem.

81 (2009) 4645–4677. doi:10.1021/ac9008012.

[173] M.A. Oturan, J.J. Aaron, Advanced oxidation processes in water/wastewater treatment: Principles and applications. A review, Crit. Rev. Environ. Sci. Technol. 44 (2014) 2577–2641. doi:10.1080/10643389.2013.829765.

[174] P. Fernández-Castro, M. Vallejo, M.F. San Román, I. Ortiz, Insight on the fundamentals of advanced oxidation processes: Role and review of the determination methods of reactive oxygen species, J. Chem. Technol. Biotechnol. 90 (2015) 796–820. doi:10.1002/jctb.4634.

[175] M. Antonopoulou, E. Evgenidou, D. Lambropoulou, I. Konstantinou, A review on advanced oxidation processes for the removal of taste and odor compounds from aqueous media, Water Res. 53 (2014) 215–234. doi:10.1016/j.watres.2014.01.028.

[176] B. Garza-Campos, E. Brillas, A. Hernández-Ramírez, A. El-Ghenymy, J.L. Guzmán-Mar, E.J. Ruiz-Ruiz, Salicylic acid degradation by advanced oxidation processes. Coupling of solar photoelectro-Fenton and solar heterogeneous photocatalysis, J. Hazard. Mater. 319 (2016) 34–42. doi:10.1016/j.jhazmat.2016.02.050.

[177] F.C. Moreira, R.A.R. Boaventura, E. Brillas, V.J.P. Vilar, Electrochemical advanced oxidation processes: A review on their application to synthetic and real wastewaters, Appl. Catal. B Environ. 202 (2017) 217–261. doi:10.1016/j.apcatb.2016.08.037.

[178] I. Sirés, E. Brillas, M.A. Oturan, M.A. Rodrigo, M. Panizza, I. Sires, E. Brillas, M.A. Oturan, M.A. Rodrigo, M. Panizza, Electrochemical advanced oxidation processes: Today and tomorrow. A review, Environ. Sci. Pollut. Res. 21 (2014) 8336–8367. doi:10.1007/s11356-014-2783-1.

[179] A. Rey, J. Carbajo, C. Adán, M. Faraldos, A. Bahamonde, J.A. Casas, J.J. Rodriguez, Improved mineralization by combined advanced oxidation processes, Chem. Eng. J. 174 (2011) 134–142. doi:10.1016/j.cej.2011.08.061.

[180] S. Malato, P. Fernández-Ibáñez, M.I. Maldonado, J. Blanco, W. Gernjak, Decontamination and disinfection of water by solar photocatalysis: Recent overview and trends, Catal. Today. 147 (2009) 1–59. doi:10.1016/j.cattod.2009.06.018.

[181] N. Klamerth, N. Miranda, S. Malato, A. Agüera, A.R. Fernández-Alba, M.I. Maldonado, J.M. Coronado, Degradation of emerging contaminants at low concentrations in MWTPs effluents with mild solar photo-Fenton and TiO2, Catal. Today. 144 (2009) 124–130. doi:10.1016/j.cattod.2009.01.024.

[182] N. Miranda-García, M.I. Maldonado, J.M. Coronado, S. Malato, Degradation study of 15 emerging contaminants at low concentration by immobilized TiO2 in a pilot plant, Catal. Today. 151 (2010) 107–113. doi:10.1016/j.cattod.2010.02.044.

[183] M. Pelaez, N.T. Nolan, S.C. Pillai, M.K. Seery, P. Falaras, A.G. Kontos, P.S.M. Dunlop, J.W.J. Hamilton, J.A. Byrne, K. O'Shea, M.H. Entezari, D.D. Dionysiou, A review on the visible light active titanium dioxide photocatalysts for environmental applications, Appl. Catal. B Environ. 125 (2012) 331–349. doi:10.1016/j.apcatb.2012.05.036.

[184] C.P. Athanasekou, V. Likodimos, P. Falaras, Recent developments of TiO2 photocatalysis involving advanced oxidation and reduction reactions in water, J. Environ. Chem. Eng. 6 (2018) 7386–7394. doi:10.1016/j.jece.2018.07.026.

[185] M.R. Prairie, L.R. Evans, B.M. Stange, S.L. Martinez, An Investigation of TiO2 Photocatalysis

for the Treatment of Water Contaminated with Metals and Organic Chemicals, Environ. Sci. Technol. 27 (1993) 1776–1782. doi:10.1021/es00046a003.

[186] P. Cheng, C. Deng, M. Gu, X. Dai, Effect of urea on the photoactivity of titania powder prepared by sol-gel method, Mater. Chem. Phys. 107 (2008) 77–81. doi:10.1016/j.matchemphys.2007.06.051.

[187] R. Zhang, L. Gao, Q. Zhang, Photodegradation of surfactants on the nanosized TiO2prepared by hydrolysis of the alkoxide titanium, Chemosphere. 54 (2004) 405–411. doi:10.1016/S0045-6535(03)00588-5.

[188] S. Son, S.H. Hwang, C. Kim, J.Y. Yun, J. Jang, Designed synthesis of SiO2/TiO2 core/shell structure as light scattering material for highly efficient dye-sensitized solar cells, ACS Appl. Mater. Interfaces. 5 (2013) 4815–4820. doi:10.1021/am400441v.

[189] U.I. Gaya, A.H. Abdullah, Heterogeneous photocatalytic degradation of organic contaminants over titanium dioxide: A review of fundamentals, progress and problems, J. Photochem. Photobiol. C Photochem. Rev. 9 (2008) 1–12. doi:10.1016/j.jphotochemrev.2007.12.003.

[190] O. Palchik, J. Zhu, A. Gedanken, Microwave assisted preparation of binary oxide nanoparticles, J. Mater. Chem. 10 (2000) 1251–1254. doi:10.1039/a908795h.

[191] K. (Guy) Vibulyaseak, S. (Benz) Deepracha, M. Ogawa, Immobilization of titanium dioxide in mesoporous silicas: Structural design and characterization, J. Solid State Chem. 270 (2019) 162–172. doi:10.1016/j.jssc.2018.09.043.

[192] R.K. Sharma, S. Sharma, S. Dutta, R. Zboril, M.B. Gawande, Silica-nanosphere-based organic-inorganic hybrid nanomaterials: Synthesis, functionalization and applications in

catalysis, Green Chem. 17 (2015) 3207–3230. doi:10.1039/c5gc00381d.

[193] S.X. Lu, L. Dai, W.G. Xu, C.X. Ma, Synthesis with Microwave-Assisted Sol-Gel Method and Photocatalytic Activity of Quantum-Sized TiO_2 under Solar and Ultraviolet Irradiation, Adv. Mater. Res. 399–401 (2011) 666–672. doi:10.4028/www.scientific.net/amr.399-401.666.

[194] E. Brillas, A review on the degradation of organic pollutants in waters by UV photoelectro-fenton and solar photoelectro-fenton, J. Braz. Chem. Soc. 25 (2014) 393–417. doi:10.5935/0103-5053.20130257.

[195] M.A. Oturan, P.V. Nidheesh, M. Zhou, Electrochemical advanced oxidation processes for the abatement of persistent organic pollutants, Chemosphere. 209 (2018) 17–19. doi:10.1016/j.chemosphere.2018.06.049.

[196] A. Hernández-Ramírez, E. Brillas, B.R. Garza-Campos, J.L. Guzmán-Mar, L.H. Reyes, E.J. Ruiz-Ruiz, Coupling of solar photoelectro-Fenton with a BDD anode and solar heterogeneous photocatalysis for the mineralization of the herbicide atrazine, Chemosphere. 97 (2013) 26–33. doi:10.1016/j.chemosphere.2013.10.044.

[197] F.C. Moreira, S. Garcia-Segura, V.J.P. Vilar, R.A.R. Boaventura, E. Brillas, Decolorization and mineralization of Sunset Yellow FCF azo dye by anodic oxidation, electro-Fenton, UVA photoelectro-Fenton and solar photoelectro-Fenton processes, Appl. Catal. B Environ. 142–143 (2013) 877–890. doi:10.1016/j.apcatb.2013.03.023.

[198] A.R.F. Pipi, I. Sirés, A.R. De Andrade, E. Brillas, Application of electrochemical advanced oxidation processes to the mineralization of the herbicide diuron, Chemosphere. 109 (2014) 49–55. doi:10.1016/j.chemosphere.2014.03.006.

[199] S.O. Ganiyu, M. Zhou, C.A. Martínez-Huitle, Heterogeneous electro-Fenton and photoelectro-Fenton processes: A critical review of fundamental principles and application for water/wastewater treatment, Appl. Catal. B Environ. 235 (2018) 103–129. doi:10.1016/j.apcatb.2018.04.044.

[200] S.O. Ganiyu, N. Oturan, S. Raffy, G. Esposito, E.D. Van Hullebusch, M. Cretin, M.A. Oturan, Electrochimica Acta Use of Sub-stoichiometric Titanium Oxide as a Ceramic Electrode in Anodic Oxidation and Electro-Fenton Degradation of the Beta-blocker Propranolol : Degradation Kinetics and Mineralization Pathway, Electrochim. Acta. 242 (2017) 344–354. doi:10.1016/j.electacta.2017.05.047.

[201] M. Zhou, M.A. Oturan, Electro-Fenton Process, Springer Singapore, Singapore, 2018. doi:10.1007/978-981-10-6406-7.

[202] J.F. Pérez, J. Llanos, C. Sáez, C. López, P. Cañizares, M.A. Rodrigo, On the design of a jet-aerated microfluidic flow-through reactor for wastewater treatment by electro-Fenton, Sep. Purif. Technol. 208 (2019) 123–129. doi:10.1016/j.seppur.2018.04.021.

[203] H. Nsubuga, C. Basheer, A. Jalilov, M.B. Haider, A.A. Al-Saadi, Droplet flow-assisted heterogeneous electro-Fenton reactor for degradation of beta-blockers: response surface optimization, and mechanism elucidation, Environ. Sci. Pollut. Res. (2019). doi:10.1007/s11356-019-04551-1.

[204] Montgomery, Rushing, Heath; Karl, Andrew; Wisnowski, James. Design and Analysis of Experiments by Douglas Montgomery: A Supplement for Using JMP(R). Copyright © 2013, SAS Institute Inc., Cary, North Carolina, USA. ALL RIGHTS RESERVED. For additional SAS resources, vi, Des. Anal. Exp. (2013).

[205] Y. Hu, H.L. Tsai, C.L. Huang, Phase transformation of precipitated TiO2 nanoparticles, Mater. Sci. Eng. A. 344 (2003) 209–214. doi:10.1016/S0921-5093(02)00408-2.

[206] M. Carbone, A. Nesticò, N. Bellucci, L. Micheli, G. Palleschi, Enhanced performances of sensors based on screen printed electrodes modified with nanosized NiO particles, Electrochim. Acta. 246 (2017) 580–587. doi:10.1016/j.electacta.2017.06.074.

[207] N. Oturan, A.K. Abdessalem, M.A. Oturan, M. Dachraoui, N. Bellakhal, Experimental design methodology applied to electro-Fenton treatment for degradation of herbicide chlortoluron, Appl. Catal. B Environ. 78 (2007) 334–341. doi:10.1016/j.apcatb.2007.09.032.

Vitae

Name :Hakimu Nsubuga

Nationality :Ugandan

Email :hakinsubuga@yahoo.com

Permanent Address : C/o, Chemistry Department, Islamic University in Uganda-P. O Box 2555, Mbale Main Campus- Uganda

Present Address : Chemistry Department, KFUPM, Dhahran Saudi Arabia

A-Academic Background

University	Department	Award	Year
King Fahd University of petroleum and Minerals	Chemistry	PhD	2018
King Fahd University of petroleum and Minerals	Chemistry	MSc	2014
Makerere University-Kampala, Uganda	Chemistry	BSc	2007
Institute of Teacher Education Kyambogo, Uganda	Chemistry	Diploma	1999
Makobore High School-Uganda	Sciences	Advanced Certificate	1997
Nyamitanga Sec. School-Uganda	Sciences	Ordinary Certificate	1994

B-Work experience

University	Department	Designation	Year
King Fahd University of petroleum & Minerals	Chemistry	Lecturer B	2014-2019
King Fahd University of petroleum & Minerals	Chemistry	Research Assistant	2011-2014
Islamic University in Uganda	Chemistry	Teaching Assistant	2008-2010
Secondary schools	Chemistry	Secondary teacher	1999-2008

C. Selected research articles (https://scholar.google.com/citations?user=Pkp-jMkAAAAJ&hl=en)

S/N	**Journal**
1	H. Nsubuga, C. Basheer, H. Muhammad Baseer, R. Bakdash, Sol-gel based biogenic silica composite as green nanosorbent for chemometric optimization of micro-solid-phase extraction of beta blockers, **Journal of Chromatography A**,554, 2018, 16-27.

2	H. Nsubuga, C. Basheer, A. Jalilov, M.B. Haider, A.A. Al-Saadi, Droplet flow-assisted heterogeneous electro-Fenton reactor for degradation of beta-blockers: response surface optimization, and mechanism elucidation, **Environmental Science and Pollution Research** (2019). doi:10.1007/s11356-019-04551-1.
3	H. Nsubuga, C. Basheer, M.M. Bushra, M.H. Essa, M.H. Omar, A.M. Shemsi, Microwave-assisted digestion followed by parallel electromembrane extraction for trace level perchlorate detection in biological samples, **Journal of Chromatography B,** 1012, 2016, 1-7.
4	H. Nsubuga, C. Basheer, H.A.S. Al-Muallem, A.N. Kalanthoden, Isolation, characterization and evaluation of photochemical potential of rice husk-based furfural via continuous flow reactor, **Journal of environmental chemical engineering,** 4, 2016, 857-863.

Filed Patents (Under Processing)

1-Chanbasha Basheer, Hakimu Nsubuga, Muhammad B. Haider, New Flow Assisted heterogeneous Electro-Fenton System for degradation of organic pollutants (Oblom ref. 520045US)

2- Chanbasha Basheer, Hakimu Nsubuga, Sol-gel functionalized graphite electrode for electro-Fenton degradation of organic pollutants (Oblom Ref. 521298US)

Conferences attended

1- Hakimu Nsubuga; Muhammad Haider Baseer; Chanbasha, Statistical analysis of beta-blockers degradation using droplet assisted electro-Fenton system and biogenic silica nanocomposite as a heterogeneous catalyst -9th Students Forum May 1-2,2018-Bld 60 KFUPM- **Oral presentation.**

2-Hakimu Nsubuga; Muhammad Haider Baseer; Chanbasha Basheer, Biogenic Silica Supported Iron as a Catalyst for Electro-Fenton Assisted Degradation of Beta-blockers-Student Research Poster Day at KFUPM-Chemistry department (3-4, Jun, 2017)-**Poster presentation**

4-Hasan Ali Saleh Al-Muallem, Hakimu Nsubuga, Chanbasha Basheer, Furfural synthesis from rice husk: a comparative study and its applications-Petroenvironment 2016-Al-khobar-KSA-**Oral Presentation.**